



University of Natural Resources
and Life Sciences, Vienna
Department of Biotechnology

Department für Biotechnologie

Departmentleiter:

Univ.Prof. Dipl.-Ing. Dr.nat.techn. Reingard Grabherr

Betreuer:

Assoc. Prof. Dr. Johannes Grillari

Dr. Markus Schosserer

The role of specialized ribosomes in aging and disease

Dissertation zur Erlangung des akademischen Grades Doctor rerum
naturalium technicarum an der Universität für Bodenkultur Wien

Eingereicht von:

Dipl.-Ing. Clemens Heissenberger

Wien, Juni 2020

Der Gipfel der Ignoranz ist ein Mensch, der von einer Pflanze oder einem Tier sagt: "Wozu soll das gut sein"? Wenn Fauna und Flora im Lauf der Äonen etwas geschaffen haben, das wir lieben, aber nicht verstehen, wer außer einem Narren würde Teile wegwerfen, die nutzlos scheinen? Jedes Rädchen und Schraubchen aufzubewahren, ist die wichtigste Voraussetzung für intelligentes Tüfteln.

- *Aldo Leopold*

Declaration

I hereby declare that I am the sole author of this work. No assistance other than that which is permitted has been used. Ideas and quotes taken directly or indirectly from other sources are identified as such. This written work has not yet been submitted in any part.

Clemens Heissenberger

Date, Signature

Acknowledgements

A doctoral project is not (or if so, please tell me how) accomplished by a single person, just according to the motto “Art is I, science is we – from Claude Bernard”. Dozens of helping hands are needed to drive success. Many great people have helped, accompanied, criticized and supported me in all regards during the last 4 years. I am deeply grateful to my direct supervisor Markus Schosserer for giving me the opportunity to work on such a challenging, yet captivating project. He never failed to inspire me with fascinating and sometimes really obscure ideas to think outside the box to “get the big picture”. He continuously challenged and supported me in every possible aspect. Thank you Markus for everything and making me a well-educated scientist.

I want to thank Giovanni (Johannes Grillari) for giving me the opportunity to start and finish this project, guiding my work where necessary and giving me the freedom to develop and try my own ideas. The theory of “try and error” is sometimes a brutal one, but after the day, you should have learned a bit and move a step forward.

I am much obliged to the IMICS and Grillari/Schosserer group members for their help, friendship and the (most of the time) relaxed working atmosphere. Thanks Nick, Peter, Marcus, Nina, Moha and the rest of the “IMICS-gang” for the valuable time, especially the great and unique discussions at Pizza-Tuesdays. Thanks Fabian for all the statistic lectures and all the help throughout the thesis and our project. Thanks Madhu for being my best Indian friend. You’ve taught me how to cook proper Dehli food and how to make your body accepting chillies. Thanks Stefan for your great personality and your good mood. I will miss your laughter. Thanks Lisa for the great time, particularly for being the “Team NSUN5”. It was an unforgettable time in the AKH while handling our grey-haired friends, while preparing isolated tissues for FACS analysis (with Austropop) and many more great occasions (bee-keeping lectures, Jolly, Rommé, Solero, Vamed, Koala, Kräutergesöff, ho, ect.). And Ingo, please stay as you are, I hope you are aware that you have a unique talent ignoring people and noise while crushing through the literature. Overall, I have to admit; it was the best time in my life with you guys. We accomplished tons of work, had tons of fun and had tons of goose! I’ll never forget this great chapter of my life.

I am much obliged to former and current members of our research group. Thank you all for your encouraging feedback and fruitful discussions. In particular, I want to mention Vera, Luci, Regina, Elena, Teresa, Tamas and Anton.

Finally, I want to express my deepest gratitude to my family and friends, my parents, my siblings and my beloved granny. Thanks to my deep friends (in alphabetical order) Benj, Benji, Finki, Holzi und Sepi, for making life more exciting and for being there for me during the worst and the good times.

Most importantly, thank you, Tanja, for always supporting me, often times absorbing the emotional load of this project but most importantly for being the best friend and partner I can imagine.

Abstract

Ribosomes are monolithic biological nanomachines, responsible for protein synthesis. Emerging evidence suggests that ribosomes are not build up equally, but that they rather differ in their composition. In humans, they are comprised of approximately 80 different ribosomal proteins and four different ribosomal RNAs. Both, ribosomal proteins and RNA are prone to be modified in manifold ways. Around 2-3% of all nucleotides of ribosomal RNA are specifically decorated with certain chemical structures.

The ribosomal RNA methyltransferase NSUN5 was previously identified as being implicated in biological aging and stress response in simple model organisms like yeast, worms and flies. The role of NSUN5 in humans and mice was not clear so far and not described in literature, thus the aim of this thesis was its functional characterisation. In the present study, we generated cell lines, which are devoid of NSUN5 and compared their ribosomal function to unmodified cells to build a direct link between this specific ribosomal RNA modification and a potentially altered function of the ribosome. In particular, we could demonstrate that NSUN5 is essential for proper cell growth and lack of NSUN5 decreases overall protein synthesis in mammalian cells. Furthermore, via ultra-structure microscopy, we verified that human NSUN5 is localized in the cells' nucleoli and specifically responsible for the methylation of cytosine 3782 on 28S ribosomal RNA. Moreover, we also generated a Nsun5 knockout mouse and could already observe biological consequences upon loss of this methyltransferase in these animals.

In addition, this thesis also addressed the characterisation of another RNA methyltransferase, NSUN-1 in *Caenorhabditis elegans*, the biological role of which was assessed in the nematode for the first time. We could demonstrate that NSUN-1 is responsible for the specific methylation of cytosine 2982 on 26S rRNA. Experiments have shown that NSUN-1 is required for adequate development, as loss of NSUN-1 leads to sterility of wildtype animals, resulting in adult animals lacking matured oocytes. Moreover, locomotion and resistance against heat were improved upon loss of *nsun-1*, especially in mid-aged nematodes.

Consequently, this work will contribute to a better understanding of ribosomal modifications in aging and disease.

Kurzfassung

Ribosomen sind gigantische biologische Nanomaschinen, die für Proteinsynthese verantwortlich sind. Immer mehr Studien zeigen, dass Ribosomen nicht gleich aufgebaut sind, sondern unterschiedliche Zusammensetzungen haben können. Ribosomen bestehen aus ungefähr 80 verschiedenen ribosomalen Proteinen und vier verschiedenen ribosomalen RNAs. Sowohl ribosomale Proteine als auch RNA neigen dazu modifiziert zu werden und zwar in vielfältiger Art und Weise. Geschätzt 2-3% aller Nukleotide ribosomaler RNA sind spezifisch mit bestimmten chemischen Strukturen modifiziert.

Die ribosomale RNA Methyltransferase NSUN5 wurde kürzlich als Protein identifiziert, welches im biologischen Alterungsprozess sowie in der Stressantwort in einfachen Modelorganismen wie Hefen, Fadenwürmern und Fliegen eine Rolle spielt. Die biologische Funktion von NSUN5 in Menschen und Mäusen war kaum erforscht. Aus diesem Grund war das Ziel dieser Arbeit die erstmalige funktionelle Charakterisierung dieses Proteins. Wir generierten Zelllinien ohne NSUN5 und verglichen deren ribosomale Funktion mit nicht modifizierten Zellen um eine direkte Verbindung zwischen dieser spezifischen ribosomalen RNA Modifikation und einer potentiell veränderten Funktion von Ribosomen herstellen zu können. Wir konnten zeigen, dass NSUN5 essentiell für adäquates Zellwachstum ist und der Verlust von NSUN5 zu geringerer Proteinsynthese in Säugerzellen führt. Weiters verifizierten wir via Ultrastruktur-Mikroskopie die Lokalisation von humanem NSUN5 in den Nukleoli und demonstrierten, dass NSUN5 für die spezifische Methylierung am Cytosin 3782 der 28S ribosomalen RNA verantwortlich ist. Weiters generierten wir außerdem eine Nsun5 Knockout Maus und konnten bereits die ersten biologischen Konsequenzen des Verlusts dieser Methyltransferase bei diesen Tiere feststellen.

Diese Arbeit adressierte auch die Charakterisierung einer weiteren RNA Methyltransferase, nämlich NSUN-1 in *Caenorhabditis elegans*. Die biologische Funktion dieser wurde hiermit in Nematoden das erste Mal untersucht. Wir konnten zeigen, dass NSUN-1 verantwortlich für die spezifische Methylierung am Cytosin 2982 auf der 26S ribosomalen RNA ist. Experimente zeigten, dass NSUN-1 für eine normale Entwicklung benötigt wird. Der Verlust von NSUN-1 führt zur Sterilität dieser Fadenwürmer und bewirkt bei erwachsenen Tieren fehlerhafte und

unterentwickelte Oozyten. Darüber hinaus zeigte sich bei Würmern ohne *nsun-1* verbesserte Fitness und Resistenz gegen Hitzestress.

Somit wird diese Arbeit zu einem besseren Verständnis von ribosomalen Modifikationen und deren Rolle im Alterungsprozess sowie in verschiedenen Pathologien beitragen.

Table of contents

Declaration.....	III
Acknowledgements	V
Abstract	VII
Kurzfassung.....	IX
Table of contents.....	XI
1 Introduction	1
1.1 The mechanisms of aging.....	1
1.2 Model organisms in aging research.....	2
1.2.1 <i>Caenorhabditis elegans</i>	3
1.2.2 <i>Mus musculus</i>	4
1.2.3 Human cell culture and clinical studies	4
1.3 Hallmarks of aging.....	6
1.3.1 Genomic instability	7
1.3.2 Telomere attrition.....	7
1.3.3 Deregulated nutrient sensing	8
1.3.4 Stem cell exhaustion.....	9
1.3.5 Altered intercellular communication.....	10
1.3.6 Mitochondrial dysfunction	11
1.3.7 Cellular senescence	12
1.3.8 Epigenetic alterations.....	14
1.3.9 Loss of proteostasis	15
1.4 Ribosomes – the underestimated monolithic machine	16
1.4.1 Ribosome biogenesis	16
1.4.2 Heterogenous ribosomes	17
1.4.3 Ribosomopathies	21
1.4.4 Composition of RPs.....	22
1.4.5 Modifications of RPs	23
1.4.6 Paralogs of RPs.....	23
1.4.7 Types of rRNA	24
1.4.8 rRNA modifications	25
1.4.8.1 2'-O methylations	26
1.4.8.2 Pseudouridylations	27

1.4.8.3	Base methylations.....	29
1.4.8.3.1	NSUN5.....	32
1.4.8.3.2	NSUN1.....	33
1.4.8.3.3	RRP8/NML.....	34
2	Aims of the thesis	36
3	Results.....	37
3.1	Loss of the ribosomal RNA methyltransferase NSUN5 impairs global protein synthesis and normal growth	37
3.1.1	NSUN5 is the human homolog of Rcm1p	37
3.1.2	Loss of NSUN5 impairs growth of cells and mice	40
3.1.3	NSUN5 methylates C3782 of human and C3438 of mouse 28S ribosomal RNA	43
3.1.4	Two conserved cysteines of NSUN5 are required for its RNA methyltransferase activity and normal proliferation	46
3.1.5	RNA polymerase I activity and the N-terminal domain are required for nucleolar localization of NSUN5	48
3.1.6	Loss of NSUN5 reduces global protein translation but does not affect ribosome biogenesis and fidelity	51
3.1.7	Partial loss of NSUN5 in Williams-Beuren-Syndrome is sufficient to reduce m ⁵ C3782	54
3.1.8	Discussion and Conclusion	56
3.1.9	Additional Discussion	60
3.1.10	Supplemental Data	62
3.2	The ribosomal RNA m⁵C methyltransferase NSUN-1 modulates healthspan and oogenesis in <i>Caenorhabditis elegans</i>	70
3.2.1	NSUN-1 is responsible for writing m ⁵ C at position C2982 on <i>C. elegans</i> 26S rRNA	70
3.2.2	The somatic tissue-specific depletion of <i>nsun-1</i> extends healthy lifespan	74
3.2.3	The somatic tissue-specific depletion of <i>nsun-1</i> affects body size, fecundity, and gonad maturation	77
3.2.4	NSUN-1 is required for the transition of meiotic germ cells to mature oocytes	80
3.2.5	NSUN-1 is not essential for pre-rRNA processing and global protein synthesis	83
3.2.6	mRNAs encoding cuticle collagens are translationally repressed upon <i>nsun-1</i> knockdown.....	86
3.2.7	Discussion and Conclusion	89
3.2.8	Additional Discussion	92
3.2.9	Supplemental Data	94
4	Conclusions and Outlook.....	101
5	Material and Methods	104
5.1	Mammalian cell culture	104

5.1.1	Cells animals and ethics	104
5.1.2	Isolation and immortalization of mouse embryonic fibroblasts	105
5.1.3	Generation of NSUN5 KO HeLa cells by CRISPR-Cas9.....	105
5.1.4	Transfection of mammalian cells.....	105
5.1.5	NSUN5 knock-down by shRNA	106
5.1.6	Generation and stable transfection of GFP-mNsun5 BACmid.....	107
5.1.7	Cell number and cell size determination	107
5.1.8	Weight and body composition measurement.....	108
5.1.9	Food intake	108
5.1.10	Antibodies	109
5.2	Molecular Biology and Imaging	110
5.2.1	Site directed mutagenesis of NSUN5 in pCI-neo and lentiviral vectors	110
5.2.2	Generation of NSUN5-GFP truncation mutants	110
5.2.3	Western blots	111
5.2.4	RNA isolation and cDNA synthesis.....	111
5.2.5	RT-qPCR.....	112
5.2.6	Bisulfite conversion, PCR amplification and sequencing.....	112
5.2.7	Combined bisulfite restriction analysis (COBRA).....	113
5.2.8	Immunofluorescence staining of cells	113
5.2.9	Actinomycin D and α -Amanitin exposure.....	114
5.2.10	O-propargyl-puromycin (OPP) assay	114
5.2.11	Quantification of rRNA	115
5.2.12	Reporter assays to characterize translational fidelity and IRES translation.....	115
5.2.13	OPP labelling <i>in vivo</i>	117
5.2.14	Polysome profiling	117
5.2.15	In vitro translation assay.....	118
5.2.16	Multiple protein sequence alignment of Rcm1p and NSUN family members	119
5.2.17	Statistics	119
5.3	<i>C. elegans</i>	119
5.3.1	Worm strains and culture conditions	119
5.3.2	RNAi knockdown.....	120
5.3.3	Differential Interference Contrast (DIC) microscopy.....	120
5.3.4	Mobility.....	120
5.3.5	Lifespan assays.....	121
5.3.6	Thermotolerance	122
5.3.7	Body size	122

5.3.8	Brood size analysis	122
5.3.9	Global protein synthesis by puromycin incorporation	122
5.3.10	Polysome profiling	123
5.3.11	RNA Seq	123
5.3.12	RT-qPCR.....	125
5.3.13	3-D ribosome structure.....	126
5.3.14	m ⁵ C detection by COBRA assay	126
5.3.15	HPLC analysis of m ⁵ C.....	126
5.3.16	Pre-rRNA processing analysis	126
5.3.17	Statistics and sample size estimation	127
6	References.....	128
7	Appendix.....	148
7.1	Abbreviations	148
7.2	Thesis related publication.....	150
7.2.1	A novel <i>Caenorhabditis elegans</i> proteinopathy model shows changes in mRNA translational frameshifting during aging – Cell Physiol Biochem. 2019	150
7.2.2	Cellular senescence and quiescence are associated with altered ribosomal RNA methylation and processing – bioRxiv preprint.....	150
7.3	Curriculum vitae.....	179

1 Introduction

1.1 The mechanisms of aging

The process of aging is commonly defined as progressive decline in biological function that affects the prevailed majority of organisms and inevitably leads to death (Maynard Smith 1959). Aging is a multiplex process in which a steady accumulation of damage on molecular, cellular and organismal level occurs. This deterioration of certain biological processes is the primary risk factor for a myriad of aging-associated diseases and goes hand in hand with pathologies such as cancer, cardiovascular disorders, diabetes, macular degeneration, and several neurodegenerative diseases like Alzheimer's and Parkinson's disease (Kirkwood 2005; Vijg and Campisi 2008; Gems and Partridge 2013; López-Otín et al. 2013).

A plethora of hypotheses attempting to explain and untangle the riddle of aging have emerged over the past decades. The "Stochastic Theory" presumes that a time-dependent decline in cellular functions is the result of damage to essential biomolecules. Damage is triggered either extrinsically (UV light) or intrinsically (reactive oxygen species (ROS)). The "Oxidative Stress Theory of Aging" states that the steady and immanent accumulation of ROS leads to a decline of cellular function (Harman 2003; Lipsky and King 2015). Another prominent example is the "Antagonistic Pleiotropy Hypothesis" postulated more than six decades ago by Georgy Williams. The underlying idea is that some genes that increase fitness early in life, have negative effects later on. Such genes could be favoured naturally during evolution as they do not exert adverse effects on reproduction (Williams 1957). In recent years, many of these genes were discovered, showing a potential to enhance the life -and/or healthspan either being absent or suppressed.

The rate of aging is controlled by various genetic pathways and biochemical processes which are often highly conserved in evolution. These pathways, which are fundamental for extending the lifespan and maintaining cellular integrity, either affect the cellular stress response system or govern energy intake, sensing and allocation of nutrients. Changes in the expression level of single genes within these essential pathways can alter the lifespan of model organisms dramatically (Alic and Partridge 2015).

Recently, researchers subsumed the existing knowledge on aging and categorized relevant biological events into nine hallmarks. Those hallmarks, illustrated in figure 1 are: Genomic instability, epigenetic alterations, telomere perturbations, loss of proteostasis, mitochondrial dysfunction, stem cell exhaustion, cellular senescence, deregulated nutrient sensing and altered intercellular communication (López-Otín et al. 2013). Hallmarks are described in more detail in the following sections 1.3.1 to 1.3.9.

Over the past few years, the mindset in the field of aging research adapted in a way that the major aim shifted from increasing the overall lifespan towards increasing healthspan, referring to an extension of the healthy period of life where an individual does not suffer from any disease. So far, the aging process is still poorly understood, but scientists all over the world are eager to improve the knowledge in order to avoid, or at least postpone, age-related diseases and physical decline in humans.

1.2 Model organisms in aging research

During the last decades, some very useful model organisms have emerged for genetic studies and, in particular, for aging research. Among these model organisms are the nematode *Caenorhabditis elegans*, the fruit fly *Drosophila melanogaster*, the mouse *Mus musculus*, as well as human cell and organoid cultures. Although *Drosophila melanogaster* is a great model to study aging, I will not describe it in detail in this chapter, since no experiments with fruit flies were conducted in this doctoral thesis.

For being suitable as a proper model organism, some general aspects have to be taken into account, such as generation time, the possibility of genetic manipulation and the conservation of genes to finally translate the findings to humans. The major advantage of simple model organisms like *Caenorhabditis elegans* compared to mammals is that a “molecular toolbox” exists and can be easily applied to specifically manipulate the genome. Also, the potential economic benefit should be noted, because cultivating nematodes is much less expensive, in all regards, compared to human cell culture or mouse studies. Due to the low complexity, for instance in their nervous -and immune system, they do not serve as a good model for respective genes that are not conserved and therefore can not be studied. Nevertheless,

these abovementioned models are great tools to understand the basic mechanisms of proteins and pathways in the aging process. Regardless of the fact that models exhibit advantages and disadvantages, no model will ever reach the exact complexity of humans.

1.2.1 *Caenorhabditis elegans*

Caenorhabditis elegans is a small, transparent roundworm that is naturally occurring in soil worldwide. Concerning its classification, *C. elegans* belongs to the nematode phylum. Adult animals are about 1 mm in length and possess exactly 959 (hermaphrodites) or 1031 (males) cells. The main characteristics of this organism are the rapid life cycle allowing for the possibility to breed a large, isogenic population (Brenner 1974; Fire et al. 1998). The vast majority of worms within a population are self-fertilizing hermaphrodites, whereas only around 0.2% are males (Shakes et al. 2009; Zarkower 2006). *C. elegans* has a maximum lifespan of approximately one month and RNAi can easily be achieved by feeding recombinant bacteria expressing dsRNA targeting a gene of interest (Fire et al. 1998). These features make *C. elegans* a perfectly suited model for studying aging, which is why it became the first organism in which long-lived mutants were discovered (Kenyon et al. 1993; Johnson 1990). Compared to yeast, *C. elegans* is closer related to mammals and allows the study of different tissues and cell types. Interestingly, approximately 70% of all human genes have an ortholog in the *C. elegans* genome (Kaletta and Hengartner 2006). Moreover, around 40% of disease-associated genes in humans have orthologs in the worms' genome (Culetto and Sattelle 2000). Hence, findings in *C. elegans* have often direct relevance for human health and disease and can pave the ground for interventions in the end applied in humans.

Nonetheless, also worms have their limitations. Since, adult *C. elegans* only have post-mitotic cells, comparisons to higher organisms in which proliferation and cell renewal is of relevance, can hardly be made. Moreover, nematodes anatomically differ from vertebrates and their nervous -and immune system show only rudimentary complexity.

1.2.2 *Mus musculus*

Compared to *C. elegans*, the mouse *mus musculus* belongs to mammals and is thus much closer related to *homo sapiens*. In fact, the majority of aging related mechanisms and nutrient sensing pathways are well conserved between mice and humans making them a valuable model in general research. Manifold genetic tools are available, for instance conditional knockouts, where individual tissues and developmental stages can be manipulated and studied in detail. Moreover, mice of many different genetic backgrounds have been developed the last decades allowing to study for instance immune-compromised mice and their tumor progression or long-lived dwarf mice and their improved stress resistance to some negative stimuli (Fontana et al. 2010; Kenyon 2005; Masoro 2005). However, the maximum lifespan of approximately 36 months makes lifespan studies very labour-, cost- and time-intensive. Hence, mouse studies need to be planned concisely and in accordance to a positive approval from the corresponding ethic authorities in the respective country. Indeed, we can not omit studies in mice until we, as scientists, have the chance to perform experiments in human-like models (e.g. organ-on-a-chip and other microfluidic systems or chimeric studies where human organs are grown in pigs). Studies in laboratory animals, in particular in mice, are certainly necessary in order to avoid poorly conceived clinical trials in humans for establishing therapies counteracting aging and diseases.

1.2.3 Human cell culture and clinical studies

Analysing long-lived human cohorts scattered around the world, in particular in parts of Italy and Japan, do provide important pieces of the puzzle of understanding aging (Pawlikowska et al. 2009; Suh et al. 2008; Willcox et al. 2008; Kojima et al. 2004). Another interesting study analyzed the offspring of long-lived parents for various genetic traits and immunologic parameters (Westendorp et al. 2009).

Genome editing in humans to study aging is of course not an option, also due to justified ethical concerns. However, cell culture based research, using human based material is an essential tool in science. Generally, human cells used in the lab can be separated into two groups. Firstly, immortalized cell lines like HeLa, HEK, and many others and secondly, primary

cells, isolated from tissue which resemble a more physiological condition compared to immortalized cells. A disadvantage of immortalized cells is the aneuploidy, the irregular set of chromosomes. It could be the case that HeLa cells consist of around 80 chromosomes, whereas healthy human cells only have exact 46 (Landry et al. 2013; Macville et al. 1999).

Premature aging phenotypes are often characterized by mutations in DNA damage repair mechanisms. These syndromes such as Werner -and Cockayne Syndrome and Bloom's disease are principally inherited (von Zglinicki et al. 2005; Kyng and Bohr 2005). Besides aging research, especially research on DNA repair mechanisms can be performed in isolated primary cells of these patients suffering from those maladies.

As described in section 1.3.7 Cellular Senescence, DNA damage, stress or aberrant oncogenic signalling have been described to participate in the induction of senescence, but the underlying mechanisms are not yet fully understood. We have to better understand how and why several tissues functionally decline *in vivo* and how cells escape and re-enter the cell-cycle and transform into tumor cells (Ressler et al. 2006; Minamino et al. 2002; Yousefzadeh et al. 2020).

Conclusively, human derived cells used *in-vitro* will of course never be totally comparable to complex *in-vivo* studies of human cells, tissues and/or organs.

1.3 Hallmarks of aging

As already abovementioned, scientist around the world subsumed the knowledge on aging and grouped relevant biological events into nine hallmarks. The prerequisites for being qualified as a hallmark are manifestation during aging, aggravation leading to accelerated aging and experimental amelioration leading to an increased lifespan. Furthermore, the hallmarks of aging are grouped into primary, antagonistic and integrative hallmarks. Primary hallmarks are characterized as being unequivocally unfavourable such as dysfunctional proteostasis and DNA damage. Antagonistic hallmarks are related to the abovementioned theory, referring to genes/cellular events that are beneficial at low levels but detrimental at high levels. A prominent example thereof and one of the hallmarks of aging is cellular senescence. On the one hand, steady accumulation of senescent cells within the body results in several malfunctions and an aged phenotype (Acosta et al. 2013; Coppé et al. 2008; Hubackova et al. 2012; Krtolica et al. 2001; Nelson et al. 2012), while on the other hand, senescence is a potential safeguard preventing cells turning into malignancies. Integrative hallmarks directly influence tissue homeostasis and are the result of primary and antagonistic hallmarks. Integrative hallmarks are ultimately responsible for the functional decline of cells and tissues associated with aging.



Figure 1: Illustration of the postulated nine major hallmarks of aging including primary, antagonistic and integrative hallmarks (López-Otín et al. 2013).

1.3.1 Genomic instability

The outcome of some progeria syndromes, such as Werner -and Bloom syndrome, are the consequence of a lifelong accumulation of DNA damage (Burtner and Kennedy 2010). The genomic integrity and stability are constantly challenged by exogenous -and endogenous threats like toxic chemicals, biological agents, spontaneous mutations, replication errors and ROS. Organisms evolved a complex system of finely-tuned repair mechanisms to shelter the genome from deleterious alterations (Hoeijmakers 2009). However, as long as DNA has to replicate, errors will accumulate over time. Thus, genomic instability poses a greater problem to aged individuals. Recently, studies showed that defective DNA repair has been linked to some human progeroid syndromes and to accelerated aging and on the contrary, enhanced DNA repair can delay aging-associated deteriorations in flies (Garschall et al. 2017) and mice (Honig and Vo; Murga et al. 2009; Gregg et al. 2012).

1.3.2 Telomere attrition

Some chromosomal regions, such as telomeres, are more susceptible to DNA damage than others (Blackburn et al. 2006). Telomeres provide the protection of DNA caps at the end of chromosomes. These protective caps are composed of TTAGGG DNA repeats and normally form a loop structure, also called the T-loop (Griffith et al. 1999). Telomeres shrink with every cell division and importantly, this telomere shortening provides an explanation for replicative senescence, also known as the “Hayflick limit” (Hayflick 1965). If the telomeres reach a critical length, rendering them prone for replication errors, cells enter replicative senescence, a state of growth arrest (Olovnikov 1996). Telomere perturbation occurs concomitantly with aging in mammals. Interestingly, in some pathologies, such as idiopathic pulmonary fibrosis, dyskeratosis congenita and aplastic anaemia, shortening of telomeres is accelerated. DNA damage at telomeres leads to DNA-damage response (DDR) which results in cell-cycle arrest and induces apoptosis -and/or senescence of pertained cells (Fumagalli et al. 2012; Hewitt et al. 2012).

An enzyme called telomerase, acts as a reverse transcriptase and can derogate the discrepancy of telomere shortening. Telomerase synthesizing the DNA repeats to the 3′- ends

of the chromosomes (Greider and Blackburn 1985). Telomerase is usually expressed in stem- and progenitor cells and normally repressed in postnatal somatic cells resulting in the progressive shortening of telomeres. Whereas adequate function of telomerase is crucial for chromosomal integrity, mutations of telomerase are associated with age related disorders including organ dysfunction and, in particular, increased cancer risk (Armanios 2013). Ectopic expression of telomerase in telomerase-devoid human cells suffices to render mortal cells immortal without oncogenic transformation (Han and Brunet 2012). Moreover, a study suggests that longer telomeres are associated with better overall health in centenarians (Terry et al. 2008). In conclusion, these facts clearly implicate the importance of the telomere, its preservation by telomerase and the link to replicative senescence and apoptosis for human aging.

1.3.3 Deregulated nutrient sensing

Nutrients such as amino acids, sugars or lipids are relatively simple components involved in a myriad of biochemical reactions. “The disposable soma theory” describes the competition for nutrients and energy between longevity and reproduction (Alic and Partridge 2015). When amino acids are scarce but needed, proteins can provide a reservoir for amino acids by utilizing recycling programs like proteasome-mediated degradation or autophagy (Efeyan et al. 2015). Caloric restriction (CR) is defined as decreased calorie intake without malnutrition. CR was shown to enhance lifespan in several model organisms, from yeast to non-human primates (Madeo et al. 2015; Weir et al. 2017; Longo 2019; Fontana et al. 2013, 2018). In CR, autophagy is induced, resulting in diverse beneficial effects on aging (Galluzzi et al. 2015). Recent studies claimed that the effects of reduced food intake on organismal lifespans are not the consequence of reduced nutrient availability, but rather of the altered nutrient signalling pathways (Alic and Partridge 2015; Efeyan et al. 2015). This effect was profoundly illustrated in fruit flies. There, the dietary restriction mediated lifespan extension was partly reversed upon applying food derived odors only (Libert et al. 2007). Interestingly, the most essential signalling pathways are evolutionary conserved from baker’s yeast, to worms, flies and humans (Fontana et al. 2013; Barzilai et al. 2012). Prominent pathways include the insulin/insulin-like growth factor (IGF) signalling (IIS), the mTOR (mechanistic target of

rapamycin) signalling and AMP-activated protein kinase (AMPK) signalling. The mTOR pathway is sensing high amino acid concentrations, the AMPK pathway is sensing high AMP levels and sirtuins are sensing high NAD⁺ levels. All these pathways are responding to the presence of nutrients, repressing or activating downstream targets to direct the available energy towards what is needed within a cell under specific circumstances. This nutrient signalling is often deregulated in diseases and aging (Efeyan et al. 2015). Genetic or pharmacological interventions reducing the activity of IIS or TOR pathway improve health and lifespans in model organisms and can delay the progression of some age-related pathologies (Selman et al. 2008). Additionally, periodic fasting without losing weight seems to be sufficient to delay aging in rodents (Longo and Mattson 2014).

1.3.4 Stem cell exhaustion

Stem cells possess the ability to differentiate into various fully functionable cell types like osteocytes, myocytes, chondrocytes and many others. The steady decline of regenerative potential and capacity of cells and tissues is another profound characteristic of aging (López-Otín et al. 2013). Hematopoiesis recedes with age, leading to a reduction of adaptive immune cells (Shaw et al. 2010) resulting in the fact that around 10% of the people over the age of 65 are anaemic (López-Otín et al. 2013). Also, recent studies have shown that a similar functional attrition of stem cells can be found in essentially all adult stem cell compartments in mice, the forebrain, muscle fibers and bone (Conboy and Rando 2012; Gruber et al. 2006; Molofsky et al. 2006). Another report showed that aged mice have an overall reduction of cell-cycle activity of hematopoietic stem cells (HSCs), leading to fewer cell divisions in old HSCs compared to young ones (Rossi et al. 2007). Interestingly, transplantation of muscle-derived stem cells from young donor mice to progeroid mice was shown to extend animals' lifespan and to improve physiological parameters of tested animals, even in tissues where donor stem cells could not be detected. This finding suggests that the overall benefit derive from systemic effects caused, for instance, by secretion factors (Rossi et al. 2007). Similarly, special systemic factors originated from young mice were shown in parabiosis experiments to derogate the decline in neural and muscle stem cell function in old animals (Conboy et al. 2005; Villeda et al. 2011). Additionally, telomere attrition is a relevant cause for stem cell exhaustion in several

tissues (Flores et al. 2005). Taken together, these facts emphasize the pivotal role of stem cells and their renewal capacity in the process of aging.

1.3.5 Altered intercellular communication

Aging is of course not restricted to single cells, it rather affects microstructures and/or tissues throughout the body. Compelling evidence suggests that the intercellular communication (neuronal, paracrine, endocrine) within a tissue is implied in physiological aging (Laplante and Sabatini 2012; Rando and Chang 2012; Russell and Kahn 2007; Zhang et al. 2013). When cells die or reside in a cellular state like senescence, they secrete an enormous number of biomolecules such as cytokines, chemokines, growth factors, proteases and other proinflammatory factors. A part of the secretome (SASP factors) of senescent cells are extracellular vesicles (EVs). Various stressors and the pathological status of cells and tissues affect EV secretion. Recent reports demonstrated that senescent cells possess an enhanced EV secretion compared to its non-senescent counterpart (Jeon et al. 2019; Takahashi et al. 2017; Terlecki-Zaniewicz et al. 2018). Interestingly, EVs secreted from senescent cells can harbour nucleic acids as well as proteins as cargo, which can influence surrounding cells and tissues in a paracrine fashion (Terlecki-Zaniewicz et al. 2018, 2019; Borghesan et al. 2019). Moreover, a state of low-grade inflammation was recently postulated as “inflammaging” (Cevenini et al. 2013). The accumulation of damage to tissues and organs over time, the secretion of proinflammatory cytokines like interleukin 1 and 8 (IL1, IL8), might be the triggers of inflammaging in mammals (Salminen et al. 2012). One prominent factor influencing cellular microenvironments is the transcription factor nuclear factor kappa-light-chain-enhancer of activated B cells (NF- κ B). NF- κ B is activated when stress and cellular damage occur. Pharmacological NF- κ B inhibition improves aging and repels senescence in progeroid mice suffering from DNA damage repair defects (Osorio et al. 2012; Tilstra et al. 2012). Furthermore, aging-associated pathologies such as skin atrophy, muscle weakness, bone fragility and impaired neurogenesis are associated with reduced levels of gonadotropin-releasing hormone (GnRH). Similarly, administration with GnRH slows down aging in mice (Zhang et al. 2013). Aging related alterations in one tissue can augment to others via the blood

stream, harbouring several soluble, proinflammatory molecules like cytokines and chemokines.

1.3.6 Mitochondrial dysfunction

Cells have to constantly cope with potentially harmful agents such as ROS, which results in oxidative damage of biomolecules. Already some decades ago, the “Free radical theory of aging” was postulated, suggesting ROS as the central cause for accelerated aging (Harman 1956). Oxidative damage through ROS leakage can result in mitochondrial membrane permeability, detrimental for cells. Moreover, aged mitochondria are less productive in generating adenosine 5'-triphosphate (ATP), the main energy source in biochemical processes. Mitochondrial dysfunction may be implied in apoptotic signalling and inflammation (Kroemer et al. 2007; Green et al. 2011). Mitochondrial dysfunction seems to be linked to hormesis, hypothesizing that mild harm leads to a beneficial response, while severe mitochondrial dysfunction on the other hand leads to pathologies. Cells have evolved a clear up system called mitophagy in order to eliminate damaged and distorted mitochondria, preventing cells from inflammation and ultimately from cell death (Green et al. 2011). The precise multi-layered connections between aging and mitochondrial dysfunction have yet to be elucidated.

In the past few years, the notion of ROS has changed. Potentially, ROS is not solely seen as a noxious agent, as adequate ROS levels are implied in the stress response and can promote longevity pathways under certain conditions (Hekimi et al. 2011; Wang and Hekimi 2015). This beneficial effect was evidenced in a study showing that mild mitochondrial dysfunction had positive effects on the lifespan of model organisms (Merkwirth et al. 2016). Hence, moderate ROS levels can support the stress response. Taken together, mitochondrial function plays a pivotal role in cellular fitness and aging.

1.3.7 Cellular senescence

Although cellular senescence is a tumor suppressive mechanism and adequate presence of senescent cells has beneficial functions in wound healing, there is emerging evidence that chronic presence of senescent cells in tissues is directly linked to many age-related pathologies (Demaria et al. 2014; Jun and Lau 2010; Naylor et al. 2013). Senescence, originating from DNA damage, is characterized by an irreversible cell-cycle arrest, the accumulation of senescence-associated β -galactosidase (SA- β -gal) and the acquisition of a flattened and enlarged cell morphology (Campisi and d'Adda di Fagagna 2007). Hence, these cells cannot convey accumulated DNA damage to their next generation, preventing them from turning into cancer cells. Senescence associated cell-cycle arrest is induced via the p53-p21^{CIP1} or the p16^{INK4a}-Rb axis. Cellular senescence is often investigated *in vitro* by either using replicative senescent cells (see section 1.3.2 Telomere attrition) or using stress-induced premature senescent (SIPS) cells induced by various triggers like UV irradiation, oncogenes and oxidative stress.

Although arrested in G1 or G2 phase, senescent cells are still metabolically active. They are commonly thought to exert negative effects to the surrounding tissue by secreting a complex mixture of pro-inflammatory molecules, such as cytokines, chemokines, matrix metalloproteases and growth factors, referred to as the senescence associated secretory phenotype (SASP). The SASP accounts for chronically inflamed and pro-tumorigenic tissue environments, resulting in a vicious cycle of progressive functional loss of tissues and organs (Acosta et al. 2013; Coppé et al. 2008; Hubackova et al. 2012; Krtolica et al. 2001; Nelson et al. 2012). Up to now, strong evidence suggests that the presence of cellular senescence *in vivo* and the number of senescent cells vary in different tissues but rise with age and are thereupon believed to contribute to the aging phenotype (Wang et al. 2009). Recently, a study showed that in 10 of 13 tested mouse tissues, the expression of senescent markers like p16 and p21 significantly increased with age. Exceptions are three muscle tissues. Thus, it is conceivable that in myocytes, senescence only plays a minor role (Yousefzadeh et al. 2020).

Senescent intimal foam cells can accumulate at sites of atherosclerosis and drive the formation and maturation of atheromata (Childs et al. 2016). Furthermore, adipogenesis is inhibited by senescent fat progenitor cells, which in turn secrete high levels of activin A.

Similarly, elevated levels of activin A were also found in blood and fat tissue of old mice (Xu et al. 2015). Moreover, the generation of senescent cells can be induced by chemotherapeutics, total body irradiation or joint replacement surgeries leading to weight loss, liver damage, reduced hematopoietic stem cells or osteoarthritis (Baar et al. 2017; Chang et al. 2016; Jeon et al. 2017).

In order to attenuate the negative effects of cellular senescence, three strategies have been proposed. Firstly, delaying the acquisition of a senescent phenotype and subsequently the loss of functionality, secondly attenuating the negative effects of senescent cells and thirdly selectively eliminating senescent cells with senolytic substances (Naylor et al. 2013; Soto-Gamez and Demaria 2017; Tchkonina et al. 2013). Recent reports found that selective elimination of senescent cells in mice extends the median lifespan and attenuates deterioration of tissues and organs with age (Baker et al. 2016; Valiathan et al. 2016). Interventions that reduce the expression of SASP factors, without revoking the growth arrest, should be able to curtail the negative effect and support the surrounding tissue. Until today, many SASP inhibitors were identified, including glucocorticoids, metformin, rapamycin and JAK inhibitors (Soto-Gamez and Demaria 2017). Another promising strategy is the specific removal of senescent cells by the immune system or via selective elimination with the help of senolytic molecules, such as navitoclax, fisetin, dasatinib, quercetin or the FOXO4 inhibiting peptide (Chang et al. 2016; Baar et al. 2017; Zhu et al. 2016, 2017). Lifelong clearance of p16-positive cells in a progeria mouse model using the INK-ATTAC transgene delayed the onset of some age-related pathologies (Baker et al. 2011). A similar outcome was shown in naturally aged mice when clearing p16-positive cells, resulting in lifespan extension, delayed tumorigenesis and attenuated age-related disorders of several organs (Baker et al. 2016).

Within my doctoral study, we also investigated the role of ribosome specialization in senescent cells. For using a model which is as close to humans as possible, we examined human derived fibroblasts (HDFs) from female mid-aged donors. In particular, we assessed the 2'-O methylation pattern of ribosomal RNA (rRNA) in senescence in these cells (Yang et al. 2020). Moreover, we evaluated the translational capacity of senescent and quiescent HDFs with the aim to find specific ribosome modifications of ribosomal proteins (RPs) or rRNA distinctive solely in senescence (manuscript in preparation).

1.3.8 Epigenetic alterations

Epigenetic alterations typically include changes in the overall DNA methylation pattern, chromatin remodelling and histone modifications. In recent days, many epigenetic marks and alterations were uncovered, but the exact role of those still remains largely unknown. Modifications of methylation marks occur for instance, when DNA is damaged and repair proteins have to remove the epigenetic mark to attain the DNA and repair it. Thereupon, the removed epigenetic mark can be replaced correctly, incorrectly or even omitted.

Epigenetic perturbations typically occur during aging and are ordinarily reversible. Changes in the DNA methylation pattern are not uniform, meaning that ectopical overexpression or deletion of responsible methyltransferases will not be sufficient to restore the methylation pattern in humans. Nevertheless, new therapeutic targets to improve life -and healthspan are constantly emerging. In fact, epigenetic alterations heavily rely on environmental conditions such as temperature, pressure and nutrients (Fraga and Esteller 2007; Han and Brunet 2012). Thus, also great effort is spent on understanding epigenetics in the context of biopharmaceutical research, for example in Chinese hamster ovary (CHO) cells used for producing human therapeutics during a chemostat fermentation which is happening – at our department (Marx et al. 2018).

Transcriptional re-programming is one of the most evident cause and/or consequence in aging. Locus specific increase or loss of heterochromatin may regulate genes affecting longevity or aging in general. For instance, it was shown previously that loss of H3K27me3 causes an upregulation of SASP genes (Shah et al. 2013b). Such epigenetic changes certainly affect all cells and tissues throughout life, possibly contributing to aging and cancer (Talens et al. 2012). Moreover, deletion of components important for histone methylation (e.g. ASH-2 trithorax complex) extends the lifespan of flies and nematode worms (Siebold et al. 2010; Maro et al. 2011). So far, the precise role of epigenetic-based histone modifications in aging are not well known, although it is strongly suggested that gain or loss of epigenetic marks plays a profound role in gene expression and aging. Beside DNA, also RNA can be heavily modified and decorated with diverse modifications. Up to now, the role of RNA modifications in aging is scarcely understood and we I am eager to shed light on this specific topic within the next few chapters in my doctoral thesis.

1.3.9 Loss of proteostasis

Impaired protein homeostasis is associated with aging and disease and is therefore postulated as a primary hallmark of aging (Powers et al. 2009). Accurate proteostasis is defined as equilibrium between protein synthesis and degradation. Most scientists around the globe addressed proteostasis mainly by means of protein degradation. In this case, proper proteostasis utilizes mechanisms stabilizing correctly folded proteins and the degradation of aberrant, unfolded or non-functional proteins. Stabilization of proteins is mostly assured by heat shock proteins and chaperones, whereas recycling of proteins is executed either by the ubiquitin-proteasome or the autophagy-lysosomal pathway. If the balance between native and misfolded, unfolded or aggregated proteins shifts towards the latter, the needed equilibrium is out of balance. Hence, deregulated proteostasis is implied in some age-related pathologies such as Alzheimer's disease, cataracts and Parkinson's disease (Powers et al. 2009).

Also, dysfunctional autophagy is linked to some neurodegeneration and cancer and a general decline in molecular chaperones occurs during aging (Hartl et al. 2011; Koga et al. 2011; Mizushima et al. 2008). On the contrary, genetic interventions which promote proper proteostasis have been shown to delay physiological aging in mammals (Zhang and Cuervo 2008). Recent studies found that treatment with rapamycin can extend the lifespan of several model organisms by inhibiting the mTOR pathway (Powers et al. 2006; Robida-Stubbs et al. 2012; Bjedov et al. 2010).

Rare is known about how ribosomes, the gigantic molecular machines, control and adapt protein synthesis. Approximately, 2-3% of rRNA nucleotides can be modified, adumbrate an putative important role of those RNA modifications to fine-tune the translational process (Sharma and Lafontaine 2015). Ribosomes are not only comprised of rRNA, human 80S ribosomes are also composed of around 80 different RPs. Most of the RPs are assembled within or on the ribosomal surface. In the next chapter, I will describe the miracle of ribosomes in detail and hopefully can show how complex the build-up and composition of ribosomes can be.

1.4 Ribosomes – the underestimated monolithic machine

1.4.1 Ribosome biogenesis

Ribosome biogenesis requires a substantial amount of energy and is a tightly regulated cellular process (Kressler et al. 2010). As illustrated in figure 2, it needs all three RNA polymerases, as well as other non-ribosomal factors aiding the rRNA processing. RNA polymerase I is responsible for the transcription of 28S, 18S and 5.8S rRNAs in the nucleolus as a single 47S pre-rRNA. RNA polymerase III transcribes the 5S rRNA in the nucleus. After transcription, the pre-rRNAs are extensively decorated with specific methylations and pseudouridylations (Shi et al. 2017; Simsek et al. 2017; Genuth and Barna 2018; Xue and Barna 2012). Table 1 summarizes rRNAs and RPs of *Homo sapiens*, *Mus musculus*, *Caenorhabditis elegans* and *Escherichia coli*.

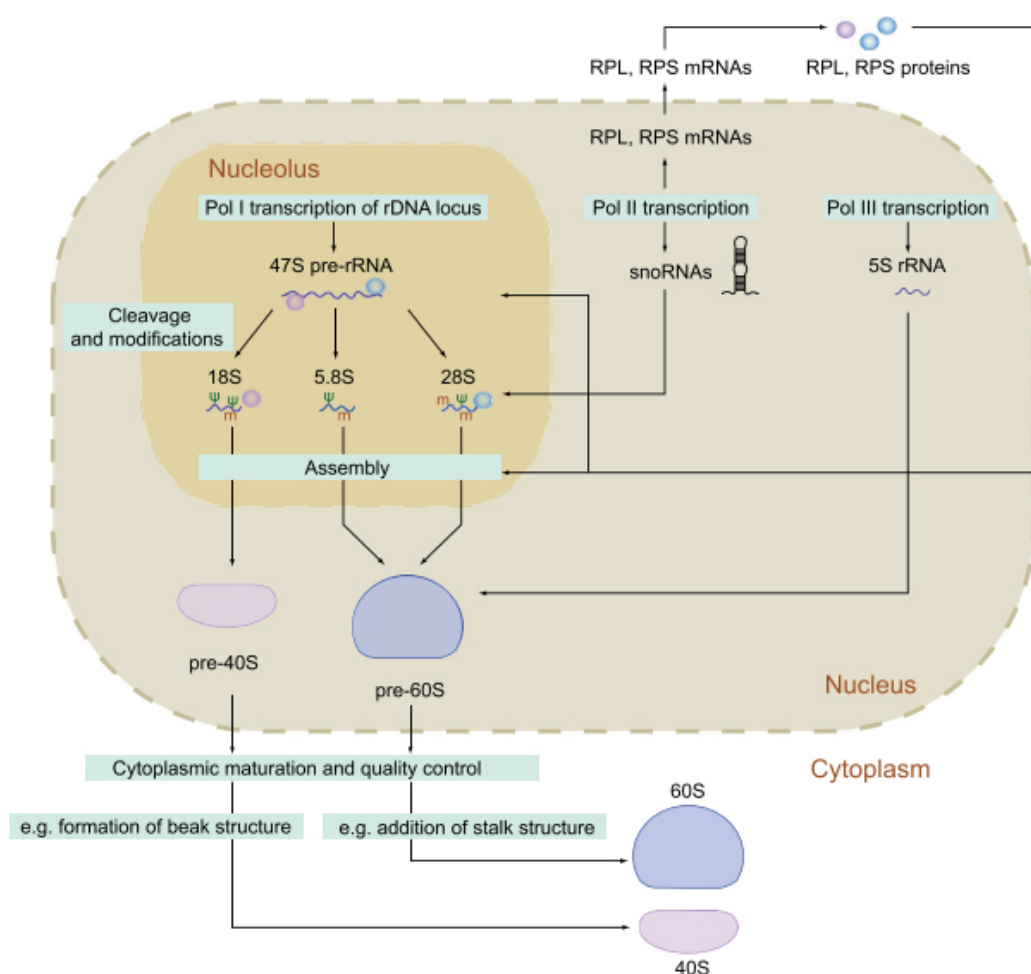


Figure 2: Overview of ribosome biogenesis including all three RNA polymerases (Guo 2018).

Sequence-specific small nucleolar RNAs (snoRNAs) guide the catalytically active enzymes to the modification target site of the rRNA (Sloan et al. 2017). Although emerging evidence exists that diverse ribosome biogenesis plays a part in ribosome function, the exact biological role of most of the rRNA modifications still remains to be answered (Baxter-Roshek et al. 2007). mRNA blueprints are transcribed by RNA polymerase II. Ribosomes, monolithic nanomachines, are not only assembled by four different rRNAs, but a main part are the around 80 different RPs. After translation in the cytoplasm, RPs enter the nucleus and assemble on pre-rRNAs during transcription. Subsequently, the pre-rRNAs are cleaved into mature 28S, 18S and 5.8S rRNA as the RPs assemble. The large ribosomal subunit comprises the 28S, 5.8S, 5S rRNA and 47 RPs and is formally known as 60S. The small ribosomal subunit consists of the 18S rRNA and 33 RPs (Ban et al. 2014). Upon assembly, the large and small subunit are then shuttled into the cytoplasm in a controlled and coordinated fashion (Henras et al. 2008; Johnson et al. 2002).

Table 1: Ribosome composition in different eukaryotes and *E. coli* as a member of prokaryotes

		<i>Homo sapiens</i>	<i>Mus musculus</i>	<i>Caenorhabditis elegans</i>	<i>Escherichia Coli</i>
Full ribosome	Sedimentation coefficient	80S	80S	80S	70S
Large subunit	rRNA	28S rRNA 5S rRNA 5.8S rRNA	28S rRNA 5S rRNA 5.8S rRNA	26S rRNA 5S rRNA 5.8S rRNA	23S rRNA 5S rRNA
	Proteins	47	47	47	33
Small subunit	rRNA	18S rRNA	18S rRNA	18S rRNA	16S rRNA
	Proteins	33	33	33	22

1.4.2 Heterogenous ribosomes

Ribosomes are massive macromolecules with a mass of approximately three mega daltons, consisting of four different rRNAs and 80 RPs (Khatter et al. 2015; Natchiar et al. 2017). Until a few years ago, ribosomes were seen as a uniform molecular entity with the conventional depiction that all ribosomes are composed identically. Protein synthesis engrosses around half of a mammalian cell's ATP supply (Princiotta et al. 2003). Heterogeneity of ribosomes means that ribosomes can vary in composition of their proteins, rRNA, or the post-

transcriptional and post-translational modifications of both kind of components (Figure 3). Studies focusing on heterogeneous ribosomes suggest that their composition can influence their way of function, while preserving their main duties, namely decoding and peptidyl transfer. During protein synthesis, mRNAs are read in the decoding site of the small subunit whereas the large subunit accommodates the peptidyl transferase centre (PTC), where the oligopeptide is joined together, as well as the terminal exit tunnel. A fully assembled and translating ribosome harbours three tRNAs between the subunits, i) the A-site tRNA (aminoacyl-tRNA), ii) the P-site tRNA (peptidyl-tRNA) and iii) the E-site tRNA (unloaded tRNA and the nascent polypeptide) (Steitz 2008). Upon initiation, the P-site is occupied by Met-tRNA^{Met}, whereas the A-site remains unloaded. Then, tRNAs with specific anti codons can bind correctly to the mRNA codon and the A-site. During elongation, the A-site tRNA advances to the P-site where peptide bond formation occurs. Nascent polypeptides are then formed and emerge from the ribosome through the E-site (Voorhees and Ramakrishnan 2013). The tRNA resided at the A-site is proceeding to the P-site via a ratchet-like movement which implicates the rotation of both subunits allowing the ribosome's progression relative to the mRNA blueprint (Zhou et al. 2014).

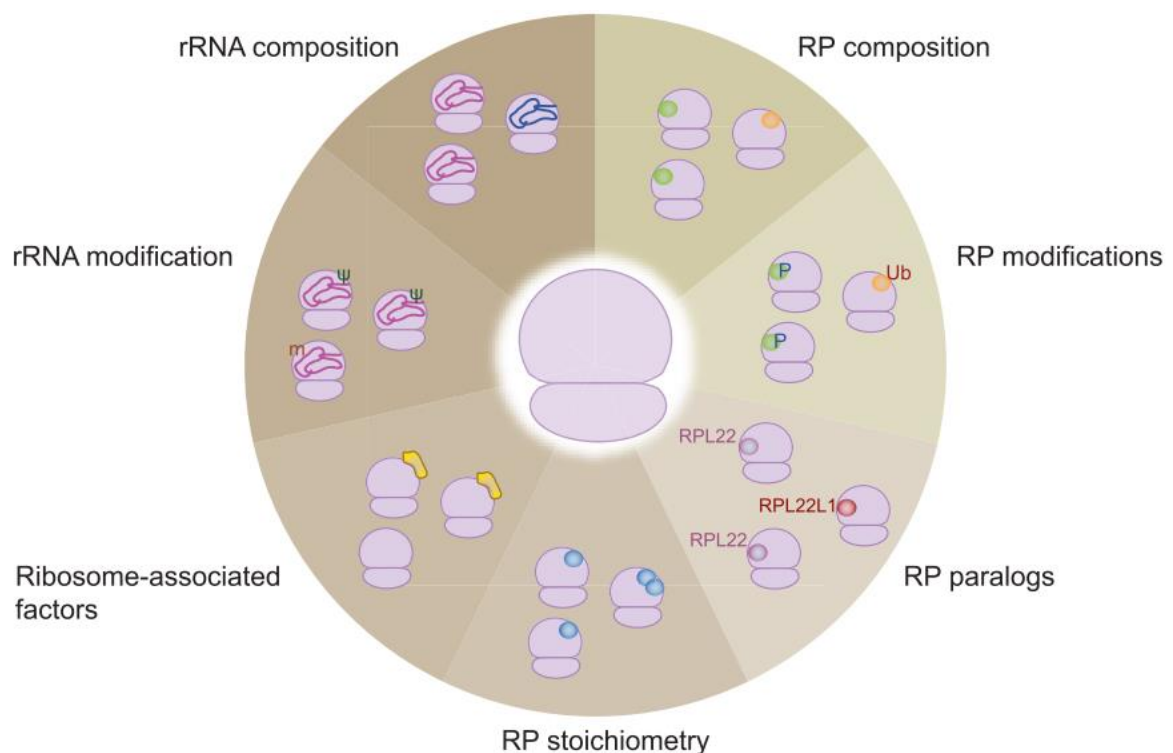


Figure 3: How ribosomes can be heterogeneous. Both, rRNA as well as RPs can be heavily modified (Guo 2018).

Functional ribosome heterogeneity can be defined as variations in ribosome composition, which affect its activity and thereby change the output of synthesized proteins. In principle, heterogeneous ribosomes can arise through different rRNA types, rRNA modifications, composition of RPs, paralogs of RPs, the stoichiometry of RPs, modifications of RPs and other ribosome-associated factors (Guo 2018; Xue and Barna 2012; Genuth and Barna 2018). Differences in the composition can then result in an altered preference for certain mRNAs, mRNA motifs, as well as changes in the ribosomal fidelity leading to erroneous and aberrant proteins due to alternative start- or stop-codon usage. Gene expression is regulated in a multiplex fashion, such as transcription, translation, splicing, mRNA stability, protein stability, but yet it is not known how and to what extent regulation by ribosome customization plays a role in that picture. Recently, heterogeneous ribosomes have been found to exist in tissues with the preference for translating specific subsets of mRNAs. There are many cases where protein abundance does not correlate with mRNA abundance and *vice versa*. Thus, it seems that the rate of translation (by any means) can offer another layer of gene expression regulation (Schwanhäusser et al. 2011). While transcriptional regulation happens within minutes (Gasch et al. 2000), it still needs high engagement of the transcriptional factors, mRNA export and translation. On the contrary, a post-translational change in RPs or the addition/removal of a RP from the ribosome solely requires a single step. This single-step-adaption can theoretically occur extremely fast (Ferretti and Karbstein 2019). The temporal control of gene expression is crucial because organisms, unicellular as well as multicellular, need to promptly respond to environmental fluctuations like osmolarity, nutrient availability, temperature, etc. Furthermore, fabrication of specialized ribosomes might not be that costly, since rapidly growing cells constantly produce new ribosomes anyway. In addition, some RPs can be replaced during the lifetime of a ribosome (Lilleorg et al. 2019; Mathis et al. 2017). Indeed, traditional transcriptional induction only allows genes to be up-regulated, while the idea of specialized ribosomes could facilitate such regulation by allowing for a concurrent up- and down-regulation of some mRNAs. Locati et al. recently showed that mammals undergo turnover of their set of ribosomes after the first initial developmental stages, probably reflecting the possibility that these “old” ribosomes are potentially damaged as they were deposited into oocytes prior to the animal’s birth (Locati et al. 2017). As cells experience a turnover and generally a large change in ribosome numbers, the theory of specialized ribosomes could be a great explanation of how an organism shifts the ribosome population

through specialization towards what is needed (Ramagopal and Ennis 1984; Jacobs et al. 1985). Many hints supporting the hypothesis of specialized ribosomes were gathered during the last 40 years. The slime mold *Dictyostelium discoideum* was shown to completely exchange its ribosomes including different RPs and modifications of them when transitioning between certain stages of its life cycle (Ramagopal 1990). Heterozygous mutations of RPs in minute mutants of *D. melanogaster* lead to the manifestation of abnormally thin and short bristles, a prolonged development and impaired fertility and viability (Marygold et al. 2007).

Although the plethora of examples provide compelling evidence for ribosome heterogeneity, proving that these differences in ribosome composition have functional consequences remains challenging because most manipulations also affect the ribosome number (Segev and Gerst 2018; Steffen et al. 2012; Palumbo et al. 2017; Cheng et al. 2019; Ferretti and Karbstein 2019). The “ribosome concentration hypothesis” considers reduced ribosome numbers in many experimental setups used to study functional relationships of specialized ribosomes (Mills and Green 2017; Ferretti et al. 2017). Also, as initiation is the limiting step in translation, considering that subunits assemble first with mRNAs, initiation rates should be proportional to the ribosome concentration (Lackner et al. 2007; Shah et al. 2013a). Experimental obstacles can be the handling of biochemicals used to study functional ribosomes because some chemicals (e.g. salts, detergents and others), heat, pH and pressure can affect ribosomal

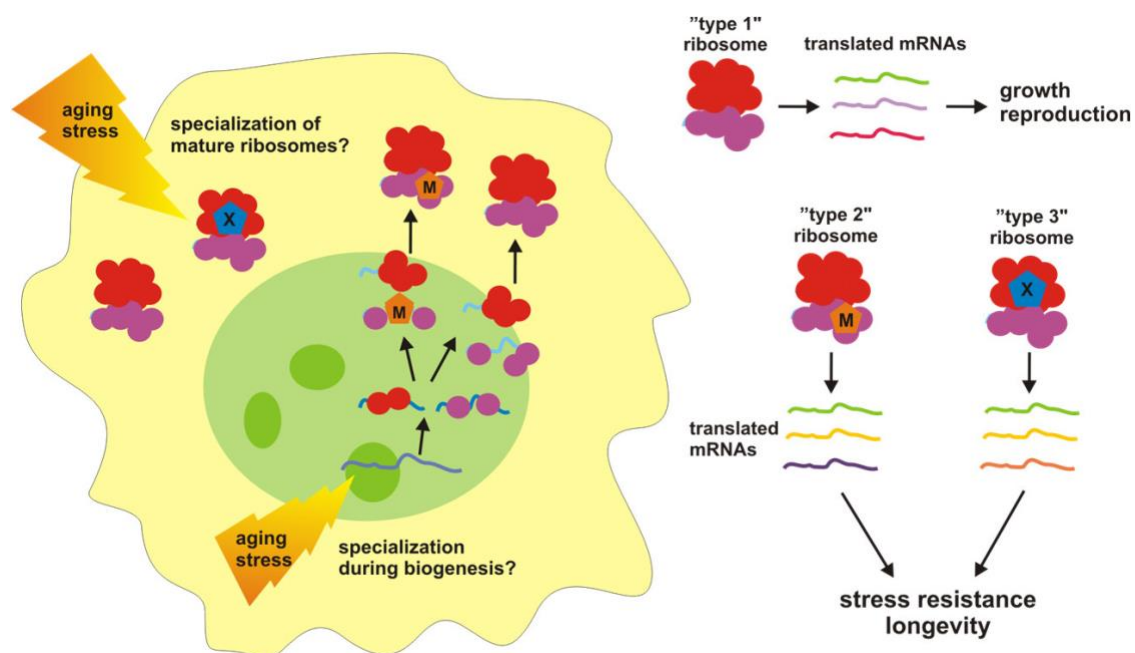


Figure 4: Scheme of specialized ribosomes affecting gene-expression. The illustration was created by Dr. Markus Schosserer. Dr. Schosserer gave me the permission.

stability. Moreover, as ribosome degradation starts on mRNAs (Cole et al. 2009), it remains challenging to entirely rule out that ribosomes lacking some modifications or proteins are not degradation intermediates. Special caution has to be warranted when evaluating experiments of specialized ribosomes, as already cellular perturbations (knock-outs or knock-ins of RPs or base modifications) can generate stable ribosome degradation products or non-functional intermediates that might be wrongly mistaken for specialized ribosomes (Ferretti and Karbstein 2019). Figure 4 explains how specialized ribosomes could work and act “specialized” in terms of specific gene expression as an answer to environmental changes leading finally to increased stress resistance or improved health- and lifespan.

1.4.3 Ribosomopathies

Ribosomopathies are a group of human congenital disorders linked to defects of ribosomal components, in particular RPs and ribosome biogenesis factors. Some of these disorders are characterized by a hypo-proliferative phenotype such as anaemia, congenital anomalies, increased risk for cancer or bone marrow failure (De Keersmaecker et al. 2015; Ruggero and Shimamura 2014). One prominent example is Diamond-Blackfan anaemia (DBA), which is linked to mutations in 11 different RP encoding genes (Narla and Ebert 2010). Other examples are X-linked dyskeratosis congenita, Treacher Collins -and Schwachman-Diamond syndrome. The question, why defective ribosomes lead to tissue-specific abnormalities, as ribosomes are essential organelles and crucial for cellular survival, needs to be answered. Anyway, this discrepancy has two consequences. First, cells may not produce enough properly functional ribosomes to satisfy the metabolic demands. This possibly can account for hypo-proliferation, in particular in high proliferative cells like hematopoietic cells. Second, insufficient quantities of one or more RPs, base modifications or specific post-translational modifications (PTMs) can result in too few functional ribosomes, which ultimately leads to molecular stress. Emerging research indicates that these defective ribosomes show specific deficiencies in translational fidelity.

In conclusion, scientist have to thoroughly keep track of the experimental setup and the resulting data in respective studies, to further convince this and other fields of the existence

of specialized ribosomes, posing a fast and reliable cellular command to adjust gene expression implying direct physiological consequences.

1.4.4 Composition of RPs

Although the catalytic mode of action of ribosomes is carried out by rRNA, most RPs are crucial for their proper function. So far, RPs were thought as being present in equimolar ratios, assembled within ribosomes. RPs exhibit manifold functions: structural integrity, fidelity, binding of initiation-, elongation- and release factors and some directly can bind to mRNA. (Hinnebusch 2017; Haimov et al. 2017; Korostelev 2011). Several recent studies found changes in the RP stoichiometry in different experimental setups. One example, exposing yeast to high osmolarity or high pH causes ribosomes to become Rps26 deficient and subsequently renders yeast cells more tolerant to those stressors (Ferretti et al. 2017; Shi et al. 2017; Loveland et al. 2016). Deficiency of RPs in mammalian cells is related to the induction of autophagy (Artero-Castro et al. 2015). In mouse embryonic stem cells (ESCs), the RP content varied in isolated ribosomes and was associated with the rate of growth and the number of ribosomes bound to a single mRNA (Slavov et al. 2015). However, there is enough evidence demonstrating that ribosomes, in some circumstances, lack the full set of RPs. Nonetheless, scepticism regarding ribosome heterogeneity arising from a varying set of RPs is plausible. In fact, in human cells, turnover of RPs located in the nucleolus is rather fast (6 h) compared to RPs in the cytoplasm (> 30 h). Also, proteins with the fastest turnover were shown to be predominantly RPs in the nucleolus. This finding propose the idea that a subset of proteins, RPs, are putatively more specialized in function and occur within the nucleolus as opposed to throughout the cell (Lam et al. 2007; Boisvert et al. 2012). Thus, it appears vague that an exchange of ribosome-assembled RPs and cytoplasmic RPs can occur in an adequate amount of time (Ballesta and Remacha 1996). How cells control RP stoichiometry and what triggers the initial impulse to add or remove specific RPs respectively need further investigations.

1.4.5 Modifications of RPs

Another very straightforward option leading to customized ribosomes are PTMs of RPs (Genuth and Barna 2018). Such adaptations can be conducted rapidly and do not require the construction of new ribosomes. Although there are many known PTMs on RPs, in most cases it remains unclear whether they participate in specific gene regulation or not (Ferretti and Karbstein 2019). Generally, PTMs of RPs have been discovered in plants (Carroll et al. 2008), yeast (Lee et al. 2002) and human cells (Yu et al. 2009; Zeidan et al. 2010; Odintsova et al. 2003). One example of a PTM affecting ribosomal function is the hydroxylation of the conserved Rps23/uS12. This RP is important for faithful translation and for avoiding translation of premature stop-codons. Mutations of the hydroxylated proline of Rps23/uS12 are linked to defects in ribosome biogenesis and polysome formation in yeast (Loenarz et al. 2014; Singleton et al. 2014). Likewise, loss of the methylation site of Rpl3/uL3 decreases translational fidelity (Al-Hadid et al. 2016). Up to now, it is not known if cells govern PTM of the abovementioned RPs to exert translational control in certain growth conditions.

1.4.6 Paralogs of RPs

Million years ago, a genome duplication event in *Saccharomyces cerevisiae* occurred. Thus, 59 out of 78 RP genes were duplicated into A and B isoforms with highly similar, if not identical, coding sequences (Kellis et al. 2004; Gasch et al. 2000). Despite the fact that paralogs have an almost identical amino acid sequence, recent studies suggest that paralogs can convey specific functions of ribosomes (Samir et al. 2018; Komili et al. 2007; Segev and Gerst 2018). A prominent example is Rps26 with its paralogs *Rps26A* and *Rps26B*. Whereas deletion of the minor paralog *Rps26B* has minimal effects, deletion of *Rps26A* results in slow growth and other phenotypes. Intriguingly, this effect can be rescued by supplementing either Rps26A or B in Δ Rps26A cells, manifesting that the phenotypes arise from insufficient levels of Rps26 and not of one of the specific isoforms (Strittmatter et al. 2006).

The majority of mammalian RPs do not have any paralogous genes. A special case is RPS4 which is encoded by three genes on the X and Y chromosome (Fisher et al. 1990). All three paralogs are highly expressed but only RPS4Y2 is specifically expressed in the prostate and

testis, suggesting the existence of sex-specific ribosomes (Lopes et al. 2010; Sugihara et al. 2010). Some differences of paralog levels might arise at the level of transcription and are regulated during cellular growth, stress or other extrinsic triggers. For instance, both paralogs of Rpl13 are equally expressed during vegetative growth, but when cells enter quiescence, Rpl13A is reduced eightfold (Parenteau et al. 2011; Petibon et al. 2016).

1.4.7 Types of rRNA

As mentioned in the previous chapters, ribosomes are composed of four different rRNAs residing within two subunits. Intriguingly, the mystery of nature features fascinating examples of how ribosome heterogeneity can be accomplished. In most organisms rDNA is encoded in multiple (ranges from 1 to hundreds) of repetitive operons throughout their genome. The majority of bacteria and archaea possess between 1 and 15 rDNA operons, which are sometimes not identical (Sun et al. 2013). Likewise, *in E. coli* are seven rDNA operons with highly similar, but not identical, sequences (Hillebrand et al. 2005). The promoters of these rDNA operons are differentially responsive to different stimuli. Thus, the production and accumulation of distinct pools of ribosomal species is enhanced under various environmental conditions (Kurylo et al. 2018). In this study from Kurylo and colleagues, they demonstrated that under nutrient limitations, *E. coli* switches the rDNA templates and thereby changing its 16S rRNA composition. The resulting ribosomes render bacteria resistant to tetracycline, indicating functional differences for these ribosomes.

The best known case of rRNA heterogeneity is the malaria parasite *Plasmodium*, it expresses three distinct types of rRNA at different stages of life (Gunderson et al. 1987; Laplante and Sabatini 2012). The biological function of the rRNA subtypes are still not well resolved (van Spaendonk et al. 2001; Velichutina et al. 1998; Qi et al. 2015). Another interesting example was shown in a zebrafish study, where two distinct ribosomal subtypes, maternal and somatic, of 5.8S, 18S and 28S rRNA were found in *Danio rerio* (Locati et al. 2017). Heterogeneity of different types of rRNA is also present in higher eukaryotes. In mice and humans, many rDNA operons throughout the genome are variable and transcription from individual loci can diverge across tissues and over time of a cell's lifecycle (Parks et al. 2018).

As ribosome synthesis is happening within minutes, using different transcripts of rRNA is only marginally helpful for an immediate response to acute stress conditions. Instead, this option of ribosome specialization is, most likely, more useful for an ameliorated adaption and tolerance to new environments.

1.4.8 rRNA modifications

Per definition, the term “epitranscriptomics” encloses all alterations to the transcriptome without a change in the sequence of the ribonucleotides (Saletore et al. 2012). Similar to that, “epigenetics” include changes to the genome without affecting the nucleotide sequence. rRNA modifications are most commonly pseudouridines and 2'-O methylations of the ribose sugar whereas only a few base modifications are characterized. Up to now, around 104 pseudouridines and 112 2'-O modifications (Taoka et al. 2018) decorating human rRNAs are known. In total, 2-3% of the approximately 7000 nucleotides distributed over the four rRNAs are modified (Penzo et al. 2016; Sharma and Lafontaine 2015). Catalysis of those modifications is accomplished either by specific snoRNA-guided or snoRNA-independent stand-alone enzymes (Penzo et al. 2016; Sloan et al. 2017). RNA modifications expand the natural repertoire of the four nucleotides and thus contribute to ribosome heterogeneity, possibly altering the ribosome's structure, stability and function (Schosserer et al. 2015; Heissenberger et al. 2019). It seems that most modified residues are highly conserved from yeast to humans and are located in or close to the decoding site (DCS), PTC or subunit interface (Penzo et al. 2015; Natchiar et al. 2017; Sharma and Lafontaine 2015; Sloan et al. 2017).

As illustrated in figure 5, simple prokaryotes and eukaryotes share the majority of nucleotide modifications in the inner core of the ribosome. Eukaryotes have evolutionarily evolved an additional shell of modifications around the ribosome's centre (Natchiar et al. 2017). The expanded eukaryotic repertoire propose the hypothesis that these organisms developed a mechanism for fine-tuning translation at the level of rRNA modifications. The fact that rRNA modifications exist in all three kingdoms of life suggests a biological function rather than an accidental evolutionary trait (Machnicka et al. 2012; Cantara et al. 2011).

While individual removal of most rRNA modifications typically has minor consequences on growth and survival, the loss of some indeed shows detrimental phenotypes. It seems to be a yet unclear layer to regulate gene expression, but emerging evidence renders the idea that cells can (specifically?) fine-tune the function of ribosomes (Guo 2018; Ferretti and Karbstein 2019; Heissenberger et al. 2019).

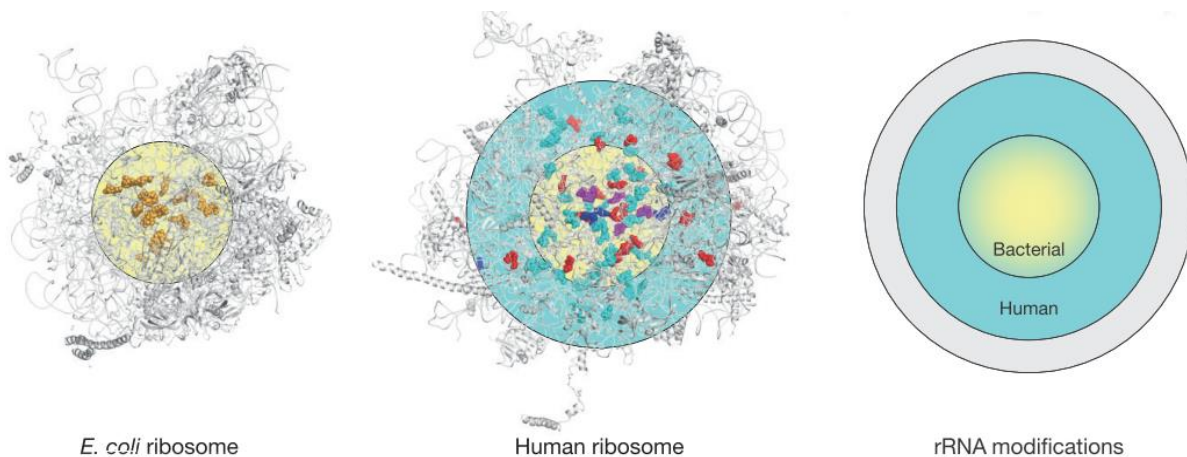


Figure 5: Evolution shows how ribosome modifications have evolved from *E. coli* to humans (Natchiar 2017).

1.4.8.1 2'-O methylations

Recently, quantitative mass spectrometry of human cells listed 112 2'-O methylations decorating rRNA. The majority of these modifications are introduced co-transcriptionally in the nucleolus, concomitantly with ribosomal assembly and pre-rRNA processing (Lafontaine 2015). The synthesis of 2'-O methylations involves a family of antisense box C/D snoRNAs (also known as SNORDs). Catalysis is executed by fibrillarin, a conserved rRNA methyltransferase. Almost all snoRNAs form transient 9 – 20 bp long double stranded RNAs with pre-rRNA where the nucleotide substrate for methyl group catalysis occupies a specific position. This fixed position seems to be always the fifth nucleotide upstream a conserved sequence motif found in all snoRNAs, the D or D' box (Cavaillé et al. 1996; Hebras et al. 2020). Additionally, it was shown that there are snoRNAs lacking any obvious rRNA-pairing potential (Dupuis-Sandoval et al. 2015). 2'-O methylations favour an A-form RNA helix and enhance base stacking which increases the RNA rigidity (Prusiner et al. 1974). The study of 2'-O ribose methylations has recently been boosted, due to now available modern methods like RP-HPLC

(Yang et al. 2016), sequence-based methods like RiboMeth-seq (Krogh et al. 2016; Birkedal et al. 2014; Yang et al. 2020) and quantitative mass spectrometry (qMS) (Taoka et al. 2018). Previous reports showed that the vast majority of known 2'-O methylated sites were found to be fully methylated. Otherwise, some sites, especially in human cancer cells, were found to be fractionally modified ranging from ~56 to 90%, paving the ground for potential therapeutics in the future (Taoka et al. 2018; Krogh et al. 2016).

The importance of 2'-O methylations for organismal health was recently shown, as genetic ablation of the fibrillarin gene resulted in complete lethality in very early development in mice (Newton et al. 2003) and impairment of zebrafish development (Bouffard et al. 2018; Higa-Nakamine et al. 2012). Another study in yeast demonstrated that loss of 2'-O methylated pre-rRNA leads to growth impairment at non-permissive temperature (Hebras et al. 2020). The molecular mode of action is likely achieved by altering chemical and structural properties of modified nucleotides, which affects rRNA folding, conformation and reactivity with ribosome associated factors. As mentioned above, many of those modifications are located in conserved and functional rRNA regions, DCS, the PTC and the inter-subunit domain (Sharma and Lafontaine 2015; Sloan et al. 2017; Krogh et al. 2016; Heissenberger et al. 2019). However, the precise regulatory mechanism of each individual modification, in particular in context of different circumstances concerning nutrient, growth, differentiation and development, remains to be untangled.

1.4.8.2 Pseudouridylations

The second most abundant and widespread nucleoside modification is the isomerization of uridine (U) to pseudouridine (Ψ), known as rRNA pseudouridylation. Taoka and colleagues recently found 104 Ψ sites decorating rRNA in human cells (Taoka et al. 2018). Ψ -formation is catalysed by an evolutionarily conserved protein family of pseudouridine synthases (PUSs). PUSs can act via two distinct modes of action, on the one hand as stand-alone enzymes or on the other hand through an RNA-dependent mechanism involving antisense box H/ACA snoRNAs (Hamma and Ferré-D'Amaré 2006). Moreover, Ψ residues also tend to cluster in the centre of ribosomes near functionally important regions like the PTC and DCS (Decatur and Fournier 2002). Recent advances in high-throughput Ψ -sequencing shed new light on the role

of RNA pseudouridylation in cells, similarly to 2'-O methylations of the ribose, adding a further layer to regulate gene expression via ribosome heterogeneity (Karijolich et al. 2015). A steady improvement of techniques investigating pseudouridines on RNA led to the discovery of novel Ψ sites within different types of RNA that were previously not known to be modified, including mainly mRNAs from yeast to mammals (Carlile et al. 2014; Li et al. 2015; Schwartz et al. 2014). Ψ are well conserved in prokaryotes and eukaryotes and the number of Ψ increases drastically from bacteria to eukaryotes, implying a possible fine-tuning mechanism towards adapted gene expression via specialized ribosomes (Ofengand 2002). Surprisingly, the majority of the identified Ψ sites are dynamically inducible within cells and are predominantly catalysed by stand-alone PUSs (Schwartz et al. 2014; Rintala-Dempsey and Kothe 2017).

Emerging evidence has been built up, indicating that mutations in genes encoding PUSs provide important links to certain impairments resulting in pathologies and severe syndromes as well as cancer in humans (Rintala-Dempsey and Kothe 2017). The altered biochemical properties of Ψ compared to uridine can affect RNA biogenesis, structure, function and therefore poses the ability to fine-tune gene expression via modifying rRNAs and tRNAs (Guzzi et al. 2018). Ψ favours an A-form RNA helix, which provides additional hydrogen bonding capacity and enhances thermal stability. However, mutations of dyskerin (*DKC1* gene) in mammals have been linked to a prominent ribosomopathy, namely X-linked Dyskeratosis Congenita (X-DC). Patients suffering from X-DC show signs of bone marrow failure, skin abnormalities and enhanced cancer susceptibility (Dokal 2000; Alter et al. 2009). Lack of Ψ seems to render ribosomes “non-functional” (e.g. translate less and/or unfavourable genes, translate mRNAs harbouring internal ribosomal entry sites (IRES) elements and exhibit decreased fidelity) leading to severe outcomes. Two mutations affecting the catalytic domain *DKC1* are associated with a severe variant of X-DC known as Hoyeraal-Hreidarsson (HH) syndrome. In brief, the HH syndrome is a severe multisystem disorder affecting mainly young males. This malady is characterized by cerebellar hypoplasia, microcephaly, immunodeficiency and aplastic anaemia (Dokal 2000). The molecular mechanisms by which ribosomes lacking Ψ modifications are impaired regarding translational function and control need to be answered in future studies.

1.4.8.3 Base methylations

Apart from more abundant 2'-O methylations and pseudouridines, only eight different types of base modifications are present on rRNA. According to current estimations, on the human 80S rRNA, eight different base modifications can be found. 7 modifications on the human 18S rRNA: two acetylated cytosine (ac^4C), two *N,N*-dimethyladenosine (m^6_2A), one *N*⁶-methyladenosine (m^6A), one *N*-methylguanosine (m^7G) and one *N*-methyl-*N*-aminocarboxypropylpseudouridine ($\text{m}^1\text{acp}^3\psi$). 5 modifications on the 28S rRNA: one *N*¹-methyladenosine (m^1A), two C⁵-methylcytosine (m^5C), one *N*³-methyluridine (m^3U) and also one m^6A (Taoka et al. 2018).

Methylation of the fifth carbon of cytosine (m^5C) has been found in various types of RNA (tRNA, mRNA and rRNA). Hence, it seems obvious that they might possess a particularly beneficial role in terms of structure, mRNA binding and chemical stability (Sharma and Lafontaine 2015).

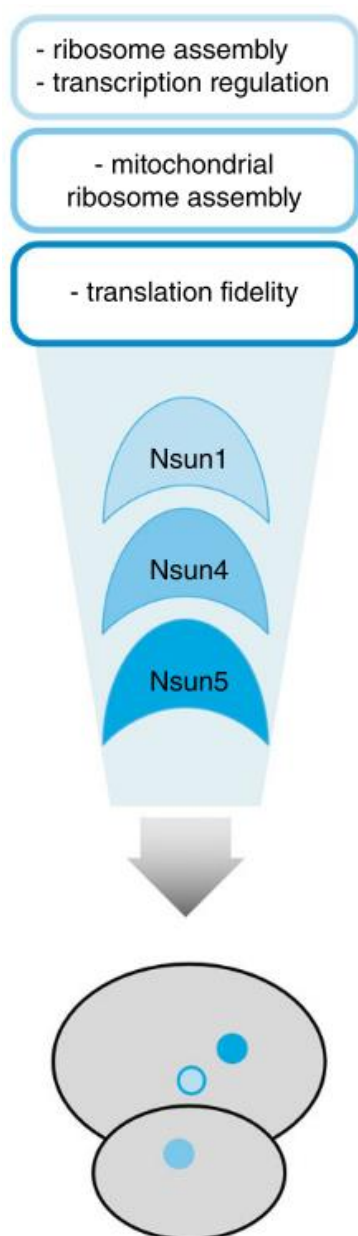


Figure 6: Overview of the three members of NSUN protein family modifying rRNA, whereas NSUN4 is methylating mitochondrial rRNA (Lusser 2019).

Interestingly, no m^5C sites have been uncovered on the eukaryotic 18S rRNA (Edelheit et al. 2013; Janin et al. 2019). The two methylated cytosines that are known on human/yeast 28S/25S rRNA, are mediated independently by NSUN1 and NSUN5 respectively (enzymes described in more detail in the following section) (Bourgeois et al. 2015; Motorin et al. 2010; Heissenberger et al. 2019; Schosserer et al. 2015). All currently identified m^5C methyltransferases either belong to the NOL1/NOP2/SUN (NSUN) family or to DNA methyltransferase 2 (DNMT2) (Bujnicki 2004; Motorin et al. 2010). The biochemical property of m^5C is to expand the lipophilic surface of the base which promotes base stacking and stabilizes the RNA by enhancing thermal stability of bonding with guanine (Motorin et al. 2010). The mammalian NSUN protein family comprises seven genes: NSUN1, NSUN2, NSUN3, NSUN4, NSUN5, NSUN6 and NSUN7 (Trixl and Lusser 2019). Three of those are depicted schematically in figure 6, whereas NSUN4 is shown to be responsible for methylating mitochondrial rRNA.

As most rRNA modifications, the vast majority of modified residues is highly conserved from yeast to humans and occur, in close orientation to the DCS, PTC or the inter subunit space.

Table 2: Position, type, and stoichiometry of modified nucleotides found in human rRNAs. The abbreviations for nucleotides are as follows: Ψ , pseudouridine; Am, 2'-O-methyladenosine; Cm, 2'-O-methylcytidine; Gm, 2'-O-methylguanosine; Um, 2'-O-methyluridine; Ψ m, 2'-O-methylpseudouridine; m¹A, 1-methyladenosine; m⁶₂A, N6, N6-dimethyladenosine; m⁵C, 5-methylcytidine; m⁷G, 7-methylguanosine; m³U, 3-methyluridine; m⁶A, N6-methyladenosine; ac⁴C, N4-acetylcytidine; m¹acp³ Ψ , 1-methyl-3-(3-amino-3-carboxypropyl)pseudouridine. Underline denotes the modified nucleotides newly identified in Taoka et al. 2018, Nucleic Acids Research, doi: 10.1093/nar/gky811 (Taoka et al. 2018).

rRNA	Modified nu- cleotide	Type ^a	Percent modifi- cation	rRNA	Modified nu- cleotide	Type ^a	Percent modifi- cation	rRNA	Modified nu- cleotide	Type ^a	Percent modifi- cation	rRNA	Modified nu- cleotide	Type ^a	Percent modifi- cation
5.8S	14	Um	5	18S	1004	Ψ	97	28S	1768	Ψ	100	28S	3866	Cm	99
5.8S	55	Ψ	60	18S	1031	Am	97	28S	1769	Ψ	100	28S	3878	Gm	98
5.8S	69	Ψ	61	<u>18S</u>	<u>1045</u>	Ψ	<u>92</u>	28S	1779	Ψ	100	28S	3899	Ψ	100
5.8S	75	Gm	87	18S	1046	Ψ	100	28S	1847	Ψ	95	28S	3904	Um	96
				18S	1056	Ψ	93	28S	1849	Ψ	95	28S	3923	Gm	80
18S	27	Am	100	18S	1081	Ψ	94	28S	1858	Am	96	28S	3938	Ψ	93
18S	34	Ψ	100	18S	<u>1136</u>	Ψ	<u>7</u>	28S	1868	Cm	35	28S	4020	Gm	83
18S	36	Ψ	82	18S	1174	Ψ	100	28S	2338	Cm	99	28S	4032	Cm	100
18S	93	Ψ	87	18S	1177	Ψ	100	28S	2350	Am	100	28S	4166	Gm	98
18S	99	Am	99	<u>18S</u>	<u>1232</u>	Ψ	<u>98</u>	28S	2351	Gm	100	28S	4190	m ⁶ A	100
18S	105	Ψ	99	18S	1238	Ψ	97	28S	2352	Cm	90	28S	4197	Um	97
18S	109	Ψ	99	18S	1244	Ψ	100	28S	2388	Am	73	28S	4198	Gm	92
18S	116	Um	98	18S	1248	m ¹ acp ³ Ψ	100	28S	2402	Um	87	28S	4263	Ψ	98
18S	119	Ψ	94	18S	1272	Cm	47	28S	2409	Cm	98	28S	4266	Ψ	90
18S	121	Um	98	18S	1288	Um	98	28S	2411	Gm	90	28S	4269	Ψ	93
18S	159	Am	96	18S	1326	Um	100	28S	2495	Ψ	92	28S	4276	Um	88
18S	166	Am	100	18S	1328	Gm	100	<u>28S</u>	<u>2619</u>	Ψ	<u>90</u>	28S	4282	Ψ	83
18S	172	Um	96	18S	1337	ac ⁴ C	79	28S	2774	Am	84	28S	4323	Ψ	95
18S	174	Cm	92	18S	1347	Ψ	98	28S	2791	Cm	93	28S	4331	Ψ	93
18S	210	Ψ	83	18S	1367	Ψ	98	28S	2802	Am	92	28S	4340	Gm	99
18S	218	Ψ	100	18S	1383	Am	98	28S	2811	Cm	87	28S	4362	Gm	97
18S	296	Ψ	25	18S	1391	Cm	95	28S	2824	Um	99	28S	4373	Ψ	96
18S	354	Um	20	18S	1442	Um	78	28S	2826	Ψ	20	28S	4390	Ψ	99
18S	406	Ψ	87	18S	1445	Ψ	90	28S	2830	Ψ	9	28S	4393	Ψ	97
18S	428	Um	76	18S	1447	Gm	34	28S	2848	Cm	72	28S	4401	Ψ	89
18S	436	Gm	76	18S	1490	Gm	100	28S	2863	Gm	49	28S	4412	Ψ	100
18S	462	Cm	100	18S	1625	Ψ	79	<u>28S</u>	<u>3606</u>	<u>Gm</u>	<u>96</u>	28S	4417	m ⁵ C	100
18S	468	Am	99	18S	1639	m ⁷ G	100	28S	3616	Ψ	89	28S	4426	Cm	98
18S	484	Am	97	18S	1643	Ψ	96	28S	3618	Ψ	95	28S	4427	Ψ	98
18S	509	Gm	98	18S	1668	Um	8	28S	3674	Ψ	99	28S	4441	Ψ	87
18S	512	Am	83	18S	1678	Am	94	28S	3680	Cm	100	<u>28S</u>	<u>4463</u>	Ψ	<u>17</u>
18S	517	Cm	100	18S	1692	Ψ	98	28S	3694	Ψ	100	28S	4464	Gm	91
18S	572	Ψ	97	18S	1703	Cm	92	28S	3697	Am	88	28S	4468	Um	100
18S	576	Am	96	18S	1804	Um	86	28S	3703	Am	100	28S	4469	Gm	100
18S	590	Am	72	18S	1832	m ⁶ A	99	28S	3709	Ψ	72	28S	4470	Ψ	100
18S	601	Gm	89	18S	1842	ac ⁴ C	99	28S	3713	Ψ	98	28S	4491	Ψ	91
18S	609	Ψ	90	18S	1850	m ⁶ ₂ A	94	28S	3723	Gm	83	28S	4493	Am	87
<u>18S</u>	<u>621</u>	<u>Cm</u>	<u>62</u>	18S	1851	m ⁶ ₂ A	94	28S	3737	Ψ	85	28S	4500	m ³ U	120
18S	627	Um	99					28S	3739	Am	90	28S	4502	Ψ	100
18S	644	Gm	98	28S	389	Am	98	28S	3741	Ψ	100	28S	4506	Cm	100
18S	649	Ψ	93	28S	391	Am	98	28S	3743	Ψ	100	28S	4522	Ψ	98
18S	651	Ψ	93	28S	1303	Gm	71	28S	3747	Ψ	100	28S	4541	Am	43
18S	668	Am	99	28S	1309	m ¹ A	100	28S	3749	Ψ	100	28S	4546	Ψ	100
18S	681	Ψ	67	28S	1310	Am	44	28S	3761	m ⁵ C	100	28S	4549	Ψ	100
18S	683	Gm	99	28S	1313	Am	100	28S	3764	Am	96	28S	4560	Am	37
18S	686	Ψ	95	28S	1327	Cm	92	28S	3771	Gm	100	28S	4588	Gm	75
18S	797	Cm	68	28S	1509	Gm	99	28S	3787	Cm	80	28S	4590	Um	82
18S	799	Um	98	28S	1511	Am	99	28S	3797	Ψ m	100	28S	4593	Gm	100
18S	801	Ψ	100	28S	1521	Am	109	28S	3801	Ψ	50	28S	4598	Ψ	92
18S	814	Ψ	100	28S	1523	Ψ	88	28S	3804	Am	92	28S	4606	Ψ	42
18S	815	Ψ	100	28S	1569	Ψ	68	28S	3809	Am	100	28S	4607	Gm	100
18S	822	Ψ	99	28S	1612	Gm	100	28S	3820	Cm	100	28S	4643	Ψ	39
18S	863	Ψ	95	28S	1664	Ψ	97	28S	3823	Ψ	66	28S	4659	Ψ	87
18S	866	Ψ	88	28S	1670	Ψ	96	28S	3830	Ψ	92	28S	4937	Ψ	81
18S	867	Gm	28	28S	1731	Ψ	100	28S	3832	Ψ	100	28S	4966	Ψ	86
<u>18S</u>	<u>897</u>	<u>Ψ</u>	<u>23</u>	<u>28S</u>	<u>1747</u>	<u>Gm</u>	<u>89</u>	<u>28S</u>	<u>3846</u>	<u>Am</u>	<u>43</u>	<u>28S</u>	<u>4975</u>	<u>Ψ</u>	<u>72</u>
18S	918	Ψ	42	<u>28S</u>	<u>1760</u>	<u>Um</u>	<u>70</u>	28S	3848	Cm	67				
18S	966	Ψ	89	28S	1766	Ψ	40	28S	3863	Ψ	33				

1.4.8.3.1 NSUN5

NSUN5 is a conserved rRNA methyltransferase belonging to the NOL1/NOP2/SUN domain family. The Sun-domain containing protein NSUN5 is highly conserved from yeast to humans. The S-adenosyl methionine-binding pocket (SAM) serves as active site that also accommodates two conserved cysteines which are essential for adequate protein function, namely C308 and C359 (King et al. 1999; Heissenberger et al. 2019). Until now, the only known substrate of the yeast homolog of NSUN5, Rcm1, is C2278 on 25S rRNA (Schosserer et al. 2015; Gigova et al. 2014; Sharma et al. 2013), while C2381 on 26S rRNA is methylated by NSUN-5, the worms' homolog (Schosserer et al. 2015) and C3782 on 28S rRNA is methylated by the human NSUN5 (Heissenberger et al. 2019; Janin et al. 2019). Additionally, we recently reported that lack of a single, conserved m⁵C on 25S rRNA alters ribosome function leading to a “reprogramming” of the ribosome towards translation of mRNAs involved in cellular stress-responses (Schosserer et al. 2015). Furthermore, deletion of NSUN5 extended the lifespan and stress resistance in yeast, worms and flies (Schosserer et al. 2015).

The locus of human NSUN5 is located on chromosome 7. A rare, developmental disorder, called Williams-Beuren syndrome (WBS) is caused by a large heterozygous deletion at chromosome 7q11.23, including NSUN5 amongst around 25 other genes. Signs of WBS include mental retardation, heart problems and physical impairments (Doll and Grzeschik 2001; Schubert 2009). In Nsun5 knockout mice, cognitive deficits as well as abnormalities in the development of certain brain regions were observed, potentially pointing towards the role of Nsun5 in the manifestation of WBS (Zhang et al. 2018; Yuan et al. 2019; Chen et al. 2019).

Apart from WBS, NSUN5 is also associated with other diseases like cancer. A recent study showed that decreased levels of NSUN5 by epigenetic silencing promote long-term survival of glioma patients and render those brain cancers more sensitive to bioactive compounds generating oxidative stress (Janin et al. 2019).

With our study we could show that loss of a single modification on rRNA can significantly alter cellular growth, cell size and proliferation, as well as reduce bulk protein synthesis. We characterized human NSUN5 and its target cytosine, the catalytical function, and cellular localization for the first time (Heissenberger et al. 2019).

This newly generated knowledge might contribute to the development of strategies for improving health of WBS and e.g. glioma patients as well as aged subjects in general.

1.4.8.3.2 NSUN1

NSUN1 (also known as NOP2 or P120) is a rRNA methyltransferase adding a m⁵C methylation on the large subunit as well. The localization of NSUN1 is predominantly in the nucleolus but it is also present in the cytoplasm in early mouse embryogenesis. Human NSUN1 was shown to be responsible for methylating m⁵C4447 on 28S rRNA (Schaefer et al. 2008; Squires et al. 2012; Bourgeois et al. 2015), yeast Nop2 on the other hand for m⁵C2870 on 25S rRNA (Sharma et al. 2013). Already few years ago, Nop2 was shown to be essential for ribosome biogenesis of the large subunit in yeast (Sharma et al. 2013). Further relevance of this protein was evidenced by some recent reports showing that NSUN1 is involved in the development of mammalian preimplantations (Cui et al. 2016). Cui and colleagues found that NSUN1 has an indispensable role during blastocyst development. Other reports state that low levels of NSUN1 reduce cell growth of leukaemia cells, which is in agreement with findings that NSUN1 promotes cell proliferation. When applying RNAi targeting NSUN1, mouse embryos die at the morula stage. In those embryos, a global reduction of rRNAs and mRNAs was observed (Hong et al. 1997; Cui et al. 2016). Furthermore, high NSUN1 expression levels result in increased tumor aggressiveness and increased 5-azacytidine (5-AZA) resistance in two different leukemia cell lines (Bantis et al. 2004; Saijo et al. 2001; Cheng et al. 2018). Human NSUN1 was shown to be overexpressed in some human cancers, thus it was suggested to use NSUN1 as a prognostic biomarker for lung adenocarcinomas (Sato et al. 1999). Beside cancer, NSUN1 is also associated with the 'Cri du chat' syndrome caused by a deletion on chromosome five (Wu et al. 2005). Considering these reports and our work, NSUN1 might be considered as an example of 'antagonistic pleiotropy', being indispensable early in life, but having negative effects on health later.

Table 3: Summary table of the target m⁵C substrate as well as synonyms found in literature of NSUN5 and NSUN1 from humans to yeast.

rRNA methyltransferase	<i>Homo sapiens</i>	<i>Mus musculus</i>	<i>Drosophila melanogaster</i>	<i>Caenorhabditis elegans</i>	<i>Saccharomyces cerevisiae</i>
Name/Synonym	NSUN5	Nsun5	dNsun5	NSUN-5	Rcm1
NSUN5	3782 ¹	3438 ²	3620 ³	3381 ⁴	2278 ⁵
Name/Synonym	NSUN1, NOL1, NOP2, P120	Nsun1	unknown	NSUN-1	Nop2
NSUN1	4447 ⁶	unknown	unknown	2982 ⁷	2870 ⁸

1.4.8.3.3 RRP8/NML

Nucleomethylin (NML)/ribosomal RNA-processing protein 8 (RRP8) is a nucleolar protein implicated in the assembly of the energy-dependent nucleolar silencing complex (eNoSC). NML is a rRNA methyltransferase harbouring the capacity to modify rRNA at m¹A residues. Yeast Rrp8p was shown to be responsible for m¹A645 base methylation on 25S rRNA (Sharma et al. 2018). Likewise, *C. elegans* RRP-8 methylates m¹A674 on 26S rRNA (Yokoyama et al. 2018). Human NML has a Rossmann-fold methyltransferase-like domain and binds to SAM (Murayama et al. 2008). Moreover, NML is responsible for the methylation at position m¹A1322 on 28S rRNA (Sharma et al. 2018).

m¹A methylations add a positive charge to the nucleotide residue to increase the basicity of adenosine, disturbing Watson-Crick pairing and strongly altering RNA topology (Wu et al. 2005). In brief, under low nutrient conditions the eNoSC complex suppresses rDNA transcription to save energy and improve cellular survival (Wu et al. 2005). The binding of NML to rRNA is inhibited, thus enhanced binding of sirtuin1 (SIRT1) to NML occurs (Murayama et al. 2008). These results suggest that NML can direct and regulate gene expression in a way

¹ Heissenberger et al. 2019, Janin et al. 2019

² Heissenberger et al. 2019

³ Schosserer et al. 2015

⁴ Schosserer et al. 2015

⁵ Sharma et al. 2013, Schosserer et al. 2015, Gigova et al. 2014

⁶ Schaefer et al. 2008, Squires et al. 2012, Bourgeois et al. 2015

⁷ Heissenberger et al. 2020, Navarro et al. 2020

⁸ Sharma et al. 2013, Sloan et al. 2017

that under glucose deprivation, NML represses rDNA transcription and under normal nutrient availability, NML adds a specific methylation mark on the large subunit to render ribosomes fully functionable. NML^{-/-} mice usually die at embryonal stage (E10.5 and 12.5), whereas most embryos exhibit impaired erythropoiesis and decreased growth (Murakami et al. 2018).

2 Aims of the thesis

Ribosomes are not static, monolithic machines, but dynamically respond to environmental factors. This potentially specific response can be explained by the fast exchange of compartments of the ribosome. Heterogeneity of ribosomes means that they can vary in the composition of their proteins, rRNA, or the post-transcriptional and post-translational modifications to both kind of components. Compelling evidence suggests that this diversity can influence the ribosome's function. Up to now, the biological role of the two rRNA methyltransferases, namely NSUN1 and NSUN5 is not clear.

Project 1: This project is aiming to characterize NSUN5 in human cells for the first time. At this point, not much was known about the cellular localization and the RNA substrate. Hence, we hypothesized that NSUN5 is required for rRNA methylation.

Project 2: The second project is aiming to provide a characterization of NSUN-1 in *C. elegans* for the first time. Indeed, in nematodes, the biological function of NSUN-5 is well characterized by our research group and others. Therefore, a logic step forward is to decipher the molecular and biological function for NSUN-1 as well.

Since neither human NSUN5 nor *C. elegans* NSUN-1 were described in literature so far, the aim of the thesis is their functional characterization; especially in the context of cellular and organismal aging.

3 Results

3.1 Loss of the ribosomal RNA methyltransferase NSUN5 impairs global protein synthesis and normal growth⁹

Modifications of ribosomal RNA expand the nucleotide repertoire and thereby contribute to ribosome heterogeneity and translational regulation of gene expression. One particular m⁵C modification of 25S ribosomal RNA, which is introduced by Rcm1p, was previously shown to modulate stress responses and lifespan in yeast and other small organisms. Here, we report that NSUN5 is the functional orthologue of Rcm1p, introducing m⁵C3782 into human and m⁵C3438 into mouse 28S ribosomal RNA. Haploinsufficiency of the NSUN5 gene in fibroblasts from William Beuren syndrome patients causes partial loss of this modification. The N-terminal domain of NSUN5 is required for targeting to nucleoli, while two evolutionary highly conserved cysteines mediate catalysis. Phenotypic consequences of NSUN5 deficiency in mammalian cells include decreased proliferation and size, which can be attributed to a reduction in total protein synthesis by altered ribosomes. Strikingly, Nsun5 knockout in mice causes decreased body weight and lean mass without alterations in food intake, as well as a trend towards reduced protein synthesis in several tissues. Together, our findings emphasize the importance of single RNA modifications for ribosome function and normal cellular and organismal physiology.

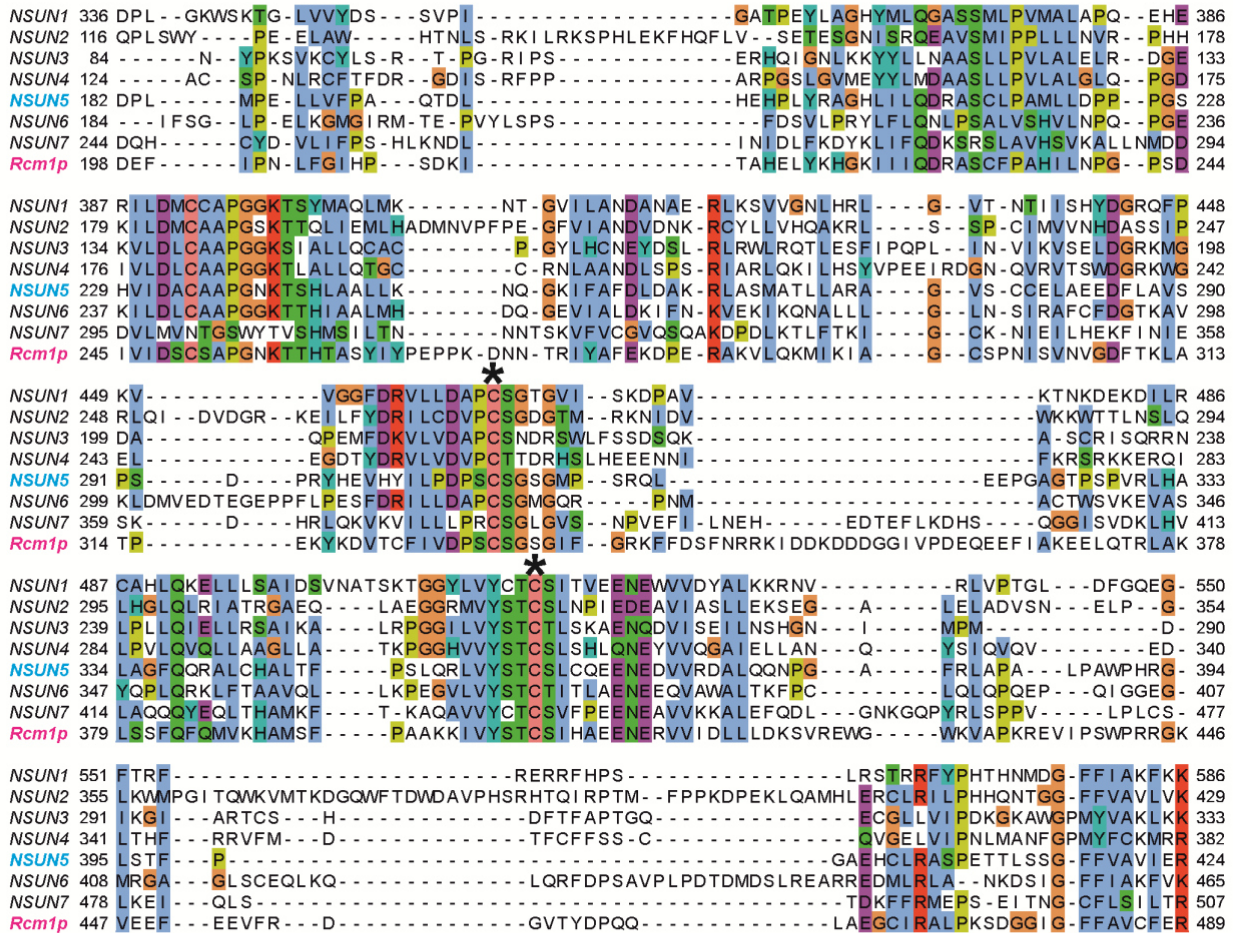
3.1.1 NSUN5 is the human homolog of Rcm1p

We previously found that depletion of Rcm1p/NSUN-5/Nsun5 extends lifespan in the model organisms *Saccharomyces cerevisiae*, *C. elegans* and *Drosophila melanogaster* (Schosserer et al. 2015). To further investigate the underlying molecular functions and their conservation in mammals, we aligned the protein sequence of Rcm1p from *S. cerevisiae* to all seven human NSUN-family members (Figure 7A and Figure 14) to identify a putative mammalian homolog.

⁹ These data were already published (Heissenberger et al. 2019, doi: 10.1093/nar/gkz1043). Personal contributions: Planned experiments: Figure 2, 3, 5, 6, 7, Suppl., Performed experiments: Figure 2, 3, 4, 5, 6, 7, Suppl., Analysed data: Figure 2, 3, 4, 5, 6, 7, Suppl. and wrote the manuscript.

Evolutionary conservation was highest in the catalytic region, which contains the SAM-binding pocket and cysteines at positions C308 and C359, which are considered to be required for covalent binding and release of the RNA substrate in other RNA methyltransferases (Schosserer et al. 2015; King and Redman 2002; Hussain et al. 2013). Subsequent phylogenetic analysis suggested that Rcm1p is closest related to human NSUN5 (Figure 7B), which we therefore decided to investigate further.

A



B

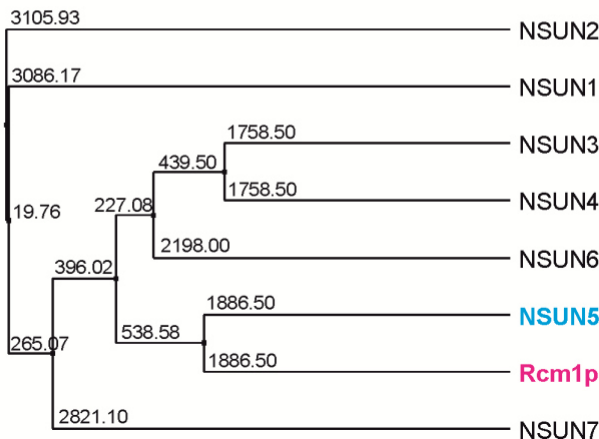


Figure 7: NSUN5 is the closest human homolog of Rcm1p. **A**, The multiple protein sequence alignment of Rcm1p and the human NSUN protein family is shown. The sequences were cropped as follows: NSUN1 (336-586), NSUN2 (116-429), NSUN3 (84-333), NSUN4 (124-382), NSUN5 (182-424), NSUN6 (184-465), NSUN7 (244-507) and Rcm1p (198-489). The full-length alignment is shown in Figure 14. Colours indicate similarities. Two highly conserved cysteines required for covalent RNA substrate binding and subsequent release are indicated by asterisks (*). **B**, Based on this alignment, the depicted phylogenetic tree was constructed. Numbers indicate phylogenetic distances. NSUN5 (cyan) is the closest human homolog of yeast Rcm1p (magenta).

3.1.2 Loss of NSUN5 impairs growth of cells and mice

To study functional consequences of NSUN5 depletion in a human cell model, we applied CRISPR-Cas9 to homozygously delete NSUN5 in HeLa cells. In order to prevent transcription of functional mRNA, we decided to target the second exon of the NSUN5 gene and subsequently screened clones originating from single cells for loss of NSUN5. We were indeed able to isolate a single clone which showed complete absence of NSUN5 protein expression (Figure 8A). Sanger sequencing of genomic DNA from this clone revealed a translocation from chromosome 4q into intron 1/exon 2 of the NSUN5 locus (Figure 15). This led to loss of NSUN5 mRNA, as confirmed by RT-qPCR (Figure 15).

During cultivation and expansion of this clone, we noticed that cells appeared smaller and proliferated slower than the parental HeLa cell line. To quantify this phenomenon, we measured more than 6,000 single cells and indeed observed a small but significant decrease of 3.5% in median cell diameter in NSUN5 KO compared to control HeLa cells (Figure 8B). To exclude the possibility that this reduction of cell size was due to off-target effects of CRISPR-Cas9, we stably introduced a BACmid containing the GFP-tagged mouse *Nsun5* gene together with its endogenous promotor (Poser et al. 2008) into NSUN5 KO (NSUN5 KO GFP-mNsun5) and control HeLa (HeLa GFP-mNsun5) cells. Western blot analysis confirmed expression of GFP-mNsun5 at the correct size (Figure 16A), while fluorescence microscopy revealed localization predominantly in the nucleoli and in the nucleoplasm (Figure 16B). Indeed, expression of GFP-mNsun5 partially rescued the size defect in NSUN5 KO GFP-mNsun5 compared to HeLa GFP-mNsun5 cells (Figure 8B). The remaining small but significant difference in size might be due to steric effects caused by fusion to GFP or unexpected differential regulation of the mouse genomic locus contained in the BACmid used by the human transcriptional machinery.

To quantify our observation that loss of NSUN5 also decreases proliferation, we seeded equal numbers of HeLa, NSUN5 KO, HeLa GFP-mNsun5 and NSUN5 KO GFP-mNsun5 cells and recorded cell numbers every day. Indeed, HeLa cells reached approximately 40% higher cell numbers after three days (Figure 8C), which was also reflected by a steeper growth curve (Figure 8D). Ectopic expression of GFP-mNsun5 slightly suppressed proliferation of HeLa cells, but not of NSUN5 KO cells (Figure 8C, D). To further confirm these results in normal cells, we

introduced four different small hairpin RNAs (shRNAs) targeting NSUN5, as well as a non-hairpin forming control, into three different strains of human dermal fibroblasts (HDFs). After puromycin selection, reduced expression of NSUN5 mRNA was confirmed by RT-qPCR (Figure 17A) and reduced cell numbers were observed in all fibroblast strains transduced with shRNA constructs compared to the non-hairpin forming control (Figure 17B). To exclude the possibility that the reduction of cell numbers was due to acute transduction stress, we reseeded one of the HDF strains at the same cell numbers and again, a decrease in proliferation upon NSUN5 depletion was evident (Figure 17C).

To assess the consequences of Nsun5 loss in mammals *in vivo*, we deleted exon 1 of the Nsun5 gene in C57BL/6J mice by CRISPR/Cas9, which resulted in Nsun5 knockout in the whole mouse body (Figure 17D). We confirmed that Nsun5 was indeed not expressed in these mice at mRNA and protein level by RT-qPCR and western blot (Figure 17E and 17F). When recording the weight of Nsun5 knockout and wildtype animals within the same litter at either 4 or 8 weeks of age, we observed a significant decrease in body weight by ~10% in both sexes upon loss of Nsun5, which was slightly more pronounced in females than in males (Figure 8E). A similar trend was visible in two other Nsun5 knockout mouse models, one by the International Mouse Phenotyping consortium (Dickinson et al. 2016) at 8 weeks of age (data included in Figure 8E), as well as in a recent publication by Zhang and coworkers, although not reaching statistical significance (Zhang et al. 2018). Interestingly, also adult Nsun5 knockout mice at 14 to 18 weeks of age were significantly lighter than wildtype mice. EchoMRI measurements revealed that the weight difference between wildtype and Nsun5 knockout animals was evident in lean but not in fat mass (Figure 28F). Food intake of Nsun5 knockout mice was slightly reduced compared to wildtype animals, but did not reach statistical significance (Figure 8G).

Herdy and coworkers found that NSUN5 interacts with the 5'UTR of NRAS mRNA. As RAS represents a proto-oncogene regulating cell growth, we speculated that the growth phenotypes we observed upon NSUN5 depletion might be caused by changes in RAS expression. To test this hypothesis, we measured RAS protein levels in HeLa and NSUN5 KO cells, but did not observe any differences (Figure 8H).

Taken together, these experiments clearly indicate that NSUN5 is partially required for reaching a specific cell size and for proliferation in mammals without influencing RAS protein

levels. Moreover, Nsun5 depletion resulted in reduced body weight of mice, prompting us to further investigate the underlying molecular mechanisms.

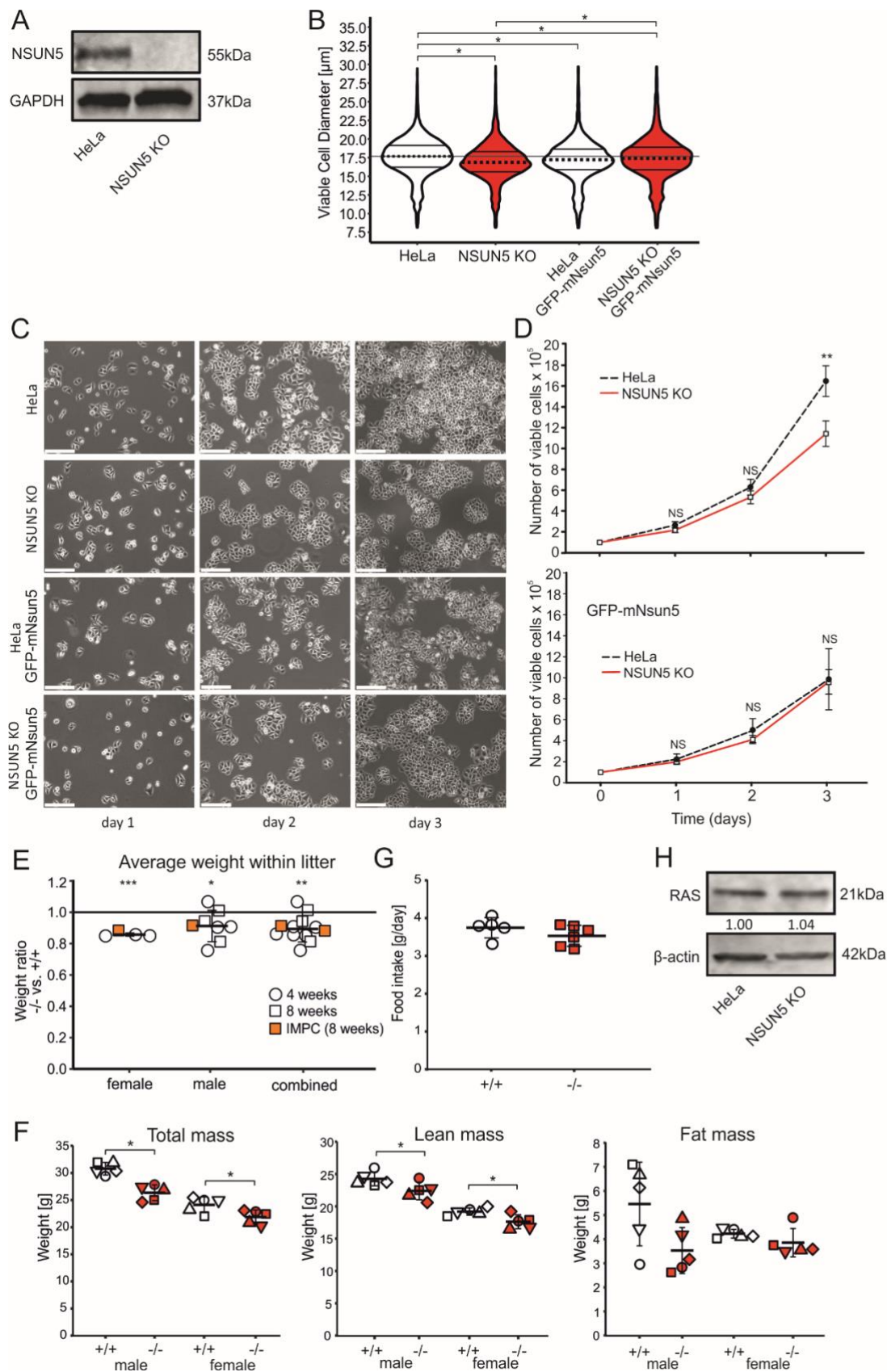


Figure 8: NSUN5 depletion decreases cell size and proliferation without affecting NRAS expression. **A**, Western blot confirms loss of NSUN5 protein expression in NSUN5 KO compared to HeLa cells. **B**, Cell size was decreased in NSUN5 KO compared to HeLa cells. Horizontal lines within the violin indicate median, first and third quartile. $n = 4$ independent experiments with $\geq 6,000$ cells. $*p \leq 0.05$, Kruskal-Wallis rank sum test with Dunn's post-hoc test. **C**, HeLa, NSUN5 KO, HeLa GFP-mNsun5 and NSUN5 KO GFP-mNsun5 cells on day 1, 2 and 3 after seeding. Representative images of 4 independent experiments are shown. Scale bar represents 50 μm . **D**, Analysis of cell proliferation by automated counting of viable cells. $n = 4$ independent experiments with $\geq 6,000$ cells each. $**p < 0.005$, two-tailed Student's t-test. ns = not significant. **E**, The weight of Nsun5 knockout mice was decreased compared to littermate controls. Each transparent data point represents the weight ratio of animals within a single litter of either 4 (circle) or 8 weeks (square) of age. $n \geq 4$ litters with 2-4 animals each. Data points represented by orange rectangles correspond to publicly available data of another Nsun5 knockout mouse model by the International Mouse Phenotyping Consortium (IMPC), with 2 knockout (-/-) versus 135 wildtype female (+/+) and 1 knockout (-/-) versus 150 wildtype (+/+) male mice at 8 weeks of age. Error bars indicate standard deviation. $*p < 0.05$, $**p < 0.005$, $***p < 0.0005$, one sample t-test against expected value of 1. **F**, Total mass, lean mass and fat mass of adult mice at the age of 14 – 18 weeks assessed by Echo-MRI. Total and lean mass were significantly decreased in Nsun5 knockout compared to wildtype mice. Fat mass revealed no significant differences upon Nsun5 knockout. Shapes of data points always refer to the same individual mouse per group. $n = 5$ per genotype and sex. Error bars indicate standard deviation. $*p < 0.05$, Welch Two Sample t-test. **G**, Food intake of male mice at the age between 15 to 19 weeks was calculated as mean of four consecutive days. No difference between wildtype (+/+) and Nsun5 knockout (-/-) mice was observed. $n = 5$ (+/+), $n = 6$ (-/-). Welch Two Sample t-test. **H**, Protein expression levels of RAS and β -Actin as loading control were analysed in HeLa and NSUN5 KO cells by western blot. Anti-Ras antibody reacts with NRAS, VRAS and HRAS. Numbers represent quantitation of RAS expression relative to β -Actin. The experiment was independently repeated two times with similar outcome.

3.1.3 NSUN5 methylates C3782 of human and C3438 of mouse 28S ribosomal RNA

Since we previously did not observe similar size and growth phenotypes in *S. cerevisiae*, *C. elegans* or *D. melanogaster* upon NSUN5 depletion (Schosserer et al. 2015), we first aimed to confirm that human NSUN5 methyltransferase activity is indeed directed against a specific cytosine of 28S rRNA, as previously hypothesized in literature (Sharma and Lafontaine 2015; Natchiar et al. 2017; Sergiev et al. 2018) and shown in yeast, worms and human glioma cells (Janin et al. 2019; Sharma et al. 2013; Schosserer et al. 2015). Therefore, we compared the sequences of 28S rRNA of humans and mice with the sequence stretch on 25S rRNA that is methylated by Rcm1 in yeast (Figure 9A). Indeed, we observed 100% evolutionary conservation of the nucleotide sequence, as well as conservation of many other known RNA modifications, indicating functional importance of this region. Due to the high similarity, we hypothesized that NSUN5 might methylate C3782 in humans and C3438 in mice, respectively. To test this hypothesis, we performed bisulfite treatment of total RNA, followed by reverse

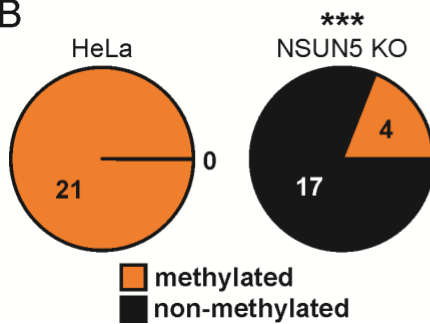
transcription, PCR amplification, TOPO-cloning and Sanger-sequencing of 21 individual clones from HeLa and NSUN5 KO cells, each. All 21 sequences of normal HeLa cells showed no conversion of C3782 to uridine, indicating that this residue of 28S rRNA was fully methylated. In contrast, only 4 of 21 (19%) clones of NSUN5 KO cells were not converted (Figure 9B). Thus, NSUN5 is clearly responsible for m⁵C modification of C3782 of 28S rRNA. Our findings are corroborated by another recent study, showing that C3782 was the only methylation site altered upon ectopic expression of NSUN5 in a NSUN5 lacking glioma cell line (Janin et al. 2019).

Due to the high evolutionary conservation of the sequence stretch of 28S rRNA (Figure 9A), we hypothesized that Nsun5 methylates C3438 on 28S rRNA in mice. We tested this hypothesis by using the same approach as for HeLa cells with kidneys of Nsun5 knockout and littermate control mice. Indeed, more than half of 17 clones of wildtype mice showed methylation at C3438, in contrast to only one single clone of Nsun5 knockout animals (Figure 9C), confirming that Nsun5 is responsible for the modification of C3438 of 28S rRNA in mice.

A

H. sapiens 28S rRNA 3754 - GAG Ψ A Ψ AmC Ψ A Ψ GAC Ψ C Ψ CUUAAGGUAGCm⁵CAA AmUGCCUCG UCAUCUAAUUAG-3805
M. musculus 28S rRNA 3410 - GAGUAA CUAUGACUCUCUUAAGGUAGCm⁵CAA A UGCCUCG UCAUCUAAUUAG-3461
S. cerevisiae 25S rRNA 2250 - GAGUA Ψ AmC Ψ A Ψ GAC Ψ C Ψ CUUAAGGUAGCm⁵CAAmAmUGCCUCGmUCAUCUAAUUAG-2301

B



C

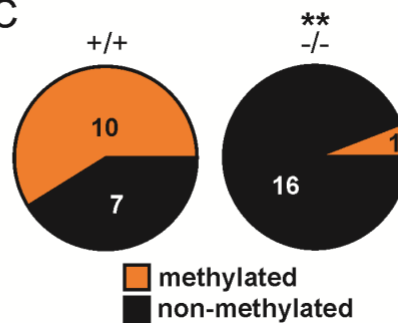


Figure 9: NSUN5 methylates C3782 of 28S rRNA in human and C3438 in murine cells. A, The sequence of 25S/28S ribosomal RNA surrounding the putative methylation site of NSUN5 (orange colour) is highly conserved between yeast, mice and humans. 2'O methylations are depicted in magenta and pseudo-uridylation (Ψ) in green. B, Bisulfite conversion and Sanger sequencing of RNA from HeLa and NSUN5 KO cells confirms C3782 methylation by NSUN5. Figures indicate numbers of clones with (orange) or without (black) methylation. Pooled results from two independent experiments are shown. Pooled n = 21 per condition. ***p < 0.0005, Fisher's exact test for count data. C, Bisulfite conversion and Sanger sequencing of RNA from kidneys of wildtype (+/+) and NSUN5 KO (-/-) mice confirms C3438 methylation by NSUN5. Numbers indicate clones with (orange) or without (black) methylation. Pooled results from two independent experiments of littermate animals are shown. Pooled n = 17 per condition. **p < 0.005, Fisher's exact test for count data.

3.1.4 Two conserved cysteines of NSUN5 are required for its RNA methyltransferase activity and normal proliferation

In order to confirm this result by a different and faster read-out, we adapted the Combined Bisulfite Restriction Analysis (COBRA) assay for detection of m⁵C2278 in yeast (Gigova et al. 2014) to human cells (Figure 10A). This approach confirmed the results from Sanger-sequencing after bisulfite conversion, also showing low potential residual methylation. To exclude artefacts from using HeLa cells and off-target effects by CRISPR-Cas9 deletion, we knocked down NSUN5 mRNA expression in HEK293 by shRNAs and observed, despite low knockdown efficiency in this cell type (Figure 18A), a trend towards loss of m⁵C3782, although not reaching statistical significance (Figure 18B).

Due to the high evolutionary conservation of NSUN5 and its rRNA target site between human and mouse, we aimed to test whether mouse Nsun5 can rescue loss of NSUN5 in human cells. Indeed, ectopic expression of endogenous levels of GFP-mNsun5 encoded on the BACmid was able to fully restore methylation of m⁵C3782 in HeLa cells (Figure 10B, C). Loss of human NSUN5 mRNA (Figure 10D) and gain of mouse Nsun5 mRNA (Figure 10E) were confirmed by RT-qPCR.

To identify amino acid residues involved in the catalysis of the methylation, we focused on two cysteine residues of NSUN5 that we considered to be essential in the binding and release of the substrate due to their conserved positioning and amino acid surroundings (Figure 14) (Schosserer et al. 2015; King and Redman 2002; Hussain et al. 2013). We then performed site directed mutagenesis to exchange these cysteines to serines (C308S and C359S). In fact, ectopic overexpression of human NSUN5 rescued C3782 methylation defects as visualized by COBRA assay, while C308S and C359S mutant versions of NSUN5 did not (Figure 10F, G). Restored NSUN5 mRNA expression was confirmed by RT-qPCR (Figure 10H). Moreover, ectopic expression of human wildtype NSUN5 in HeLa and mouse embryonic fibroblast (MEF) cells lacking NSUN5 led to increased proliferation compared to cells ectopically expressing the inactive C308S mutant (Figure 10I, J). We were not able to test the C359S mutation, as several attempts to generate stable cell lines failed. We hypothesize that this might be due to an inability to release covalently bound NSUN5 from the RNA, resulting in impaired rRNA biogenesis and consequently cellular toxicity.

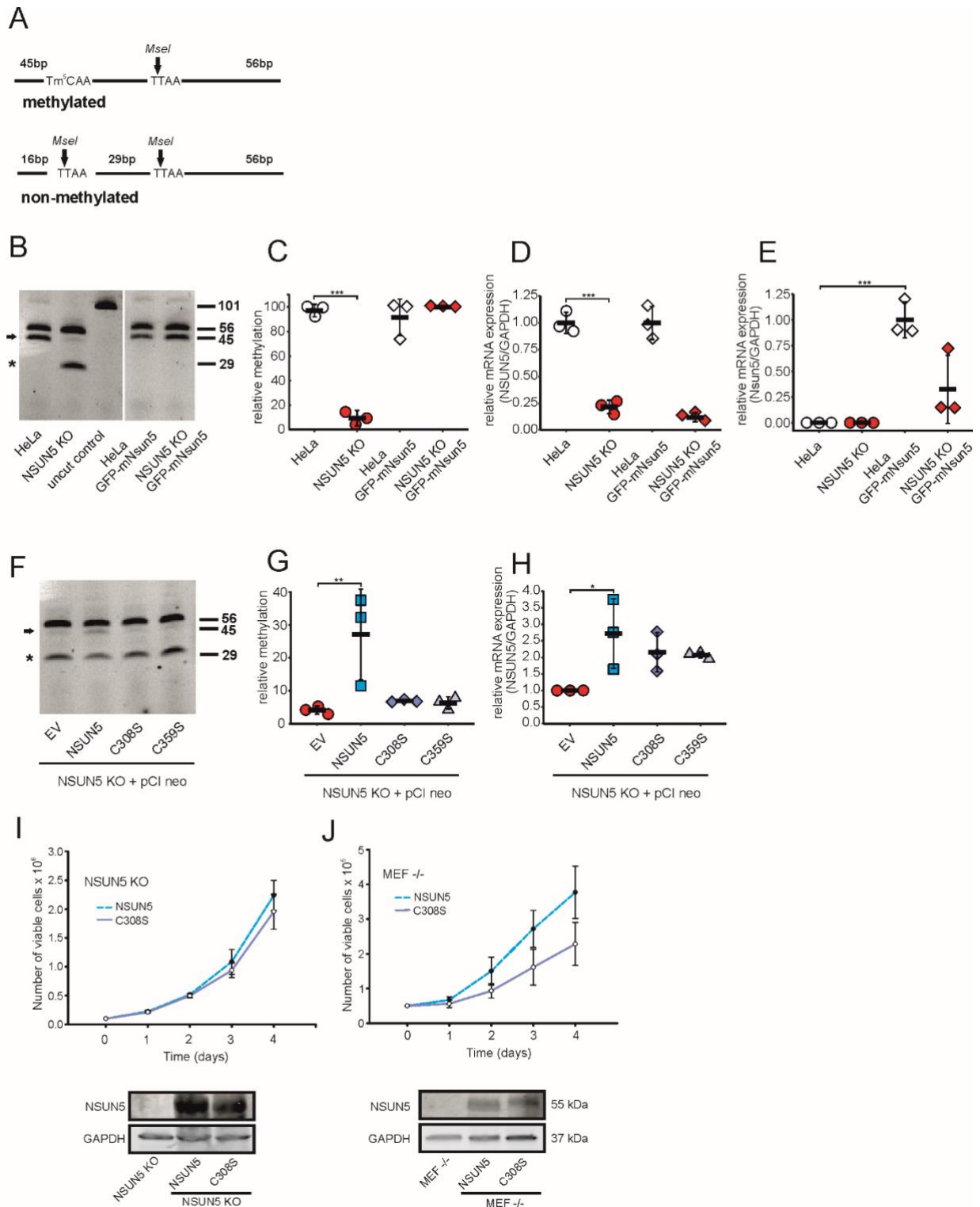


Figure 10: Two conserved cysteines of NSUN5 are required for RNA methyltransferase activity and normal proliferation. **A**, Principle of the COBRA assay to measure m⁵C3782. Digestion with MseI generates two products (56 bp and 45 bp) in the presence of m⁵C3782 and three products (56 bp, 29 bp and 16 bp) in the absence of m⁵C3782. A band at 101 bp represents the undigested PCR product. **B**, COBRA assay of HeLa, NSUN5 KO, HeLa GFP-mNSUN5 and NSUN5 KO GFP-mNSUN5 demonstrates that mouse Nsun5 fully restores methylation of C3782 upon loss of human NSUN5. A representative 20% TBE gel of MseI-digested PCR products is shown. Numbers indicate size of fragments in basepairs. Arrow indicates methylation-specific band, whereas asterisk (*) indicates band upon non-methylation. **C**, Quantitation of COBRA assay in (**B**), n = 3 independent experiments. Error bars represent standard deviation. ***p < 0.0005, One-Way-Anova followed by a post-hoc Dunnet's test. **D** and **E**,

mRNA expression levels of human NSUN5 (**D**) and mouse Nsun5 (**E**) were analysed by RT-qPCR. $n = 3$ independent experiments. Error bars represent standard deviations. $***p < 0.0005$, One-Way-Anova followed by a post-hoc Dunnet's test. **F**, Representative COBRA assay of NSUN5 KO cells stably expressing the empty pCI-neo vector (EV) or pCI-neo containing either NSUN5, NSUN5 (C308S) or NSUN5 (C359S) demonstrates the requirement of C308S and C359S for catalysis. **G**, Quantitation of COBRA assay in (**F**), $n = 3$ independent experiments. Error bars represent standard deviations. $**p < 0.005$, One-Way-Anova followed by a post-hoc Dunnet's test. **H**, Ectopic expression of NSUN5 in pCI-neo restores NSUN5 mRNA levels as analysed by RT-qPCR. $n = 3$ independent experiments. Error bars indicate standard deviations. $*p < 0.05$, One-Way-Anova followed by a post-hoc Dunnet's test. **I, J**, Analysis of cell proliferation by automated counting of viable cells comparing NSUN5 KO HeLa (**I**) or MEF $-/-$ (**J**) ectopically expressing either human NSUN5 or the C308S mutant on four consecutive days after seeding. Error bars indicate standard deviations. $n = 4$ independent experiments. Western blots confirm ectopic expression of NSUN5 in both cell types.

3.1.5 RNA polymerase I activity and the N-terminal domain are required for nucleolar localization of NSUN5

All four eukaryotic rRNAs are transcribed in the nucleolus by RNA polymerases I and III, representing the first steps of ribosome biogenesis. Consequently, the pre-ribosomal particles are exported to the cytoplasm, where mature ribosomes are assembled (Turowski and Tollervey 2015; Yarunin et al. 2005; Vannini and Cramer 2012). To test in which cellular compartment m^5C3782 is introduced by NSUN5, we performed immunofluorescence staining of HeLa cells and analysed endogenous NSUN5 localization by gated STED super resolution microscopy. Nucleoli were stained with an antibody targeting fibrillarin (Figure 11A, Figure 19). As expected and also observed for GFP-mNsun5 (Figure 16B), NSUN5 was present in the centre of nucleoli, which suggests that m^5C3782 is introduced at an early stage of ribosome biogenesis. Next, we specifically blocked RNA polymerase II and III with α -amanitin, which left the nucleolar localization of NSUN5 and fibrillarin undisturbed (Figure 11A). RNA polymerase II synthesizes mRNAs and microRNAs, while RNA polymerase III transcribes tRNAs and 5S rRNA (Vannini and Cramer 2012; Yarunin et al. 2005; Turowski and Tollervey 2016). However, when cells were exposed to 50 ng/ml actinomycin D to specifically block RNA polymerase I (Perry and Kelley 1970; Shav-Tal et al. 2005; Ochs 1997), which transcribes the pre-rRNA template that is further processed into 28S, 18S, 5.8S rRNA, both NSUN5 and fibrillarin segregated to the nucleolar caps (Figure 11A), as previously described for other nucleolar proteins as well (Shav-Tal et al. 2005).

Next, we aimed to test which part of NSUN5 is required for nucleolar localization. NSUN5 is composed of three domains: The N-terminal domain of unknown function and predicted

globular tertiary structure, the evolutionarily conserved RNA methyltransferase domain including the SAM binding pocket and two cysteines required for catalysis, as well as the C-terminal domain of unknown function (Figure 11B, Figure 14). First, we ectopically expressed full-length NSUN5 (NSUN5-GFP), as well as the C308S and C359S mutants, with a C-terminal GFP-tag in normal HeLa cells. Neither C308S nor C359S did affect nucleolar localization (Figure 11C), indicating that the catalytic activity is not required for targeting NSUN5 to its substrate. Thus, we generated truncation mutants of NSUN5-GFP and observed that complete absence of the N-terminal globular domain fully excluded NSUN5-GFP from nucleoli, while absence of the C-terminal domain only led to a slight redistribution from nucleoli towards the nucleoplasm (Figure 11C).

Taken together, these findings suggest that RNA polymerase I activity, as well as presence of the globular N-terminal domain, and to a much lesser extend also of the C-terminal domain, are required for nucleolar localization of NSUN5. Consequently, we suggest that the addition of m⁵C3782 occurs co-transcriptionally and is guided by the globular N-terminal domain of NSUN5, representing the functional targeting moiety.

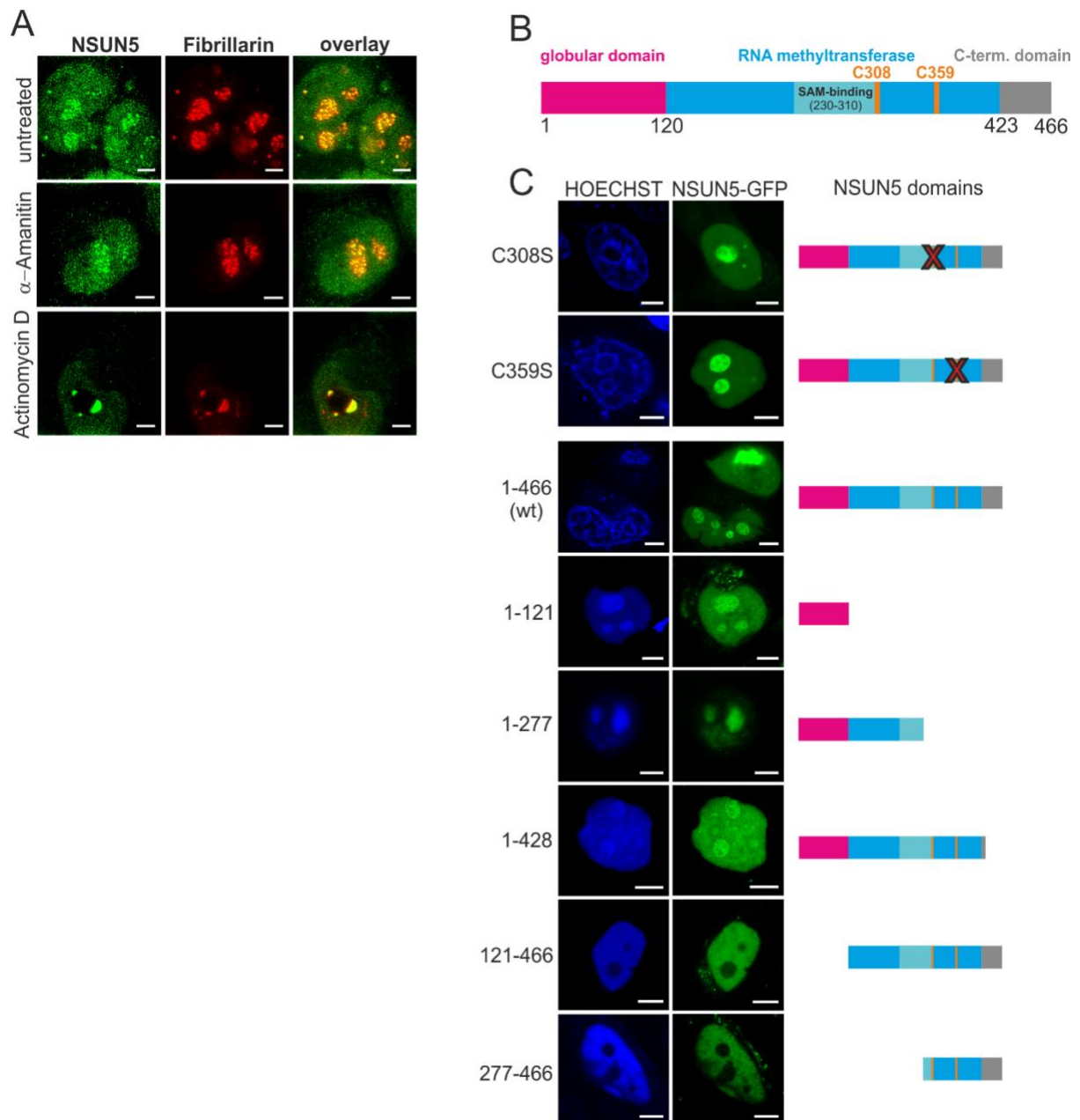


Figure 11: RNA polymerase I activity and presence of the N-terminal domain are required for nucleolar localization of NSUN5. **A**, HeLa cells were exposed to 50 $\mu\text{g}/\mu\text{L}$ α -amanitin to block RNA Polymerase II and III or 50 $\text{ng}/\mu\text{L}$ actinomycin D to block RNA Polymerase I, II and III. NSUN5 (green) and fibrillarin (red) were visualized by indirect immunofluorescence staining. Confocal gSTED microscopy reveals nucleolar localization of NSUN5 and segregation to nucleolar caps upon inhibition of RNA polymerase I. Images were processed by deconvolution and brightness and contrasts were adjusted. Scale bar represents 3 μm . The experiment was repeated twice with similar outcome (see also Figure S6). **B**, Protein domain structure of NSUN5. The N-terminal globular domain (magenta), the RNA methyltransferase domain (blue), the C-terminal domain (grey), the two cysteines required for catalysis (C308 and C359, orange) and the SAM (S-adenosyl methionine) binding site (cyan) are depicted. Numbers indicate amino acids counted from the N-terminus. **C**, HeLa cells were transfected with NSUN5 (C308S, full-length), NSUN5 (C359S, full-length), NSUN5 (1-466, full-length), NSUN5 (1-121), NSUN5 (1-277), NSUN5 (1-428), NSUN5 (121-466) and NSUN5 (277-466) as C-terminal GFP-fusions. Confocal microscopy revealed nucleolar localization of all NSUN5 constructs (green) except NSUN5 (121-466) and NSUN5 (277-466). Nuclei were counterstained with Hoechst33342 (blue). Microscopic images and NSUN5 domain structure of mutants are shown side by side. Images were processed by deconvolution and brightness and contrasts were adjusted. Scale bar represents 5 μm . The experiment was repeated twice with similar outcome.

3.1.6 Loss of NSUN5 reduces global protein translation but does not affect ribosome biogenesis and fidelity

To further elucidate molecular mechanisms that might explain the observed growth and proliferation phenotype, we aimed to investigate the potential role of m⁵C3782 in global protein translation in HeLa cells. Quantification of O-propargyl-puromycin (OPP) incorporation by flow cytometry (Nagelreiter et al. 2018) revealed median bulk translation to be reduced by about 25% in NSUN5 KO compared to control HeLa cells (Figure 12A). This reduction in protein synthesis is directly connected with the methylation activity of NSUN5, since ectopic expression of wildtype NSUN5 in NSUN5 KO cells was able to rescue OPP incorporation, while expression of the catalytically inactive mutant C308S was not (Figure 12A). Similarly, comparison of polysome profiles, which provide a snapshot of translational activity, showed an increase of 80S monosomes compared to polysomes upon loss of NSUN5 (Figure 12B, C).

To confirm that alterations to the ribosome itself, and not the number of ribosomes or other extrinsic factors, which might also be influenced by loss of NSUN5, are responsible for decreased bulk protein synthesis, we decided to analyse translation in vitro. For this aim, we depleted ribosomes from a HeLa cell lysate by ultracentrifugation and spiked this extract with equal amounts of purified ribosomes from either control HeLa cells or NSUN5 KO cells, as well as with ³⁵S-Methionine to quantify protein synthesis. Thereby, we observed a significant reduction in ³⁵S-Methionine incorporation upon loss of NSUN5, whereas the size distribution of newly synthesized proteins appeared to be similar (Figure 12D). Omission of the supernatant, which contains several components necessary for translation including mRNA, tRNAs, initiation, elongation and termination factors, did not result in protein synthesis and thereby confirmed specificity of the assay. Quantification of in vitro synthesized, radiolabelled protein over the full length of the autoradiogram revealed a reduction by 60% in NSUN5 KO compared to control HeLa cells (Figure 12E). We confirmed equal loading of extracts by Coomassie gels and equal amounts of ribosomes by ethidium bromide staining for 5S and 5.8S rRNA (Figure 12F).

Importantly, the observed protein synthesis defect in HeLa cells is not associated with decreased amounts of mature ribosomes per cell, as quantified by comparing 28S and 18S

bands from HeLa and NSUN5 KO cells upon loading of total RNA from equal numbers of cells (Figure 20A). Furthermore, loss of NSUN5 in HeLa cells did not induce any obvious alterations in ribosome biogenesis, as evidenced by northern blot analysis with two specific pre-rRNA probes (Figure 20B-E).

Cancer cells, such as HeLa or glioblastoma, and cells of embryonic origin, such as MEFs, require high global protein translation rates to maintain their fast proliferation behaviour. For this reason, we decided to measure protein translation also in MEFs, as well as in various normal tissues of wildtype and *Nsun5* knockout mice in vivo by injection of OPP. OPP labelling of *Nsun5* deficient MEFs indeed revealed a substantial reduction in overall protein synthesis, which could be rescued by ectopic expression of human NSUN5, but not by the C308S mutant (Figure 12G). Interestingly, quantification of OPP incorporation into liver, kidney, lung and bone marrow also showed a trend towards decreased protein synthesis in *Nsun5* knockout animals compared to littermate controls (Figure 12H), but to a lesser extent than in MEFs.

Since we previously observed that loss of *Rcm1*, the NSUN5 orthologue in yeast, increased stop-codon read-through (Schosserer et al. 2015), and depletion of *nsun-5* in a polyglutamine-frameshifting *C. elegans* model caused elevated -1 translational frameshifting upon osmotic stress (Adamla et al. 2019), we aimed to test if loss of human NSUN5 also influences stop-codon read-through or perturbs translational fidelity in other ways. However, the recognition of any of the three stop-codons was not affected in NSUN5 KO compared to control HeLa cells upon transient transfection of dual luciferase-based reporter constructs (Figure 20F). Moreover, neither translational frameshifting induced by viral sequences (Harger and Dinman 2003) (Figure 20G), nor amino acid misincorporation (Ke et al. 2017; Azpurua et al. 2013) were altered upon NSUN5 loss (Figure 20H). Additionally, recognition of internal ribosome entry sites (IRES) (Figure 20I), which was previously reported to be affected by pseudouridines in rRNA (Penzo et al. 2015), was not different in NSUN5 KO versus control HeLa cells.

Taken together, our findings indicate that presence of NSUN5-mediated 28S rRNA methylation is required for maintaining productive global protein synthesis, but not translational fidelity, IRES recognition or ribosome biogenesis in mammals.

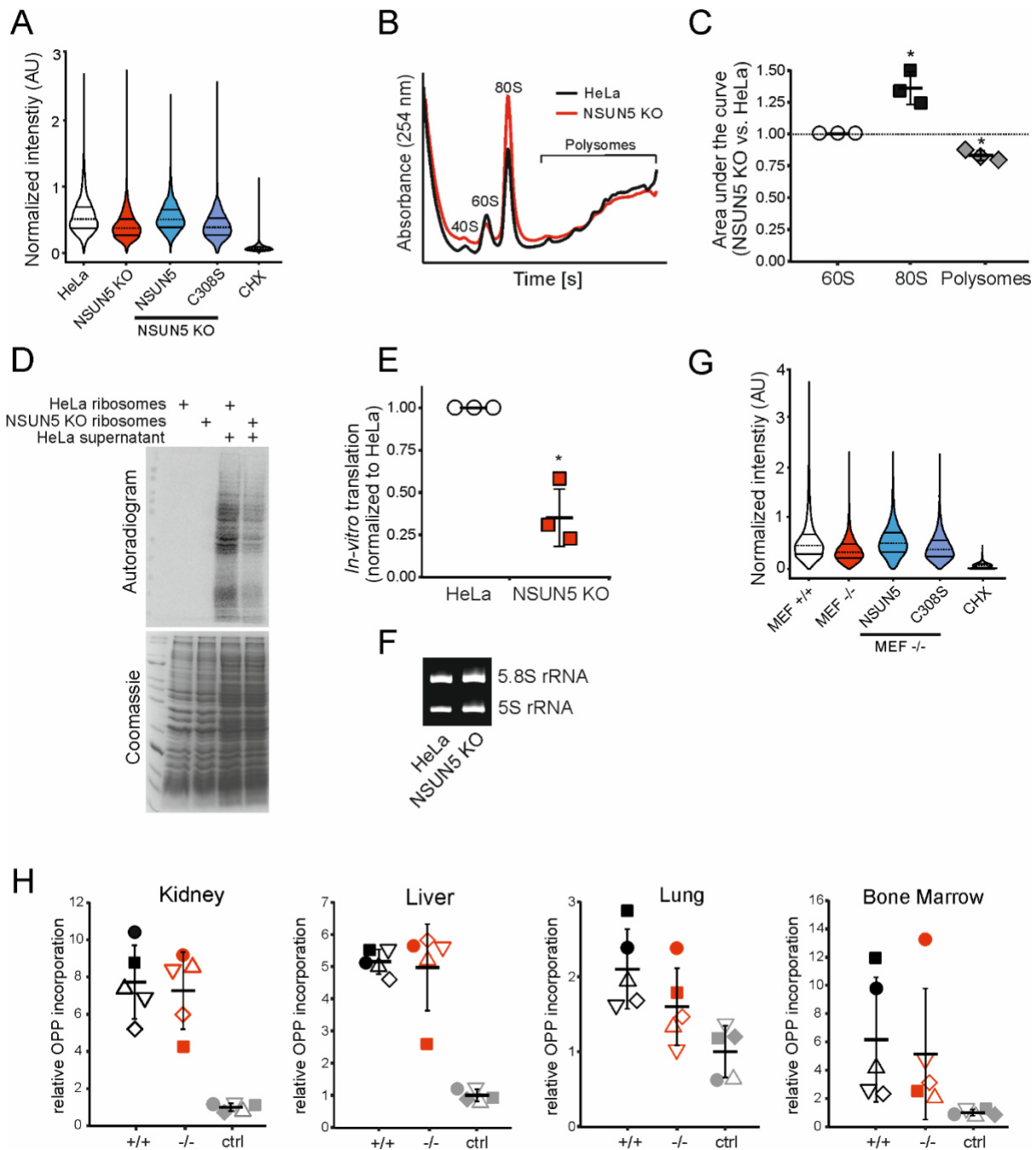


Figure 12: Loss of NSUN5 reduces global protein translation but does not affect fidelity. **A**, Total protein synthesis, analysed by OPP incorporation and flow cytometry, was reduced in NSUN5 KO compared to control HeLa cells and could be rescued by ectopic expression of NSUN5 but not by the C308S mutant. Specificity was verified by cycloheximide (CHX) exposure or omission of OPP (data not shown). Horizontal lines within the violin represent median, first and third quartile. Pooled data from 4 independent replicates are shown. 5,000 cells of each condition were randomly selected for analysis and normalized to the sum of fluorescence intensities of all selected cells within the replicate. 95% confidence intervals (CI) by Kruskal-Wallis rank sum test with Dunn's post-hoc test: HeLa = -0 to 0; NSUN5 KO = -27.3 to -25.3; NSUN5 KO ectopically expressing NSUN5 = -1.8 to 0.4; NSUN5 KO ectopically expressing C308S = -25.0 to -22.8; CHX = -87.3 to -85.5. **B**, Loss of NSUN5 increases the 80S monosome peak compared to polysomes in HeLa cells. Polysome profiling was performed three times independently, representative profiles are shown. **C**, Quantification of polysome profiles by calculating the area under the 60S, 80S and polysome peak, respectively. Data were normalized to 60S. Error bars indicate standard deviation. * p < 0.05, one sample t-test against expected value of 1. **D**, Ribosomes of control HeLa and NSUN5 KO cells were purified and spiked into ribosome-free supernatant of HeLa cells. Autoradiogram shows decreased

amounts of nascent in vitro translated proteins upon NSUN5 loss. Purified ribosomes without supernatant verified specificity and Coomassie staining confirmed equal loading. **E**, Quantitation of autoradiograms demonstrate less in vitro translation in NSUN5 KO compared to control HeLa cells. Error bars indicate standard deviation. * $p < 0.05$, one sample t-test against expected value of 1. **F**, Ethidium bromide staining of a denaturing polyacrylamide gel confirms equal loading of purified ribosomes. **G**, Total protein synthesis, analysed by OPP incorporation and flow cytometry, of MEF $-/-$ was reduced compared to MEF $+/+$ cells and could be rescued by ectopic expression of NSUN5 but not by the C308S mutant. Specificity was verified by cycloheximide (CHX) exposure or omission of OPP (data not shown). Horizontal lines within the violin represent median, first and third quartile. Pooled data from 3 independent replicates are shown. 5,000 cells of each condition were randomly selected for analysis and normalized to the sum of fluorescence intensities of all selected cells within the replicate. 95% confidence intervals (CI) by Kruskal-Wallis rank sum test with Dunn's post-hoc test: MEF $+/+$ = -0 to 0; MEF $-/-$ = -29.2 to -26.1; MEF $-/-$ ectopically expressing NSUN5 = -8.3 to 11.6; MEF $-/-$ ectopically expressing C308S = -18.7 to -15.5; CHX = -87.1 to -84.7. **H**, Total protein synthesis in vivo was analysed by injection of OPP and flow cytometry of single cell suspensions of kidney, liver, lung and bone marrow. Specificity was verified by injection of PBS (ctrl). N = 5 animals per condition in two independent experiments (indicated by either filled or empty symbols). Welch Two Sample t-test: Kidney: $p = 0.7313$; mean $+/+$ = 7.730, mean $-/-$ = 7.274; Liver: $p = 0.7882$, mean $+/+$ = 5.1526, mean $-/-$ = 4.9744; Lung: $p = 0.1684$, mean $+/+$ = 2.102, mean $-/-$ = 1.600; Bone marrow: $p = 0.7305$, $+/+$ = 6.162, mean $-/-$ = 5.140.

3.1.7 Partial loss of NSUN5 in Williams-Beuren-Syndrome is sufficient to reduce m⁵C3782

NSUN5 is deleted in around 95% of WBS patients (Pober 2010), who show clinical phenotypes including growth retardation, a dysmorphic face, behavioural and cognitive alterations, hypercalcaemia, as well as aortic and pulmonary stenosis (Tassabehji 2003). While haploinsufficiency of the elastin gene was unambiguously associated with the cardiovascular disease in WBS, the question which other genes are dosage-sensitive and contribute the clinical phenotype still remains unanswered (Tassabehji 2003). Recently Zhang and coworkers observed cognitive impairments in homozygous Nsun5 knockout mice, which were associated with a decrease in proliferation of oligodendrocyte precursor cells (Zhang et al. 2018).

This prompted us to further investigate the functional role of NSUN5 in WBS. To assess whether haploinsufficiency of the NSUN5 gene affects mRNA expression, we compared NSUN5 mRNA levels in HDF of two WBS patients to two healthy donors. Indeed, we observed reduced levels of NSUN5 mRNA in both cell strains derived from WBS patients (Figure 13A). Similarly, reduced expression of NSUN5 protein was detected by western blot (Figure 13B), while nucleolar localization of endogenous NSUN5 was not altered (Figure 13C). To test whether the partial loss of NSUN5 is also sufficient to reduce methylation of C3782, we performed COBRA assay and indeed observed decreased C3782 methylation in HDF from two WBS patients compared to two healthy donors (Figure 13D, E).

Thus, we conclude that NSUN5 expression is lower in HDF from WBS patients compared to cells from healthy donors on both mRNA and protein level. Furthermore, reduced NSUN5 expression also results in decreased C3782 methylation. However, further studies in heterozygous Nsun5 knockout mice are required to assess whether the reduced gene dosage by Nsun5 haploinsufficiency is enough to induce similar cognitive deficits that were observed in Nsun5 full knockout mice (Zhang et al. 2018; Yuan et al. 2019; Cheng et al. 2018).

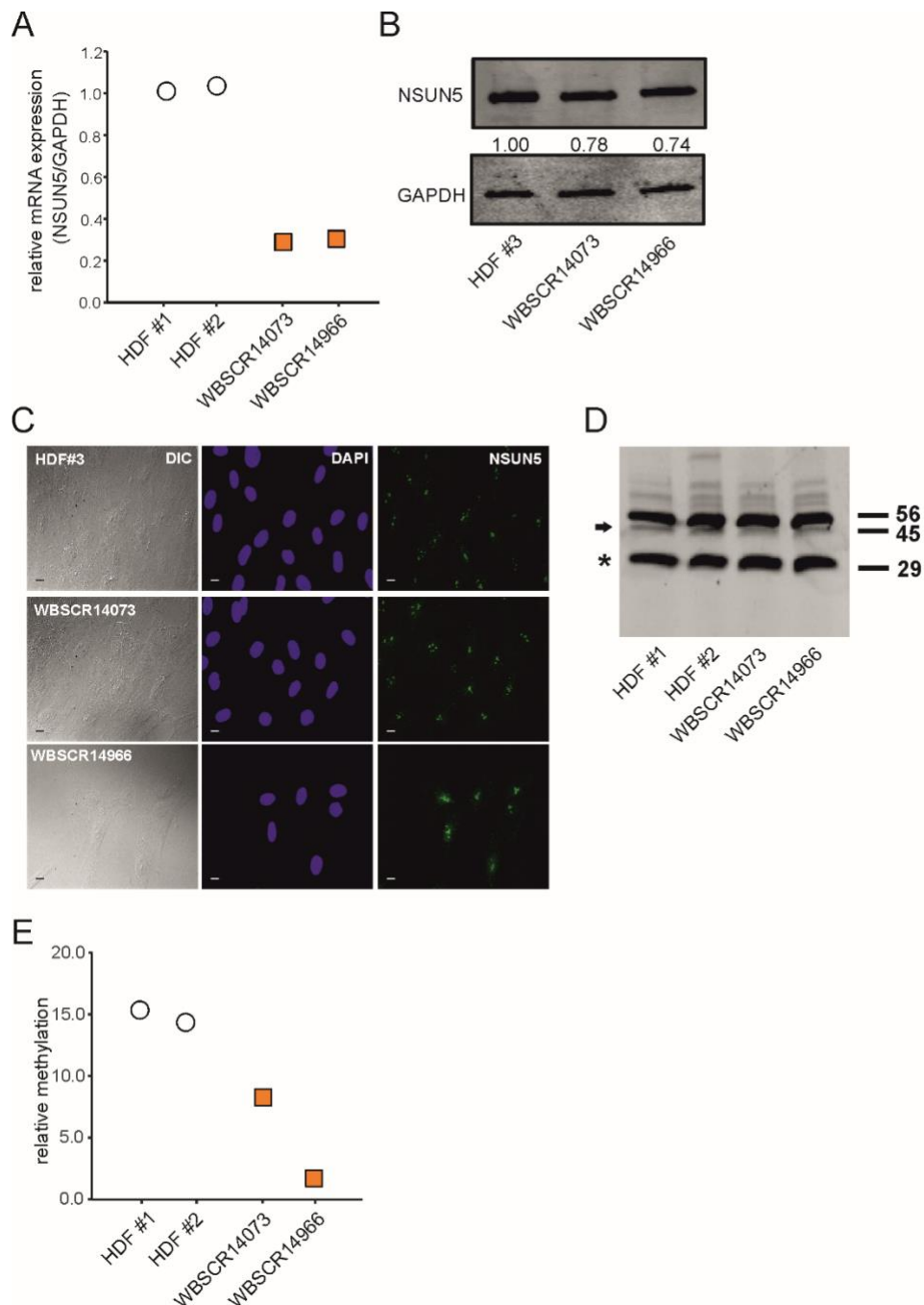


Figure 13: Partial loss of NSUN5 in Williams-Beuren-Syndrome is sufficient to reduce m⁵C3782. **A**, Relative expression levels of NSUN5 mRNA of two healthy donors as well as two WBS patients were determined by RT-qPCR. **B**, Protein expression levels of NSUN5 were measured in fibroblasts of a healthy donor and two WBS

patients. **C**, DIC and IF images of fibroblasts of a healthy donor and the two WBS patients. NSUN5 is stained in green and nuclei are counterstained with DAPI. Scale bar represents 10 μ m. **D**, COBRA assay of fibroblasts of two healthy donors and two WBS patients indicates that methylation of C3782 is decreased in WBS. A representative 20% TBE gel of MseI-digested PCR products is shown. Numbers indicate size of fragments in basepairs. Arrow indicates methylation-specific band, whereas asterisk (*) indicates band upon non-methylation. **E**, Quantitation of COBRA assay in (**D**).

3.1.8 Discussion and Conclusion

We here report that loss of NSUN5 induces growth phenotypes in mice and different mammalian cells, which is likely connected to the requirement of NSUN5 for ribosomal RNA modification and normal global protein translation, especially in highly proliferative cells. However, we can also not fully rule out that NSUN5 directly disturbs one of the main growth pathways or RAS activity without interfering with RAS protein levels. But how might loss of m⁵C3782 affect the ribosome?

Upon assembly of the SSU and LSU to active 80S ribosomes, the eukaryote-specific bridge eB14 is formed, which directly contacts rRNA base modifications of both subunits including m⁵C3782. This residue, which we have shown to be methylated by NSUN5, is located within helix 70, domain IV on 28S rRNA and interacts with RPL41, a small but highly positively charged protein and main constituent of eB14, which expands from the 60S and protrudes into a binding pocket of the 40S DCS (Tibshirani et al. 2011). Although not much is known about the presence and precise function of the eB14 bridge in humans (Sharma and Lafontaine 2015; Tibshirani et al. 2011; Natchiar et al. 2017), NSUN5-guided methylation of C3782 might play an important part in its formation and thereby modulate global protein translation.

Accumulating evidence for the presence of “specialized ribosomes”, which are generated in response to various stimuli and promote the selection of specific mRNAs for translation (Genuth and Barna 2018; Xue and Barna 2012), fuels the hypothesis that presence or absence of certain rRNA modifications might contribute to ribosome heterogeneity on a structural and functional level. Our discovery that NSUN5, being required for the addition of a specific methylation to 28S rRNA in humans and mice, co-localizes with fibrillarin in the centre of nucleoli suggests that addition of m⁵C3782 might constitute an early event during ribosome biogenesis happening co-transcriptionally, as was already reported for 2’O-methylations

introduced by fibrillarin (Kos and Tollervey 2010; Turowski and Tollervey 2015). As m⁵C3782 is located in the core of mature ribosomes, this site appears unlikely to be accessible for hypothetical cytoplasmic RNA methylases or de-methylases. Since the response time of transmitting a signal via NSUN5-guided methylation of rRNA in the nucleolus to mature (specialized) ribosomes leading ultimately to altered mRNA translation patterns would be rather slow compared to other cellular regulatory loops, we consider it hardly probable that NSUN5 plays an active role in the translational regulation of gene expression. Nonetheless, the identification of potential upstream regulators of NSUN5 expression and activity is important and will be further studied, as tight regulation of NSUN5 expression levels seems to be crucial for cellular fitness.

Recent studies revealed almost complete methylation at C3782 in HeLa (Khoddami et al. 2019) and at C3438 in mouse embryonic stem cells (Legrand et al. 2017). However, as we found only partial methylation in mouse kidney, it will be interesting to determine in future studies if these discrepancies are caused by artefacts due to the much lower sequencing depth of our approach. In addition, methylation levels might be influenced by the tissue context or the proliferative capacity of cells.

Equally important will be the identification of potential additional RNA substrates of NSUN5 by global bisulfite sequencing, Aza-IP or miCLIP (Khoddami and Cairns 2013; Khoddami et al. 2019; Trixl and Lusser 2019; Legrand et al. 2017; Hussain et al. 2013), which will also clarify whether the recently described physical association of NSUN5 with NRAS mRNA in cytoplasmic extracts (Herdy et al. 2018) results in NRAS mRNA methylation, or if NSUN5 fulfils other non-canonical functions there. Surprisingly and contradictory to the study by Herdy and coworkers (Herdy et al. 2018), we did not observe cytoplasmic localization of NSUN5, neither with two different antibodies detecting endogenous NSUN5, nor by ectopic expression of different GFP-tagged NSUN5 constructs. This suggests that either only small amounts of NSUN5 shuttle to the cytoplasm, or that extracts used for pulldowns might have contained small residual amounts of nuclear proteins and mRNAs. Anyhow, since RAS is an important stimulator of mTORC1 activity (Mendoza et al. 2011), it thereby promotes cytoplasmic translation and growth further downstream. Thus, subtle differences in RAS signalling and molecular function between different organisms might partially explain why loss of NSUN5

impairs growth in mice and human cells, but not in yeast, worm and fly (Schosserer et al. 2015).

We previously reported that NSUN5 orthologs modulate the chronological lifespan of yeast, as well as organismal lifespan of *C. elegans* and *D. melanogaster*. Importantly, this lifespan extension was conditional to reduced nutrient availability and was not accompanied by any obvious phenotypical alterations, such as body size, locomotion or feeding behaviour (Schosserer et al. 2015). *C. elegans* and *D. melanogaster* are predominantly post-mitotic organisms, thus impaired proliferation of cells is unlikely to affect organismal fitness and depletion of Rcm1 in yeast only extended chronological, but not replicative lifespan (Schosserer et al. 2015). Further experiments with our Nsun5 knockout mouse model will clarify, if loss of Nsun5 is able to modulate healthy lifespan of a complex model organism with characteristics of both chronological and replicative ageing.

In contrast to the small model organisms, we here discovered that loss of NSUN5 or catalytic mutation impairs ribosome function and reduces size and proliferation in mammalian cells, as well as the body weight of mice. These disagreements might be due to important differences between the models. NSUN5 depletion reduced bulk protein translation in mammalian cells, while a similar response was only evoked in yeast and *C. elegans* by exposure to stress such as hydrogen peroxide (Schosserer et al. 2015) or high salt concentrations (Gigova et al. 2014; Adamla et al. 2019). This might indicate that loss of m⁵C3782 renders ribosomes instable, which yeast and nematodes in contrast to mammalian cells are able to compensate under unstressed conditions.

Also, cells with high proliferation rates, such as cancer cells (HeLa, certain glioma cell lines under oxidative stress (Janin et al. 2019)) and immortalized cell lines (MEF), seem to be sensitive to loss of NSUN5, while in mice several normal tissues with low proliferation rates, including kidney, liver, lung and bone marrow were only mildly affected. Thus, we hypothesize that blunted expression of Nsun5, either by knockout or endogenous hypermethylation of its promoter, will mostly influence highly proliferative tissues of the adult mouse, which might explain the relatively mild general phenotype. Indeed, differential regulation of NSUN5 expression in various tissues was recently demonstrated to happen at epigenetic level, since methylation of the NSUN5 promoter was high in some glioma cell lines and primary tumors,

but low in cervical and other malignancies (Janin et al. 2019). Thus, it will be interesting to determine epigenetic silencing of the NSUN5 locus also in various normal tissue contexts.

Importantly, the ancestral gene NSUN5, which we here investigated, has two additional copies (NSUN5B and NSUN5C) in the same chromosomal region related to WBS. All three gene products are described to be ubiquitously expressed and showing tissue-specific patterns (Schubert 2009). Weak expression of NSUN5 and high background staining of available antibodies did not allow us to assess which of the predicted genes are indeed expressed. However, only full-length NSUN5 is likely to participate in methylation of rRNA, because NSUN5B and NSUN5C roughly correspond to GFP-tagged truncation mutants, which did not localize to nucleoli. However, we cannot rule out specific functions of these genes in the cytoplasm or in another tissue context.

One of the main features of WBS is a mild to moderate cognitive impairment, including reduced cerebral volume by 13% (Li et al. 2009; Thompson 2005). Recently, Zhang and coworkers described a novel Nsun5 knockout mouse model in the same C57BL/6J genetic background as our Nsun5 knockout mice. They demonstrated that loss of Nsun5 led to deficits in spatial learning and memory capacity, which might be connected to WBS pathology (Yuan et al. 2019; Zhang et al. 2018). Our data presented here further support this hypothesis in several ways: (i) Reduced proliferation of oligodendrocyte precursor cells in Nsun5 knockout mice (Zhang et al. 2018) is most likely a general consequence of Nsun5 depletion, as we observed similar proliferation deficits in several other primary and immortalized cell types, (ii) alterations of ribosomes and protein translation, which we also observed upon NSUN5 loss, are frequently linked to other neuronal pathologies (Lehmkuhl and Zarnescu 2018; Scheper et al. 2007), and (iii) we were able to demonstrate that primary fibroblasts from WBS patients indeed showed decreased NSUN5 mRNA and protein levels resulting in a reduction of m⁵C3782, which clearly indicates that gene-dosage by haploinsufficiency of the NSUN5 gene in WBS is relevant. However, further studies with other cell types, more donors and advanced disease models, such as mice heterozygous for the Nsun5 gene, are required to draw definite conclusions and identify further symptoms that might be linked to NSUN5 haploinsufficiency. Better understanding of these molecular mechanisms will then potentially allow the development of novel therapeutics targeting the cognitive phenotype of WBS.

3.1.9 Additional Discussion¹⁰

As described herein, we have created a CRISPR/Cas9 based full Nsun5 knockout in mammalian cells. On the one hand we established NSUN5 knockout in HeLa cells and on the other hand we generated a Nsun5 knockout mouse model (C57BL/6J genetic background) by disruption of exon 1 and intron 1 with two loxP-sites. These systems allowed us to create the link between NSUN5, the specific rRNA modification and normal global protein translation, the latter being particularly affected by NSUN5 loss in highly proliferative cells. A combination of experiments demonstrated that upon loss of NSUN5, the overall protein synthesis was reduced, cell size and proliferation capacity were hampered. Remarkably, body weight of Nsun5 knockout mice was reduced compared to the control group. In the case of NSUN5, the results pointed towards the fact that loss of m⁵C3782 renders ribosomes unstable, which yeast and nematodes in contrast to mammalian cells are able to compensate under unstressed conditions.

Mammalian cells with high proliferation rates, such as cancer cells (HeLa, certain glioma cell lines under oxidative stress) and immortalized cell lines (MEF), seem to be susceptible to loss of NSUN5, whereas normal mouse tissues including kidney, liver, lung and bone marrow were only mildly affected. A recent report demonstrated that differential regulation of NSUN5 expression is happening at epigenetic level, since methylation of the NSUN5 promotor was high in some gliomas and primary tumors, but low in cervical and other malignancies (Heissenberger et al. 2019; Janin et al. 2019).

Some diseases are linked to defects of ribosomal components. Most of them are characterized by a hypo-proliferative phenotype such as congenital anomalies, anaemia and bone marrow failure in humans (De Keersmaecker et al. 2015). One example where NSUN5, amongst many other genes, is heterozygously deleted, is WBS. This malady is characterized by a mild to moderate cognitive impairment, including a reduction of cerebral volume by approximately 13% (Zhang et al. 2018). They further demonstrated that loss of Nsun5 led to deficits in memory capacity and spatial learning, which is likely to be connected to the WBS

¹⁰ This part is not included in the published manuscript (Heissenberger et al. 2019).

pathology. We were able to demonstrate that primary fibroblasts from WBS patients showed decreased

NSUN5 mRNA as well as protein levels resulting in a reduction of m⁵C3782 on 28S rRNA, which clearly indicates the gene-dosage relationship of the NSUN5 gene in WBS pathologies.

[illegible]




 N-terminal globular domain
 RNA methyltransferase domain
 C-terminal domain

Figure 14: Related to Figure 7 and Figure 11B: Full-length protein sequence alignment of Rcm1p and the human NSUN protein family. The full-length multiple protein sequence alignment of Rcm1p and the NSUN family (NSUN1 – NSUN7) is depicted. Colours indicate similarities. Two highly conserved cysteins required for covalent RNA substrate binding and subsequent release are indicated by asterisks (*). Protein domains of NSUN5 are highlighted by colours, as specified in the included legend.

A



B

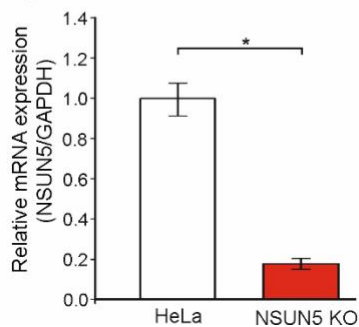


Figure 15: Related to Figure 8: CRISPR-Cas9 mediated gene editing of the NSUN5 locus reduced NSUN5 mRNA expression in HeLa. **A**, Sanger sequencing of genomic DNA from NSUN5 KO cells reveals translocation from genomic region 4q into the guide-RNA (gRNA) target site between intron 1 and exon 2 of the NSUN5 locus. An alignment of nine TOPO-sequencing clones with the NSUN5 reference sequence (NSUN5_reference.seq) is shown. Introns are highlighted in green, exons in orange and the gRNA in grey. **B**, NSUN5 mRNA expression was measured by RT-qPCR of HeLa and NSUN5 KO cells and showed decreased NSUN5 mRNA expression in NSUN5 KO cells. Error bars indicate standard deviation. n = 3 independent replicates. *p < 0.05, Student's t-test.

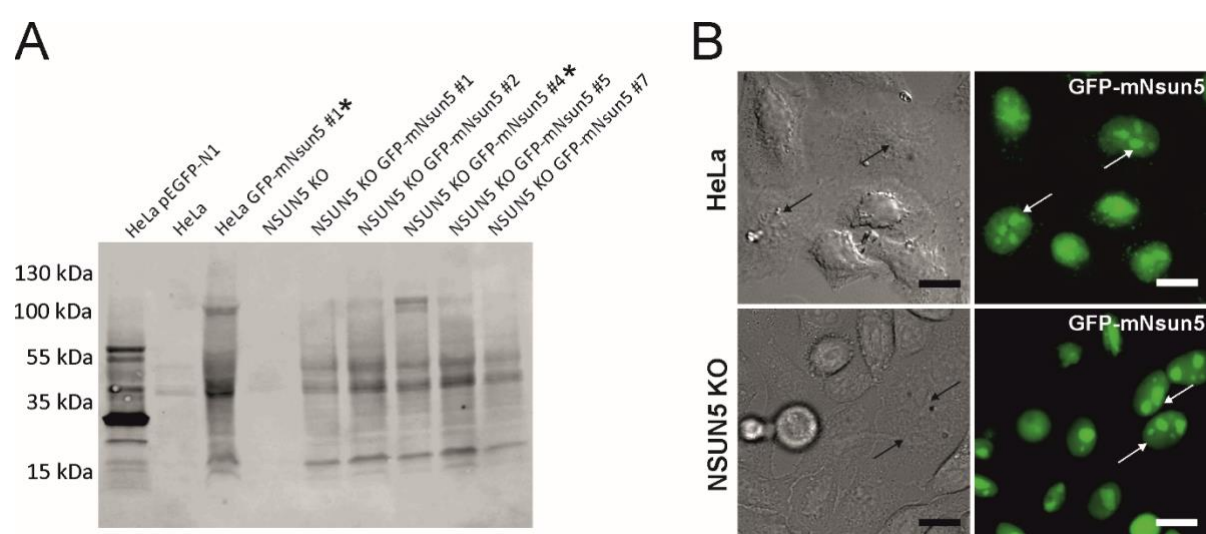


Figure 16: Related to Figure 8: Generation of stable HeLa and NSUN5 KO cell lines expressing endogenous levels of GFP-tagged mouse Nsun5. **A**, Western blot of GFP-Nsun5 constructs shows screening and selection of stable cell lines expressing BACmid-encoded GFP-mNsun5 in HeLa and NSUN5 KO cells. HeLa transiently expressing GFP (HeLa + pEGFP-N1) were included as control. Asterisks (*) indicate selected cell lines. Probing with α -GFP confirms the expected size of GFP-mNsun5 at around 80 kDa and of free GFP at 25 kDa. **B**, Fluorescence microscopy of HeLa GFP-mNsun5 and NSUN5 KO GFP-mNsun5 indicates localization of GFP-mNsun5 in nucleoli and nucleoplasm. Arrows indicate nucleoli. Scale bars represent 15 µm.

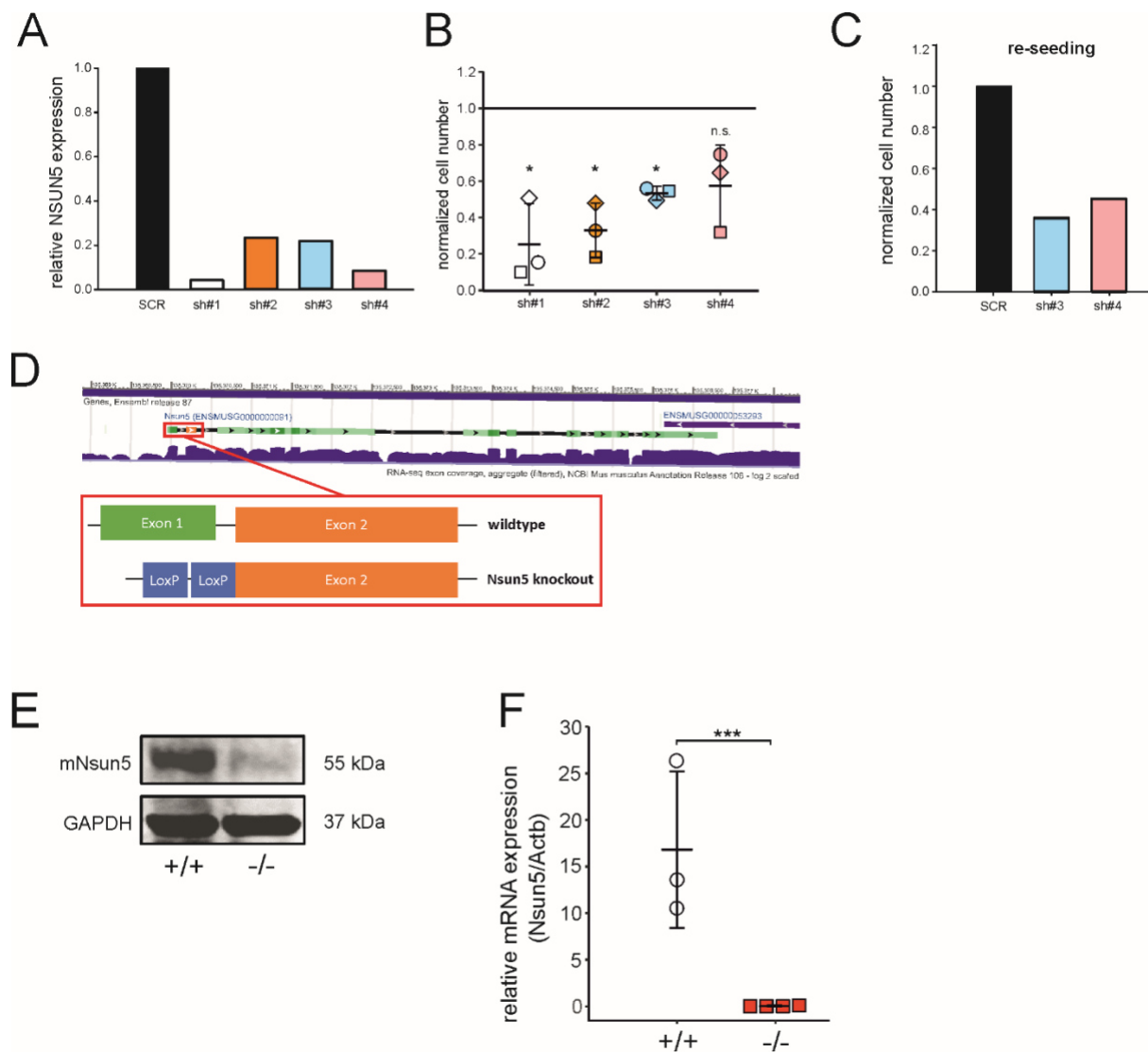


Figure 17: Related to Figure 8: Loss of NSUN5 decreases proliferation of primary cells and body weight of mice. **A**, RT-qPCR reveals knockdown of NSUN5 mRNA in fibroblasts upon transduction with four different shRNAs against NSUN5, compared to a non-hairpin forming control (SCR). **B**, Cell numbers of shRNA-transduced fibroblast strains were recorded after selection of stable transformants (10 – 31 days post transduction) and normalized to the SCR control. $n = 3$ independent experiments with strains from three different donors. $*p \leq 0.05$, n.s. = not significant, one sample t-test against expected value of 1. **C**, SCR, sh#3 and #4 of one replicate (squares in panel B) were re-seeded at equal cell numbers after selection of stable transformants (10 days post transduction) and counted 10 days after re-seeding. **D**, The design of the Nsun5 knockout mouse model is depicted. Exon 1, intron 1 and parts of exon 2 were replaced by two LoxP sites. **E**, Western blot confirms loss of Nsun5 protein expression in kidneys of wildtype (+/+) and knockout (-/-) mice. GAPDH was used as loading control. The blot was probed with Santa Cruz α -NSUN5. **F**, RT-qPCR confirms loss of Nsun5 mRNA expression. Data were normalized to Actb. Error bars indicate standard deviation. $n \geq 3$ animals. $***p < 0.005$. One-Way Anova followed by post-hoc Dunnet's test.

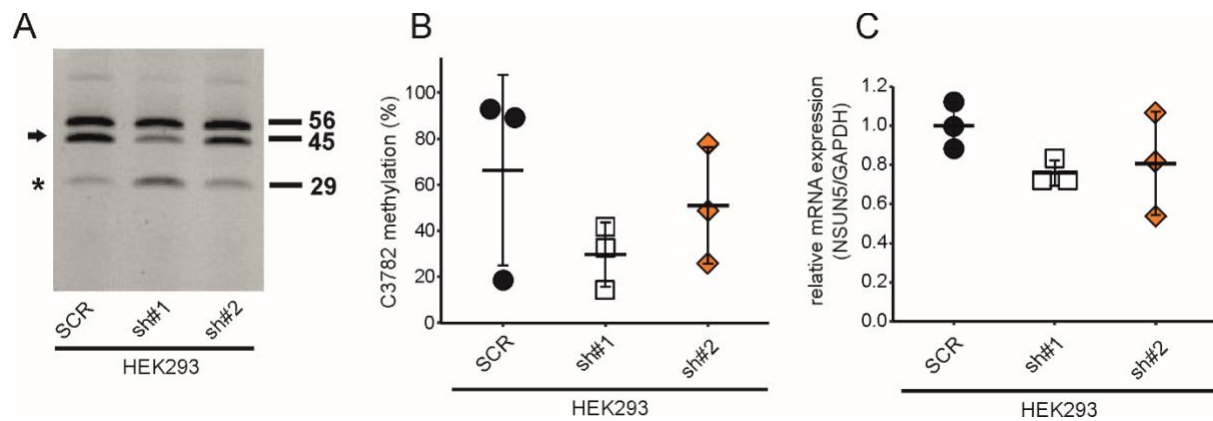


Figure 19: Related to Figure 10: shRNA-mediated knockdown of NSUN5 in HEK293 cells indicates a trend towards impaired C3782 methylation. **A**, COBRA assay indicates a trend towards decreased C3782 methylation in HEK293 cells upon shRNA-mediated knockdown of NSUN5. Arrow depicts the 45 bp fragment, representing methylation and the asterisk (*) indicates the 29 bp fragment, representing non-methylation. **B**, Quantification of the COBRA assay. $n = 3$ independent experiments. One-way Anova followed by Dunnet's post-hoc test does not reveal statistical significance. **C**, Relative expression levels of NSUN5 mRNA were determined by RT-qPCR. $n = 3$ independent experiments. One-way Anova followed by Dunnet's post-hoc test does not reveal statistical significance.

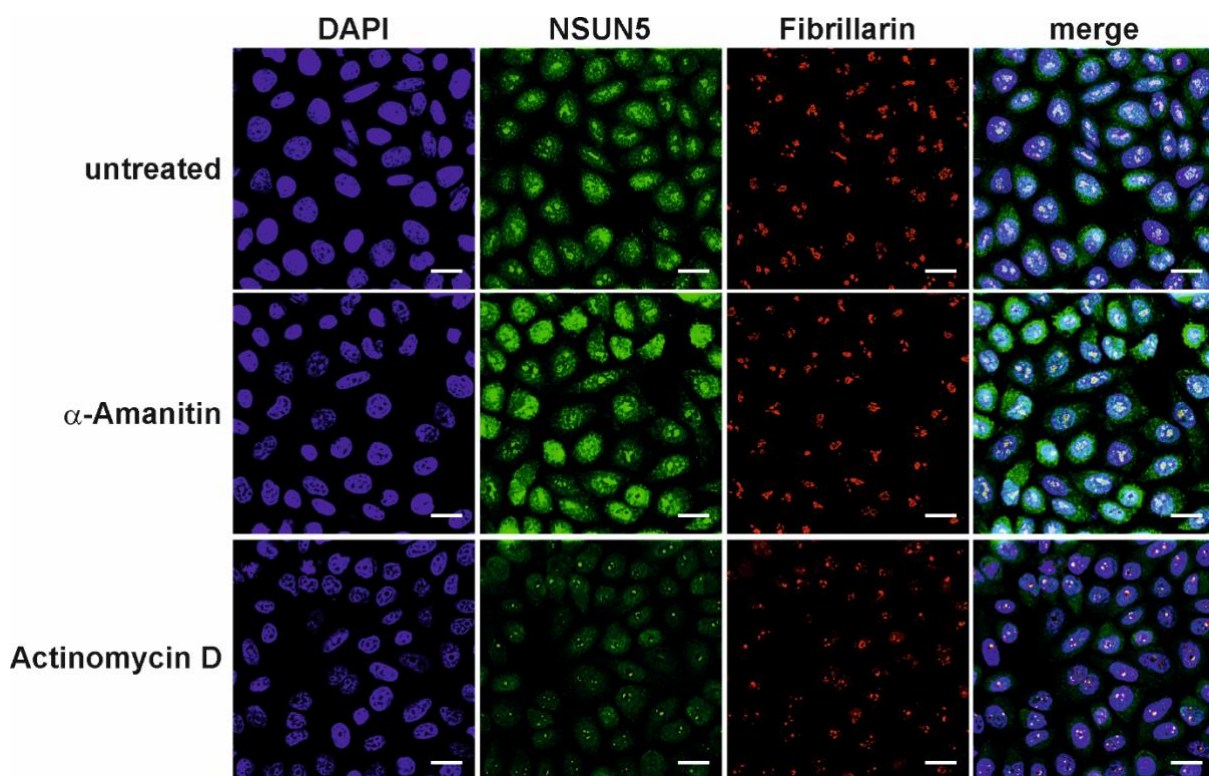


Figure 18: Related to Figure 11: RNA polymerase I activity targets NSUN5 to the nucleolus. HeLa cells were exposed to 50 $\mu\text{g}/\mu\text{L}$ α -Amanitin to block RNA Polymerase II and III or 50 $\text{ng}/\mu\text{L}$ Actinomycin D to block RNA Polymerase I, II and III. NSUN5 (green) and Fibrillarin (red) were visualized by indirect immunofluorescence staining. Fluorescence microscopy reveals nucleolar localization of NSUN5 and segregation to nucleolar caps upon inhibition of RNA polymerase I. Nuclei were counterstained with DAPI (blue). Images were processed by deconvolution and brightness and contrasts were adjusted. Scale bar represents 15 μm .

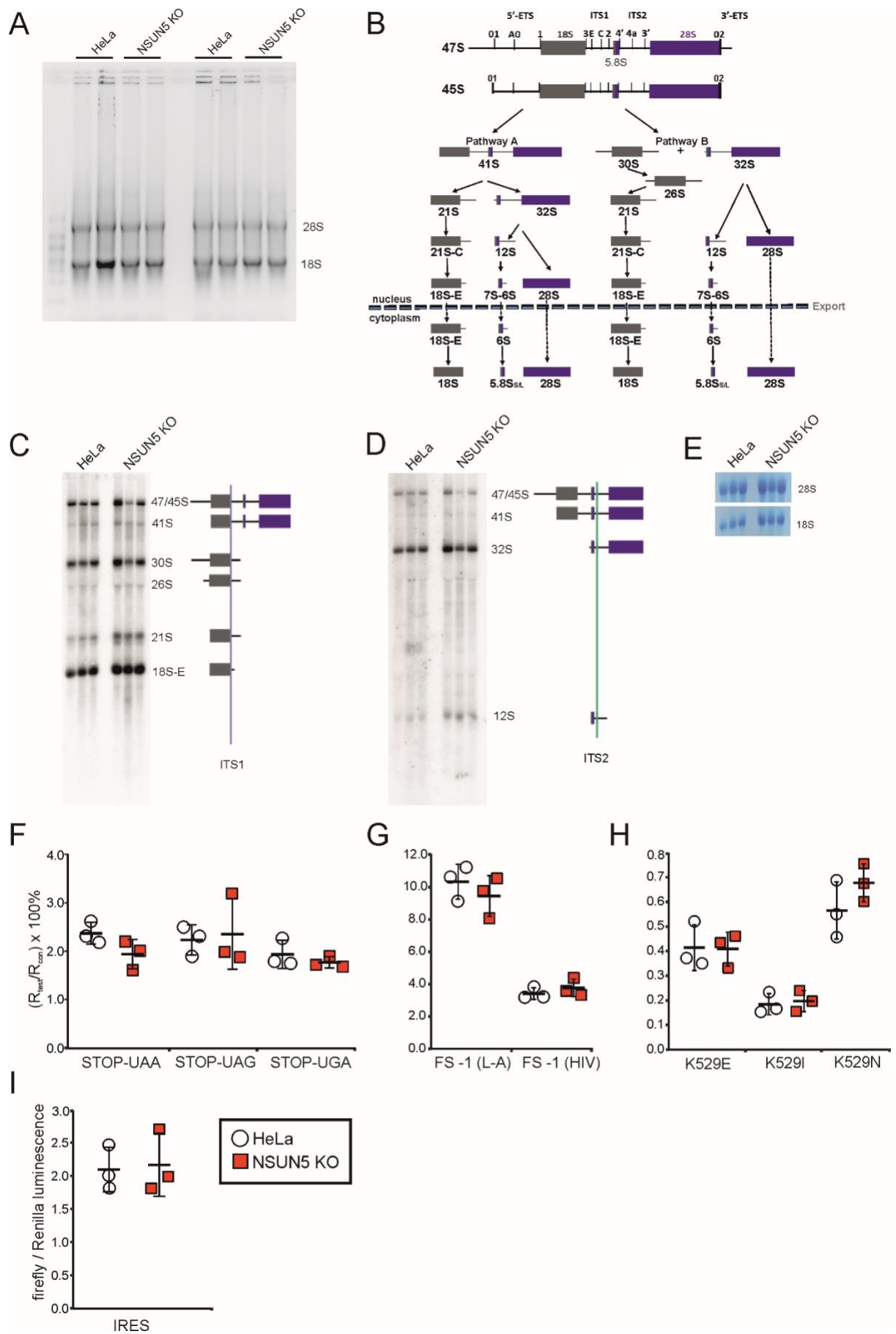


Figure 20: Related to Figure 12: Quantification of mature ribosomes and analysis of ribosome biogenesis did not reveal changes upon loss of NSUN5. **A**, Quantification of 28S and 18S rRNA fragments show no differences in mature ribosomes of HeLa compared to NSUN5 KO cells. $n = 2$ independent experiments with 2 technical replicates each. **B**, Scheme of human ribosome biogenesis. **C-E**, Northern blots using two specific pre-rRNA probes, ITS1 (**C**) and ITS2 (**D**), indicate no alterations in ribosome biogenesis in HeLa compared to NSUN5 KO cells. Methylene blue staining of 28S and 18S rRNA confirms equal loading (**E**). $n = 3$ replicates. **F-I**, Dual luciferase reporter assays show no statistically significant difference in translational fidelity upon loss of NSUN5 in HeLa cells as measured by read-through of all three stop codons (**F**), -1 frameshifting induced by viral sequences (FS -1 (L-A) and FS -1 (HIV)) (**G**), as well as amino acid misincorporation into the first (K529E), second (K529I) and third (K529N) codon position (**H**). Normalized luminescence relative to the respective control plasmids is shown. $n = 3$ independent replicates. Error bars indicate standard deviation. Two sample t-tests of control HeLa vs. NSUN5 KO. **I**, IRES-dependent translation as measured by a dual luciferase reporter assay does not reveal a significant difference between control HeLa and NSUN5 KO cells. $n = 3$ independent replicates. Error bars indicate standard deviation. Two sample t-tests of control HeLa vs. NSUN5 KO.

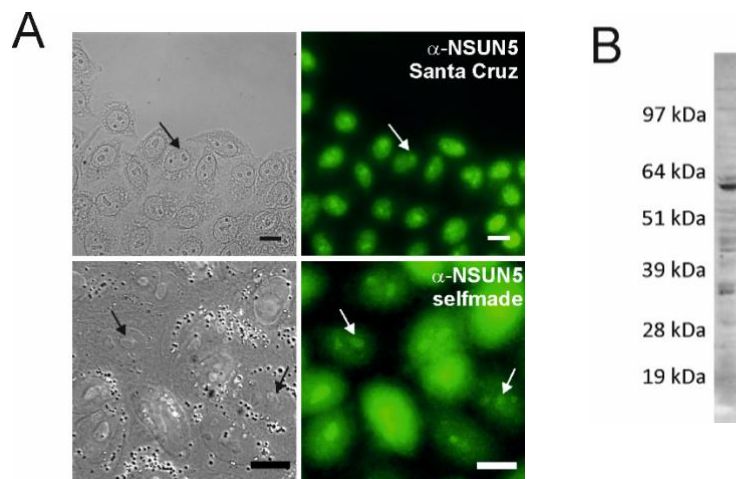


Figure 21: Related to experimental procedures: Characterization of selfmade anti-NSUN5 antibody. **A**, Brightfield and fluorescence microscopy showed similar nucleolar staining of endogenous NSUN5 in HeLa cells with both commercial and selfmade NSUN5 antibodies. Arrows indicate nucleoli. Scalebars represent 15 μ m. **B**, Western blot of a HeLa cell lysate probed with the selfmade α -NSUN5 antibody revealed a prominent band at ~60 kDa.

3.2 The ribosomal RNA m⁵C methyltransferase NSUN-1 modulates healthspan and oogenesis in *Caenorhabditis elegans*¹¹

Our knowledge about the repertoire of ribosomal RNA modifications and the enzymes responsible for installing them is constantly expanding. Previously, we reported that NSUN-5 is responsible for depositing m⁵C at position C2381 on the 26S rRNA in *Caenorhabditis elegans*.

Here, we show that NSUN-1 is writing the second known 26S rRNA m⁵C at position C2982. Depletion of *nsun-1* or *nsun-5* improved locomotion at midlife and resistance against heat stress, however, only soma-specific knockdown of *nsun-1* extended lifespan. Moreover, soma-specific knockdown of *nsun-1* reduced body size and impaired fecundity, suggesting non-cell-autonomous effects. While ribosome biogenesis and global protein synthesis were unaffected by *nsun-1* depletion, translation of specific mRNAs was remodelled leading to reduced production of collagens, loss of structural integrity of the cuticle and impaired barrier function.

We conclude that loss of a single enzyme required for rRNA methylation has profound and highly specific effects on organismal physiology.

3.2.1 NSUN-1 is responsible for writing m⁵C at position C2982 on *C. elegans* 26S rRNA

Previously, we showed that an m⁵C modification is introduced at position C2381 on the 26S rRNA of *C. elegans* large ribosomal subunit by NSUN-5 (Adamla et al. 2019; Schosserer et al. 2015), which is required to modulate animal lifespan and stress resistance (Schosserer et al. 2015). On this basis, we were interested to learn if other related rRNA methyltransferases in *C. elegans* might display similar properties.

¹¹ These data are published as a pre-print (Heissenberger et al. 2020, doi: <https://doi.org/10.1101/2020.03.16.993469>) and are currently under revision in eLife. Personal contributions: Planned experiments: Figure 1, 2, 3, 4, 5, 6, Suppl., Performed experiments: Figure 1, 2, 3, 4, 5, 6, Suppl., Analysed data: Figure 1, 2, 3, 4, 5, 6, Suppl. and wrote the manuscript.

Therefore, we investigated the RNA substrate of NSUN-1 (also formerly known as NOL-1, NOL-2 or W07E6.1) and its potential roles in worm physiology. NSUN-1 is also a member of the NOP2/Sun RNA methyltransferase family. Since there are only two known m⁵C residues on worm 26S rRNA (Trixl and Lusser 2019; Sharma and Lafontaine 2015b), one of them at C2381, being installed by NSUN-5, we speculated that NSUN-1 might be required for introducing the second m⁵C residue at position C2982. Notably, both 26S m⁵C sites are localized close to important functional regions of the ribosome, and they are highly conserved during evolution (Figure 22A,B).

In order to test if NSUN-1 is involved in large ribosomal subunit m⁵C methylation, 26S rRNA was purified from worms treated with siRNAs specific to NSUN-1-encoding mRNAs on sucrose gradients, digested to single nucleosides and analysed by quantitative HPLC. In our HPLC assay, the m⁵C nucleoside eluted at 12 min, as established with a m⁵C calibration control (data not shown).

The depletion of NSUN-1 was conducted in two genetic backgrounds: N2 (wildtype), and NL2099 (an RNAi-hypersensitive strain due to mutation in *rrf-3*) (Figure 22 and 28). Treating N2 worms with an empty control vector, not expressing any RNAi, did not significantly reduce the levels of 26S rRNA m⁵C methylation (Figure 22C, 97% instead of 100%). Interestingly, treating N2 worms with an RNAi construct targeting *nsun-1* led to a reduction of 26S rRNA m⁵C methylation by 35% (Figure 22C). In the NL2099 strain, *nsun-1* RNAi treatment also led to a reduction of 26S rRNA m⁵C methylation by 26% (Figure 22D).

As there are only two known modified m⁵C residues on worm 26S rRNA, and since one of them is introduced by NSUN-5 (Adamla et al. 2019; Schosserer et al. 2015), a complete loss of NSUN-1 activity was expected to result in a 50% decrease in m⁵C methylation. However, protein depletion achieved with RNAi is usually not complete. It is not clear why the level of m⁵C depletion was not higher in the RNAi hypersensitive strain in comparison to the N2 strain; nonetheless, RNAi-mediated depletion of *nsun-1* significantly reduced the levels of 26S rRNA m⁵C modification in both worm strains, thus, we conclude that NSUN-1 is responsible for 26S rRNA m⁵C methylation.

We analysed the 26S rRNA m⁵C levels in a *nsun-5* deletion strain as control (strain JGG1, Figure 22E). In this case, we observed a near 2-fold reduction in methylation (58% residual), as

expected from the known involvement of NSUN-5 in modification at position C2381. When *nsun-1* was additionally depleted by RNAi in the *nsun-5* knockout animals, the level of 26S rRNA m⁵C was further reduced to 43%, again in agreement with our conclusion that NSUN-1 is responsible for methylating the second position, C2982.

To further prove that NSUN-1 is not involved in C2381 modification, methylation levels at this position were specifically tested by Combined Bisulfite Restriction Analysis (COBRA) assay in animals depleted of *nsun-1* or *nsun-5*. This method is based on bisulfite conversion of total RNA, followed by PCR amplification and restriction digest, yielding two bands in case of methylation at C2381 and three bands in case of non-methylation (Adamla et al. 2019). As expected, only *nsun-5* depletion strongly reduced methylation at C2381, and there was no residual m⁵C2381 in the *nsun-5* knockout strain, while *nsun-1* RNAi had no effect on modification at this position (Figure 22F). Bisulfite sequencing is well-known to be sensitive to RNA secondary structure (Warnecke et al. 2002), which likely explains why, despite repeated attempts, we could not monitor modification at position C2982 by use of this technique.

In conclusion, NSUN-1 and NSUN-5 are each responsible for installing one m⁵C onto the worm 26S rRNA, with NSUN-1 being responsible for position C2982 and NSUN-5 for position C2381 under the *bona fide* assumption that indeed only two m⁵C positions are present as described (Sharma and Lafontaine 2015).

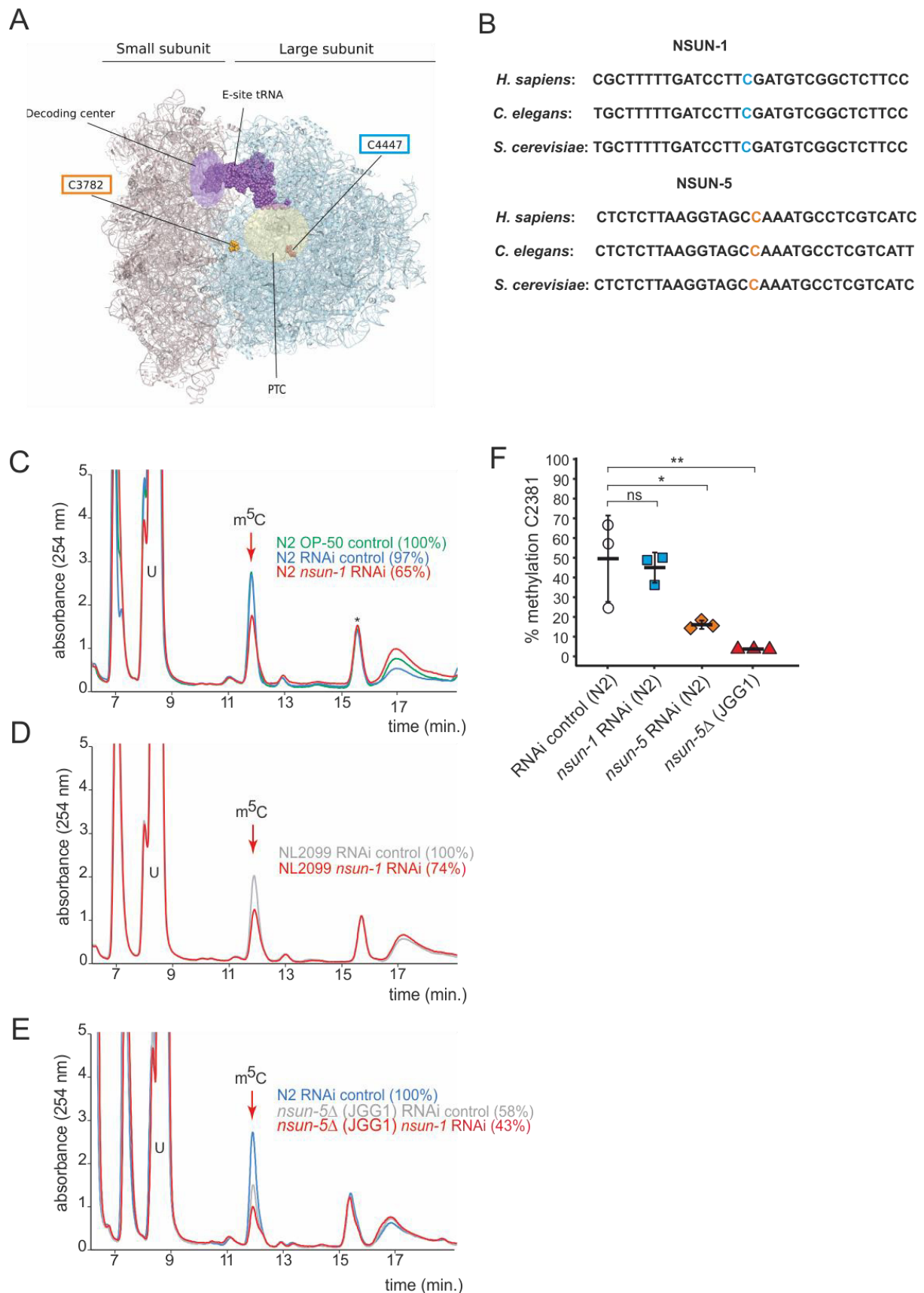


Figure 22: NSUN-1 is responsible for large ribosomal subunit 26S rRNA m⁵C methylation. **A**, Location of the two eukaryotic large ribosomal subunit m⁵C residues within the 3D structure of the human ribosome. For reference, important functional sites are indicated (DCS = decoding site, PTC = peptidyl transferase centre). In *C. elegans*, NSUN-1 is responsible for m⁵C2982 (this work) while NSUN-5 installs m⁵C2381 (Schosserer et al.

2015). **B**, Regions surrounding the sites modified by NSUN-1 and NSUN-5 are evolutionarily conserved between yeast, worms and humans. The modified cytosine is indicated. **C-E**, Purified 26S rRNA was isolated by sucrose gradient centrifugation, digested to single nucleotides and analysed by quantitative HPLC. *nsun-1* knockdown consistently leads to a decrease of m⁵C levels. **C**, N2 worms were analysed as either: untreated (OP-50), treated with an RNAi control or with a *nsun-1* targeting RNAi. **D**, NL2099 RNAi hypersensitive worms were treated with the RNAi control or with the *nsun-1* targeting RNAi. **E**, N2 strain treated with RNAi control and the *nsun-5* deletion strain (JGG1) treated with control RNAi or a *nsun-1* targeting RNAi. For quantification of m⁵C peak area, the peak was normalized to the peak eluting at 16 min (asterisk). **F**, Quantification of the enzymatic activity of NSUN-5 using the COBRA assay for N2 worms, subjected to either *nsun-5* or *nsun-1* RNAi, and the *nsun-5* mutant strain JGG1 (*nsun-5Δ*). Loss of *nsun-5* leads to significantly decreased methylation levels at C2381, whereas *nsun-1* RNAi does not alter methylation at this site (three independent biological replicates, one-way ANOVA with Dunnett's post test, $\alpha=0.05$, * $P<0.05$, ** $P<0.01$).

3.2.2 The somatic tissue-specific depletion of *nsun-1* extends healthy lifespan

Next, we investigated if knockdown of *nsun-1* modulates healthy lifespan in a similar fashion as *nsun-5* (Schosserer et al. 2015). For this aim, we depleted *nsun-1* by RNAi in N2 wildtype animals starting from day 0 of adulthood and, surprisingly, did not observe any extension of mean or maximum lifespan (Figure 23A). Consequently, we also evaluated the stress resistance of adult worms upon *nsun-1* or *nsun-5* depletion, as an increased health at an advanced age often improves resilience to adverse events (Lithgow et al. 1994). Indeed, depletion of either *nsun-1* or *nsun-5* increased resistance to heat stress compared to the RNAi control (Figure 23B). Similarly, we tracked the movement of animals exposed to either empty vector control or RNAi directed against *nsun-1* or *nsun-5* in a time course analysis, starting at day 1 of adulthood up to day 16. Interestingly, we observed a trend towards increased average speed in all three independent experiments at day 8 of adulthood in both *nsun-1* (+47.8%) and *nsun-5* (+34.7%) depleted animals compared to the control, and, to a lesser extent at day 12 (*nsun-1* RNAi: +10.2%, *nsun-5* RNAi: +73.5% compared to the control) (Figure 23C). Thus, while *nsun-1* knockdown does not extend lifespan, it improves the healthspan parameters thermotolerance and locomotion (Bansal et al. 2015; Rollins et al. 2017).

Intrigued that depletion of *nsun-1* did not extend the lifespan of *C. elegans* in a similar fashion as *nsun-5* did when whole adult animals were treated with RNAi, we reasoned that performing tissue-specific depletion of *nsun-1* might help us to further elucidate a possible effect on lifespan. We focused on the comparison of the germline and somatic tissues, because somatic maintenance and ageing are evolutionarily tightly connected (Kirkwood and Holliday 1979), and signals from the germline modulate *C. elegans* lifespan (Hsin and Kenyon

1999). In addition, only loss of soma- but not germline-specific eIF4E isoforms, which are central regulators of cap-dependent translation, extend nematode lifespan (Syntichaki et al. 2007). To test if *nsun-1* has similar specificity, we made use of worm strains sensitive to RNAi only in either the germline or somatic tissues. This is achieved, on the one hand by mutation of *rrf-1*, which is required for amplification of the dsRNA signal specifically in the somatic tissues (Sijen et al. 2001; Kumsta and Hansen 2012), and, on the other hand by functional loss of the argonaute protein *ppw-1* rendering the germline resistant to RNAi (Tijsterman et al. 2002). Interestingly, germline-specific *nsun-1* RNAi had no effect on animal lifespan (Figure 23D), but depletion of *nsun-1* in somatic tissues reproducibly increased mean lifespan by ~10% (Figure 23E).

In conclusion, both NSUN-1 and NSUN-5 m⁵C rRNA methyltransferases modulate thermotolerance and mobility of wildtype nematodes at midlife. Whole-animal *nsun-5* depletion expands mean lifespan by 17% (Schosserer et al. 2015), and in contrast to this, a 10% lifespan extension is only detected after depletion of *nsun-1* specifically in the somatic tissues.

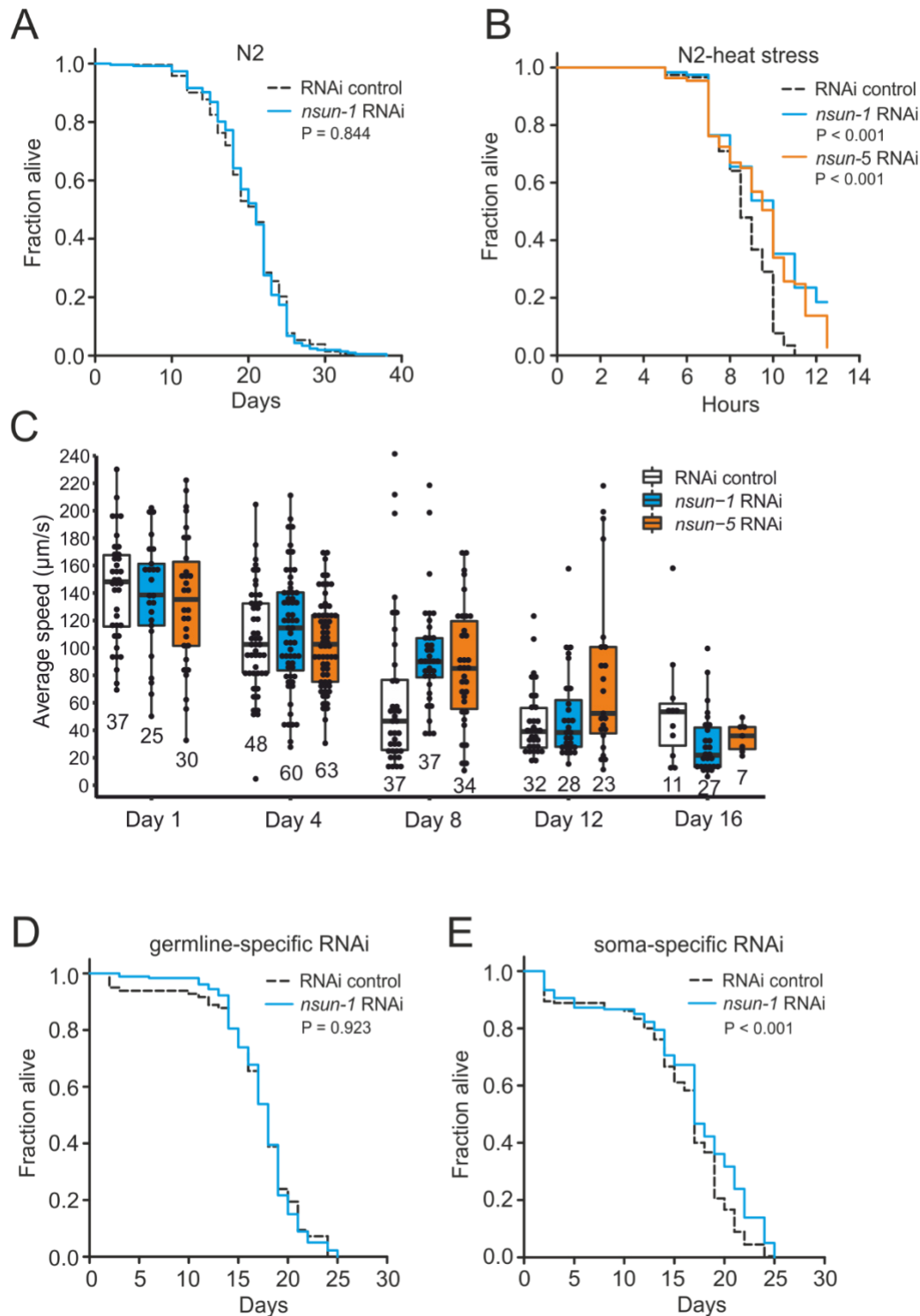


Figure 23: Depletion of *nsun-1* and *nsun-5* improves thermotolerance and locomotion. **A**, *nsun-1* whole-body RNAi (N2 wildtype strain) does not affect lifespan. Three pooled independent biological replicates are shown. Pooled $n \geq 208$ animals per condition, log-rank test, not significant. **B**, N2 wildtype animals treated with either *nsun-1* or *nsun-5* RNAi and subjected to heat stress (35°C) show increased survival compared to the RNAi control. Three pooled independent biological replicates are shown. Pooled $n \geq 90$ animals per condition, log rank, $P < 0.05$. **C**, Average speed [$\mu\text{m/s}$] of N2 wildtype worms as indicator of the health status was measured at day 1, 4, 8, 12 and 16 of adulthood. Movies of animals treated with either RNAi control, *nsun-1* or *nsun-5* RNAi were captured. One representative experiment is shown. Three biological replicates were performed with

similar outcome. Pooled $n \geq 20$ animals per condition at day 1. The black line indicates median. Two-way ANOVA $P < 0.01$ (for interaction day:RNAi treatment) **D-E**, Lifespan analysis of germline- (NL2098) and soma-specific RNAi strains (NL2550). Worms were treated with either RNAi control or *nsun-1* RNAi. Only soma-specific knockdown of *nsun-1* results in increased lifespan (**E**) while germline-specific knockdown does not (**D**) (two independent biological replicates, pooled $n(\text{NL2098}) \geq 160$ animals per condition, log-rank, not significant, pooled $n(\text{NL2550}) \geq 145$ per condition, log-rank, $P < 0.01$). A summary of the individual replicates of lifespan and thermotolerance experiments is provided in Table 3.

3.2.3 The somatic tissue-specific depletion of *nsun-1* affects body size, fecundity, and gonad maturation

The ‘disposable soma theory’ of ageing generally posits that long-lived species exhibit impaired fecundity and reduced number of progeny. The underlying cause is that energy is invested in the maintenance of somatic tissues instead of rapid reproduction (Kirkwood and Holliday 1979). In keeping with this theory, we expected that the absence of *nsun-1* in somatic tissues, which increased longevity, may reduce fecundity. Therefore, we first measured the brood size upon *nsun-1* and *nsun-5* depletion by RNAi. After reaching adulthood but before egg-laying, worms were transferred to individual wells of cell culture plates containing NGM-agar and fed with bacteria expressing the specific RNAi or, as control, the empty vector. Egg production was impaired upon *nsun-1* knockdown (reduced by 42%), but, surprisingly, this was not the case upon *nsun-5* knockdown (reduced by 2%) (Figure 24A). Egg production ceased rapidly after day one in all conditions (Figure 24 and 29A).

Thus far, all the experiments were performed on worms subjected to adult-onset *nsun-1* knockdown, as animals depleted of *nsun-1* during development were smaller and were infertile upon adulthood. To follow up on these observations, we measured mRNA expression levels of both m⁵C rRNA methyltransferases at different developmental stages including eggs, L1/L2 larvae, L3 larvae, L4 larvae and young adults. RT-qPCR indicated that both *nsun-1* and *nsun-5* mRNA levels constantly increase during development (Figure 24B). The same observation applied to mRNA levels of *nsun-2* and *nsun-4* (Figure 24 and 29B), indicating that all four members of the NSUN-protein family might play important roles during development.

To further assess whether *nsun-1* expression is indeed necessary for progressing faithfully through larval stages, we captured images of young adult animals subjected to larval-onset RNAi. The disparity in body size between RNAi control and *nsun-1* RNAi was apparent,

whereby *nsun-1* depleted animals showed reduced length by approximately 20%. Interestingly, this reduced body size was not seen upon *nsun-5* RNAi treatment (Figure 24C,D).

In addition, we imaged 3-day old animals using differential interference contrast (DIC) microscopy. Worms subjected to *nsun-1* knockdown displayed morphological alterations, specifically the gonad appeared severely distorted (Figure 24E). In contrast, RNAi control and *nsun-5* RNAi showed comparable morphology of distal and proximal gonads (Figure 24E). Consequently, we hypothesized that *nsun-1* RNAi treated worms might be arrested in early L4 larval stage when the gonad is not yet fully developed and animals still grow, instead of reaching normally adulthood after 3 days like RNAi control or *nsun-5* RNAi treated nematodes. To test this, we used the TP12 *kals12[col-19::GFP]* translational reporter strain, which expresses COL-19::GFP specifically upon reaching adulthood, but not during larval stages. Surprisingly, larval-onset RNAi against *nsun-1* or *nsun-5* did not reveal differences in the expression of COL-19::GFP as compared to RNAi control, suggesting that neither *nsun-1* nor *nsun-5* induce larval arrest (Figure 24F). Together with the reduced brood size upon adult-onset RNAi, these findings imply that loss of *nsun-1* induces phenotypic changes in the reproductive organs of *C. elegans* independent of development.

Since knockdown of *nsun-1* extended lifespan only when it was applied to somatic tissues, we hypothesized that body length might also be affected when these tissues are specifically targeted for depletion. To test this, we depleted *nsun-1* specifically in the germline or in somatic tissues using tissue-specific RNAi strains and measured body size during three consecutive days after adulthood was reached. While germline-specific knockdown of *nsun-1* did not induce any changes in body size (Figure 24G), soma-specific knockdown revealed a decrease in body length by 23% on day 1, 11% on day 2 and 12% on day 3 compared to the RNAi control (Figure 24H), phenocopying *nsun-1* depletion in wildtype animals after whole animal RNAi. Similarly, no effect of *nsun-1* knockdown was evident in another germline-specific RNAi strain, which was recently developed to enhance germline specificity (Zou et al. 2019) (Figure 24 and 29C).

In conclusion, *nsun-1* but not *nsun-5* depletion impairs body size and morphology of the gonad and leads to a significant reduction of brood size. Furthermore, these phenotypes are also observed when *nsun-1* is specifically knocked-down in somatic tissues, but not when depleted in the germline only.

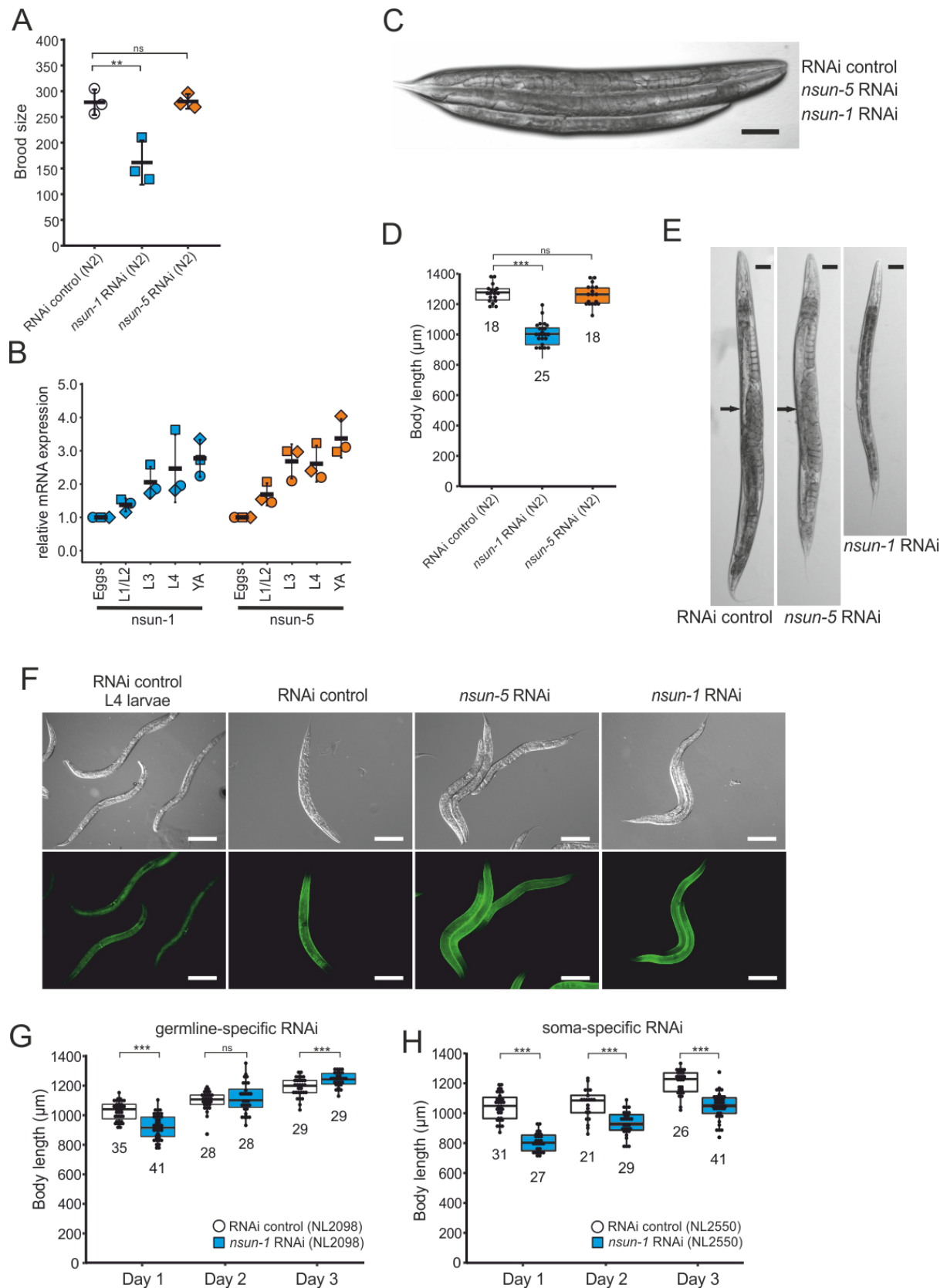


Figure 24: Loss of *nsun-1* reduces body size and impairs fecundity. **A**, Brood size analysis of adult-onset RNAi exposed animals. Eggs of individual worms were counted and the total number of eggs per worm is shown. Knockdown of *nsun-1* but not *nsun-5* induced a significant reduction in brood size compared to control RNAi (three independent experiments, $n = 5$ per condition and per experiment, one-way ANOVA with Dunnett's post test, $\alpha=0.05$, $**P<0.01$). Error bars indicate standard deviation. **B**, RT-qPCR analysis of wild-type animals at

different stages of development (eggs, L1/L2 larvae, L3 larvae, L4 larvae and young adults). *tba-1* was used for normalization and expression is shown relative to eggs. Error bars represent standard deviation of three biological replicates, one-sample t-test against expected value of 1 with multiple comparison correction by Holm's method did not reveal significant differences. **C**, Representative DIC images of larval-onset RNAi exposed nematodes show that only *nsun-1* but not *nsun-5* RNAi decreased the body length and altered general morphology compared to the RNAi control. Scale bar, 100 μ m. **D**, Quantification of mean body length of 1-2-day old adult worms. The body size of *nsun-1* RNAi treated worms was significantly reduced compared to the RNAi control and *nsun-5* RNAi. The experiment was independently performed two times and one representative replicate is shown. $n(\text{RNAi control}) = 18$, $n(\text{nsun-1 RNAi}) = 25$, $n(\text{nsun-5 RNAi}) = 19$, one-way ANOVA with Dunnett's post, $\alpha=0.05$, $***P<0.001$. Error bars represent standard deviation. **E**, Larval-onset *nsun-1* RNAi-treated adults had reduced body size and lacked embryos (arrow). Scale bar, 50 μ m. **F**, Loss of *nsun-1* did not impair expression of the adult-specific marker *col-19::GFP*. The TP12 strain was used and young adult animals treated with either control RNAi, *nsun-1* RNAi or *nsun-5* RNAi were imaged in DIC and fluorescent mode. L4 control RNAi worms, which did not express GFP specifically in the hypodermis, were used as negative control. Scale bar, 200 μ m. **G-H**, Soma- but not germline-specific *nsun-1* RNAi phenocopied the mean body length defect upon whole body *nsun-1* knockdown. The germline-specific NL2098 strain (**G**) and the soma specific NL2550 (**H**) strain were used and measured on three consecutive days after reaching adulthood. $n \geq 21$ for each day and condition. Two independent experiments were performed and one representative replicate is shown. Two-tailed t-test, $***P<0.001$. Error bars represent standard deviation.

3.2.4 NSUN-1 is required for the transition of meiotic germ cells to mature oocytes

To further investigate the mechanisms underlying impaired fecundity upon *nsun-1* knockdown, we analysed the morphology of the gonad in *nsun-1* depleted animals in more detail. The germline of adult hermaphrodites resides within the two U-shaped arms of the gonad, which contains germ cells at various stages of differentiation (Figure 24A). The gonad is sequentially developing from the proliferative germ cells near the distal tip cell, through the meiotic zone into the loop region, finally culminating in fully-formed oocytes in the proximal gonad (Pazdernik and Schedl 2013). The limiting factor for fecundity in self-fertilizing hermaphrodites is sperm produced in the spermatheca (Hodgkin and Barnes 1991).

Upon visualizing the germline cell nuclei with DAPI-staining, no oocytes were observed in worms after knockdown of *nsun-1* in contrast to RNAi control treated animals (Figure 24B). The mitotic zone at the distal end of the gonad appeared normal in *nsun-1* depleted animals, whereas oocyte production starting at the pachytene zone was hampered. Analysis of *GFP::RHO-1* and *NMY-2::GFP* expressing worm strains, which specifically express GFP in the germline, confirmed our observations (Figure 24C and 30). The gonads of control and *nsun-5* RNAi treated animals appeared normal, clearly depicting the different stages of *in-utero*

embryo development, whereas the germline of *nsun-1* RNAi treated animals displayed a strikingly altered morphology.

Since other phenotypes observed upon *nsun-1* depletion were detected in soma- but absent from germline-specific RNAi treated strains, we hypothesized that the somatic part of the gonad might specifically require NSUN-1 for normal oocyte production. Indeed, soma-specific depletion of *nsun-1* phenocopied the distorted gonad morphology of wildtype animals exposed to *nsun-1* RNAi (Figure 25D). Remarkably, upon germline-specific knockdown of *nsun-1*, the gonad appeared completely unaffected (Figure 25E and 31).

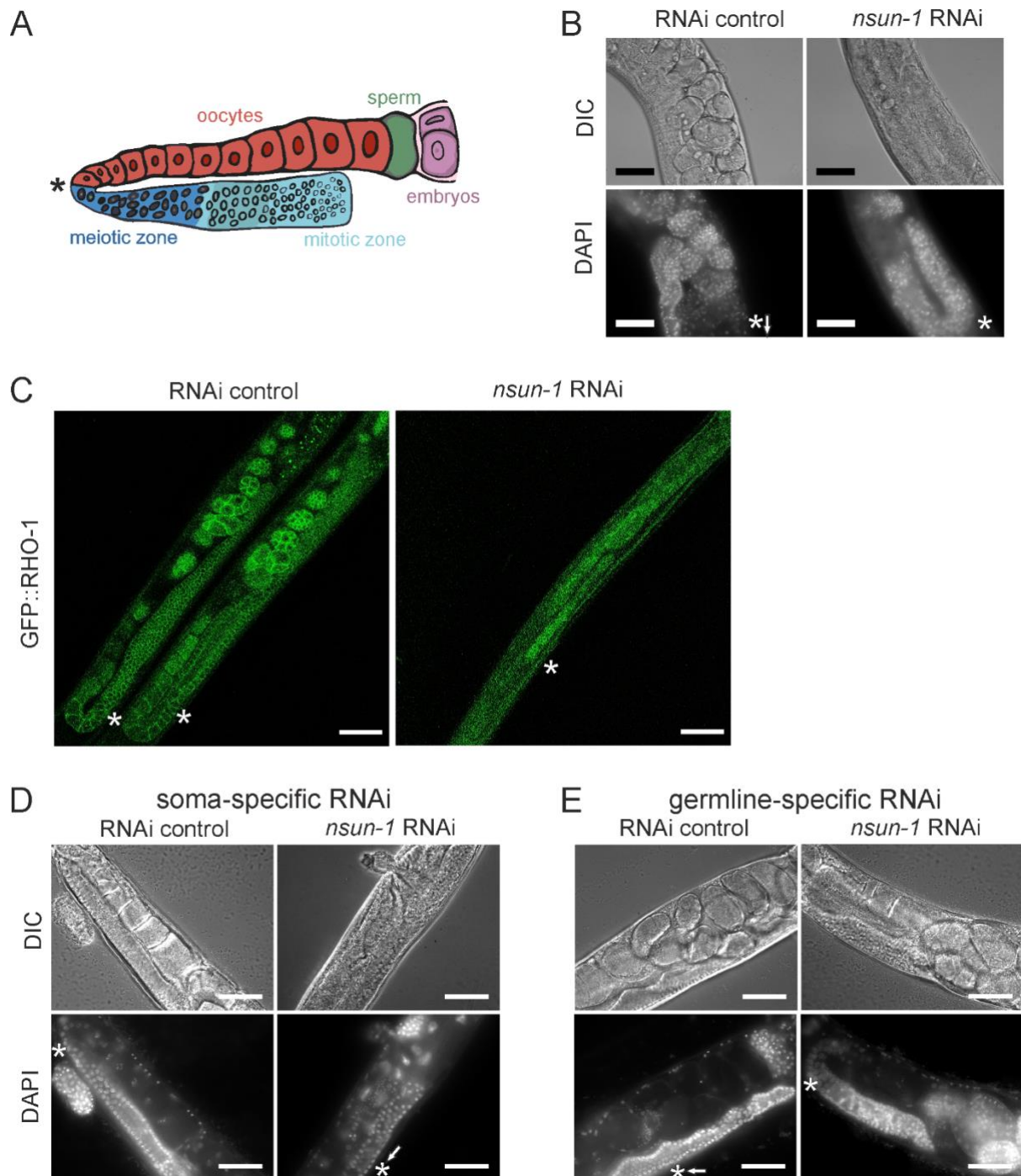


Figure 25: Soma-specific depletion of *nsun-1* blocks oogenesis. **A**, Schematic of one gonad arm in *C. elegans*. Germ cell replication starts in the distal mitotic zone. After passing through the meiotic zone, oocytes further mature and are fertilized by sperm produced in the spermatheca. In panels **A-E**, an asterisk indicates the gonadal region impaired in *nsun-1* RNAi exposed animals. This area corresponds to the transition between the meiotic zone and oocyte maturation. **B**, Microscopic image of one gonad arm of young adult worms subjected to either control or *nsun-1* RNAi. Worms were imaged in DIC mode and nuclei of fixed animals were stained with DAPI. Scale bar, 40 μ m. **C**, Confocal imaging of the gonad-specific GFP::RHO-1 expressing SA115 strain revealed altered gonad morphology upon *nsun-1* knockdown (see also Figure 4—figure supplement 1). Scale bar, 40 μ m. **D-E**, Soma- but not germline-specific *nsun-1* RNAi phenocopied altered gonad morphology upon whole body *nsun-1* depletion. NL2550 was used for soma- (**D**) and NL2098 for germline-specific knockdown (**E**). One gonad arm of one representative 2-day old adult animal was imaged in DIC mode and nuclei were stained with DAPI following fixation. Scale bar, 40 μ m.

3.2.5 NSUN-1 is not essential for pre-rRNA processing and global protein synthesis

Since the only known function of NSUN-1 and NSUN-5 is m⁵C methylation of rRNA, we reasoned that methylation-induced alterations of ribosome biogenesis and function might explain the observed phenotypes. Therefore, we tested if the presence of NSUN-1 or NSUN-5 is required for ribosomal subunit production and pre-rRNA processing. To this end, total RNA was extracted from worms treated with *nsun-1* RNAi, separated by denaturing agarose gel electrophoresis and processed for northern blot analysis (Figure 26A,B). Again, two reference worm strains were used (N2 and NL2099). Upon *nsun-1* knockdown, we observed a mild accumulation of the primary pre-rRNA transcript and of its immediate derivative, collectively referred to as species “a” (Figure 26A, (Bar et al. 2016; Saijou et al. 2004)), as well as a mild accumulation of the pre-rRNAs “b” and “c” (Figure 26A,B, see lane 1 and 3 as well as 5 and 6). Again, these findings were observed in both worm backgrounds tested, N2 and NL2099.

For comparison, we also analysed rRNA processing in *nsun-5* deletion worms (JGG1 strain) in presence and absence of NSUN-1 (*nsun-1* RNAi in JGG1). In both cases, we noted an important reduction in the overall production of ribosomal RNAs (Figure 26B,C), with an apparent increase of rRNA degradation (seen as an increase in accumulation of metastable RNA fragments, in particular underneath the 18S rRNA). Furthermore, we observed that NSUN-1 is not required for mature rRNA production as shown by the unaffected levels of mature 18S and 26S rRNAs (Figure 26C). This was confirmed by determining the 26S/18S ratio, which was 1.0 as expected since both rRNAs are produced from a single polycistronic transcript (Figure 26C). The levels of the other two mature rRNAs (5S and 5.8S) were also unaffected (Figure 26 and 32). This behaviour was shown in both worm backgrounds, N2 and NL2099, used. The overall decrease in mature ribosome production observed in *nsun-5* deletion worms did not affect the ratio of mature ribosomal subunits (26S/18S ratio of 1.0) (Figure 26C). In agreement with the reduced amounts of 18S and 26S rRNA observed in *nsun-5* deletion worms, total amounts of all precursors detected were reduced (Figure 26B). Analysis of low molecular weight RNAs by acrylamide gel electrophoresis, revealed absence of NSUN-5 to severely inhibit processing in the internal transcribed spacer 2 (ITS2), which separates the 5.8S and 26S

rRNAs on large precursors. This was illustrated by the accumulation of 3'-extended forms of 5.8S, and of short RNA degradation products (Figure 26 and 32, see lanes 3 and 4). Depletion of *nsun-1* partially suppressed the effect of *nsun-5* deletion: the overall production of mature rRNA and, in particular, the amount of mature 26S rRNA was increased (ratio of 1.2) (Figure 26C). Consistently, the accumulation of 3'-extended forms of 5.8S and of short RNA degradation products was reduced (Figure 26 and 32).

In order to test if mature ribosomes of animals lacking any of the two m⁵C rRNA methyltransferases might be functionally defective, we analysed global protein synthesis by incorporation of puromycin in N2 worms treated with either RNAi control, *nsun-1* or *nsun-5* RNAi. Worms were exposed to puromycin for three hours at room temperature. Following lysis, puromycin incorporation was measured by western blot with an anti-puromycin antibody (Figure 26D). Quantification of three independent experiments revealed no changes in global protein synthesis (Figure 26E). We also performed polysome profiling which provides a “snapshot” of the pool of translationally active ribosomes. Comparison and quantification of profiles obtained from control and *nsun-1* knockdown nematodes did not reveal any differences in the distribution of free subunits, monosomes and polysomes (Figure 26F,G). This agrees with the absence of global protein translation inhibition in the metabolic (puromycin) labelling assay (Figure 26E).

In conclusion, NSUN-1 is not required for rRNA processing nor for global translation. On the contrary, the amounts of ribosomal subunits were reduced in the absence of NSUN-5. The ribosomal biogenesis alterations observed upon *nsun-5* depletion result from a combination of processing inhibitions in ITS2 and increased rRNA intermediates turnover. However, global translation was not detectably affected.

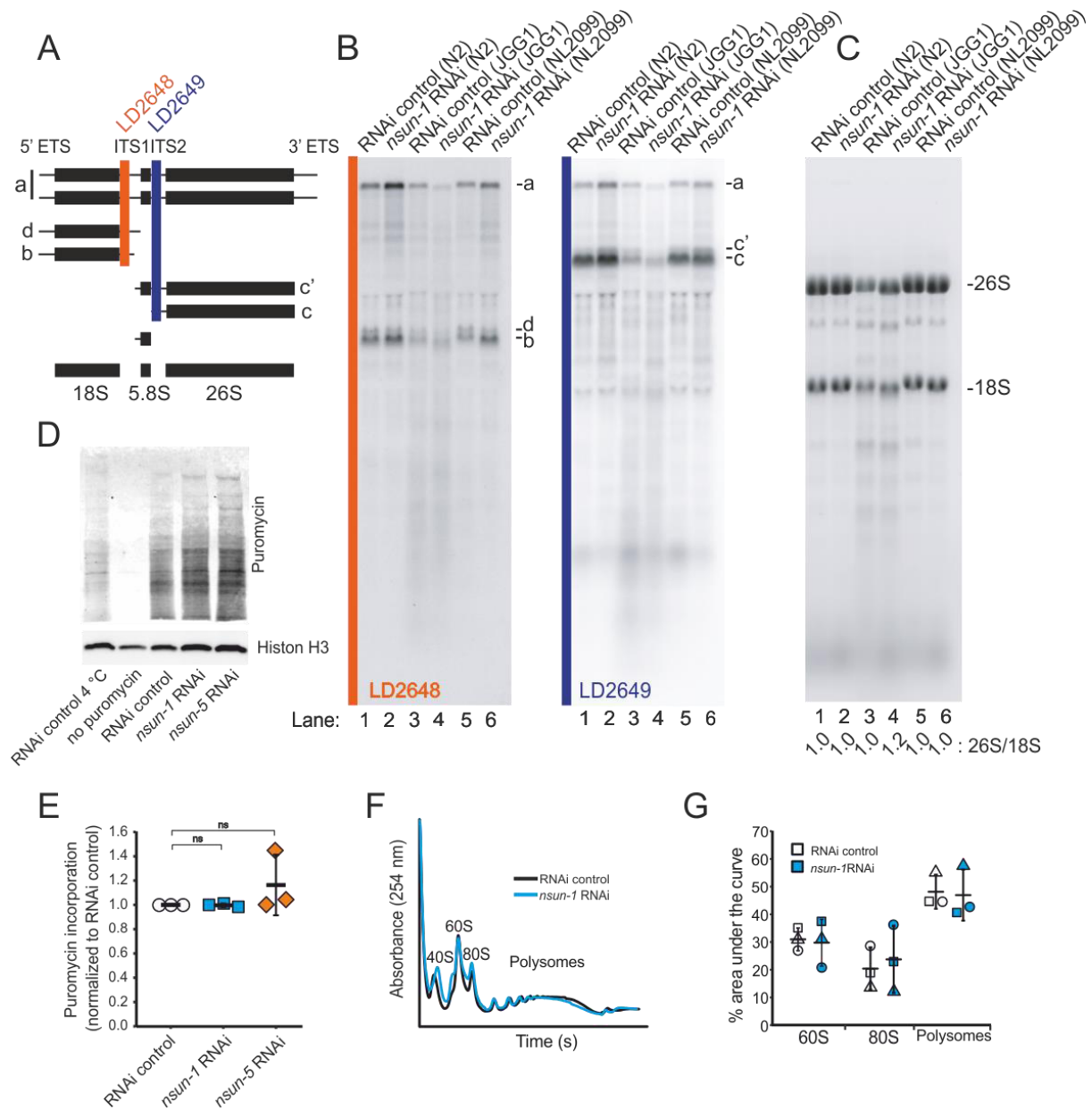


Figure 26: NSUN-1 and NSUN-5 are only partially required for rRNA processing and not for global translation. **A**, Schematics of pre-rRNA processing intermediates in *C. elegans* and probes (LD2648 and LD2649) used in pre-rRNA processing analysis (see panel B). **B**, Pre-rRNA processing analysis. Total RNA extracted from the indicated strains were separated on denaturing agarose gels and processed for northern blotting. The probes (LD2648 and LD2649) used to detect the pre-rRNA intermediates a, b, c, c', and d are indicated. **C**, Steady-state levels of mature rRNAs (18S and 26S) analysed by ethidium bromide staining and quantified by densitometry. The 26S/18S ratio is indicated. **D**, Total protein synthesis of N2 animals treated with RNAi control, nsun-1 or nsun-5 RNAi. RNAi control treated worms at either 4°C or without puromycin exposure were used as negative controls. Protein synthesis was measured by puromycin exposure for 3 h and western blot using a puromycin-specific antibody. The experiment was performed in three independent replicates. One representative replicate is shown. Histone H3 was used as loading control. **E**, Quantification of western blots in D (three biological replicates, one-sample t-test against an expected value of 1, $\alpha=0.05$, not significant). **F-G**, Polysome analysis indicating that global translation is not affected by nsun-1 depletion. Free small subunit (40S), large subunit (60S), monosome (80S) and polysome fractions were detected by UV₂₅₄ monitoring. Representative profiles are shown. **G**, Quantification of 60S, 80S and polysome fractions of three independent experiments reveals no changes between nsun-1 knockdown and RNAi control.

3.2.6 mRNAs encoding cuticle collagens are translationally repressed upon *nsun-1* knockdown

Since depletion of *nsun-1* did not affect global protein synthesis, we hypothesized that loss of 26S rRNA m⁵C methylation might modulate the translation of specific mRNAs, as was previously observed after Rcm1 (NSUN-5 homolog) depletion in yeast (Schosserer et al. 2015). To test this possibility, we isolated mRNAs contained in the polysome fraction, systematically sequenced them by RNAseq and compared their respective abundance in polysomes versus total mRNAs contained in the lysate before fractionation. We considered only protein-coding mRNAs with a minimum fold change of 2 between translome and transcriptome and an adjusted p-value cut-off at 0.05 (Figure 27A). The translation of more mRNAs was repressed (RNAi control: 599, *nsun-1* RNAi: 536) than promoted (RNAi control: 94, *nsun-1* RNAi: 84). Since the composition of 3' UTRs can affect translation (Tushev et al. 2018), we analysed GC-content, length and minimal free folding energy of all coding, promoted and repressed mRNAs in our dataset (Figure 27B). Interestingly, all three features significantly differed between RNAi control and *nsun-1* RNAi in promoted and repressed mRNAs ($p < 0.05$), while they remained unchanged when analysing all coding mRNAs present in the dataset. These findings suggest that loss of *nsun-1* causes the translation of specific subsets of mRNAs based on the composition and length of their 3'UTRs. Moreover, 3'UTRs of mRNAs repressed by *nsun-1* depletion were exclusively and significantly enriched ($p < 0.001$) for several binding motifs of ASD-2, GLD-1 and RSP-3. All three RNA binding proteins play essential roles in *C. elegans* development (Lee and Schedl 2010; Longman et al. 2000) and were not differentially regulated in the transcriptome between *nol-1* RNAi and RNAi control.

To further understand the mechanistic link between differential translation and the phenotypes observed upon *nsun-1* knockdown, we performed GO-term enrichment analysis. Among others, GO terms associated with collagens, structural integrity of the cuticle and embryo development were significantly enriched amongst those mRNAs, which were translationally repressed by *nsun-1* knockdown (Figure 27C).

Since three collagens (*col-35*, *col-36* and *col-37*) were also among the five most strongly repressed genes upon loss of *nsun-1* (Figure 27A), we decided to assess whether collagen deposition is indeed altered. For this aim, we performed a specific histological staining

protocol in which young collagen is stained blue and mature collagen is stained pink to brownish-red (Teuscher et al. 2019; Herovici 1963). While young adult worms exposed to RNAi control showed presence of both young and mature collagen, animals subjected to *nsun-1* RNAi displayed a strikingly reduced collagen deposition compared to the cytoplasmatic counter-stain (yellow) (Figure 27D).

Interestingly, we repeatedly observed an increased fraction of animals displaying gonad extrusion upon *nsun-1* RNAi, which might be caused by loss of cuticle structural integrity. To quantify this phenotype, we classified mid-aged animals according to the grade of gonad extrusion into three categories: i) no visible signs of gonad extrusion, ii) mild extrusion, or iii) severe extrusion (Figure 27 and 32). Upon *nsun-1* depletion, 134 of 220 animals (~60%) showed mild to severe extrusion of the gonad (categories ii and iii), while no extrusion was observed in any of the tested 50 RNAi control nematodes (Figure 27E). To assess further physiological consequences of altered collagen deposition, we tested cuticle barrier activity. This assay is based on the principle Hoechst33342 dye being membrane permeable, but cuticle impermeable. As previously described by Ewald et al. 2015, worms were grouped into four categories: i) not permeable (no stained nuclei in the animal tail region), ii) mildly permeable (< 5 stained nuclei), iii) permeable (5-10 stained nuclei), or iv) highly permeable (>10 stained nuclei) (Figure 27 and 32). Consistent with a change of several collagens, *nsun-1* RNAi caused cuticle permeability (categories ii, iii and iv) in 26 of 46 animals (~56%) compared to only 5 of 51 RNAi control animals (~10%) (Figure 27F).

Taken together, this indicates that NSUN-1 is partially required for translation of several cuticle collagens, which might not only explain the loss of gonad integrity, but also the increased cuticle permeability upon *nsun-1* depletion. Moreover, several mRNAs whose translation depends on NSUN-1 are associated with embryogenesis and enriched for binding motifs of known regulators of nematode development.

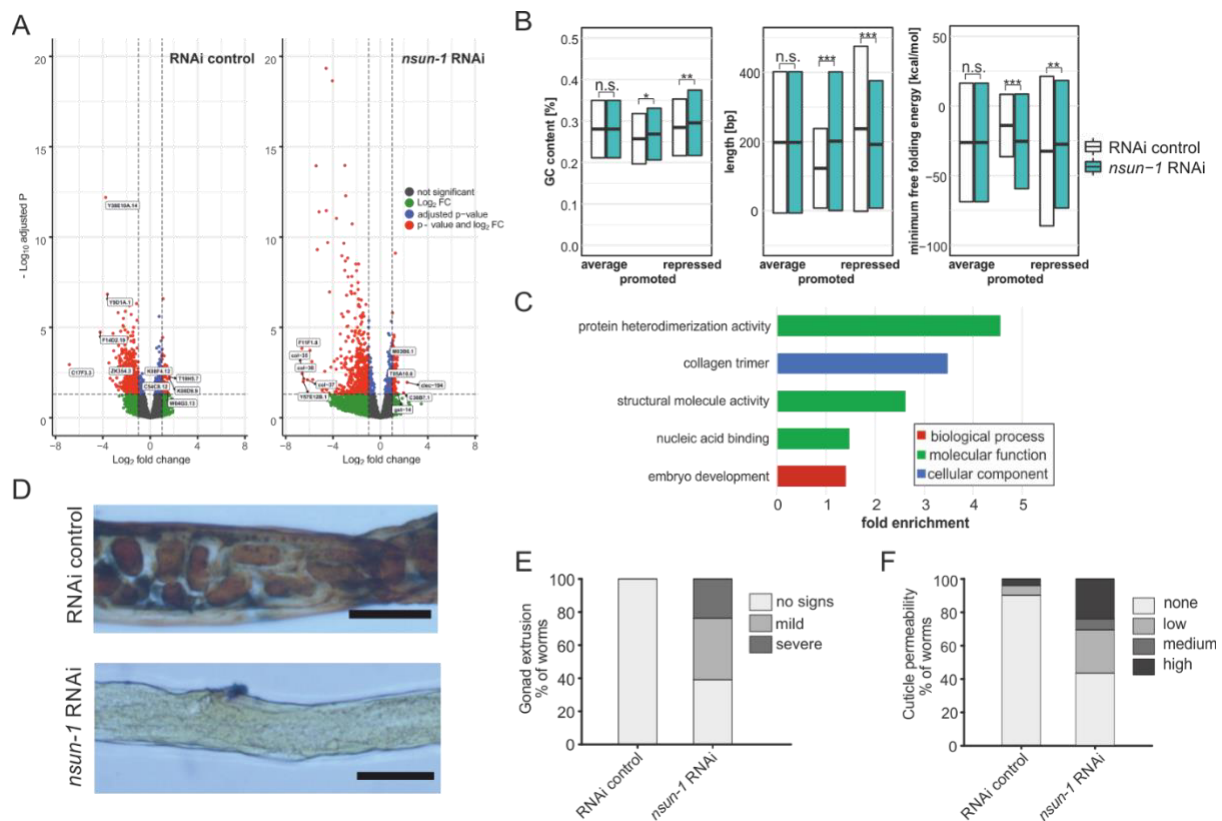


Figure 27: *nsun-1* depletion modulates selective translation of collagens and induces gonad extrusion and loss of barrier function. **A**, Volcano plots of selectively translated genes after RNAi control and *nsun-1* RNAi exposure. Significantly regulated genes (adjusted $p < 0.05$ and fold-change > 2) between polysome fraction and total mRNAs are depicted in red, genes with a two-fold up- or down-regulation but an adjusted p-value (FDR/Benjamini and Hochberg) above 0.05 in green, genes with an adjusted p-value below 0.05 but less than two-fold change in expression in blue, and not significantly regulated genes in grey. The top five up- or down-regulated genes based on their fold change are indicated. **B**, Characteristics of the 3'UTRs of mRNAs with significantly promoted or repressed polysome enrichment (adjusted $p < 0.1$, fold-change > 2). GC content (in %), length (in bp) and minimum free folding energy [kcal/mol] are shown. Boxes indicate mean \pm SD (for GC content and length) or mean \pm SEM (for minimum free folding energy). Wilcoxon rank sum test, * $p < 0.05$, ** $p < 0.01$, *** $p < 0.001$. **C**, Biological GO terms enriched among genes with repressed translation (adjusted $p < 0.1$, fold-change > 2) upon *nsun-1* depletion. Modified Fisher's exact test, $p < 0.05$. **D**, Histological staining (Herovici) to assess collagen deposition. Worms exposed to control RNAi show presence of both young (blue) and mature (pink to brownish-red) collagen whereas animals subjected to *nsun-1* RNAi display less collagen deposition. The cytoplasm is counterstained in yellow. Representative images of the region surrounding the gonad are shown. Two independent experiments with a minimum of 10 animals each were performed with similar outcome. Scale-bar, 80 μ m. **E**, Quantification of gonad extrusion upon *nsun-1* depletion compared to RNAi control. 8-9 day old adult animals were classified into three categories according to the severance of gonad extrusion ('no signs', 'mild', 'severe', see Figure 6–figure supplement 1A). The experiment was independently performed two times with similar outcome. One representative replicate is shown. $n \geq 50$ animals per replicate. Modified Fisher's exact test on the raw count values, $p < 0.001$. **F**, Quantification of cuticle barrier function upon *nsun-1* depletion compared to RNAi control. Young adult animals were exposed to Hoechst 33342, which is membrane-permeable but cuticle-impermeable. Stained nuclei were counted exclusively in the tail region to exclude intestinal autofluorescence and classified into four categories accordingly ('none', 'low', 'medium', 'high', see Figure 6–figure supplement 1B). Three independent experiments were pooled. $n(\text{RNAi control}) = 51$, $n(\text{nsun-1 RNAi}) = 46$. Modified Fisher's exact test on the raw count values, $p < 0.001$.

3.2.7 Discussion and Conclusion

Although rRNAs are universally modified at functionally relevant positions, little is known about the biological functions and pathological roles of RNA methylation sites, or about their potential readers, writers and erasers (Sharma and Lafontaine 2015b). In this work we have investigated the molecular and physiological roles of two structurally related Sun-domain-containing RNA methyltransferases, NSUN-1 and NSUN-5 in *C. elegans*, each responsible for writing one m⁵C mark on 26S rRNA. We further describe NSUN-1 as a *bona fide* m⁵C rRNA writer enzyme that, if missing, directly entails physiological and developmental consequences. We conclude that, molecularly, loss of NSUN-1 function leads to translational remodelling with profound consequences on cell homeostasis, exemplified by loss of cuticle barrier function, and highly specific developmental defects, including oocyte maturation failure. We further suggest that extrusion of the gonad and loss of cuticle barrier function are directly caused by reduced expression of collagens, while the developmental defects are associated with altered expression of several important developmental regulators. We summarized the observed RNAi phenotypes in different strain backgrounds in Table 2.

According to the ‘disposable soma theory of aging’, a balance between somatic repair and reproduction exists. Depending on the current environment, an organism may direct the available energy either to maintenance of the germline and thereby ensuring efficient reproduction, or to the homeostasis of somatic cells including the prevention of DNA damage accumulation (Kirkwood and Holliday 1979). While most of the known genetic and nutritional interventions increase the lifespan of organisms, they antagonistically also reduce growth, fecundity and body size (Kapahi 2010; Kenyon et al. 1993). Indeed, reduction of overall protein synthesis by genetic, pharmacological or dietary interventions was reproducibly shown to extend longevity in different ageing model organisms (Chiocchetti et al. 2007; Masoro 2005; Kaeberlein et al. 2005; Curran and Ruvkun 2007; Pan et al. 2007; Hansen et al. 2007). These reports clearly established protein synthesis as an important regulator of the ageing process at the interface between somatic maintenance and reproduction. Thus, we were surprised to find that despite their ability to modulate healthy ageing and to methylate rRNA, neither NSUN-1 nor NSUN-5 were required for global protein synthesis in worms under the conditions tested. In the case of NSUN-5 depletion, we previously found overall

translation to be decreased in mammalian cells (Heissenberger et al. 2019), but not in yeast (Schosserer et al. 2015). We reasoned that the higher complexity of mammalian ribosomes and associated factors might render them more vulnerable to alterations of rRNA secondary structure, for example by loss of a single base modification, than ribosomes from yeast and nematodes.

As ribosome biogenesis or global translational activity *per se* were not severely affected by loss of NSUN-1, the idea of a mechanism to ‘specialize’ the ribosome by rRNA modifications for selective mRNA translation seems attractive (Simsek and Barna 2017). Indeed, lack of NSUN-1 and presumably the methylation at C2982 resulted in decreased translation of mRNAs containing GLD-1 and ASD-2 binding sites. These two proteins are closely related members of the STAR protein family involved in mRNA binding, splicing and nuclear export of mRNAs. While the molecular functions of ASD-2 are only poorly understood, the role of GLD-1 in embryonic development is well characterized (Lee and Schedl 2010). GLD-1 levels are highest in the pachytene (also referred to as meiotic zone), where GLD-1 acts as a translational repressor of mRNAs modulating oogenesis. At the transition zone between the pachytene and the diplotene, GLD-1 levels sharply decrease and previously repressed mRNAs are consequently translated. Since the gonads of *nsun-1* knockdown animals appeared defective precisely at this transition and GLD-1 target mRNAs were repressed, we speculate that either ribosomes lacking the methylation at C2982 have generally low affinity for these mRNAs, or that translational repression by GLD-1 is never fully relieved. Although the expression of GLD-1 itself was not differentially regulated between control and *nsun-1* depleted animals at transcription or translation level (Supplemental Data File 1 and 3), multiple direct or indirect interactions with NSUN-1 to modulate ribosome function are still conceivable and will require further studies.

Previously, Curran and Ruvkun reported that depletion of *nsun-1* (W07E6.1) by adult-onset RNAi was able to extend lifespan in *C. elegans* (Curran and Ruvkun 2007). The authors used for their high throughput screen a strain carrying a mutation in the *eri-1* gene, rendering it hypersensitive to RNAi in the whole body, but especially in neurons and in the somatic gonad (Kennedy et al. 2004). In this study, we conducted a whole-body knockdown in N2 wildtype animals, but could not verify these previous findings on lifespan, although thermotolerance and the health status of mid-aged nematodes, as assessed by quantifying locomotion

behaviour, were elevated. However, when knocking-down *nsun-1* specifically in somatic tissues, but not in the germline, we observed a lifespan extension. The N2 wildtype strain is usually resistant to RNAi in the somatic gonad and neurons. Thus, we hypothesize that depletion of *nsun-1* specifically in the somatic part of the gonad is required for lifespan extension, which is only effectively realised in the *eri-1* and *ppw-1* mutant strains, but not in N2 wildtype animals. Intriguingly, these findings further suggest possible non-cell-autonomous effects of single RNA methylations, since modulation of NSUN-1 levels in somatic cells profoundly affected distinct cells of the germline.

The developing gonad of L1 larvae consists of two primordial germ cells and two surrounding somatic gonad precursor niche cells. The crosstalk between these two cell types, which form the germline and somatic part of the gonad at later stages of larval development, was already described to modulate ageing and stress responses. Laser depletion of both primordial germ cells extends lifespan via insulin/IGF-signalling, while animals with an additional depletion of the two somatic gonad precursor cells have a normal lifespan (Hsin and Kenyon 1999). Of potential relevance to our study is a recent report by Ou and coworkers, who demonstrated that IFE-4 regulates the response to DNA damage in primordial germ cells in a non-cell-autonomous manner via FGF-like signalling. Soma-specific IFE-4 is involved in the specific translation of a subset of mRNA including *egl-15*. Thereby, IFE-4 regulates the activity of CEP-1/p53 in primordial germ cells despite not being present there (Ou et al. 2019). We thus hypothesize that selective translation of mRNAs by specialized ribosomes, either generated by association with translational regulators such as IFE-4, or by RNA modifications as described here, might serve as a general mechanism to tightly control essential cellular processes even in distinct cells and tissues.

Elucidating the precise mechanism is of importance, as human NSUN1 (also known as NOP2 or P120) was shown to be required for mammalian preimplantation development (Cui et al. 2016) and thus indicates evolutionary conservation. Cui and colleagues found that NSUN1 has an indispensable role during blastocyst development within their experimental setup. Additionally, other groups reported that low levels of NSUN1 reduce cell growth in leukaemia cells, which is in line with findings that NSUN1 promotes cell proliferation. Moreover, high NSUN1 expression results in increased tumour aggressiveness and augmented 5-azacytidine (5-AZA) resistance in two leukaemia cell lines (Cheng et al. 2018; Bantis et al. 2004; Saijo et

al. 2001). Thus, NSUN1 might be considered as an example of ‘antagonistic pleiotropy’. According to this theory, genes can be indispensable early in life but negligible later, for instance after sexual reproduction. While NSUN1 appears to be essential for normal development, it might increase tumour aggressiveness later in life, especially in highly proliferative cells and tissues.

3.2.8 Additional Discussion¹²

In the second project, we conclude that molecularly, loss of NSUN-1 leads to translational remodelling with profound consequences on cell homeostasis. This is manifested by loss of cuticle barrier function and highly specific developmental defects, in particular oocyte maturation failure. We suggest that upon loss of NSUN-1, the expression of responsible collagen genes is repressed, causing leaky cuticle barrier function. Counterintuitively to our findings, when using an *nsun-1* catalytic mutant, where the first (from N to C terminus) cysteine is exchanged to an alanine, Navarro and colleagues did not observe infertility in assessed nematodes. This finding suggests that the observed phenotype is not, at least in part, directly linked to the methylation itself, but to other functions of NSUN-1. Nonetheless, when applying RNAi targeting *nsun-1*, they observed the same developmental phenotype we did (Navarro et al. 2020).

Cui and colleagues found that human NSUN1 has an indispensable role during blastocyst maturation (Cui et al. 2016). Other reports showed that low levels of NSUN1 reduce cell growth while high expression levels result in increased tumor aggressiveness (Cheng et al. 2018; Bantis et al. 2004; Saijo et al. 2001). Taken together, NSUN1 might be considered as a gene referring to the ‘antagonistic pleiotropy theory’, being indispensable early in life for normal development, but negligible after sexual reproduction as it might increase tumor aggressiveness and negatively affects highly proliferative cells and tissues.

As the ‘disposable soma theory of aging’ postulates, a balance between somatic repair and reproduction governs the organism’s energy. While most genetic and nutritional interventions are known to increase the lifespan, they antagonistically also reduce growth,

¹² This part is not included in the published pre-print (Heissenberger et al. 2020).

fecundity and body size (Kapahi 2010; Kenyon et al. 1993). As aging research is eager to increase the healthy lifespan, we assessed locomotion and heat resistance as well-known healthspan parameters in nematodes. While the lifespan was shown to be unaffected, locomotion and resistance against heat were improved upon loss of *nsun-1*. Further, we were surprised to find that despite their ability to modulate healthy aging and to methylate rRNA, neither NSUN-1 nor NSUN-5 were required for normal global protein synthesis in worms under the conditions tested. Remarkably, in the case of NSUN5 depletion, we previously found an overall reduction of protein synthesis in mammalian cells (Heissenberger et al. 2019), but not in yeast (Schosserer et al. 2015). Moreover, NSUN5 orthologs modulate the chronological lifespan of yeast, worms and flies. This lifespan extension was conditional to reduced nutrient availability and not accompanied by any obvious phenotypical alterations in body size or locomotion. We reasoned that higher complexity of mammalian ribosomes compared to yeast and nematodes (see Figure 5) might render them more vulnerable to alterations of rRNA secondary structure, for example by loss of a single base modification.

3.2.9 Supplemental Data

Table 4: Comparison of phenotypes after *nsun-1* and *nsun-5* depletion (in green) soma-specific effects, n.d.: not determined

Phenotype	<i>nsun-1</i> RNAi	<i>nsun-5</i> RNAi
Lifespan	<ul style="list-style-type: none"> - Unaffected in whole adult treatment - Unaffected after germline-specific depletion - Increased by ~10% after soma-specific depletion 	<ul style="list-style-type: none"> - Increased by ~17% in whole adult treatment (Schosserer et al., 2015)
Stress resistance (heat) in adults	Increased	Similarly increased
Locomotion at midlife	Increased	Similarly increased
Brood size (fecundity)	Reduced (2-fold)	Unaffected
Adult animal size	<ul style="list-style-type: none"> - Reduced by ~20% after soma-specific depletion and whole body depletion - Unaffected after germline-specific depletion 	Unaffected
Gonad morphology	<ul style="list-style-type: none"> - Impaired at meiotic to oocyte transition - Gonad extrusion (possibly caused by loss of cuticle integrity) - Unaffected after germline-specific depletion 	Unaffected
Pre-rRNA processing	Unaffected	Affected
Collagen expression	Affected (translational remodeling)	n.d.
Cuticle permeability	increased	n.d.

Table 5: Related to Figure 23: Summary of individual lifespan and thermotolerance experiments

strain	treatment	replicate	mean survival	s.d.	dead/ total	P-value
N2	RNAi control	1	20.8 days	± 0.9	47/75	0.579
N2	<i>nsun-1</i> RNAi	1	20.7 days	± 0.8	52/75	
N2	RNAi control	2	18.9 days	± 0.6	75/90	0.694
N2	<i>nsun-1</i> RNAi	2	18.9 days	± 1.1	74/90	
N2	RNAi control	3	20.7 days	± 0.3	87/90	0.474
N2	<i>nsun-1</i> RNAi	3	21.0 days	± 0.4	82/90	
NL2550	RNAi control	1	16.5 days	± 0.4	66/90	0.009
NL2550	<i>nsun-1</i> RNAi	1	18.0 days	± 0.4	68/90	
NL2550	RNAi control	2	18.6 days	± 0.3	83/90	<0.001
NL2550	<i>nsun-1</i> RNAi	2	20.2 days	± 0.4	75/90	
NL2098	RNAi control	1	16.7 days	± 0.3	80/90	0.289
NL2098	<i>nsun-1</i> RNAi	1	17.0 days	± 0.3	89/90	
NL2098	RNAi control	2	19.2 days	± 0.3	87/90	0.068
NL2098	<i>nsun-1</i> RNAi	2	18.4 days	± 0.3	88/90	
GR1373	RNAi control	1	18.9 days	± 0.3	104/120	0.065
GR1373	<i>nsun-1</i> RNAi	1	19.6 days	± 0.4	103/120	
GR1373	RNAi control	2	18.7 days	± 0.3	109/120	0.137
GR1373	<i>nsun-1</i> RNAi	2	19.2 days	± 0.2	113/120	
N2	heat / RNAi control	1	9.0 hours	± 0.3	25/25	control
N2	heat / <i>nsun-1</i> RNAi	1	13.0 hours	± 1.4	15/19	0.005
N2	heat / <i>nsun-5</i> RNAi	1	11.3 hours	± 1.2	19/22	0.377
N2	heat / RNAi control	2	8.4 hours	± 0.2	47/47	control
N2	heat / <i>nsun-1</i> RNAi	2	16.7 hours	± 1.2	33/51	<0.001
N2	heat / <i>nsun-5</i> RNAi	2	11.0 hours	± 0.2	43/43	<0.001
N2	heat / RNAi control	3	8.6 hours	± 0.2	45/45	control
N2	heat / <i>nsun-1</i> RNAi	3	7.7 hours	± 0.2	49/49	0.001
N2	heat / <i>nsun-5</i> RNAi	3	7.8 hours	± 0.2	44/44	0.003

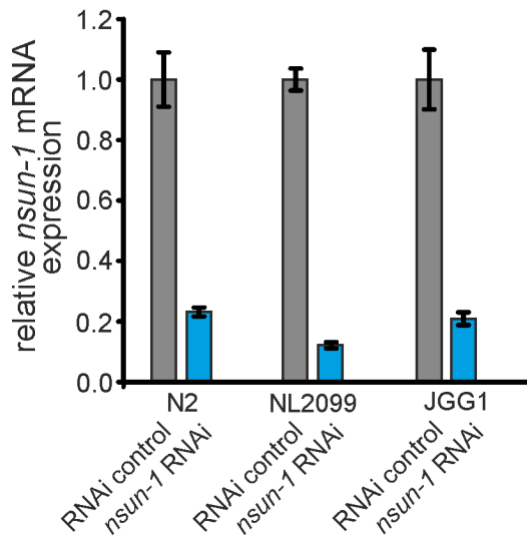


Figure 28: Related to Figure 22: RNAi effectively depletes *nsun-1* in *C. elegans*. Quantification of *nsun-1* mRNA levels using RT-qPCR in N2, NL2099 and JGG1 nematode strains. Worms were subjected to control and *nsun-1* RNAi. *nsun-1* mRNA levels were decreased to approximately 20% in N2 and JGG1, as well as to 10% in the RNAi hypersensitive strain NL2099. *act-1* was used for normalization. Error bars represent standard deviation of four technical replicates. This experiment was repeated independently with similar outcome.

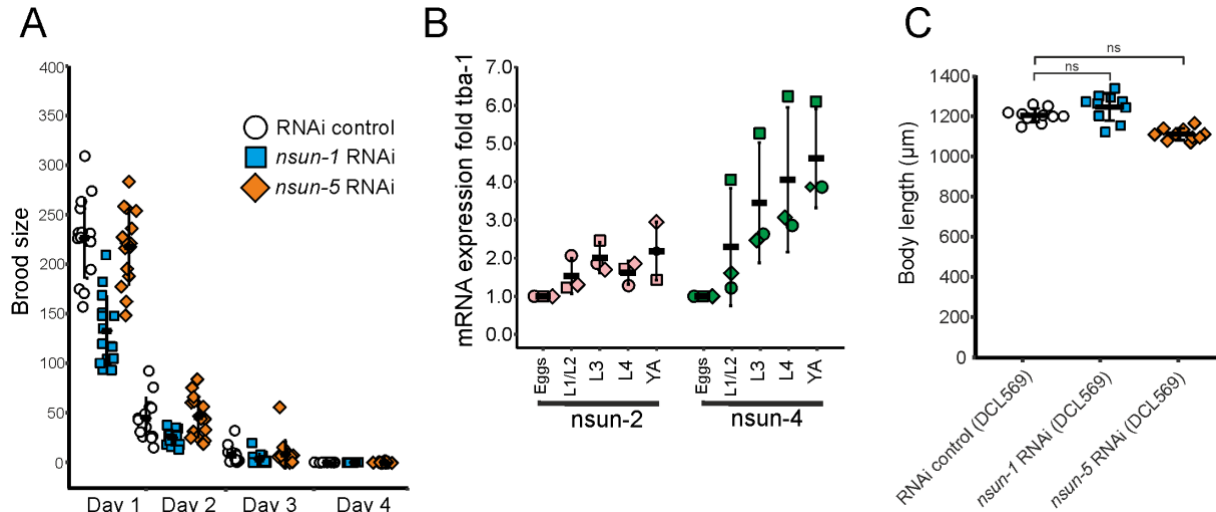


Figure 29: Related to Figure 24: *nsun-1* depleted worms display impaired fecundity. **A**, Brood size analysis of adult-onset RNAi exposed animals. Eggs of individual worms were counted every day until day 4 of adulthood. Knockdown of *nsun-1*, but not *nsun-5*, inflicted a reduced brood size compared to control RNAi. Three pooled independent experiments are shown. $n = 5$ per condition and per experiment. Error bars indicate standard deviation. **B**, RT-qPCR analysis of developing wild-type animals (eggs, L1/L2 larvae, L3 larvae, L4 larvae and young adults) revealed enhanced mRNA expression of *nsun-2* and *nsun-4* during development. Three independent biological experiments are shown. *tba-1* was used for normalization. Error bars represent standard deviation. **C**, Body size of 1-2 day old adult worms of a germline-specific RNAi strain (DCL569) was measured. The body size of *nsun-1* and *nsun-5* RNAi treated animals was not changed compared to RNAi control. $n(\text{all conditions}) = 10$, one-way ANOVA with Dunnett's post, $\alpha=0.05$, not significant. Error bars represent standard deviation.

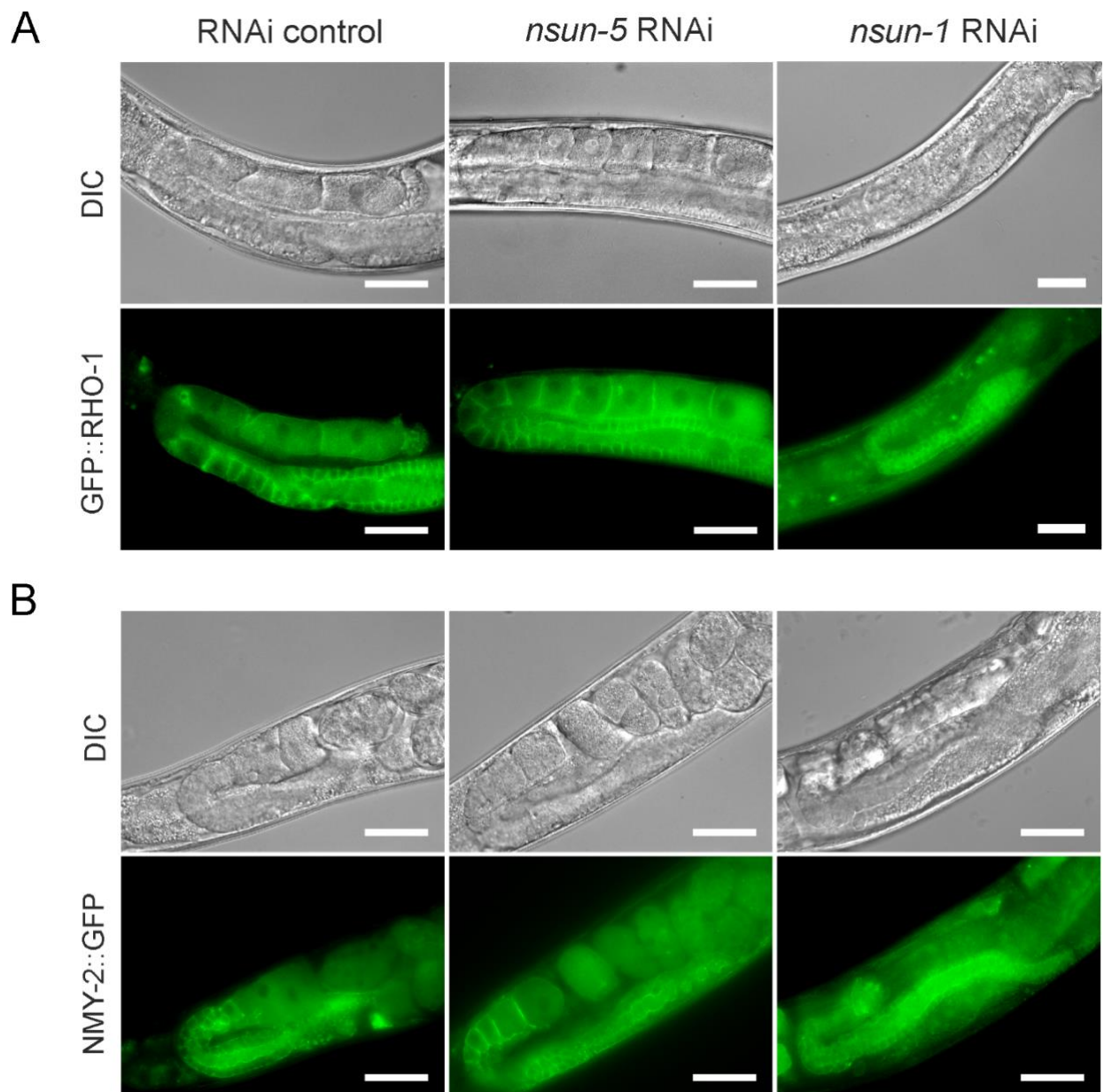
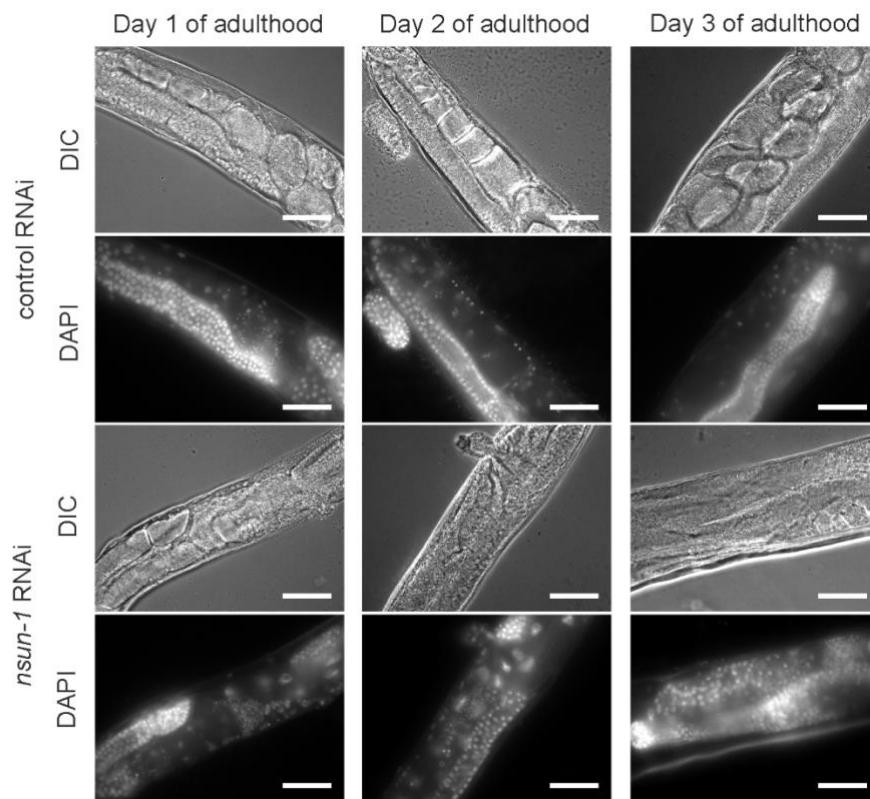


Figure 30: Related to Figure 25:: *nsun-1* but not *nsun-5* depletion inflicts a defect in oogenesis: A, B, Gonad specific expression of GFP::RHO-1 (SA115 strain) (**A**) and NMY-2::GFP (JJ1473 strain) (**B**) were used to visualize the morphology of the germline after *nsun-1* and *nsun-5* knockdown. Scale bar represents 40 μ m. Oocyte maturation starting from the loop region was impaired in *nsun-1* RNAi, but not in *nsun-5* RNAi treated animals.

A

soma-specific RNAi



B

germline-specific RNAi

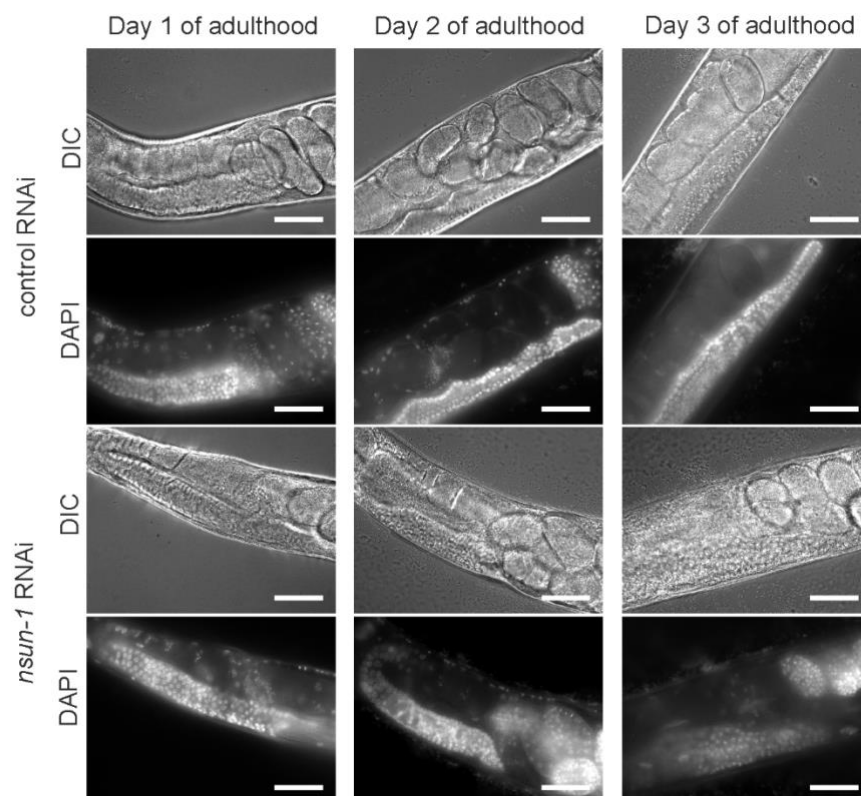


Figure 31: Related to Figure 25: Somatic- but not germline specific nsun-1 depletion causes defective oogenesis. A-B, Soma- but not germline-specific nsun-1 RNAi phenocopies altered gonad morphology of whole body nsun-1 depletion. NL2550 was used for soma- (A) and NL2098 for germline-specific knockdown (B). The gonad of 1-, 2- and 3-day old animals was imaged in DIC mode and nuclei were stained with DAPI following fixation. In the soma-specific strain maturing oocytes and embryos were observed only in RNAi control but not in nsun-1 RNAi subjected worms. The germline-specific strain remained entirely unaffected. Scale bar represents 40 μ m.

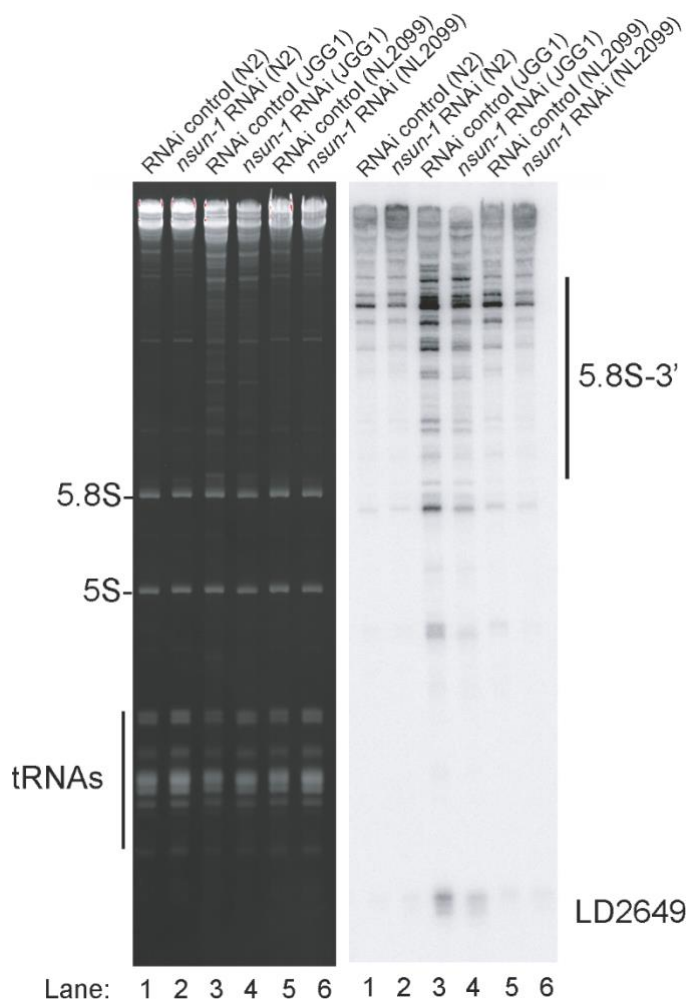


Figure 32: Related to Figure 26: nsun-5 but not nsun-1 RNAi alters 5.8S rRNA maturation. In the absence of nsun-5 (JGG1 strain, lane 3 and 4) the 3'-extended forms of 5.8S and short RNA degradation products accumulated. Upon co-depletion of nsun-1 (lane 4), such an accumulation is partially suppressed. When comparing the 5.8S and 5S, as well as tRNAs, no change can be observed between control and nsun-1 RNAi treated animals in the three different worm strains (N2, JGG1 and NL2099).

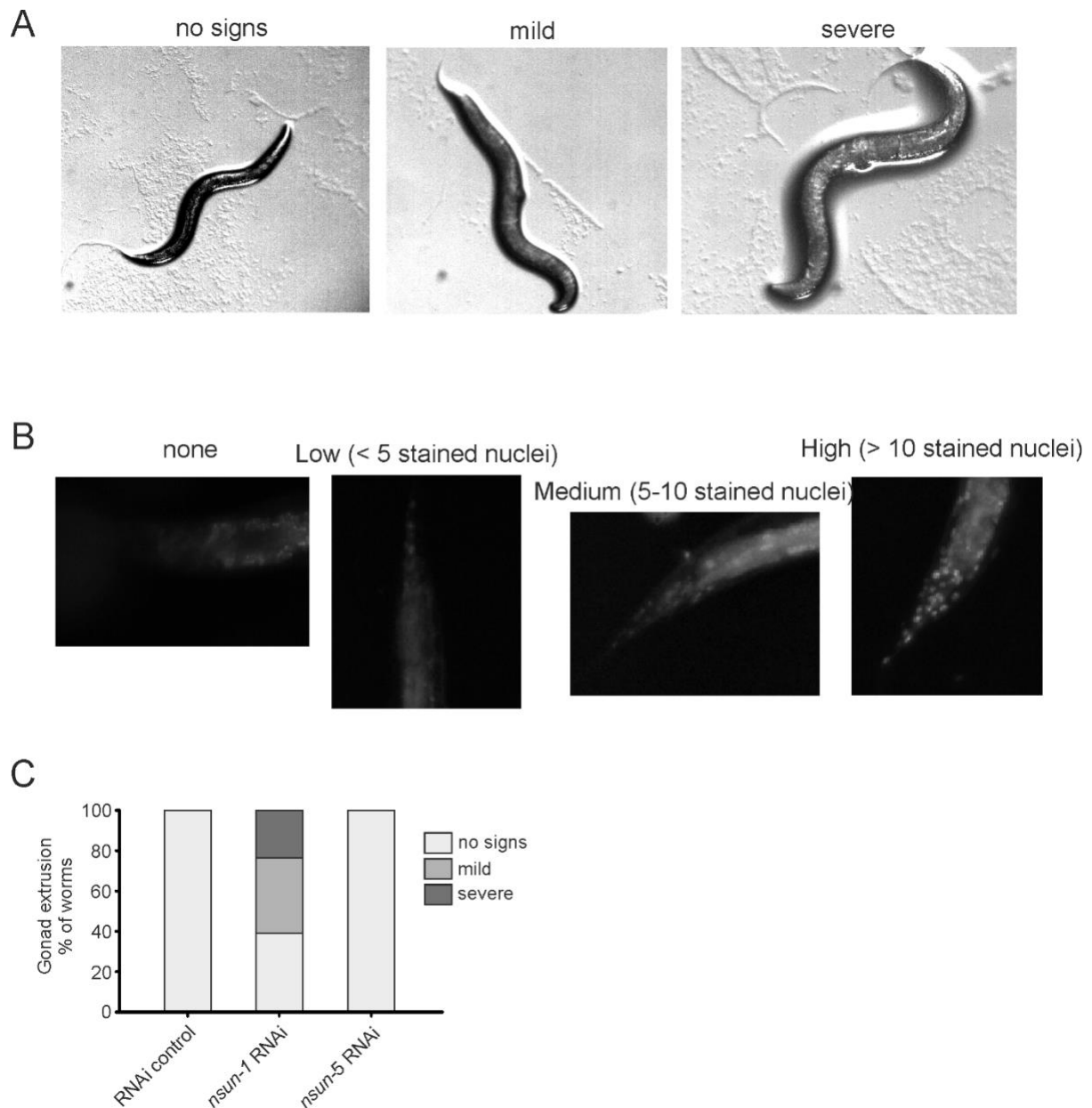


Figure 33: Related to Figure 27: *nsun-1* depletion affects gonad integrity and barrier function. **A**, Knockdown of *nsun-1* increased the rate and severity of gonad extrusion. Mid-aged worms at day 8-9 of adulthood were classified into three categories according to the severance of gonad extrusion ('no signs', 'mild', 'severe', see arrowhead). Representative images of the categories are shown here. **B**, Reduced levels of *nsun-1* affected barrier function. Young adult animals were incubated in 1 μ g/mL Hoechst 33342, which is membrane-permeable but cuticle-impermeable. Permeability was assessed by counting nuclear Hoechst staining in the tail region (see arrowhead). Young adult animals were classified into four categories ('no staining', 'low (< 5 stained nuclei)', 'medium (5-10 stained nuclei)', 'high (>10 stained nuclei)'). Representative images of the different categories are shown here. **C**, Analysis of gonad extrusion including the results of *nsun-5* RNAi. The experiment was independently performed two times with similar outcome. One representative replicate is shown. $n \geq 50$ animals per replicate.

4 Conclusions and Outlook

Although rRNA modifications are universally found in all kingdoms of life, little is known about the direct biological functions of rRNA methylation sites, or about the putative readers, writers and erasers. Within this thesis, I have investigated the molecular and physiological roles of two Sun-domain-containing RNA methyltransferases, NSUN1 and NSUN5. These enzymes harbour commonly two highly conserved cysteines. One of which is required for the covalent adduct formation and the other for the protein-rRNA release following m⁵C catalysis (King and Redman 2002). Each of them was shown to be responsible for writing one m⁵C mark on 26S/28S rRNA in nematodes and mammals respectively. No other m⁵Cs can be found on rRNA, as the small subunit is devoid of such modifications.

Emerging evidence of how heterogeneity of ribosomes affect gene expression and cellular fitness points out that scientists are eager to enlarge our knowledge in this regard. It is time to push the field of epitranscriptomics to better understand how individual cells, tissues and simple organisms control one of the most fundamental biological processes, namely protein synthesis. A plethora of publications has shown the importance of ribosomal heterogeneity (accomplished either genetically or by environmental changes concerning temperature, pressure, milieu, ect.) affecting the ribosomal function and thus the physiology of respective cells. A major obstacle to conclusively prove the existence of specialized ribosomes is to show the directly resulting biological function of one (or more) modifications of the ribosome, i.e. via *in-vitro* translation or similar experiments. For example, an exchange of “mutant” to “control” 40S or 60S subunit respectively in an *in-vitro* translation experiment would be sophisticated but meaningful at the same time. Furthermore, the practical handling of cells, ribosomes and other organelles can affect the ribosomal composition (nutrients, temperature, salts, pH, ect.), so experiments should be executed with utmost caution not to create artefacts. Additionally, ribosomal decay has been shown to start on the bound mRNA, adding an additional layer of complexity to the problem. As most experiments just offer a “snapshot” of the current cells’ fitness, one has to be very careful in interpreting results from MS, RNA-Seq, Ribo-Seq and WB, because it cannot be ruled out exclusively that the absence or presence of ribosome intermediates is falsifying the results.

Nonetheless, in this work I could show that already single rRNA modifications (in this case m⁵C), mediated by the two Sun-domain rRNA methyltransferases NSUN1 and NSUN5, can have a striking impact on living nematodes and on human cells and mice. We demonstrated that loss of NSUN1 or NSUN5 results in loss of the corresponding specific methylation on the large ribosomal subunit in all used model systems. Furthermore, we evaluated and characterized the localization of NSUN5 in human cells as well as NSUN-1 in *C. elegans* for the first time.

In the last four years, I also have worked with RRP8 (see chapter 1.4.8.3.3) as a different rRNA methyltransferase not belonging to the NSUN family. As the results look quite promising, we are currently writing a grant proposal. Moreover, I have cooperated within my colleague's project in assessing the whole 2'-O methylation pattern in human derived fibroblast cells. In particular, we analysed senescent, quiescent and proliferating HDF cells in order to get insights how ribosomes are build-up and modified in cellular senescence (Yang et al. 2020). Another fruitful collaboration ended in an co-authorship. There, we analysed the context of NSUN-5, amongst others, in a frameshifting *C. elegans* model during aging (Adamla et al. 2019).

At that point, we can say that the absence of m⁵C marks influences ribosomes and renders them more vulnerable to stress or other stimuli. Personally, I think it seems obvious that ribosomal heterogeneity is crucial, as nature has evolved such a great set of modifications during evolution. As studies showed, the majority of rRNA modifications in prokaryotes, as well as in eukaryotes, are located in the core of ribosomes and/or being located between the large and small subunit where peptidyl transfer and decoding occur. Why should nature have kept all these modifications if not needed to fine-tune translation and adapt to current environmental conditions? I hope that the reader of my doctoral thesis is convinced enough not to deny the presence of specialized ribosomes or, at least, start not neglecting it. Indeed, it is clear to me that we have to be very careful to control our experimental systems to conclusively and directly connect certain modifications to changes in ribosomal function and finally certain phenotypes. It needs a tremendous amount of effort to understand why and how cells can adapt gene expression via altered ribosomes. At the same time, it is also needed to understand the few orphan maladies based on erroneous ribosomes and we have to seek for future therapeutics to treat those patients. Adequate proteostasis, as a primary hallmark,

strongly implicates the importance of ribosomes in all its facets. How ribosomes are build up, work and adapt to environmental changes in different species should be a primary goal of us scientists in the field of aging research.

Hence, investing in something that is relevant for everybody, namely the aging process, should be of interest to everyone. I hope I could provide a few more pieces in the large mosaic that is the basic biological processes – translation.

5 Material and Methods ¹³

5.1 Mammalian cell culture

5.1.1 Cells animals and ethics

HeLa and HEK293 cells were purchased from ATCC. HeLa cells were cultured in RPMI (F1215, Biochrom) and HEK293 cells in DMEM (F0435, Biochrom), each supplemented with 10% fetal calf serum (FCS) and 4 mM L-glutamine (G7513; Sigma).

Human dermal fibroblasts (HDF) from healthy female donors were obtained from Evercyte GmbH (Vienna, Austria). The two dermal fibroblast cell strains from Williams Beuren Syndrome (WBS) patients were a kind gift from Dr. Aleksander Hinek (The Hospital for Sick Children, Toronto, Canada). WBSCR14073 was isolated from a skin biopsy of a 6 years old male patient and WBSCR14966 from a skin biopsy of a 3 months old female patient as described previously. Both strains show haploinsufficiency of the NSUN5 gene (Urbán et al. 2002). All human dermal fibroblast strains were cultured in DMEM/Ham's F-12 (1:1 mixture) (F4815, Biochrom) supplemented with 10% FCS and 4 mM L-glutamine (G7513; Sigma).

NSUN5 knockout mice were generated by Applied Stem Cell Inc. by disruption of exon 1 and intron 1 with two loxP-sites by CRISPR-Cas9. Mice were crossed into the C57BL/6J background 10 times.

Experiments with Nsun5 knockout mice were approved by the animal ethics commission of the Medical University of Vienna and by the Austrian Federal Ministry of Education, Science and Research (BMBWF-66.009/0199-V/3b/2018). The generation of anti-NSUN5 antibodies was approved by the Austrian Federal Ministry of Science and Research (BMBWF-66.016/6-II/3b/2011).

¹³ The content of chapter 5.1 and 5.2 were already published (Heissenberger et al. 2019, doi: 10.1093/nar/gkz1043)
The content of chapter 5.3 is published as a pre-print (Heissenberger et al. 2020, doi: <https://doi.org/10.1101/2020.03.16.993469>)

All cell lines and strains were tested for the absence of mycoplasmas regularly and kept at 37 °C, 7% CO₂ and 90% humidity.

5.1.2 Isolation and immortalization of mouse embryonic fibroblasts

Embryos from homozygous mating were isolated between E 12.5 and E 14.5. After removing the heads, embryos were minced and incubated with trypsin-EDTA (0.25%) at 37 °C for 30 minutes. After filtering the suspension through a cell strainer (100 µm) and harvesting cells via centrifugation, cells were seeded in cell culture flasks. For immortalization, cells were passaged every three days and 12.000 cells per cm² were seeded. After about 20 passages when cells passed crisis stage, they were passaged at a 1:10 split ratio. Mouse embryonic fibroblasts (MEFs) were cultured in DMEM (F0435, Biochrom), supplemented with 10% FCS, 4 mM L-glutamine and 0.1 mM β-mercaptoethanol.

5.1.3 Generation of NSUN5 KO HeLa cells by CRISPR-Cas9

After reaching 80% confluence, HeLa cells were transfected with an all-in-one plasmid encoding the guide RNA (CTTCACGTTCTGTGTGGCCG, designed by gUIDEbook™), as well as Cas9 and GFP (Horizon Discovery Ltd., Free CRISPR Knockout Generation Program). One day after transfection, 10⁵ GFP positive cells were isolated with a MoFlo Astrios cell sorter (Beckman Coulter) into a 12-well cell culture plate. On the next day, we performed single cell dilution in 96-well cell culture plates. Clones originating from single cells were screened for NSUN5 expression using Western blot and immunofluorescence with the self-made polyclonal NSUN5 mouse antibody.

5.1.4 Transfection of mammalian cells

Cells were grown to ~80% confluence in 6-well cell culture plates. 2 µg of plasmid DNA were mixed with 4 µL of jetPRIME transfection reagent (Polyplus transfection), vortexed and

incubated for 10 minutes. The mixture was added dropwise to the cells. Culture medium was exchanged 16 – 24 h after transfection. Lentiviruses containing NSUN5, C308S and C359S were produced by co-transfecting Lenti-X HEK-293T cells with the recombinant pLVX-IRES-Hyg plasmid and a Lenti-X Packaging Single Shot (Takara) following the supplier instructions. The transfection cocktail was removed after 24 h and replaced with fresh medium. 72 h after transfection, supernatant containing viral particles was harvested 0.45 µm filtered and stored at -80 °C before transduction. Presence of virus particles was tested using Lenti-X GoStix Plus (Takara). NSUN5 KO HeLa -and MEF -/- cells were infected with virus particles. One day after infection, antibiotic selection (400 µg/mL hygromycin) was initiated. After 5 days of selection, stably expressing cells were expanded and passaged at least three times before starting experiments in media containing 200 µg/mL hygromycin.

5.1.5 NSUN5 knock-down by shRNA

The following shRNA constructs in the pLKO.1 vector, as well as a non-hairpin forming construct as negative control (Moffat et al. 2006), were acquired from Open Biosystems: Non hairpin control (CCGCAGGTATGCACGCGT), NSUN5 shRNA #1 (AGGCAATAAGACCAGTCACT), NSUN5 shRNA #2 (AAGAGACAAGGTTTCTCCTA), NSUN5 shRNA #3 (CAAGGGAAGATCTTTGCCTT) and NSUN5 shRNA #4 (CAAGGTGCTAGTGTATGAGT).

Lentiviral particles were packaged by transfecting 293FT cells as previously described (Micutkova et al. 2011). 293FT cells were seeded into T75 cell culture flasks at cell numbers that resulted in 90-95% confluence on the day of transfection. For transfection, the culture medium was removed and cells were washed once with 10 mL PBS. 5 mL of growth medium without antibiotics were added. In a sterile 15 mL tube, 7.5 µg psPAX packaging plasmid, 2.5 µg pMD2.G envelope plasmid and 3 µg of shRNA pLKO plasmid DNA were diluted in 1.5 mL Opti-MEM I Medium (Life Technologies). In a separate sterile tube, 36 µL Lipofectamine 2000 (Life Technologies) were diluted in 1.5 mL of Opti-MEM I Medium. The Lipofectamine/Opti-MEM I suspension was gently mixed and incubated for 5 minutes at room temperature. After 5 minutes incubation, the diluted DNA was combined with diluted Lipofectamine 2000. The solution was gently mixed and incubated for 20 minutes at room temperature to allow the DNA / Lipofectamine 2000 complexes to form. The DNA / Lipofectamine 2000 complexes were

added to the cells and incubated overnight. The next day, medium was exchanged. Viruses were harvested after 48 h by centrifugation of the supernatant at 300 g for 10 minutes to remove debris. The viral supernatant was filtered through a Millex-HV 0.45 µm filter (Merck-Millipore), aliquoted into cryo tubes and stored at -80 °C. An extra vial with 10 µL of virus was frozen for quantitation of the infection titer.

For the transduction of HEK293 and HDF, 50,000 cells were seeded into one well of a 6-well plate and incubated overnight. A multiplicity of infection (MOI) of four was used with the addition of 8 µg/mL Polybrene to the medium. The next day, medium was exchanged. 3 days after transduction puromycin (500 ng/mL) was added to the medium and the medium containing puromycin was exchanged every three days. After 6-8 days the selection was finished and the knockdown efficiency was evaluated by RT-qPCR and western blot.

5.1.6 Generation and stable transfection of GFP-mNsun5 BACmid

GFP-mNsun5 BACmid was generated by fusing mouse Nsun5 contained in a BAC-clone to the C-terminus of EGFP using the NFLAP tagging cassette (Poser et al. 2008b) by the Quick & Easy BAC Modification Kit (GeneBridges).

The GFP-mNsun5 BACmid was amplified in *E. coli* and purified using the Large Construct Purification Kit (Qiagen) following the manufacturer's instructions. Transfection into HeLa cells was performed using Metafectene Pro (Biontex GmbH) following the manufacturer's instructions. 3 days after transfection, 800 µg/mL G418 were applied for selection. Single colonies emerged two weeks after transfections and were screened for GFP-mNsun5 expression and correct intracellular localization by Western blot and fluorescence microscopy.

5.1.7 Cell number and cell size determination

Viable cell number and cell size were determined by ViCell (Beckmann Coulter). 0.5 - 1 x 10⁵ cells per well were seeded in 6-well culture plates and total viable cell numbers were determined on consecutive days until 100% confluency was reached. Microscopic images

were acquired with an inverted microscope (Leica, DM IL LED) using a 10x/NA 0.22 objective and phase contrast. Insertion of scale bars, as well as brightness and contrast adjustments were done with Image J (Version 1.52 e).

5.1.8 Weight and body composition measurement

Mice of the same litter were weighed at either 4 or 8 weeks of age. Weight ratio per litter was calculated according to this formula, with 2-4 mice per litter:

$$\text{weight ratio} = \frac{\text{mean weight } N\text{sun5}^{-/-} \text{ animals [g]}}{\text{mean weight } N\text{sun5}^{+/+} \text{ animals [g]}}$$

Body composition of awake un-anesthetized male and female mice between 14 and 18 weeks of age was analysed using EchoMRI-100H (EchoMRI LCC) in a non-invasive manner. The weight of these mice was also recorded.

5.1.9 Food intake

Male mice between 15 and 19 weeks of age were caged separately. After an adaption period of one week, food was weighed on four consecutive days and the mean food intake for each mouse was calculated.

5.1.10 Antibodies

The following primary and secondary antibodies were used for western blot (WB) and immunofluorescence (IF) at indicated dilutions:

target	manufacturer	product #	host	conjugate	WB	IF
NSUN5	Santa Cruz	sc-376147	mouse	-	1 : 250	1 : 100
NSUN5	selfmade	-	mouse	-	1 : 2,000	1 : 250
β-Actin	Sigma	A-5441	mouse	-	1 : 5,000	-
GAPDH	Thermo Fisher Scientific	MA5-15738	mouse	-	1 : 5,000	-
Fibrillarin	Abcam	ab5821	rabbit	-	-	1 : 1,000
KRAS, HRAS and NRAS	Abcam	ab55193	mouse	-	1 : 1,000	-
GFP	Abcam	ab290	rabbit	-	1 : 2,500	
mouse IgG	Jackson Immunoresearch	115-485-146	goat	Dyelight 488	-	1 : 1,000
rabbit IgG	Jackson Immunoresearch	111-485-144	goat	Dyelight 488	-	1 : 1,000
rabbit IgG	Jackson Immunoresearch	111-505-144	goat	Dyelight 549	-	1 : 1,000
rabbit IgG	Jackson Immunoresearch	111-495-144	goat	Dyelight 649	-	1 : 1,000
mouse IgG	Life Technologies	O6380	goat	Oregon Green 488	-	1 : 1,000
rabbit IgG	Jackson Immunoresearch	111-065-144	goat	Biotin	-	1 : 1,000
mouse IgG	Life Technologies	A21057	goat	Alexa Fluor 680	1 : 10,000	-
rabbit IgG	Licor	926-32211	goat	IRDye 800CW	1 : 10,000	-

For the generation of the polyclonal mouse NSUN5 antibody, recombinant HIS-tagged NSUN5 was expressed in *Escherichia coli* in the pET30a vector and purified using Ni-NTA Agarose beads (Qiagen) under denaturing conditions following the manufacturer's protocol. Recombinant HIS-NSUN5 was used for the immunization of mice. Crude serum from a single mouse was used. A characterization of this antibody is shown in Figure 21.

5.2 Molecular Biology and Imaging

5.2.1 Site directed mutagenesis of NSUN5 in pCI-neo and lentiviral vectors

The QuickChange II Site-Directed Mutagenesis Kit (Agilent) was applied for exchanging C308 and C359 of NSUN5 in pCI-neo to serines following the manufacturer's instructions. For producing lentiviral particles, the cDNA sequence of wildtype NSUN5 and the two point mutants, C308S and C359S, were cloned into the pLVX-IRES-Hyg expression plasmid (Takara) using *In-Fusion*[®] HD *Cloning* (Takara) with a sense (5'-CGGTGAATTCCTCGAATGGGGCTGTATGCTGCAG-3') and an antisense (5'-TAGAACTAGTCTCGACTATGTGCAAGGCGGTGTGC-3') primer at the XhoI restriction site.

5.2.2 Generation of NSUN5-GFP truncation mutants

The following full-length and truncated versions of NSUN5 were generated by PCR from HeLa cDNA (numbers represent amino acids counted from the N-terminus of the protein, bold letters indicate restriction sites): NSUN5(1-466)-GFP (5'-gataCTCGAGatggggctgtatgctgcagctgc-3' and 5'-ttagGAATTCatgtgcaaggcggtgtgcaag-3'), NSUN5(1-121)-GFP (5'-gataCTCGAGatggggctgtatgctgcagctgc-3' and 5'-ttagGAATTCccaggtcctcattccggctcacac-3'), NSUN5(1-277)-GFP (5'-gataCTCGAGatggggctgtatgctgcagctgc-3' and 5'-ttagGAATTCaagagacgccagccgggcca-3'), NSUN5(1-428)-GFP (5'-gataCTCGAGatggggctgtatgctgcagctgc-3' and 5'-ttagGAATTCatggcacctcgacccgttcaatta-3'), NSUN5(121-466)-GFP (5'-gataCTCGAGatgttgaagtgggatccaggcctg-3' and 5'-ttagGAATTCatgtgcaaggcggtgtgcaag-3'),

NSUN5(277-466)-GFP (5'-gataCTCGAGatgtgctgtgaactggctgaggagg-3' and 5'-ttagGAATTCatgtgcaaggcggtgtgcaag-3'). Purified PCR products were cloned into pEGFP-N1 by restriction digest with XhoI and EcoRI.

5.2.3 Western blots

Cells were lysed in RIPA-buffer (150 mM NaCl, 1% NP-40, 0.5% sodium deoxycholate, 0.1% SDS, 50 mM Tris/HCl pH 8.0), sonicated for 30 cycles (30 s on / 30 s off) with a Bioruptor Plus sonicator (Diagenode) and mixed with SDS-PAGE sample buffer (60 μ M Tris/HCl pH 6.8, 2% SDS, 10% glycerol, 0.0125% bromophenol blue and 1.25% β -mercaptoethanol). Mouse kidneys were cut in small pieces, lysed in RIPA-buffer, sonicated for 30 cycles (30 s on / 30 s off) and centrifuged briefly. The supernatant was mixed with SDS-PAGE sample buffer.

Lysates were heated to 95 °C for 10 min and cooled on ice. Electrophoresis was performed using 4-15% Mini-PROTEAN[®] TGX Gels (BioRad) in Laemmli-Buffer (25 mM Tris, 250 mM glycine and 0.1% SDS) (Laemmli 1970) at 150 V for approximately one hour. The protein bands were transferred from SDS-PAGE gels to a PVDF-membrane (Bio Rad) at 25 V and 1.3 A for 3 min. Afterwards the membrane was incubated for 1 h in Blocking Buffer (PBS containing 0.1% Tween-20 and 3% non-fat dry milk), followed by primary antibodies in Blocking Buffer for either one hour at room temperature or overnight at 4 °C. After three washes with PBS containing 0.1% Tween-20 for 5 min each, secondary antibodies in Blocking Buffer were added and incubated for 1 h at room temperature. After three consecutive washes in PBS containing 0.1% Tween-20, and one final wash in PBS without Tween-20, detection was performed on the Odyssey Infrared Imager (LI-COR) at 700 and 800 nm.

5.2.4 RNA isolation and cDNA synthesis

Cells were lysed in TRI Reagent (Sigma) and RNA was isolated following the manufacturer's protocol. Whenever applicable, total RNA was isolated with Direct-zol[™] RNA Kit (Zymo Research). RNA quality and concentration were quantified with an ND-1000 (NanoDrop)

spectrometer. cDNA was synthesised from 500 ng of total RNA using High-Capacity cDNA Reverse Transcription Kit (Applied Biosystems).

5.2.5 RT-qPCR

Target gene expression levels were quantified from cDNA using the 5x HOT FIREPol® EvaGreen® qPCR Mix Plus (Medibena) on a Rotor-Gene Q cyclor (Qiagen) with gene-specific primers: GAPDH (human): 5'-CGACCACTTTGTCAAGCTCA-3' and 5'-TGTGAGGAGGGGAGATTCAG -3', Actb (mouse): 5'-AGAGGGAAATCGTGCGTGAC-3' and 5'-CAATAGTGATGACCTGGCCGT -3', NSUN5 (human): 5'-CTACCATGAGGTCCACTACAT-3' and 5'-CTGGCAGAGGGAGCA-3', Nsun5 (mouse): 5'-TTGCAAGAGAGCTCCAGACC-3' and 5'-AGGCAGCAAGGGATCCAAAA-3'.

5.2.6 Bisulfite conversion, PCR amplification and sequencing

Bisulfite conversion of 750 ng DNase I (Zymo Research) digested total RNA was performed using the EZ RNA Methylation™ Kit (Zymo Research). The converted RNA was eluted in 15 µL nuclease-free water and reverse-transcribed as described above. cDNA after bisulfite conversion was amplified by PCR using GoTaq® DNA polymerase (Promega), forward primer (5'-GGGAGTAATTATGATTTTGACAAGGTAG-3') and reverse primer (5'-ATAATAAATAAAAAACAATAAAAAATCTCATTCATCCATTCATACAC-3') to generate a 101 bp PCR product. After purification by agarose gel electrophoresis and QIAquick PCR Purification Kit (Qiagen), DNA was either used for COBRA assay (see below) or subjected to TOPO cloning using the TOPO TA Cloning Kit for Sequencing (Life Technologies) following the manufacturer's protocol. Purified plasmids of the indicated number of clones were sent to Sanger sequencing (eurofins Genomics).

5.2.7 Combined bisulfite restriction analysis (COBRA)

COBRA was performed as previously described (Gigova et al. 2014) with minor modifications: The PCR product after bisulfite conversion and reverse transcription was digested with MseI (New England Biolabs), resulting in either two products of 45 and 56 bp (methylated) or three bands at 16, 29 and 56 bp (non-methylated). Digested DNA samples were separated on a 20% TBE gel (Life Technologies) followed by incubation for 20 min with SYBR Safe (Life Technologies). The mean density of individual bands was quantified in Image J (Version 1.52 e) and relative methylation [%] was calculated according to this formula:

$$\text{relative methylation [\%]} = \frac{\text{methylated (45 bp band)}}{\text{methylated (45 bp band)} + \text{non methylated (29 bp band)}} * 100$$

5.2.8 Immunofluorescence staining of cells

Cells were seeded onto coverslips or into μ -slides (ibidi GmbH) and incubated over night at 37 °C. Afterwards the cells were fixed in 4% formaldehyde in PBS, washed two times with PBS for 5 min each, and permeabilized for 10 min in 1% Triton X-100 in PBS, followed by two PBS washing steps. Primary and secondary antibodies were diluted in PBS containing 2% BSA. Samples were incubated with primary and secondary antibody solutions for 30 min respectively in a humidified chamber at room temperature, each followed by four washes in PBS. Nuclei were counterstained with DAPI and images were recorded on a Leica DMI6000B epifluorescence microscope using the A4, L5 and N2.1 filter cubes. Deconvolution with Huygens Essential version 4.0.0p5 64 b (Scientific Volume Imaging) was performed when indicated in the figure legend. Cropping, insertion of scale bars and brightness and contrast adjustments were done with Image J (Version 1.52 e).

Immunofluorescence staining for gSTED microscopy was performed as described above with the following modifications: After incubation with primary antibodies and the washing, cells on coverslips were stained with Oregon Green 488 anti-mouse and Biotin anti-rabbit antibodies. After the final wash, coverslips were incubated with V500-streptavidin (Becton Dickinson) 1:250 in 2% BSA in PBS for 30 min, washed three times with PBS and mounted with Mowiol (Sigma) on slides. Counterstaining with DAPI was omitted. On the next day when

Mowiol was hardened, imaging was performed on a SP8 confocal microscope equipped with a pulsed white-light laser and gSTED (Leica Microsystems) with the following parameters: objective: HC PL APO CS2 100x/1.40 OIL, bi-directional scan at 400 Hz, pinhole = 1 Airy unit, frame accumulation = 6, line average = 6, sequential accumulation: 503 nm pulsed laser excitation / time-gated hybrid detector at 533 nm – 575 nm / 592 nm STED depletion for NSUN5 and 470 nm pulsed laser excitation / time-gated hybrid detector at 479 nm – 511 nm / 592 nm STED depletion for Fibrillarin. Deconvolution of images was performed with Huygens Professional (Scientific Volume Imaging).

5.2.9 Actinomycin D and α -Amanitin exposure

Actinomycin D and α -Amanitin treatment was performed as previously described (Müller et al. 2010). HeLa cells were seeded into μ -slides (ibidi GmbH) and incubated over night at 37 °C. On the next day, cells were incubated with 50 ng/mL Actinomycin D (Sigma) or with 50 μ g/mL α -Amanitin (Sigma). Immunofluorescence staining for NSUN5 (selfmade polyclonal mouse NSUN5 antibody) was performed as described above.

5.2.10 O-propargyl-puromycin (OPP) assay

OPP assays were performed as described previously (Nagelreiter et al. 2018b). In brief, cells were grown to ~80% confluence and incubated with 25 μ M OPP (#NU-931-05, Jena Bioscience) for 20 minutes at 37 °C, 7% CO₂. After harvesting, cells were fixed by adding 5 mL ice-cold 70% ethanol with gentle agitation on a vortex-mixer to avoid clumping. Two specificity controls were included: 1) cells not labelled with OPP and 2) cells incubated with cycloheximide (#C7698, Sigma) at a final concentration of 50 μ g/mL for 15 min prior to, as well as during incubation with OPP.

In order to visualize OPP incorporation by a fluorescent label, cells were pelleted and resuspended in 1 mL “Click Chemistry Buffer” (115 mM Tris/HCl pH 8.5, 0.1% Triton X-100). After another centrifugation, cells were re-suspended in 500 μ L freshly prepared “Click Chemistry Mix” (500 μ L “Click Chemistry Buffer”, 10.6 μ L 100 mM CuSO₄ solution, 53.3 μ L 20

mg/mL ascorbic acid solution and 1 μ L 10 mM Alexa Fluor 647 azide) and incubated for 30 min at room temperature protected from light. Subsequently, cells were washed twice with 1 mL “Wash Buffer” (100 mM Tris/HCl pH 7.4, 2 mM MgCl₂, 0.1% Triton X-100). All centrifugation steps were performed at 400 g for 5 min.

For quantitation of OPP labelling, cells were analysed by flow cytometry (Gallios flow cytometer; Beckman Coulter), using a 638 nm red diode 25 mW laser for the analysis of AF647 signals (FL6, 660/10 bandpass filter). Selection of whole single cells in G1 phase was based on forward and side scatter, as well as on DAPI staining. Analysis of fluorescence intensities was performed in Kaluza 1.2 (Beckman Coulter).

5.2.11 Quantification of rRNA

4 μ g purified total RNA were separated on a 1.2% agarose gel. Separated RNA was then transferred to a wet nylon membrane using electro-transfer at 4 °C. Crosslinking was performed in a UV-Crosslinking device (Hoefer UVC 500 Ultraviolet Crosslinker) utilizing a 254 nm light source for 30 seconds. Afterwards, the membrane was stained with methylene blue to visualize 18S and 28S rRNA. Probes (ITS1: 5′ GTCCGGGCTCCGTTAATGATC ′3 and ITS2: 5′ GGCAAGAGGAGGGCGGA ′3) were hybridized with the membrane at 38 °C to 42 °C overnight. Then membranes were exposed to imaging plates (Fuji). Signal intensities were quantified, and background was subtracted (Fuji FLA-5100 scanner and AIDA software, Raytest).

5.2.12 Reporter assays to characterize translational fidelity and IRES translation

pGL3 (WT), pGL3 (E - K529E), pGL3 (I - K529I) and pGL3 (N - K529N) to test amino-acid misincorporation were a kind gift from Vera Gorbunova. The pcDNA3 (RLUC POLYIRES FLUC) plasmid to test IRES-dependent translation was a kind gift from Nahum Sonenberg (Poulin et al. 1998). pCI-neo (control), pCI-neo (FS -1 (L-A)), pCI-neo (FS -1 (HIV)), pCI-neo (Stop-UAA), pCI-neo (Stop-UAG) and pCI-neo (Stop-UGA) to measure stop-codon read through and translational frameshifting were generated as follows:

The dual luciferase reporter constructs to analyse translational frameshifting were generously provided by Jonathan Dinman (Harger and Dinman 2003), transferred into CMV-promoter containing yeast expression vectors to generate pMK967 (control), pMK968 (FS -1 (L-A)), pMK970 (FS -1 (HIV)), pMK971 (Stop-UAA), pMK972 (Stop-UAG) and pMK973 (Stop-UGA), and further cloned into the mammalian expression vector pCI-neo. For this aim, the DNA sequence of the luciferase fusion constructs were amplified by polymerase chain reaction from pMK plasmids using Q5-Polymerase (New England Biolabs) and the CLF forward primer introducing a recombination site and the KOZAK initiation sequence at the 5' end (5'-CTAGCCTCGAGAATTGCGCCGCCACCATGACTTCGAAAGTTTATGATCCAGAACAAAG-3'), as well as the CLR reverse primer appending another recombination site at the 3' end (5'-TACCACGCGTGAATTCTTACAATTTGGACTTTCCGCCCTTCTTG-3'). The pCI-neo vector backbone was linearized by restriction digest with EcoRI-HF (New England Biolabs). Purified inserts and linearized vector DNA were consequently recombined using the In-Fusion cloning system (Takara Bio USA Inc.) according to the manufacturer's instructions.

The firefly luciferase plasmids pGL3 (WT), pGL3 (E - K529E), pGL3 (I - K529I), pGL3 (N - K529N) and pcDNA3 (RLUC POLYIRES FLUC) were mixed with pGL3 coding for Renilla luciferase for normalization in a 4:1 ratio and transfected into mammalian cells as described above. The dual-luciferase plasmids pCI-neo (control), pCI-neo (FS -1 (L-A)), pCI-neo (FS -1 (HIV)), pCI-neo (Stop-UAA), pCI-neo (Stop-UAG) and pCI-neo (Stop-UGA) were transfected without mixing with another plasmid. 48 h after transfection, translational fidelity of transfected cells was analysed by using the Dual-Luciferase assay kit (Promega). Cells were harvested by scraping in lysis buffer (25 mM Tris-HCl pH 7.8, 1% Triton X-100, 0.1% SDS, and 0.5% sodium deoxycholate) and incubation for 10 minutes at room temperature. Extracts were thoroughly mixed with luciferase reagent and luminescence was measured after 20 min incubation at room temperature on a microplate reader (Tecan, Life Sciences). Samples were then mixed with Dual-Glo® Stop & Glo® reagent (blocking firefly luciferase and initiating Renilla luciferase), incubated for 20 min at room temperature and luminescence was measured. Relative luminescence [%] to quantify translational fidelity was calculated as previously described (Harger and Dinman 2003):

$$relative\ luminescence\ [\%] = \frac{\frac{firefly\ [sample]}{Renilla\ [sample]}}{\frac{firefly\ [control]}{Renilla\ [control]}} * 100$$

5.2.13 OPP labelling *in vivo*

Mice at the age of 4-6 months were weighed and OPP was injected intraperitoneally at a concentration of 49.5 mg per kilogram of body weight (10 mM OPP in PBS, 10 µL/g). Vehicle control mice were injected with the appropriate amount of PBS. For these experiments, male mice were used, except for 4 female vehicle control mice. 1 hour after injection, mice were sacrificed by cervical dislocation. Bone marrow cells were obtained by flushing the femur and tibia with PBS/EtOH (70%). Single cell suspension of liver, kidney and lung were prepared by washing the tissues in PBS, followed by cutting and incubation with collagenase NB4 (17454, Serva) in DMEM/Ham's F12 (1.7 mg/ml) at 37°C for 30 minutes. The suspension was pushed through a G23 needle for several times in a petri dish and filtered through a cell strainer (40 µm). After centrifugation, cells were incubated with DNase I in DMEM/Ham's F12 (5 U/mL) at room temperature for 10 minutes. Cells were harvested by centrifugation, fixed in 1 ml EtOH (70%) and stored at 4 °C. For visualisation of OPP incorporation, cells were treated as described above.

5.2.14 Polysome profiling

Cells were grown to ~80% confluence and treated with 100 µg/mL cycloheximide for 10 min at 37 °C. Subsequently, cells were washed twice with ice-cold PBS containing 100 µg/mL cycloheximide and then resuspended in lysis buffer (30 mM HEPES-KOH pH 7.6, 150 mM KOAc, 5 mM MgOAc₂, 4 mM DTT, RiboLock RNase Inhibitor (ThermoFisher Scientific), 1x cOmplete™ Protease Inhibitor Cocktail (Roche), 100 µg/mL cycloheximide). Cell membranes were disrupted by passing through a 23G needle for 25 times. Cell debris were removed by centrifugation at ~15.000 g for 15 min and the resulting cleared cell lysate was layered on a linear 10-50% (w/v) sucrose gradient prepared in buffer containing 30 mM HEPES-KOH pH 7.6, 150 mM KOAc, 5 mM MgOAc₂, 4 mM DTT, 1 mM PMSF, 100 µg/mL cycloheximide and

centrifuged for 2 h 45 min at 39.000 rpm in a Beckman SW41 rotor at 4 °C. The gradient was then fractionated using a Brandel density gradient fractionation system. Polysome profiles were generated by continuous measurement of the absorbance at 254 nm. Polysome profiles within one biological replicate were normalized to the same square area under the entire profile and the peak area ratio between control HeLa and NSUN5 KO was subsequently calculated.

5.2.15 In vitro translation assay

Cells were grown to ~80% confluence, washed twice with cold PBS and resuspended in buffer containing 30 mM HEPES-KOH pH 7.6, 150 mM KOAc, 5 mM MgOAc₂, 4 mM DTT, RiboLock RNase Inhibitor (ThermoFisher Scientific) and 1x cOmplete™ Protease Inhibitor Cocktail (Roche). Cell debris were removed by centrifugation at ~15.000 g for 15 min and the resulting cleared cell lysate was layered on a 0.5 mL sucrose cushion prepared in 30 mM HEPES-KOH pH 7.6, 150 mM KOAc, 5 mM MgOAc₂ and centrifuged in a Beckman mini-ultracentrifuge for 2 h 30 min at 200.000 g in a S140AT rotor at 4 °C. The pellet (P100 - ribosome fraction) was re-suspended in HEPES-KOH pH 7.6, 150 mM KOAc and 5 mM MgOAc₂ and the supernatant (S100) was stored on ice. Ribosome content was estimated based on absorbance at 260 nm.

For in vitro translation 6.45 pmol of control HeLa or NSUN5 KO HeLa P100 were mixed with 5 µL HeLa S100 in a total volume of 20 µL and incubated for 10 min at 35 °C and 450 rpm. During this period the majority of ribosomes that were already associated with mRNAs will terminate translation. After pre-incubation, 2.1 µL of translation mixture containing 1.2 µL 10x translation cocktail (150 mM HEPES-KOH pH 7.6, 750 mM KOAc, 19.5 mM MgOAc₂, 4 mM GTP, 17.5 mM ATP, 500 µM 19 amino acids except methionine), 0.17 µL 100 mg/mL bulk yeast tRNA, 0.08 µL 3M creatine phosphate, 0.06 µL 20 mg/mL creatine phosphokinase and 0.625 µL ³⁵S-methionine) were added to the reaction (Fricker et al. 2019). In vitro translation was performed at 35 °C and rotation at 450 rpm for 30 min, stopped by the addition of 8 µL of 4x Laemmli buffer and incubation at 95 °C for 5 minutes. Proteins were separated by 10% SDS PAGE and visualized by autoradiography.

5.2.16 Multiple protein sequence alignment of Rcm1p and NSUN family members

A multiple protein sequence alignment of Rcm1p (UniProtKB: P53972), NSUN1 (UniProtKB: P46087), NSUN2 (UniProtKB: Q08J23), NSUN3 (UniProtKB: Q9H649), NSUN4 (UniProtKB: Q96CB9), NSUN5 (UniProtKB: B2RD09), NSUN6 (UniProtKB: Q8TEA1) and NSUN7 (UniProtKB: Q8NE18) was performed with T-Coffee Version_11.00.8cbe486 (Di Tommaso et al. 2011). Clustal colouring was applied. From this alignment a phylogenetic tree with average distances using BLOSSUM62 was constructed in JalView 2.10.5 (Waterhouse et al. 2009).

5.2.17 Statistics

Statistical analysis and plotting of results were done in R, version 3.5.1 (2018-07-02) [R Core Team (2017) R: A Language and Environment for Statistical Computing. Vienna, Austria: R Foundation for Statistical Computing. Retrieved from <http://www.R-project.org>]. Depending on the shape of the sample distribution, appropriate parametric or non-parametric tests were used as indicated in the figure legend. The number of replicates usually refers to independent biological replicates unless indicated otherwise.

5.3 *C. elegans*

5.3.1 Worm strains and culture conditions

The following *C. elegans* strains were used in this study: N2; JGG1 *nsun-5(tm3898)*, SA115 *unc-119(ed3)*, JJ1473 *unc-119(ed3)*, TP12 *kals12[col-19::GFP]*, DCL569 *mkcSi13[P_{sun-1}::rde-1::sun-1 3'UTR + unc-119(+)]*, NL2098 *rff-1(pk1417)* and NL2550 *ppw-1(pk2505)*. Worms were cultured following standard protocols on *Escherichia coli* OP50-seeded NGM agar plates at 20°C, unless indicated otherwise (Brenner, 1974).

5.3.2 RNAi knockdown

The *nsun-1* RNAi clones was from the J. Ahringer library (Kamath et al. 2003) and the *nsun-5* RNAi clone from the M. Vidal library (Rual et al. 2004). For inactivating *nsun-1* and *nsun-5*, feeding of double-stranded RNA expressed in bacteria was used (Timmons et al; 2001). Therefore, the HT115 strain of *E. coli*, carrying either the respective RNAi construct or the empty vector (L4440) as RNAi control, was cultured overnight in LB medium with ampicillin and tetracyclin at 37 °C. Bacteria were harvested by centrifugation, resuspended in LB medium and either 100 µL (60 mm plates) or 400 µL (100 mm plates) were plated on NGM containing 1 mM isopropyl-b-D-thiogalactoside and 25 µg/mL carbenicillin. The plates were incubated at 37 °C overnight and used within one week.

Larval-onset RNAi was achieved by bleaching adult animals. Released eggs were transferred directly to plates seeded with RNAi bacteria. Adulthood was usually reached after three days and animals were used for experiments when the RNAi control strain started to lay eggs.

In case of adult-onset RNAi, eggs were transferred to plates seeded with RNAi control bacteria. Animals were raised until egg production commenced and subsequently transferred to the respective RNAi bacteria.

5.3.3 Differential Interference Contrast (DIC) microscopy

Worms were paralyzed using 1 M sodium azide solution and mounted on 2% agar pads. Images were acquired on a Leica DMI6000B microscope with a 10x dry objective (NA 0.3) or a 63x glycerol objective (NA 1.3) in DIC brightfield mode. Cropping, insertion of scale bars and brightness and contrast adjustments were done with Image J (version 2.0.0-rc-65/1.51w; Java 1.8.0_162 [64-bit]).

5.3.4 Mobility

Animals were either synchronized by timed egg-lay (two replicates) or by hypochlorite treatment (one replicate) on RNAi control plates. When reaching adulthood, nematodes were

transferred to RNAi plates. Every few days at regular intervals, plates were rocked in order to induce movement of animals and videos were subsequently recorded for one minute. Worms were transferred to fresh plates whenever necessary. At day 16 the vast majority of worms completely ceased movement, thus we did not include any later timepoints. Notably, we did not notice any obvious aversion behavior or elevated speed at young age upon *nsun-1* or *nsun-5* RNAi, which was previously shown to be present upon depletion of other components of the translational machinery (Melo and Ruvkun 2012). Worm Lab version 4.1.1 was used to track individual animals and calculate the average speed.

5.3.5 Lifespan assays

Lifespan measurement was conducted as previously described (Schosserer et al. 2015). For lifespan assays, 90 adults per condition were transferred to plates seeded with the respective RNAi bacteria (control, *nsun-1*, *nsun-5*). Wildtype worms were pre-synchronised on NGM plates seeded with UV-killed OP50 bacteria. 50 adult worms were transferred to NGM plates and allowed to lay eggs for 15 h; then the adult worms were removed. Synchronisation by timed egg lay was performed 72 h after the pre-synchronisation by transferring 350 gravid worms from the pre-synchronisation to fresh NGM plates seeded with RNAi control bacteria and allowed to lay eggs for four hours. After 68 h, 90 young adult worms per condition were placed on fresh NGM plates containing 5 mL NGM, 100 μ L bacterial suspension and 50 μ g FUDR. This day represents day 0 in the lifespan measurement. Worms were scored as “censored” or “dead” every two to four days. Nematodes were scored as “censored” if they had crawled off the plate, were missing or died due to other causes than ageing, such as gonad extrusion. Animals were transferred to fresh plates every 3–7 days depending on the availability of the bacterial food source. Lifespans were performed at 20°C. Kaplan-Meier survival curves were plotted and log-rank statistics were calculated.

5.3.6 Thermotolerance

Thermotolerance was assessed as previously described (Vieira et al. 2017). Animals were synchronized by hypochlorite treatment and released eggs were transferred to NGM plates seeded with RNAi control bacteria and kept at 20°C. After 48 h, L4 animals were picked on RNAi control, *nsun-1* or *nsun-5* RNAi plates and exposed to RNAi for approximately three days (68 hours). Subsequently, plates were transferred to 35°C and scored every 1-2 h for survival.

5.3.7 Body size

Worms were synchronized by hypochlorite treatment and incubated in liquid S-Basal medium overnight. On the following day, eggs/L1 were transferred to RNAi plates (RNAi control, *nsun-1* and *nsun-5* RNAi). Three days later, worms were transferred to agar pads and paralyzed using sodium azide and visualized using DIC microscopy (see above).

5.3.8 Brood size analysis

Worms were synchronised by treatment with hypochlorite solution and incubated in S-Basal at room temperature overnight. L1 larvae were subsequently transferred to NGM plates seeded with RNAi control bacteria. After 48 h, L4 animals were transferred to individual wells of a 24-well plate seeded with the respective RNAi bacteria (HT115, *nsun-1*, *nsun-5*). Each well contained 1.5 mL of NGM agar and 3 µL of bacterial suspension (1:2 dilution in S-Basal). Worms were transferred to a new well every day for four consecutive days and total progeny of individual animals was counted. Per condition and experiment, five worms were analysed.

5.3.9 Global protein synthesis by puromycin incorporation

Puromycin incorporation was measured as previously described (Tiku et al. 2018) with minor modifications. Heat-inactivated OP-50 (75°C, 40 min) were provided as food source during pulse labelling. As negative controls, RNAi control treated worms were used either without

addition of puromycin or by pulse-labelling at 4°C instead of 20°C. Around 100 animals per condition were harvested for western blot analysis. Lysis was done directly in SDS loading dye (60 µM Tris/HCl pH 6.8, 2% SDS, 10% glycerol, 0.0125% bromophenol blue and 1.25% β-mercaptoethanol). Worms in SDS loading dye were homogenized with a pellet pestle for 1 min. Then, the samples were heated to 95°C and loaded on 4-15% Mini-PROTEAN® TGX gels (BioRad) in Laemmli-Buffer (25 mM Tris, 250 mM glycine and 0.1% SDS). Protein bands were transferred to PVDF-membranes (Bio Rad) at 25 V and 1.3 A for 3 min. After blocking with 3% milk in PBS, the membrane was incubated overnight at 4°C with a mixture of anti-Histone H3 (Abcam ab1791, 1:4000) and anti-puromycin (Millipore 12D10, 1:10000). After washing and secondary antibody incubation (IRDye680RD and IRDye800CW, 1:10000), the membrane was scanned on the Odyssey Infrared Imager (LI-COR). Quantification of band intensities was performed in Image J (version 2.0.0-rc-65/1.51w; Java 1.8.0_162 [64-bit]).

5.3.10 Polysome profiling

Two-day-old adult worms were used to generate polysome profiles as previously described (Rogers et al. 2011). One hundred microliter worm-pellet were homogenized on ice in 300 µL of solubilisation buffer (300 mM NaCl, 50 mM Tris-HCl (pH 8.0), 10 mM MgCl₂, 1 mM EGTA, 200 µg/ml heparin, 400 U/ml RNasin, 1.0 mM phenylmethylsulfonyl fluoride, 0.2 mg/ml cycloheximide, 1% Triton X-100, 0.1% sodium deoxycholate) using a pellet pestle. 700 µl additional solubilisation buffer were added, vortexed briefly, and placed on ice for 10 min before centrifugation at 20.000 g for 15 min at 4°C. Approximately 0.9 mL of the supernatant was applied to the top of a linear 10-50% sucrose gradient in high salt resolving buffer (140 mM NaCl, 25 mM Tris-HCl (pH 8.0), 10 mM MgCl₂) and centrifuged in a Beckman SW41Ti rotor (Beckman Coulter, Fullerton, CA, USA) at 180.000 g for 90 min at 4°C.

5.3.11 RNA Seq

Gradients were fractionated while continuously monitoring the absorbance at 260 nm. Trizol LS (Life Technologies) was immediately added to collected fractions and RNA was isolated

following the manufacturer's protocol. PolyA-selection, generation of a strand-specific cDNA library and sequencing on the HiSeq 4000 platform (Illumina) using the 50 bp SR mode was performed by GATC Biotech (Konstanz, Germany). At least 30 million reads were generated per sample.

FASTQ Trimmer by column (Galaxy Version 1.0.0) was used to remove the first 12 bases from the 5' end of each read due to an obvious base bias in this region, as detected by FastQC (Galaxy Version 0.69). Filter by quality (Galaxy Version 1.0.0) was performed using a cut-off value of 20 and only reads with a maximum number of 8 bases with quality lower than the cut-off value were retained. RNA STAR (Galaxy Version 2.6.0b-1) was used to align reads to the WBcel235 reference genome using the default options. Aligned reads with a minimum alignment quality of 10 were counted using htseq-count (Galaxy Version 0.9.1).

Differential expression was analyzed using the DEseq2 package in R. The contrast

~ batch + condition

(batch = biological replicate, condition = sample description) was applied to compare the polysome fraction to the total RNA of either RNAi control or *nsun-1* RNAi treated samples. Afterwards, results were filtered in R to contain only protein-coding genes (according to ENSEMBL annotation), genes with detectable expression (base mean > 1), a fold change of > 2 ($\log_2FC > 1$) and an adjusted p-value of < 0.05. Vulcano plots were generated in R using the EnhancedVulcano package, labelling the top 5 up- and down-regulated genes respectively.

GO term enrichment using DAVID (version 6.7) was performed as previously described (Rollins et al. 2019). Only protein-coding genes with detectable expression (base mean > 1), a fold change of > 2 and an adjusted p-value of < 0.10 were considered. For visualization, only the broadest GO terms of the GOTERM_BP_FAT, GOTERM_MF_FAT and GOTERM_CC_FAT categories, which were still significantly enriched ($FDR < 0.05$), are shown while similar terms based on the same subset of genes but lower in hierarchy were manually removed. Full results are contained in the supplements.

UTR characterization and RBP motif enrichment were performed as previously described (Rollins et al. 2019) using only protein-coding genes with detectable expression (base mean > 1), a fold change of > 2 and an adjusted p-value of < 0.10.

The raw and processed sequencing data are available from the Gene Expression Omnibus database (<https://www.ncbi.nlm.nih.gov/geo>) under accession GSE143618.

5.3.12 RT-qPCR

Samples were collected by either transferring worms individually into 1.5 mL tubes or by washing them off NGM plates using S-Basal. After three washing steps with S-Basal, 300 µL TRIzol® LS Reagent were added to approximately 100 µL residual S-Basal including worms. Subsequently, worms were homogenised with a pellet pestle for one minute, 600 µL TRIzol® LS Reagent were added and the sample was vortexed for five minutes at room temperature. Total RNA was isolated using Direct-zol™ RNA MiniPrep Kit (Zymo) according to the instructions by the manufacturer. For cDNA synthesis, 500 ng RNA were converted into cDNA using the Applied Biosystems™ High-Capacity cDNA Reverse Transcription Kit (Thermo Fisher Scientific). cDNA was amplified from total RNA using random primers. RT-qPCR was performed on a Rotor-Gene Q (QIAGEN) using HOT FIREPol® EvaGreen® qPCR Mix. The absolute amounts of mRNAs were calculated by computing a standard curve and the resulting copy numbers were normalized to the housekeeping genes *act-1* and *tba-1*. The following primers were used: *nsun-1*: 5'-TCGCCGAGATCCACAGAAAT-3' (sense) and 5'-CCACGTTCATTCCACGGTTG-3' (antisense); *nsun-2*: 5'-GCTTAAACGAGAGACGGGAGTT-3' (sense) and 5'-CACCAGTATCCTGGGCGTG-3' (antisense); *nsun-4*: 5'-TGTTGGATATGTGTGCGGCT-3' (sense) and 5'-GCGTCCTTGCGTTTTAGGAC-3' (antisense); *nsun-5*: 5'-GGCCAAGGAGAAAAGTGTG-3' (sense) and 5'-GATCCACCGATATTCGCAT-3' (antisense); *act-1*: 5'-CTACGAACTTCCTGACGGACAAG-3' (sense) and 5'-CCGGCGGACTCCATACC-3' (antisense) and *tba-1*: 5'-TCAACACTGCCATCGCCGCC-3' (sense) and 5'-TCCAAGCGAGACCAGGCTTCAG-3' (antisense).

For measuring mRNA expression during development, worms were synchronised by treatment with hypochlorite solution and the released eggs were subsequently transferred to four separate NGM plates seeded with UV-killed OP50 bacteria. Samples were taken from eggs immediately after bleaching, L1/L2 (20 h after bleaching), L3 (32 h after bleaching), L4 (46 h after bleaching) and young adults (60 h after bleaching).

5.3.13 3-D ribosome structure

The PyMOL Molecular Graphics System (Version 2.0) was used. The structure was modelled on the human 80S ribosome (PDB 6EK0).

5.3.14 m⁵C detection by COBRA assay

NSUN-5 activity was measured by the COBRA assay as previously described (Adamla et al. 2019) using the following primers: 5'-GGGAGTAATTATGATTTTCTAAGGTAG-3' (sense) and 5'-ATAATAAATAAAAACAATAAAAATCTCACTAATCCATTCATACAC-3' (antisense).

5.3.15 HPLC analysis of m⁵C

13-15µg 26S purified on sucrose gradient were digested to nucleosides and analyzed by HPLC. Peaks elutes at 12 min and as a control, a commercial 5-methylcytidine (NM03720, CarboSynth) was used. For quantification of m⁵C peak area, the peak was normalized to either the peak eluting at 16 min (asterisk on the Figure), or to the peak eluting at 8 min (U), with similar results. The results are shown for normalization to the peak eluting at 16 min.

5.3.16 Pre-rRNA processing analysis

For analysis of high-molecular weight RNA species, 3 µg total RNA was resolved on a denaturing agarose gel (6% formaldehyde/1.2% agarose) and migrated for 16 h at 65 volts. Agarose gels were transferred by capillarity onto Hybond-N+ membranes. The membrane was prehybridized for 1 h at 65 °C in 50% formamide, 5x SSPE, 5x Denhardt's solution, 1% SDS (w/v) and 200 µg/ml fish sperm DNA solution (Roche). The ³²P-labeled oligonucleotide probe (LD2648 (ITS1): CACTCAACTGACCGTGAAGCCAGTCG; LD2649 (ITS2): GGACAAGATCAGTATGCCGAGACGCG) was added and incubated for 1 h at 65 °C and then overnight at 37 °C. For analysis of low molecular weight RNA species, northern blots were

exposed to Fuji imaging plates (Fujifilm) and signals acquired with a Phosphorimager (FLA-7000; Fujifilm).

5.3.17 Statistics and sample size estimation

No explicit power analysis was used. Sample sizes estimations were partially based on our own previous empirical experience with the respective assays, as well as the cited literature.

No systematic blinding of group allocation was used, but samples were always analysed in a random order. Nematodes were randomly assigned to the experimental groups. All lifespan, stress resistance and locomotion experiments were performed by at least two different operators.

Most experiments were performed in three independent experiments, unless stated otherwise in the figure legend. Independent experiments were always initiated at different days and thus always resemble different batches of nematodes. Some experiments (RNA isolation for RNA-seq, HPLC analysis of m⁵C, pre-rRNA processing analysis) were performed once with all frozen independent batches of nematodes to minimize technical variation. No outliers were detected or removed. Criteria for censoring animals for lifespan, stress resistance and locomotion experiments are indicated in the respective chapters.

Statistical tests used, exact values of N, definitions of center, methods of multiple test correction, and dispersion and precision measures are indicated in the respective figure legends. P-value thresholds were defined as *P < 0.05, **P < 0.01 and ***P < 0.001. For RNA-seq, statistical tests and p-value thresholds are explained in detail in the “RNA-seq” chapter.

6 References

- Acosta JC, Banito A, Wuestefeld T, Georgilis A, Janich P, Morton JP, Athineos D, Kang T-W, Lasitschka F, Andrulis M, et al. 2013. A complex secretory program orchestrated by the inflammasome controls paracrine senescence. *Nat Cell Biol* **15**: 978–90. <http://www.ncbi.nlm.nih.gov/pubmed/23770676>.
- Adamla F, Rollins J, Newsom M, Snow S, Schosserer M, Heissenberger C, Horrocks J, Rogers AN, Ignatova Z. 2019. A Novel Caenorhabditis Elegans Proteinopathy Model Shows Changes in mRNA Translational Frameshifting During Aging. *Cell Physiol Biochem* **52**: 970–983.
- Al-Hadid Q, Roy K, Chanfreau G, Clarke SG. 2016. Methylation of yeast ribosomal protein Rpl3 promotes translational elongation fidelity. *RNA* **22**: 489–498. <http://rnajournal.cshlp.org/lookup/doi/10.1261/rna.054569.115>.
- Alic N, Partridge L. 2015. Europe PMC Funders Group Death and dessert : Nutrient signalling pathways and ageing. **23**: 738–743.
- Alter BP, Giri N, Savage SA, Rosenberg PS. 2009. Cancer in dyskeratosis congenita. *Blood* **113**: 6549–6557. <https://ashpublications.org/blood/article/113/26/6549/26174/Cancer-in-dyskeratosis-congenita>.
- Armanios M. 2013. Telomeres and age-related disease: How telomere biology informs clinical paradigms. *J Clin Invest* **123**: 996–1002.
- Artero-Castro A, Perez-Alea M, Feliciano A, Leal JA, Genestar M, Castellvi J, Peg V, Ramón y Cajal S, Lleonart ME. 2015. Disruption of the ribosomal P complex leads to stress-induced autophagy. *Autophagy* **11**: 1499–1519. <https://www.tandfonline.com/doi/full/10.1080/15548627.2015.1063764>.
- Azpurua J, Ke Z, Chen IX, Zhang Q, Ermolenko DN, Zhang ZD, Gorbunova V, Seluanov A. 2013. Naked mole-rat has increased translational fidelity compared with the mouse, as well as a unique 28S ribosomal RNA cleavage. *Proc Natl Acad Sci U S A* **110**: 17350–5. <http://www.pnas.org/content/110/43/17350.abstract>.
- Baar MP, Brandt RMCC, Putavet DA, Klein JDDD, Derks KWJJ, Bourgeois BRMM, Stryeck S, Rijksen Y, van Willigenburg H, Feijtel DA, et al. 2017. Targeted Apoptosis of Senescent Cells Restores Tissue Homeostasis in Response to Chemotoxicity and Aging. *Cell* **169**: 132-147.e16. <http://linkinghub.elsevier.com/retrieve/pii/S0092867417302465>.
- Baker DJ, Childs BG, Durik M, Wijers ME, Sieben CJ, Zhong J, Saltness RA, Jeganathan KB, Verzosa GC, Pezeshki A, et al. 2016. Naturally occurring p16(Ink4a)-positive cells shorten healthy lifespan. *Nature* **530**: 184–9. <http://www.ncbi.nlm.nih.gov/pubmed/26840489>.
- Baker DJ, Wijshake T, Tchkonja T, LeBrasseur NK, Childs BG, van de Sluis B, Kirkland JL, van Deursen JM. 2011. Clearance of p16Ink4a-positive senescent cells delays ageing-associated disorders. *Nature* **479**: 232–6. <http://www.ncbi.nlm.nih.gov/pubmed/22048312>.
- Ballesta JPG, Remacha M. 1996. The Large Ribosomal Subunit Stalk as a Regulatory Element of the Eukaryotic Translational Machinery. pp. 157–193 <https://linkinghub.elsevier.com/retrieve/pii/S0079660308601932>.
- Ban N, Beckmann R, Cate JHD, Dinman JD, Dragon F, Ellis SR, Lafontaine DLJ, Lindahl L, Liljas A, Lipton JM, et al. 2014. A new system for naming ribosomal proteins. *Curr Opin Struct Biol* **24**: 165–169. <https://linkinghub.elsevier.com/retrieve/pii/S0959440X14000037>.
- Bansal A, Zhu LJ, Yen K, Tissenbaum HA. 2015. Uncoupling lifespan and healthspan in Caenorhabditis elegans longevity mutants. *Proc Natl Acad Sci U S A* **112**: E277-86.
- Bantis A, Giannopoulos A, Gonidi M, Liossi A, Aggelonidou E, Petrakakou E, Athanassiades P, Athanassiadou P. 2004. Expression of p120, Ki-67 and PCNA as proliferation biomarkers in imprint smears of prostate carcinoma and their prognostic value. *Cytopathology* **15**: 25–31.
- Bar DZ, Charar C, Dorfman J, Yadid T, Tafforeau L, Lafontaine DLJ, Gruenbaum Y. 2016. Cell size and fat content of dietary-restricted Caenorhabditis elegans are regulated by ATX-2, an mTOR repressor. *Proc Natl Acad*

- Barzilai N, Huffman DM, Muzumdar RH, Bartke A. 2012. The critical role of metabolic pathways in aging. *Diabetes* **61**: 1315–22. <http://www.ncbi.nlm.nih.gov/pubmed/22618766>.
- Baxter-Roshek JL, Petrov AN, Dinman JD. 2007. Optimization of ribosome structure and function by rRNA base modification. *PLoS One* **2**: e174. <http://www.ncbi.nlm.nih.gov/pubmed/17245450>.
- Birkedal U, Christensen-Dalsgaard M, Krogh N, Sabarinathan R, Gorodkin J, Nielsen H. 2014. Profiling of Ribose Methylations in RNA by High-Throughput Sequencing. *Angew Chemie Int Ed n/a-n/a*. <http://doi.wiley.com/10.1002/anie.201408362>.
- Bjedov I, Toivonen JM, Kerr F, Slack C, Jacobson J, Foley A, Partridge L. 2010. Mechanisms of life span extension by rapamycin in the fruit fly *Drosophila melanogaster*. *Cell Metab* **11**: 35–46. <http://www.ncbi.nlm.nih.gov/pubmed/20074526>.
- Blackburn EH, Greider CW, Szostak JW. 2006. Telomeres and telomerase: the path from maize, Tetrahymena and yeast to human cancer and aging. *Nat Med* **12**: 1133–8. <http://www.ncbi.nlm.nih.gov/pubmed/17024208>.
- Boisvert F-M, Ahmad Y, Gierliński M, Charrière F, Lamont D, Scott M, Barton G, Lamond AI. 2012. A Quantitative Spatial Proteomics Analysis of Proteome Turnover in Human Cells. *Mol Cell Proteomics* **11**: M111.011429. <http://www.mcponline.org/lookup/doi/10.1074/mcp.M111.011429>.
- Borghesan M, Fafián-Labora J, Eleftheriadou O, Carpintero-Fernández P, Paez-Ribes M, Vizcay-Barrena G, Swisa A, Kolodkin-Gal D, Ximénez-Embún P, Lowe R, et al. 2019. Small Extracellular Vesicles Are Key Regulators of Non-cell Autonomous Intercellular Communication in Senescence via the Interferon Protein IFITM3. *Cell Rep* **27**: 3956–3971.e6. <https://linkinghub.elsevier.com/retrieve/pii/S221112471930734X>.
- Bouffard S, Dambroise E, Brombin A, Lempereur S, Hatin I, Simion M, Corre R, Bourrat F, Joly J-S, Jamen F. 2018. Fibrillarin is essential for S-phase progression and neuronal differentiation in zebrafish dorsal midbrain and retina. *Dev Biol* **437**: 1–16. <https://linkinghub.elsevier.com/retrieve/pii/S0012160617306188>.
- Bourgeois G, Ney M, Gaspar I, Aigueperse C, Schaefer M, Kellner S, Helm M, Motorin Y. 2015. Eukaryotic rRNA Modification by Yeast 5-Methylcytosine-Methyltransferases and Human Proliferation-Associated Antigen p120 ed. T. Preiss. *PLoS One* **10**: e0133321. <http://dx.plos.org/10.1371/journal.pone.0133321>.
- Brenner S. 1974. *Caenorhabditis elegans*. *Methods* **77**: 71–94. <http://www.pubmedcentral.nih.gov/articlerender.fcgi?artid=1213120&tool=pmcentrez&rendertype=abstract>.
- Bujnicki JM. 2004. Sequence-structure-function studies of tRNA:m5C methyltransferase Trm4p and its relationship to DNA:m5C and RNA:m5U methyltransferases. *Nucleic Acids Res* **32**: 2453–2463. <https://academic.oup.com/nar/article-lookup/doi/10.1093/nar/gkh564>.
- Burtner CR, Kennedy BK. 2010. Progeria syndromes and ageing: what is the connection? *Nat Rev Mol Cell Biol* **11**: 567–578. <http://www.ncbi.nlm.nih.gov/pubmed/20651707>.
- Campisi J, d'Adda di Fagagna F. 2007. Cellular senescence: when bad things happen to good cells. *Nat Rev Mol Cell Biol* **8**: 729–740. <http://www.ncbi.nlm.nih.gov/pubmed/17667954>.
- Cantara WA, Crain PF, Rozenski J, McCloskey JA, Harris KA, Zhang X, Vendeix FAP, Fabris D, Agris PF. 2011. The RNA modification database, RNAMDB: 2011 update. *Nucleic Acids Res* **39**: D195–D201. <https://academic.oup.com/nar/article-lookup/doi/10.1093/nar/gkq1028>.
- Carlile TM, Rojas-Duran MF, Zinshteyn B, Shin H, Bartoli KM, Gilbert W V. 2014. Pseudouridine profiling reveals regulated mRNA pseudouridylation in yeast and human cells. *Nature* **515**: 143–146. <http://www.nature.com/articles/nature13802>.
- Carroll AJ, Heazlewood JL, Ito J, Millar AH. 2008. Analysis of the Arabidopsis Cytosolic Ribosome Proteome Provides Detailed Insights into Its Components and Their Post-translational Modification. *Mol Cell*

- Proteomics* **7**: 347–369. <http://www.mcponline.org/lookup/doi/10.1074/mcp.M700052-MCP200>.
- Cavaillé J, Nicoloso M, Bachellerie J-P. 1996. Targeted ribose methylation of RNA in vivo directed by tailored antisense RNA guides. *Nature* **383**: 732–735. <http://www.nature.com/articles/383732a0>.
- Cevenini E, Monti D, Franceschi C. 2013. Inflamm-ageing. *Curr Opin Clin Nutr Metab Care* **16**: 14–20. <http://www.ncbi.nlm.nih.gov/pubmed/23132168>.
- Chang J, Wang Y, Shao L, Laberge R-M, Demaria M, Campisi J, Janakiraman K, Sharpless NE, Ding S, Feng W, et al. 2016. Clearance of senescent cells by ABT263 rejuvenates aged hematopoietic stem cells in mice. *Nat Med* **22**: 78–83. <http://www.ncbi.nlm.nih.gov/pubmed/26657143>.
- Chen P, Zhang T, Yuan Z, Shen B, Chen L. 2019. Expression of the RNA methyltransferase Nsun5 is essential for developing cerebral cortex. *Mol Brain* **12**: 74. <http://www.ncbi.nlm.nih.gov/pubmed/31462248>.
- Cheng JX, Chen L, Li Y, Cloe A, Yue M, Wei J, Watanabe KA, Shammoo JM, Anastasi J, Shen QJ, et al. 2018. RNA cytosine methylation and methyltransferases mediate chromatin organization and 5-azacytidine response and resistance in leukaemia. *Nat Commun* **9**: 1163.
- Cheng Z, Mugler CF, Keskin A, Hodapp S, Chan LY-L, Weis K, Mertins P, Regev A, Jovanovic M, Brar GA. 2019. Small and Large Ribosomal Subunit Deficiencies Lead to Distinct Gene Expression Signatures that Reflect Cellular Growth Rate. *Mol Cell* **73**: 36-47.e10. <https://linkinghub.elsevier.com/retrieve/pii/S109727651830892X>.
- Childs BG, Baker DJ, Wijshake T, Conover CA, Campisi J, van Deursen JM. 2016. Senescent intimal foam cells are deleterious at all stages of atherosclerosis. *Science* **354**: 472–477. <http://www.ncbi.nlm.nih.gov/pubmed/27789842>.
- Chiocchetti A, Zhou J, Zhu H, Karl T, Haubenreisser O, Rinnerthaler M, Heeren G, Oender K, Bauer J, Hintner H, et al. 2007. Ribosomal proteins Rpl10 and Rps6 are potent regulators of yeast replicative life span. *Exp Gerontol* **42**: 275–286.
- Cole SE, LaRiviere FJ, Merrih CN, Moore MJ. 2009. A Convergence of rRNA and mRNA Quality Control Pathways Revealed by Mechanistic Analysis of Nonfunctional rRNA Decay. *Mol Cell* **34**: 440–450. <https://linkinghub.elsevier.com/retrieve/pii/S1097276509002706>.
- Conboy IM, Conboy MJ, Wagers AJ, Girma ER, Weissman IL, Rando TA. 2005. Rejuvenation of aged progenitor cells by exposure to a young systemic environment. *Nature* **433**: 760–764. <http://www.nature.com/articles/nature03260>.
- Conboy IM, Rando TA. 2012. Heterochronic parabiosis for the study of the effects of aging on stem cells and their niches. *Cell Cycle* **11**: 2260–2267. <http://www.tandfonline.com/doi/abs/10.4161/cc.20437>.
- Coppé J-P, Patil CK, Rodier F, Sun Y, Muñoz DP, Goldstein J, Nelson PS, Desprez P-Y, Campisi J. 2008. Senescence-associated secretory phenotypes reveal cell-nonautonomous functions of oncogenic RAS and the p53 tumor suppressor. *PLoS Biol* **6**: 2853–68. <http://www.ncbi.nlm.nih.gov/pubmed/19053174>.
- Cui W, Pizzollo J, Han Z, Marcho C, Zhang K, Mager J. 2016. Nop2 is required for mammalian preimplantation development. *Mol Reprod Dev* **83**: 124–31.
- Culetto E, Sattelle DB. 2000. A role for *Caenorhabditis elegans* in understanding the function and interactions of human disease genes. *Hum Mol Genet* **9**: 869–877.
- Curran SP, Ruvkun G. 2007. Lifespan regulation by evolutionarily conserved genes essential for viability. *PLoS Genet* **3**: 0479–0487.
- De Keersmaecker K, Sulima SO, Dinman JD. 2015. Ribosomopathies and the paradox of cellular hypo- to hyperproliferation. *Blood* **125**: 1377–1382.
- Decatur WA, Fournier MJ. 2002. rRNA modifications and ribosome function. *Trends Biochem Sci* **27**: 344–351. <https://linkinghub.elsevier.com/retrieve/pii/S0968000402021096>.
- Demaria M, Ohtani N, Youssef SA, Rodier F, Toussaint W, Mitchell JR, Laberge R-M, Vijg J, Van Steeg H, Dollé

- MET, et al. 2014. An essential role for senescent cells in optimal wound healing through secretion of PDGF-AA. *Dev Cell* **31**: 722–33. <http://www.ncbi.nlm.nih.gov/pubmed/25499914>.
- Di Tommaso P, Moretti S, Xenarios I, Orobitz M, Montanyola A, Chang J-M, Taly J-F, Notredame C. 2011. T-Coffee: a web server for the multiple sequence alignment of protein and RNA sequences using structural information and homology extension. *Nucleic Acids Res* **39**: W13–7.
- Dickinson ME, Flenniken AM, Ji X, Teboul L, Wong MD, White JK, Meehan TF, Weninger WJ, Westerberg H, Adissu H, et al. 2016. High-throughput discovery of novel developmental phenotypes. *Nature* **537**: 508–514. <http://www.nature.com/articles/nature19356>.
- Dokal I. 2000. Dyskeratosis congenita in all its forms. *Br J Haematol* **110**: 768–779. <http://doi.wiley.com/10.1046/j.1365-2141.2000.02109.x>.
- Doll A, Grzeschik KH. 2001. Characterization of two novel genes, WBSCR20 and WBSCR22, deleted in Williams-Beuren syndrome. *Cytogenet Cell Genet* **95**: 20–27.
- Dupuis-Sandoval F, Poirier M, Scott MS. 2015. The emerging landscape of small nucleolar RNAs in cell biology. *Wiley Interdiscip Rev RNA* **6**: 381–397. <http://doi.wiley.com/10.1002/wrna.1284>.
- Edelheit S, Schwartz S, Mumbach MR, Wurtzel O, Sorek R. 2013. Transcriptome-Wide Mapping of 5-methylcytidine RNA Modifications in Bacteria, Archaea, and Yeast Reveals m5C within Archaeal mRNAs ed. V. De Crécy-Lagard. *PLoS Genet* **9**: e1003602. <http://dx.plos.org/10.1371/journal.pgen.1003602>.
- Efeyan A, Comb WC, Sabatini DM. 2015. Nutrient-sensing mechanisms and pathways. *Nature* **13**.
- Ewald CY, Landis JN, Porter Abate J, Murphy CT, Blackwell TK. 2015. Dauer-independent insulin/IGF-1-signalling implicates collagen remodelling in longevity. *Nature* **519**: 97–101.
- Ferretti MB, Ghalei H, Ward EA, Potts EL, Karbstein K. 2017. Rps26 directs mRNA-specific translation by recognition of Kozak sequence elements. *Nat Struct Mol Biol* **24**: 700–707. <http://www.nature.com/articles/nsmb.3442>.
- Ferretti MB, Karbstein K. 2019. Does functional specialization of ribosomes really exist? *RNA* **25**: 521–538. <http://www.ncbi.nlm.nih.gov/pubmed/30733326>.
- Fire A, Xu S, Montgomery MK, Kostas SA, Driver SE, Mello CC. 1998. Potent and specific genetic interference by double-stranded RNA in *Caenorhabditis elegans*. *Nature* **391**: 806–11. <http://www.ncbi.nlm.nih.gov/pubmed/9486653>.
- Fisher EMC, Beer-Romero P, Brown LG, Ridley A, McNeil JA, Lawrence JB, Willard HF, Bieber FR, Page DC. 1990. Homologous ribosomal protein genes on the human X and Y chromosomes: Escape from X inactivation and possible implications for Turner syndrome. *Cell* **63**: 1205–1218. <https://linkinghub.elsevier.com/retrieve/pii/009286749090416C>.
- Flores I, Cayuela ML, Blasco M a. 2005. Effects of telomerase and telomere length on epidermal stem cell behavior. *Science* **309**: 1253–1256.
- Fontana L, Nehme J, Demaria M. 2018. Caloric restriction and cellular senescence. *Mech Ageing Dev* **176**: 19–23. <http://www.ncbi.nlm.nih.gov/pubmed/30395873>.
- Fontana L, Partridge L, Longo VD. 2010. Extending healthy life span--from yeast to humans. *Science* **328**: 321–6. <http://www.pubmedcentral.nih.gov/articlerender.fcgi?artid=3607354&tool=pmcentrez&rendertype=abstract> (Accessed July 14, 2014).
- Fontana L, Partridge L, Longo VDD. 2013. Extending healthy lifespan - from yeast to humans. *Science (80-)* **328**: 321–326.
- Fraga MF, Esteller M. 2007. Epigenetics and aging: the targets and the marks. *Trends Genet* **23**: 413–8. <http://www.ncbi.nlm.nih.gov/pubmed/17559965>.
- Fricker R, Brogli R, Luidalepp H, Wyss L, Fasnacht M, Joss O, Zywicki M, Helm M, Schneider A, Cristodero M, et

- al. 2019. A tRNA half modulates translation as stress response in *Trypanosoma brucei*. *Nat Commun* **10**: 118. <http://www.ncbi.nlm.nih.gov/pubmed/30631057>.
- Fumagalli M, Rossiello F, Clerici M, Barozzi S, Cittaro D, Kaplunov JM, Bucci G, Dobrev M, Matti V, Beausejour CM, et al. 2012. Telomeric DNA damage is irreparable and causes persistent DNA-damage-response activation. *Nat Cell Biol* **14**: 355–65. <http://www.ncbi.nlm.nih.gov/pubmed/22426077>.
- Galluzzi L, Pietrocola F, Bravo-San Pedro JM, Amaravadi RK, Baehrecke EH, Cecconi F, Codogno P, Debnath J, Gewirtz DA, Karantza V, et al. 2015. Autophagy in malignant transformation and cancer progression. *EMBO J* **34**: 856–80. <http://www.ncbi.nlm.nih.gov/pubmed/25712477>.
- Garschall K, Dellago H, Gáliková M, Schosserer M, Flatt T, Grillari J. 2017. Erratum: Ubiquitous overexpression of the DNA repair factor dPrp19 reduces DNA damage and extends *Drosophila* life span. *npj Aging Mech Dis* **3**: 10. <http://www.nature.com/articles/s41514-017-0008-9>.
- Gasch AP, Spellman PT, Kao CM, Carmel-Harel O, Eisen MB, Storz G, Botstein D, Brown PO. 2000. Genomic expression programs in the response of yeast cells to environmental changes. *Mol Biol Cell* **11**: 4241–57. <http://www.ncbi.nlm.nih.gov/pubmed/11102521>.
- Gems D, Partridge L. 2013. Genetics of longevity in model organisms: debates and paradigm shifts. *Annu Rev Physiol* **75**: 621–44. <http://www.ncbi.nlm.nih.gov/pubmed/23190075>.
- Genuth NR, Barna M. 2018a. Heterogeneity and specialized functions of translation machinery: From genes to organisms. *Nat Rev Genet* **19**: 431–452. <http://dx.doi.org/10.1038/s41576-018-0008-z>.
- Genuth NR, Barna M. 2018b. The Discovery of Ribosome Heterogeneity and Its Implications for Gene Regulation and Organismal Life. *Mol Cell* **71**: 364–374.
- Gigova A, Duggimpudi S, Pollex T, Schaefer M, Koš M. 2014. A cluster of methylations in the domain IV of 25S rRNA is required for ribosome stability. *RNA* **20**: 1632–44.
- Green DR, Galluzzi L, Kroemer G. 2011. Mitochondria and the autophagy-inflammation-cell death axis in organismal aging. *Science* **333**: 1109–12. <http://www.ncbi.nlm.nih.gov/pubmed/21868666>.
- Gregg SQ, Gutiérrez V, Robinson AR, Woodell T, Nakao A, Ross MA, Michalopoulos GK, Rigatti L, Rothmel CE, Kamileri I, et al. 2012. A mouse model of accelerated liver aging caused by a defect in DNA repair. *Hepatology* **55**: 609–21. <http://www.ncbi.nlm.nih.gov/pubmed/21953681>.
- Greider CW, Blackburn EH. 1985. Identification of a specific telomere terminal transferase activity in *Tetrahymena* extracts. *Cell* **43**: 405–413.
- Griffith JD, Comeau L, Rosenfield S, Stansel RM, Bianchi A, Moss H, De Lange T. 1999. Mammalian telomeres end in a large duplex loop. *Cell* **97**: 503–514.
- Gruber R, Koch H, Doll BA, Tegtmeyer F, Einhorn TA, Hollinger JO. 2006. Fracture healing in the elderly patient. *Exp Gerontol* **41**: 1080–1093. <https://linkinghub.elsevier.com/retrieve/pii/S0531556506002853>.
- Gunderson J, Sogin M, Wollett G, Hollingdale M, de la Cruz V, Waters A, McCutchan T. 1987. Structurally distinct, stage-specific ribosomes occur in *Plasmodium*. *Science (80-)* **238**: 933–937. <https://www.sciencemag.org/lookup/doi/10.1126/science.3672135>.
- Guo H. 2018. Specialized ribosomes and the control of translation. 1–15.
- Guzzi N, Cieśła M, Ngoc PCT, Lang S, Arora S, Dimitriou M, Pimková K, Sommarin MNE, Munita R, Lubas M, et al. 2018. Pseudouridylation of tRNA-Derived Fragments Steers Translational Control in Stem Cells. *Cell* **173**: 1204–1216.e26. <https://linkinghub.elsevier.com/retrieve/pii/S0092867418302885>.
- Haimov O, Sinvani H, Martin F, Ulitsky I, Emmanuel R, Tamarkin-Ben-Harush A, Vardy A, Dikstein R. 2017. Efficient and Accurate Translation Initiation Directed by TISU Involves RPS3 and RPS10e Binding and Differential Eukaryotic Initiation Factor 1A Regulation. *Mol Cell Biol* **37**. <http://mcb.asm.org/lookup/doi/10.1128/MCB.00150-17>.
- Hamma T, Ferré-D'Amaré AR. 2006. Pseudouridine Synthases. *Chem Biol* **13**: 1125–1135.

- <https://linkinghub.elsevier.com/retrieve/pii/S1074552106003425>.
- Han S, Brunet A. 2012. Histone methylation makes its mark on longevity. *Trends Cell Biol* **22**: 42–9. <http://www.ncbi.nlm.nih.gov/pubmed/9454332>.
- Hansen M, Taubert S, Crawford D, Libina N, Lee S-JJ, Kenyon C. 2007. Lifespan extension by conditions that inhibit translation in *Caenorhabditis elegans*. *Aging Cell* **6**: 95–110.
- Harger JW, Dinman JD. 2003. An in vivo dual-luciferase assay system for studying translational recoding in the yeast *Saccharomyces cerevisiae*. *RNA* **9**: 1019–24.
- Harman D. 1956. Aging: a theory based on free radical and radiation chemistry. 298–300.
- Harman D. 2003. The free radical theory of aging. *Antioxid Redox Signal* **5**: 557–61. <http://www.ncbi.nlm.nih.gov/pubmed/14580310>.
- Hartl FU, Bracher A, Hayer-Hartl M. 2011. Molecular chaperones in protein folding and proteostasis. *Nature* **475**: 324–32. <http://www.ncbi.nlm.nih.gov/pubmed/21776078>.
- Hayflick L. 1965. THE LIMITED IN VITRO LIFETIME OF HUMAN DIPLOID CELL STRAINS. *Exp Cell Res* **37**: 614–36. <http://www.ncbi.nlm.nih.gov/pubmed/14315085>.
- Hebras J, Krogh N, Marty V, Nielsen H, Cavaillé J. 2020. Developmental changes of rRNA ribose methylations in the mouse. *RNA Biol* **17**: 150–164. <https://www.tandfonline.com/doi/full/10.1080/15476286.2019.1670598>.
- Heissenberger C, Krammer TL, Rollins JA, Nagelreiter F, Stocker I, Wacheul L, Shpylovyi A, Snow S, Grillari J, Rogers AN, et al. 2020. The ribosomal RNA methyltransferase NSUN-1 modulates healthspan and oogenesis in *Caenorhabditis elegans*. *bioRxiv* 2020.03.16.993469. <http://biorxiv.org/content/early/2020/03/18/2020.03.16.993469.abstract>.
- Heissenberger C, Liendl L, Nagelreiter F, Gonskikh Y, Yang G, Stelzer EM, Krammer TL, Micutkova L, Vogt S, Kreil DP, et al. 2019. Loss of the ribosomal RNA methyltransferase NSUN5 impairs global protein synthesis and normal growth. *Nucleic Acids Res* 1–19.
- Hekimi S, Lapointe J, Wen Y. 2011. Taking a “good” look at free radicals in the aging process. *Trends Cell Biol* **21**: 569–576.
- Henras AK, Soudet J, G rus M, Lebaron S, Caizergues-Ferrer M, Mougin A, Henry Y. 2008. The post-transcriptional steps of eukaryotic ribosome biogenesis. *Cell Mol Life Sci* **65**: 2334–59. <http://www.ncbi.nlm.nih.gov/pubmed/18408888>.
- Herdy B, Mayer C, Varshney D, Marsico G, Murat P, Taylor C, D’Santos C, Tannahill D, Balasubramanian S. 2018. Analysis of NRAS RNA G-quadruplex binding proteins reveals DDX3X as a novel interactor of cellular G-quadruplex containing transcripts. *Nucleic Acids Res* **46**: 11592–11604. <https://academic.oup.com/nar/advance-article/doi/10.1093/nar/gky861/5106999>.
- Herovici C. 1963. [Picropolychrome: histological staining technic intended for the study of normal and pathological connective tissue]. *Rev Fr Etud Clin Biol* **8**: 88–9.
- Hewitt G, Jurk D, Marques FDM, Correia-Melo C, Hardy T, Gackowska A, Anderson R, Taschuk M, Mann J, Passos JF. 2012. Telomeres are favoured targets of a persistent DNA damage response in ageing and stress-induced senescence. *Nat Commun* **3**: 708. <http://www.ncbi.nlm.nih.gov/pubmed/22426229>.
- Higa-Nakamine S, Suzuki T, Uechi T, Chakraborty A, Nakajima Y, Nakamura M, Hirano N, Suzuki T, Kenmochi N. 2012. Loss of ribosomal RNA modification causes developmental defects in zebrafish. *Nucleic Acids Res* **40**: 391–398. <https://academic.oup.com/nar/article-lookup/doi/10.1093/nar/gkr700>.
- Hillebrand A, Wurm R, Menzel A, Wagner R. 2005. The seven *E. coli* ribosomal RNA operon upstream regulatory regions differ in structure and transcription factor binding efficiencies. *Biol Chem* **386**: 523–534. <http://www.degruyter.com/view/j/bchm.2005.386.issue-6/bc.2005.062/bc.2005.062.xml>.
- Hinnebusch AG. 2017. Structural Insights into the Mechanism of Scanning and Start Codon Recognition in

- Eukaryotic Translation Initiation. *Trends Biochem Sci* **42**: 589–611.
<https://linkinghub.elsevier.com/retrieve/pii/S096800041730066X>.
- Hodgkin J, Barnes TM. 1991. More is not better: brood size and population growth in a self-fertilizing nematode. *Proceedings Biol Sci* **246**: 19–24.
- Hoeijmakers JHJ. 2009. DNA damage, aging, and cancer. *N Engl J Med* **361**: 1475–85.
<http://www.ncbi.nlm.nih.gov/pubmed/19812404>.
- Hong B, Brockenbrough JS, Wu P, Aris JP. 1997. Nop2p is required for pre-rRNA processing and 60S ribosome subunit synthesis in yeast. *Mol Cell Biol* **17**: 378–388.
<http://mcb.asm.org/lookup/doi/10.1128/MCB.17.1.378>.
- Hsin H, Kenyon C. 1999. Signals from the reproductive system regulate the lifespan of *C. elegans*. *Nature* **399**: 362–6.
- Hubackova S, Krejčíková K, Bartek J, Hodny Z. 2012. IL1- and TGFβ-Nox4 signaling, oxidative stress and DNA damage response are shared features of replicative, oncogene-induced, and drug-induced paracrine “bystander senescence”. *Aging (Albany NY)* **4**: 932–51.
<http://www.ncbi.nlm.nih.gov/pubmed/23385065>.
- Hussain S, Sajini AA, Blanco S, Dietmann S, Lombard P, Sugimoto Y, Paramor M, Gleeson JG, Odom DT, Ule J, et al. 2013. NSun2-mediated cytosine-5 methylation of vault noncoding RNA determines its processing into regulatory small RNAs. *Cell Rep* **4**: 255–261. <http://dx.doi.org/10.1016/j.celrep.2013.06.029>.
- Jacobs FA, Bird RC, Sells BH. 1985. Differentiation of rat myoblasts. Regulation of turnover of ribosomal proteins and their mRNAs. *Eur J Biochem* **150**: 255–263. <http://doi.wiley.com/10.1111/j.1432-1033.1985.tb09015.x>.
- Janin M, Ortiz-Barahona V, de Moura MC, Martínez-Cardús A, Llinàs-Arias P, Soler M, Nachmani D, Pelletier J, Schumann U, Calleja-Cervantes ME, et al. 2019. Epigenetic loss of RNA-methyltransferase NSUN5 in glioma targets ribosomes to drive a stress adaptive translational program. *Acta Neuropathol* **138**: 1053–1074. <http://www.ncbi.nlm.nih.gov/pubmed/31428936>.
- Jeon OH, Kim C, Laberge R-M, Demaria M, Rathod S, Vasserot AP, Chung JW, Kim DH, Poon Y, David N, et al. 2017. Local clearance of senescent cells attenuates the development of post-traumatic osteoarthritis and creates a pro-regenerative environment. *Nat Med* **23**: 775–781.
<http://www.ncbi.nlm.nih.gov/pubmed/28436958>.
- Jeon OH, Wilson DR, Clement CC, Rathod S, Cherry C, Powell B, Lee Z, Khalil AM, Green JJ, Campisi J, et al. 2019. Senescence cell-associated extracellular vesicles serve as osteoarthritis disease and therapeutic markers. *JCI Insight* **4**. <https://insight.jci.org/articles/view/125019>.
- Johnson AW, Lund E, Dahlberg J. 2002. Nuclear export of ribosomal subunits. *Trends Biochem Sci* **27**: 580–5.
<http://www.ncbi.nlm.nih.gov/pubmed/12417134>.
- Johnson T. 1990. Increased life-span of age-1 mutants in *Caenorhabditis elegans* and lower Gompertz rate of aging. *Science (80-)* **249**: 908–912. <https://www.sciencemag.org/lookup/doi/10.1126/science.2392681>.
- Jun J-I, Lau LF. 2010. The matricellular protein CCN1 induces fibroblast senescence and restricts fibrosis in cutaneous wound healing. *Nat Cell Biol* **12**: 676–85. <http://www.ncbi.nlm.nih.gov/pubmed/20526329>.
- Kaeberlein M, Powers RW, Steffen KK, Westman EA, Hu D, Dang N, Kerr EO, Kirkland KT, Fields S, Kennedy BK. 2005. Regulation of Yeast Replicative Life Span by TOR and Sch9 in Response to Nutrients. *Science (80-)* **310**: 1193–1196.
- Kaletta T, Hengartner MO. 2006. Finding function in novel targets: *C. elegans* as a model organism. *Nat Rev Drug Discov* **5**: 387–398.
- Kamath RS, Fraser AG, Dong Y, Poulin G, Durbin R, Gotta M, Kanapin A, Le Bot N, Moreno S, Sohrmann M, et al. 2003. Systematic functional analysis of the *Caenorhabditis elegans* genome using RNAi. *Nature* **421**: 231–7.

- Kapahi P. 2010. Protein synthesis and the antagonistic pleiotropy hypothesis of aging. *Adv Exp Med Biol* **694**: 30–7.
- Karajolich J, Yi C, Yu Y-T. 2015. Transcriptome-wide dynamics of RNA pseudouridylation. *Nat Rev Mol Cell Biol* **16**: 581–585. <http://www.nature.com/articles/nrm4040>.
- Ke Z, Mallik P, Johnson AB, Luna F, Nevo E, Zhang ZD, Gladyshev VN, Seluanov A, Gorbunova V. 2017. Translation fidelity coevolves with longevity. *Aging Cell* **16**: 988–993.
- Kellis M, Birren BW, Lander ES. 2004. Proof and evolutionary analysis of ancient genome duplication in the yeast *Saccharomyces cerevisiae*. *Nature* **428**: 617–624. <http://www.nature.com/articles/nature02424>.
- Kennedy S, Wang D, Ruvkun G. 2004. A conserved siRNA-degrading RNase negatively regulates RNA interference in *C. elegans*. *Nature* **427**: 645–9.
- Kenyon C. 2005. The plasticity of aging: Insights from long-lived mutants. *Cell* **120**: 449–460.
- Kenyon C, Chang J, Gensch E, Rudner a, Tabtiang R, Jed AF, Kirk M, Davis, Kenyon C, Chang J, et al. 1993. A *C. elegans* mutant that lives twice as long as wild type. *Nature* **366**: 461–464. <http://www.ncbi.nlm.nih.gov/pubmed/8247153>.
- Khatte H, Myasnikov AG, Natchiar SK, Klaholz BP. 2015. Structure of the human 80S ribosome. *Nature* **520**: 640–645. <http://www.ncbi.nlm.nih.gov/pubmed/25901680>.
- Khoddami V, Cairns BR. 2013. Identification of direct targets and modified bases of RNA cytosine methyltransferases. *Nat Biotechnol* **31**: 458–464. <http://www.ncbi.nlm.nih.gov/pubmed/23604283>.
- Khoddami V, Yerra A, Mosbrugger TL, Fleming AM, Burrows CJ, Cairns BR. 2019. Transcriptome-wide profiling of multiple RNA modifications simultaneously at single-base resolution. *Proc Natl Acad Sci U S A* **116**: 6784–6789. <http://www.ncbi.nlm.nih.gov/pubmed/30872485>.
- King M, Ton D, Redman KL. 1999. A conserved motif in the yeast nucleolar protein Nop2p contains an essential cysteine residue. *Biochem J* **337** (Pt 1): 29–35.
- King MY, Redman KL. 2002. RNA methyltransferases utilize two cysteine residues in the formation of 5-methylcytosine. *Biochemistry* **41**: 11218–11225. <http://www.ncbi.nlm.nih.gov/pubmed/12220187>.
- Kirkwood TB, Holliday R. 1979. The evolution of ageing and longevity. *Proc R Soc Lond B Biol Sci* **205**: 531–46.
- Kirkwood TBL. 2005. Understanding the odd science of aging. *Cell* **120**: 437–47. <http://www.ncbi.nlm.nih.gov/pubmed/15734677>.
- Koga H, Kaushik S, Cuervo AM. 2011. Protein homeostasis and aging: The importance of exquisite quality control. *Ageing Res Rev* **10**: 205–15. <http://www.ncbi.nlm.nih.gov/pubmed/20152936>.
- Kojima T, Kamei H, Aizu T, Arai Y, Takayama M, Nakazawa S, Ebihara Y, Inagaki H, Masui Y, Gondo Y, et al. 2004. Association analysis between longevity in the Japanese population and polymorphic variants of genes involved in insulin and insulin-like growth factor 1 signaling pathways. *Exp Gerontol* **39**: 1595–1598. <https://linkinghub.elsevier.com/retrieve/pii/S0531556504002736>.
- Komili S, Farny NG, Roth FP, Silver PA. 2007. Functional Specificity among Ribosomal Proteins Regulates Gene Expression. *Cell* **131**: 557–571. <https://linkinghub.elsevier.com/retrieve/pii/S0092867407011002>.
- Korostelev AA. 2011. Structural aspects of translation termination on the ribosome. *RNA* **17**: 1409–1421. <http://rnajournal.cshlp.org/cgi/doi/10.1261/rna.2733411>.
- Kos M, Tollervey D. 2010. Yeast pre-rRNA processing and modification occur cotranscriptionally. *Mol Cell* **37**: 809–20.
- Kressler D, Hurt E, Bassler J. 2010. Driving ribosome assembly. *Biochim Biophys Acta* **1803**: 673–83. <http://www.ncbi.nlm.nih.gov/pubmed/19879902>.
- Kroemer G, Galluzzi L, Brenner C. 2007. Mitochondrial membrane permeabilization in cell death. *Physiol Rev* **87**: 99–163. <http://www.ncbi.nlm.nih.gov/pubmed/17237344>.

- Krogh N, Jansson MD, Häfner SJ, Tehler D, Birkedal U, Christensen-Dalsgaard M, Lund AH, Nielsen H. 2016. Profiling of 2'-O-Me in human rRNA reveals a subset of fractionally modified positions and provides evidence for ribosome heterogeneity. *Nucleic Acids Res* **44**: 7884–7895. <https://academic.oup.com/nar/article-lookup/doi/10.1093/nar/gkw482>.
- Krtolica A, Parrinello S, Lockett S, Desprez PY, Campisi J. 2001. Senescent fibroblasts promote epithelial cell growth and tumorigenesis: a link between cancer and aging. *Proc Natl Acad Sci U S A* **98**: 12072–7. <http://www.ncbi.nlm.nih.gov/pubmed/11593017>.
- Kumsta C, Hansen M. 2012. C. elegans rrf-1 mutations maintain RNAi efficiency in the soma in addition to the germline. *PLoS One* **7**: e35428. <http://www.ncbi.nlm.nih.gov/pubmed/22574120>.
- Kurylo CM, Parks MM, Juette MF, Zinshteyn B, Altman RB, Thibado JK, Vincent CT, Blanchard SC. 2018. Endogenous rRNA Sequence Variation Can Regulate Stress Response Gene Expression and Phenotype. *Cell Rep* **25**: 236–248.e6. <https://linkinghub.elsevier.com/retrieve/pii/S2211124718314128>.
- Kyng KJ, Bohr VA. 2005. Gene expression and DNA repair in progeroid syndromes and human aging. *Ageing Res Rev* **4**: 579–602. <http://www.ncbi.nlm.nih.gov/pubmed/16246641>.
- Lackner DH, Beilharz TH, Marguerat S, Mata J, Watt S, Schubert F, Preiss T, Bähler J. 2007. A Network of Multiple Regulatory Layers Shapes Gene Expression in Fission Yeast. *Mol Cell* **26**: 145–155. <https://linkinghub.elsevier.com/retrieve/pii/S1097276507001475>.
- Laemmli UK. 1970. Cleavage of structural proteins during the assembly of the head of bacteriophage T4. *Nature* **227**: 680–5. <http://www.ncbi.nlm.nih.gov/pubmed/5432063>.
- Lafontaine DLJ. 2015. Noncoding RNAs in eukaryotic ribosome biogenesis and function. *Nat Struct Mol Biol* **22**: 11–19. <http://www.nature.com/articles/nsmb.2939>.
- Lam YW, Lamond AI, Mann M, Andersen JS. 2007. Analysis of Nucleolar Protein Dynamics Reveals the Nuclear Degradation of Ribosomal Proteins. *Curr Biol* **17**: 749–760. <https://linkinghub.elsevier.com/retrieve/pii/S096098220701202X>.
- Landry JJM, Pyl PT, Rausch T, Zichner T, Tekkedil MM, Stütz AM, Jauch A, Aiyar RS, Pau G, Delhomme N, et al. 2013. The genomic and transcriptomic landscape of a HeLa cell line. *G3 (Bethesda)* **3**: 1213–24. <http://www.pubmedcentral.nih.gov/articlerender.fcgi?artid=3737162&tool=pmcentrez&rendertype=abstract>.
- Laplanche M, Sabatini DM. 2012. mTOR signaling in growth control and disease. *Cell* **149**: 274–93. <http://www.ncbi.nlm.nih.gov/pubmed/22500797>.
- Lee M-H, Schedl T. 2010. C. elegans star proteins, GLD-1 and ASD-2, regulate specific RNA targets to control development. *Adv Exp Med Biol* **693**: 106–22.
- Lee S-W, Berger SJ, Martinovic S, Pasa-Tolic L, Anderson GA, Shen Y, Zhao R, Smith RD. 2002. Direct mass spectrometric analysis of intact proteins of the yeast large ribosomal subunit using capillary LC/FTICR. *Proc Natl Acad Sci* **99**: 5942–5947. <http://www.pnas.org/cgi/doi/10.1073/pnas.082119899>.
- Légrand C, Tuorto F, Hartmann M, Liebers R, Jacob D, Helm M, Lyko F. 2017. Statistically robust methylation calling for whole-transcriptome bisulfite sequencing reveals distinct methylation patterns for mouse RNAs. *Genome Res* **27**: 1589–1596.
- Lehmkuhl EM, Zarnescu DC. 2018. Lost in Translation: Evidence for Protein Synthesis Deficits in ALS/FTD and Related Neurodegenerative Diseases. *Adv Neurobiol* **20**: 283–301. <http://www.ncbi.nlm.nih.gov/pubmed/29916024>.
- Li HH, Roy M, Kuscuoglu U, Spencer CM, Halm B, Harrison KC, Bayle JH, Splendore A, Ding F, Meltzer LA, et al. 2009. Induced chromosome deletions cause hypersociability and other features of Williams-Beuren syndrome in mice. *EMBO Mol Med* **1**: 50–65.
- Li X, Zhu P, Ma S, Song J, Bai J, Sun F, Yi C. 2015. Chemical pulldown reveals dynamic pseudouridylation of the mammalian transcriptome. *Nat Chem Biol* **11**: 592–597.

<http://www.nature.com/articles/nchembio.1836>.

- Libert S, Zwiener J, Chu X, Vanvoorhies W, Roman G, Pletcher SD. 2007. Regulation of *Drosophila* life span by olfaction and food-derived odors. *Science* **315**: 1133–1137.
- Lilleorg S, Reier K, Pulk A, Liiv A, Tammsalu T, Peil L, Cate JHD, Remme J. 2019. Bacterial ribosome heterogeneity: Changes in ribosomal protein composition during transition into stationary growth phase. *Biochimie* **156**: 169–180. <http://www.ncbi.nlm.nih.gov/pubmed/30359641>.
- Lipsky MS, King M. 2015. Biological theories of aging. *Dis Mon* **61**: 460–6. <http://www.ncbi.nlm.nih.gov/pubmed/26490576>.
- Lithgow GJ, White TM, Hinerfeld DA, Johnson TE. 1994. Thermotolerance of a long-lived mutant of *Caenorhabditis elegans*. *J Gerontol* **49**: B270–6.
- Locati MD, Pagano JFB, Girard G, Ensink WA, van Olst M, van Leeuwen S, Nehrdich U, Spaik HP, Rauwerda H, Jonker MJ, et al. 2017. Expression of distinct maternal and somatic 5.8S, 18S, and 28S rRNA types during zebrafish development. *RNA* **23**: 1188–1199. <http://www.ncbi.nlm.nih.gov/pubmed/28500251>.
- Loenarz C, Sekirnik R, Thalhammer A, Ge W, Spivakovsky E, Mackeen MM, McDonough MA, Cockman ME, Kessler BM, Ratcliffe PJ, et al. 2014. Hydroxylation of the eukaryotic ribosomal decoding center affects translational accuracy. *Proc Natl Acad Sci* **111**: 4019–4024. <http://www.pnas.org/cgi/doi/10.1073/pnas.1311750111>.
- Longman D, Johnstone IL, Cáceres JF. 2000. Functional characterization of SR and SR-related genes in *Caenorhabditis elegans*. *EMBO J* **19**: 1625–37.
- Longo VD. 2019. Programmed longevity, youthspan, and juvenology. *Aging Cell* **18**: e12843. <http://doi.wiley.com/10.1111/accel.12843>.
- Longo VD, Mattson MP. 2014. Fasting: molecular mechanisms and clinical applications. *Cell Metab* **19**: 181–92. <http://www.ncbi.nlm.nih.gov/pubmed/24440038>.
- Lopes AM, Miguel RN, Sargent CA, Ellis PJ, Amorim A, Affara NA. 2010. The human RPS4 paralogue on Yq11.223 encodes a structurally conserved ribosomal protein and is preferentially expressed during spermatogenesis. *BMC Mol Biol* **11**: 33. <http://bmcmolbiol.biomedcentral.com/articles/10.1186/1471-2199-11-33>.
- López-Otín C, Blasco M a, Partridge L, Serrano M, Kroemer G. 2013. The hallmarks of aging. *Cell* **153**: 1194–217. <http://www.pubmedcentral.nih.gov/articlerender.fcgi?artid=3836174&tool=pmcentrez&rendertype=abstract> (Accessed July 10, 2014).
- Loveland AB, Bah E, Madireddy R, Zhang Y, Brilot AF, Grigorieff N, Korostelev AA. 2016. Ribosome•RelA structures reveal the mechanism of stringent response activation. *Elife* **5**. <https://elifesciences.org/articles/17029>.
- Machnicka MA, Milanowska K, Osman Oglou O, Purta E, Kurkowska M, Olchowik A, Januszewski W, Kalinowski S, Dunin-Horkawicz S, Rother KM, et al. 2012. MODOMICS: a database of RNA modification pathways — 2013 update. *Nucleic Acids Res* **41**: D262–D267. <http://academic.oup.com/nar/article/41/D1/D262/1050979/MODOMICS-a-database-of-RNA-modification>.
- Macville M, Schröck E, Padilla-nash H, Schro E, Keck C, Ghadimi BM, Zimonjic D, Popescu N, Ried T. 1999. Comprehensive and Definitive Molecular Cytogenetic Characterization of HeLa Cells by Spectral Karyotyping Comprehensive and Definitive Molecular Cytogenetic Characterization of HeLa Cells by Spectral Karyotyping. 141–150.
- Madeo F, Zimmermann A, Maiuri MC, Kroemer G. 2015. Essential role for autophagy in life span extension. *J Clin Invest* **125**: 85–93. <http://www.ncbi.nlm.nih.gov/pubmed/25654554>.
- Maro GS, Han S, Banko MR, Gozani O, Brunet A. 2011. NIH Public Access. **466**: 383–387.
- Marx N, Grünwald-Gruber C, Bydlinski N, Dhiman H, Ngoc Nguyen L, Klanert G, Borth N. 2018. CRISPR-Based

- Targeted Epigenetic Editing Enables Gene Expression Modulation of the Silenced Beta-Galactoside Alpha-2,6-Sialyltransferase 1 in CHO Cells. *Biotechnol J* **13**: 1700217. <http://doi.wiley.com/10.1002/biot.201700217>.
- Marygold SJ, Roote J, Reuter G, Lambertsson A, Ashburner M, Millburn GH, Harrison PM, Yu Z, Kenmochi N, Kaufman TC, et al. 2007. The ribosomal protein genes and Minute loci of *Drosophila melanogaster*. *Genome Biol* **8**: R216. <http://genomebiology.biomedcentral.com/articles/10.1186/gb-2007-8-10-r216>.
- Masoro EJ. 2005. Overview of caloric restriction and ageing. *Mech Ageing Dev* **126**: 913–922.
- Mathis AD, Naylor BC, Carson RH, Evans E, Harwell J, Knecht J, Hexem E, Peelor FF, Miller BF, Hamilton KL, et al. 2017. Mechanisms of In Vivo Ribosome Maintenance Change in Response to Nutrient Signals. *Mol Cell Proteomics* **16**: 243–254. <http://www.ncbi.nlm.nih.gov/pubmed/27932527>.
- Maynard Smith J. 1959. A Theory of Ageing. *Nature* **184**: 956–957. <http://www.nature.com/articles/184956a0>.
- Melo J, Ruvkun G. 2012. Inactivation of conserved *C. elegans* genes engages pathogen- and xenobiotic-associated defenses. *Cell* **149**: 452–66.
- Mendoza MC, Er EE, Blenis J. 2011. The Ras-ERK and PI3K-mTOR pathways: cross-talk and compensation. *Trends Biochem Sci* **36**: 320–8.
- Merkwirth C, Jovaisaite V, Durieux J, Matilainen O, Jordan SD, Quiros PM, Steffen KK, Williams EG, Mouchiroud L, Tronnes SU, et al. 2016. Two Conserved Histone Demethylases Regulate Mitochondrial Stress-Induced Longevity. *Cell* **165**: 1209–1223. <http://www.ncbi.nlm.nih.gov/pubmed/27133168>.
- Micutkova L, Diener T, Li C, Rogowska-Wrzesinska A, Mueck C, Huetter E, Weinberger B, Grubeck-Loebenstein B, Roepstorff P, Zeng R, et al. 2011. Insulin-like growth factor binding protein-6 delays replicative senescence of human fibroblasts. *Mech Ageing Dev* **132**: 468–479. <http://www.ncbi.nlm.nih.gov/pubmed/21820463>.
- Mills EW, Green R. 2017. Ribosomopathies: There's strength in numbers. *Science (80-)* **358**: eaan2755. <https://www.sciencemag.org/lookup/doi/10.1126/science.aan2755>.
- Minamino T, Miyauchi H, Yoshida T, Ishida Y, Yoshida H, Komuro I. 2002. Endothelial cell senescence in human atherosclerosis: role of telomere in endothelial dysfunction. *Circulation* **105**: 1541–4. <http://www.ncbi.nlm.nih.gov/pubmed/11927518>.
- Mizushima N, Levine B, Cuervo AM, Klionsky DJ. 2008. Autophagy fights disease through cellular self-digestion. *Nature* **451**: 1069–75. <http://www.ncbi.nlm.nih.gov/pubmed/18305538>.
- Moffat J, Grueneberg DA, Yang X, Kim SY, Kloepper AM, Hinkle G, Piqani B, Eisenhaure TM, Luo B, Grenier JK, et al. 2006. A lentiviral RNAi library for human and mouse genes applied to an arrayed viral high-content screen. *Cell* **124**: 1283–1298.
- Molofsky A V., Slutsky SG, Joseph NM, He S, Pardal R, Krishnamurthy J, Sharpless NE, Morrison SJ. 2006. Increasing p16INK4a expression decreases forebrain progenitors and neurogenesis during ageing. *Nature* **443**: 448–452. <http://www.nature.com/articles/nature05091>.
- Motorin Y, Lyko F, Helm M. 2010. 5-methylcytosine in RNA: detection, enzymatic formation and biological functions. *Nucleic Acids Res* **38**: 1415–1430. <https://academic.oup.com/nar/article-lookup/doi/10.1093/nar/gkp1117>.
- Müller C, Bremer A, Schreiber S, Eichwald S, Calkhoven CF. 2010. Nucleolar retention of a translational C/EBPalpha isoform stimulates rDNA transcription and cell size. *EMBO J* **29**: 897–909. <http://www.pubmedcentral.nih.gov/articlerender.fcgi?artid=2810377&tool=pmcentrez&rendertype=abstract>.
- Murakami S, Suzuki T, Yokoyama W, Yagi S, Matsumura K, Nakajima Y, Harigae H, Fukamizu A, Motohashi H. 2018. Nucleomethylin deficiency impairs embryonic erythropoiesis. *J Biochem* **163**: 413–423. <https://academic.oup.com/jb/article/163/5/413/4735253>.
- Murayama A, Ohmori K, Fujimura A, Minami H, Yasuzawa-Tanaka K, Kuroda T, Oie S, Daitoku H, Okuwaki M,

- Nagata K, et al. 2008. Epigenetic Control of rDNA Loci in Response to Intracellular Energy Status. *Cell* **133**: 627–639. <https://linkinghub.elsevier.com/retrieve/pii/S0092867408004595>.
- Murga M, Bunting S, Montaña MF, Soria R, Mulero F, Cañamero M, Lee Y, McKinnon PJ, Nussenzweig A, Fernandez-Capetillo O. 2009. A mouse model of ATR-Seckel shows embryonic replicative stress and accelerated aging. *Nat Genet* **41**: 891–8. <http://www.ncbi.nlm.nih.gov/pubmed/19620979>.
- Nagelreiter F, Coats MT, Klanert G, Gludovacz E, Borth N, Grillari J, Schosserer M. 2018a. ONagelreiter F, Coats MT, Klanert G, Gludovacz E, Borth N, Grillari J, Schosserer M. 2018. OPP Labeling Enables Total Protein Synthesis Quantification in CHO Production Cell Lines at the Single-Cell Level. *Biotechnol J* **13**: e1700492. <http://doi.wiley.com/10.1002/biot.201700492>.
- Nagelreiter F, Coats MT, Klanert G, Gludovacz E, Borth N, Grillari J, Schosserer M. 2018b. OPP Labeling Enables Total Protein Synthesis Quantification in CHO Production Cell Lines at the Single-Cell Level. *Biotechnol J* **13**: e1700492.
- Narla A, Ebert BL. 2010. Ribosomopathies: human disorders of ribosome dysfunction. *Blood* **115**: 3196–3205. <https://ashpublications.org/blood/article/115/16/3196/27031/Ribosomopathies-human-disorders-of-ribosome>.
- Natchiar SK, Myasnikov AG, Kratzat H, Hazemann I, Klaholz BP. 2017. Visualization of chemical modifications in the human 80S ribosome structure. *Nature* **551**: 472–477.
- Navarro IC, Tuorto F, Jordan D, Legrand C, Price J, Braukmann F, Hendrick A, Akay A, Kotter A, Helm M, et al. 2020. Translational adaptation to heat stress is mediated by 5-methylcytosine RNA modification in *Caenorhabditis elegans*. *bioRxiv* 2020.03.21.001735. <http://biorxiv.org/content/early/2020/03/23/2020.03.21.001735.abstract>.
- Naylor RM, Baker DJ, van Deursen JM. 2013. Senescent cells: a novel therapeutic target for aging and age-related diseases. *Clin Pharmacol Ther* **93**: 105–16. <http://www.ncbi.nlm.nih.gov/pubmed/23212104>.
- Nelson G, Wordsworth J, Wang C, Jurk D, Lawless C, Martin-Ruiz C, von Zglinicki T. 2012. A senescent cell bystander effect: senescence-induced senescence. *Aging Cell* **11**: 345–9. <http://www.ncbi.nlm.nih.gov/pubmed/22321662>.
- Newton K, Petfalski E, Tollervey D, Caceres JF. 2003. Fibrillarin Is Essential for Early Development and Required for Accumulation of an Intron-Encoded Small Nucleolar RNA in the Mouse. *Mol Cell Biol* **23**: 8519–8527. <http://mcb.asm.org/cgi/doi/10.1128/MCB.23.23.8519-8527.2003>.
- Ochs RL. 1997. Methods Used to Study Structure and Function of the Nucleolus. In *Methods Cell Biol.*, pp. 303–321 <https://linkinghub.elsevier.com/retrieve/pii/S0091679X08608845>.
- Odintsova TI, Müller E-C, Ivanov A V, Egorov TA, Bienert R, Vladimirov SN, Kostka S, Otto A, Wittmann-Liebold B, Karpova GG. 2003. Characterization and analysis of posttranslational modifications of the human large cytoplasmic ribosomal subunit proteins by mass spectrometry and Edman sequencing. *J Protein Chem* **22**: 249–58. <http://www.ncbi.nlm.nih.gov/pubmed/12962325>.
- Ofengand J. 2002. Ribosomal RNA pseudouridines and pseudouridine synthases. *FEBS Lett* **514**: 17–25. <http://doi.wiley.com/10.1016/S0014-5793%2802%2902305-0>.
- Olovnikov AM. 1996. Telomeres, telomerase, and aging: origin of the theory. *Exp Gerontol* **31**: 443–8. <http://www.ncbi.nlm.nih.gov/pubmed/9415101>.
- Osorio FG, Bárcena C, Soria-Valles C, Ramsay AJ, de Carlos F, Cobo J, Fueyo A, Freije JMP, López-Otín C. 2012. Nuclear lamina defects cause ATM-dependent NF- κ B activation and link accelerated aging to a systemic inflammatory response. *Genes Dev* **26**: 2311–24. <http://www.ncbi.nlm.nih.gov/pubmed/23019125>.
- Ou H-L, Kim CS, Uszkoreit S, Wickström SA, Schumacher B. 2019. Somatic Niche Cells Regulate the CEP-1/p53-Mediated DNA Damage Response in Primordial Germ Cells. *Dev Cell* **50**: 167–183.e8.
- Palumbo RJ, Fuchs G, Lutz S, Curcio MJ. 2017. Paralog-Specific Functions of RPL7A and RPL7B Mediated by Ribosomal Protein or snoRNA Dosage in *Saccharomyces cerevisiae*. *G3* **7**: 1–11.

- Genes/Genomes/Genetics* **7**: 591–606. <http://g3journal.org/lookup/doi/10.1534/g3.116.035931>.
- Pan KZ, Palter JE, Rogers AN, Olsen A, Chen D, Lithgow GJ, Kapahi P. 2007. Inhibition of mRNA translation extends lifespan in *Caenorhabditis elegans*. *Aging Cell* **6**: 111–9.
- Parenteau J, Durand M, Morin G, Gagnon J, Lucier J-F, Wellinger RJ, Chabot B, Abou Elela S. 2011. Introns within Ribosomal Protein Genes Regulate the Production and Function of Yeast Ribosomes. *Cell* **147**: 320–331. <https://linkinghub.elsevier.com/retrieve/pii/S0092867411010658>.
- Parks MM, Kurylo CM, Dass RA, Bojmar L, Lyden D, Vincent CT, Blanchard SC. 2018. Variant ribosomal RNA alleles are conserved and exhibit tissue-specific expression. *Sci Adv* **4**: eaao0665. <https://advances.sciencemag.org/lookup/doi/10.1126/sciadv.aao0665>.
- Pawlikowska L, Hu D, Huntsman S, Sung A, Chu C, Chen J, Joyner AH, Schork NJ, Hsueh W-C, Reiner AP, et al. 2009. Association of common genetic variation in the insulin/IGF1 signaling pathway with human longevity. *Aging Cell* **8**: 460–472. <http://doi.wiley.com/10.1111/j.1474-9726.2009.00493.x>.
- Pazdernik N, Schedl T. 2013. Introduction to germ cell development in *Caenorhabditis elegans*. *Adv Exp Med Biol* **757**: 1–16.
- Penzo M, Galbiati A, Tréré D, Montanaro L. 2016. The importance of being (slightly) modified: The role of rRNA editing on gene expression control and its connections with cancer. *Biochim Biophys Acta - Rev Cancer* **1866**: 330–338.
- Penzo M, Rocchi L, Brugiere S, Carnicelli D, Onofrillo C, Coute Y, Brigotti M, Montanaro L. 2015. Human ribosomes from cells with reduced dyskerin levels are intrinsically altered in translation. *FASEB J* **29**: 3472–3482.
- Perry RP, Kelley DE. 1970. Inhibition of RNA synthesis by actinomycin D: Characteristic dose-response of different RNA species. *J Cell Physiol* **76**: 127–139.
- Petibon C, Parenteau J, Catala M, Elela SA. 2016. Introns regulate the production of ribosomal proteins by modulating splicing of duplicated ribosomal protein genes. *Nucleic Acids Res* **44**: 3878–3891. <https://academic.oup.com/nar/article-lookup/doi/10.1093/nar/gkw140>.
- Pober BR. 2010. Williams-Beuren syndrome. *N Engl J Med* **362**: 239–52. <http://www.ncbi.nlm.nih.gov/pubmed/20089974>.
- Poser I, Sarov M, Hutchins JR a, Hériché J, Pozniakovsky A, Weigl D, Nitzsche A, Hegemann B, Bird AW, Pelletier L, et al. 2008a. BAC TransgeneOmics: a high-throughput method for exploration of protein function in mammals. *Nat Methods* **5**: 409–415.
- Poser I, Sarov M, Hutchins JR, Heriche JK, Toyoda Y, Pozniakovsky A, Weigl D, Nitzsche A, Hegemann B, Bird AW, et al. 2008b. BAC TransgeneOmics: a high-throughput method for exploration of protein function in mammals. *Nat Methods* **5**: 409–415.
- Poulin F, Gingras AC, Olsen H, Chevalier S, Sonenberg N. 1998. 4E-BP3, a new member of the eukaryotic initiation factor 4E-binding protein family. *J Biol Chem* **273**: 14002–7.
- Powers ET, Morimoto RI, Dillin A, Kelly JW, Balch WE. 2009. Biological and chemical approaches to diseases of proteostasis deficiency. *Annu Rev Biochem* **78**: 959–991. <http://www.ncbi.nlm.nih.gov/pubmed/19298183>.
- Powers RW, Kaerberlein M, Caldwell SD, Kennedy BK, Fields S. 2006. Extension of chronological life span in yeast by decreased TOR pathway signaling. *Genes Dev* **20**: 174–84. <http://www.ncbi.nlm.nih.gov/pubmed/16418483>.
- Princiotta MF, Finzi D, Qian S-B, Gibbs J, Schuchmann S, Buttgerit F, Bennink JR, Yewdell JW. 2003. Quantitating protein synthesis, degradation, and endogenous antigen processing. *Immunity* **18**: 343–54. <http://www.ncbi.nlm.nih.gov/pubmed/12648452>.
- Prusiner P, Yathindra N, Sundaralingam M. 1974. Effect of ribose O(2')-methylation on the conformation of nucleosides and nucleotides. *Biochim Biophys Acta - Nucleic Acids Protein Synth* **366**: 115–123.

<https://linkinghub.elsevier.com/retrieve/pii/S0005278774903256>.

- Qi Y, Zhu F, Eastman RT, Fu Y, Zilversmit M, Pattaradilokrat S, Hong L, Liu S, McCutchan TF, Pan W, et al. 2015. Regulation of *Plasmodium yoelii* Oocyst Development by Strain- and Stage-Specific Small-Subunit rRNA ed. L.M. Weiss. *MBio* **6**. <https://mbio.asm.org/lookup/doi/10.1128/mBio.00117-15>.
- Ramagopal S. 1990. Induction of cell-specific ribosomal proteins in aggregation-competent nonmorphogenetic *Dictyostelium discoideum*. *Biochem Cell Biol* **68**: 1281–1287. <http://www.nrcresearchpress.com/doi/10.1139/o90-190>.
- Ramagopal S, Ennis HL. 1984. Decay and synthesis of ribosomal proteins during *Dictyostelium discoideum* development. *Mol Gen Genet MGG* **194**: 466–470. <http://link.springer.com/10.1007/BF00425559>.
- Rando TA, Chang HY. 2012. Aging, rejuvenation, and epigenetic reprogramming: resetting the aging clock. *Cell* **148**: 46–57. <http://www.ncbi.nlm.nih.gov/pubmed/22265401>.
- Ressler S, Bartkova J, Niederegger H, Bartek J, Scharffetter-Kochanek K, Jansen-Dürr P, Wlaschek M. 2006. p16INK4A is a robust in vivo biomarker of cellular aging in human skin. *Aging Cell* **5**: 379–89. <http://www.ncbi.nlm.nih.gov/pubmed/16911562>.
- Rintala-Dempsey AC, Kothe U. 2017. Eukaryotic stand-alone pseudouridine synthases – RNA modifying enzymes and emerging regulators of gene expression? *RNA Biol* **14**: 1185–1196. <https://www.tandfonline.com/doi/full/10.1080/15476286.2016.1276150>.
- Robida-Stubbs S, Glover-Cutter K, Lamming DW, Mizunuma M, Narasimhan SD, Neumann-Haefelin E, Sabatini DM, Blackwell TK. 2012. TOR signaling and rapamycin influence longevity by regulating SKN-1/Nrf and DAF-16/FoxO. *Cell Metab* **15**: 713–24. <http://www.ncbi.nlm.nih.gov/pubmed/22560223>.
- Rogers AN, Chen D, McColl G, Czerwieniec G, Felkey K, Gibson BW, Hubbard A, Melov S, Lithgow GJ, Kapahi P. 2011. Life span extension via eIF4G inhibition is mediated by posttranscriptional remodeling of stress response gene expression in *C. elegans*. *Cell Metab* **14**: 55–66.
- Rollins JA, Howard AC, Dobbins SK, Washburn EH, Rogers AN. 2017. Assessing Health Span in *Caenorhabditis elegans*: Lessons From Short-Lived Mutants. *J Gerontol A Biol Sci Med Sci* **72**: 473–480.
- Rollins JA, Shaffer D, Snow SS, Kapahi P, Rogers AN. 2019. Dietary restriction induces posttranscriptional regulation of longevity genes. *Life Sci alliance* **2**.
- Rossi DJ, Bryder D, Seita J, Nussenzweig A, Hoeijmakers J, Weissman IL. 2007. Deficiencies in DNA damage repair limit the function of haematopoietic stem cells with age. *Nature* **447**: 725–729. <http://www.nature.com/articles/nature05862>.
- Rual J-F, Ceron J, Koreth J, Hao T, Nicot A-S, Hirozane-Kishikawa T, Vandenhaute J, Orkin SH, Hill DE, van den Heuvel S, et al. 2004. Toward improving *Caenorhabditis elegans* phenome mapping with an ORFeome-based RNAi library. *Genome Res* **14**: 2162–8.
- Ruggero D, Shimamura A. 2014. Marrow failure: a window into ribosome biology. *Blood* **124**: 2784–2792. <https://ashpublications.org/blood/article/124/18/2784/33387/Marrow-failure-a-window-into-ribosome-biology>.
- Russell SJ, Kahn CR. 2007. Endocrine regulation of ageing. *Nat Rev Mol Cell Biol* **8**: 681–91. <http://www.ncbi.nlm.nih.gov/pubmed/17684529>.
- Saijo Y, Sato G, Usui K, Sato M, Sagawa M, Kondo T, Minami Y, Nukiwa T. 2001. Expression of nucleolar protein p120 predicts poor prognosis in patients with stage I lung adenocarcinoma. *Ann Oncol Off J Eur Soc Med Oncol* **12**: 1121–5.
- Saijou E, Fujiwara T, Suzaki T, Inoue K, Sakamoto H. 2004. RBD-1, a nucleolar RNA-binding protein, is essential for *Caenorhabditis elegans* early development through 18S ribosomal RNA processing. *Nucleic Acids Res* **32**: 1028–1036.
- Saletore Y, Meyer K, Korlach J, Vilfan ID, Jaffrey S, Mason CE. 2012. The birth of the Epitranscriptome: deciphering the function of RNA modifications. *Genome Biol* **13**: 175.

- <http://genomebiology.biomedcentral.com/articles/10.1186/gb-2012-13-10-175>.
- Salminen A, Kaarniranta K, Kauppinen A. 2012. Inflammaging: disturbed interplay between autophagy and inflammasomes. *Aging (Albany NY)* **4**: 166–75. <http://www.ncbi.nlm.nih.gov/pubmed/22411934>.
- Samir P, Browne CM, Rahul, Sun M, Shen B, Li W, Frank J, Link AJ. 2018. Identification of Changing Ribosome Protein Compositions using Mass Spectrometry. *Proteomics* **18**: 1800217. <http://doi.wiley.com/10.1002/pmic.201800217>.
- Sato G, Saijo Y, Uchiyama B, Kumano N, Sugawara S, Fujimura S, Sato M, Sagawa M, Ohkuda K, Koike K, et al. 1999. Prognostic Value of Nucleolar Protein p120 in Patients With Resected Lung Adenocarcinoma. *J Clin Oncol* **17**: 2721–2721. <http://ascopubs.org/doi/10.1200/JCO.1999.17.9.2721>.
- Schaefer M, Pollex T, Hanna K, Lyko F. 2008. RNA cytosine methylation analysis by bisulfite sequencing. *Nucleic Acids Res* **37**: e12–e12. <https://academic.oup.com/nar/article-lookup/doi/10.1093/nar/gkn954>.
- Scheper GC, van der Knaap MS, Proud CG. 2007. Translation matters: protein synthesis defects in inherited disease. *Nat Rev Genet* **8**: 711–23.
- Schossere M, Minois N, Angerer TB, Amring M, Dellago H, Harreither E, Calle-Perez A, Pircher A, Gerstl MP, Pfeifenberger S, et al. 2015. Methylation of ribosomal RNA by NSUN5 is a conserved mechanism modulating organismal lifespan. *Nat Commun* **6**: 6158.
- Schubert C. 2009. The genomic basis of the Williams – Beuren syndrome. *Cell Mol Life Sci* **66**: 1178–1197. <http://link.springer.com/10.1007/s00018-008-8401-y>.
- Schwanhäusser B, Busse D, Li N, Dittmar G, Schuchhardt J, Wolf J, Chen W, Selbach M. 2011. Global quantification of mammalian gene expression control. *Nature* **473**: 337–42. <http://www.ncbi.nlm.nih.gov/pubmed/21593866>.
- Schwartz S, Bernstein DA, Mumbach MR, Jovanovic M, Herbst RH, León-Ricardo BX, Engreitz JM, Guttman M, Satija R, Lander ES, et al. 2014. Transcriptome-wide Mapping Reveals Widespread Dynamic-Regulated Pseudouridylation of ncRNA and mRNA. *Cell* **159**: 148–162. <https://linkinghub.elsevier.com/retrieve/pii/S0092867414010988>.
- Segev N, Gerst JE. 2018. Specialized ribosomes and specific ribosomal protein paralogs control translation of mitochondrial proteins. *J Cell Biol* **217**: 117–126. <https://rupress.org/jcb/article/217/1/117/39158/Specialized-ribosomes-and-specific-ribosomal>.
- Selman C, Lingard S, Choudhury AI, Batterham RL, Claret M, Clements M, Ramadani F, Okkenhaug K, Schuster E, Blanc E, et al. 2008. Evidence for lifespan extension and delayed age-related biomarkers in insulin receptor substrate 1 null mice. *FASEB J* **22**: 807–818.
- Sergiev P V, Aleksashin NA, Chugunova AA, Polikanov YS, Dontsova OA. 2018. Structural and evolutionary insights into ribosomal RNA methylation. *Nat Chem Biol* **14**: 226–235. <http://www.nature.com/doi/10.1038/nchembio.2569>.
- Shah P, Ding Y, Niemczyk M, Kudla G, Plotkin JB. 2013a. Rate-Limiting Steps in Yeast Protein Translation. *Cell* **153**: 1589–1601. <https://linkinghub.elsevier.com/retrieve/pii/S0092867413006557>.
- Shah PP, Donahue G, Otte GL, Capell BC, Nelson DM, Cao K, Aggarwala V, Cruickshanks HA, Rai TS, McBryan T, et al. 2013b. Lamin B1 depletion in senescent cells triggers large-scale changes in gene expression and the chromatin landscape. *Genes Dev* **27**: 1787–99. <http://www.ncbi.nlm.nih.gov/pubmed/23934658>.
- Shakes DC, Wu JC, Sadler PL, LaPrade K, Moore LL, Noritake A, Chu DS. 2009. Spermatogenesis-specific features of the meiotic program in *Caenorhabditis elegans*. *PLoS Genet* **5**.
- Sharma S, Hartmann JD, Watzinger P, Klepper A, Peifer C, Kötter P, Lafontaine DLJ, Entian K. 2018. A single N¹-methyladenosine on the large ribosomal subunit rRNA impacts locally its structure and the translation of key metabolic enzymes. 1–16.
- Sharma S, Lafontaine DLJ. 2015a. “View From A Bridge”: A New Perspective on Eukaryotic rRNA Base Modification. *Trends Biochem Sci* **40**: 560–575. <http://www.ncbi.nlm.nih.gov/pubmed/26410597>.

- Sharma S, Lafontaine DLJ. 2015b. 'View From A Bridge': A New Perspective on Eukaryotic rRNA Base Modification. *Trends Biochem Sci* **40**: 560–575.
- Sharma S, Yang J, Watzinger P, Kötter P, Entian KD. 2013. Yeast Nop2 and Rcm1 methylate C2870 and C2278 of the 25S rRNA, respectively. *Nucleic Acids Res* **41**: 9062–9076.
- Shav-Tal Y, Blechman J, Darzacq X, Montagna C, Dye BT, Patton JG, Singer RH, Zipori D. 2005. No Title. **16**: 2395–2413. <http://www.ncbi.nlm.nih.gov/pubmed/15758027>.
- Shaw AC, Joshi S, Greenwood H, Panda A, Lord JM. 2010. Aging of the innate immune system. *Curr Opin Immunol* **22**: 507–13. <http://www.ncbi.nlm.nih.gov/pubmed/20667703>.
- Shi Z, Fujii K, Kovary KM, Genuth NR, Röst HL, Teruel MN, Barna M. 2017. Heterogeneous Ribosomes Preferentially Translate Distinct Subpools of mRNAs Genome-wide. *Mol Cell* **67**: 71-83.e7.
- Siebold AP, Banerjee R, Tie F, Kiss DL, Moskowitz J, Harte PJ. 2010. Polycomb Repressive Complex 2 and Trithorax modulate Drosophila longevity and stress resistance. *Proc Natl Acad Sci U S A* **107**: 169–174.
- Sijen T, Fleenor J, Simmer F, Thijssen KL, Parrish S, Timmons L, Plasterk RH, Fire A. 2001. On the role of RNA amplification in dsRNA-triggered gene silencing. *Cell* **107**: 465–76.
- Simsek D, Barna M. 2017. An emerging role for the ribosome as a nexus for post-translational modifications. *Curr Opin Cell Biol* **45**: 92–101.
- Simsek D, Tiu GC, Flynn RA, Byeon GW, Leppek K, Xu AF, Chang HY, Barna M. 2017. The Mammalian Ribosome Interactome Reveals Ribosome Functional Diversity and Heterogeneity. *Cell* **169**: 1051-1065.e18. <http://dx.doi.org/10.1016/j.cell.2017.05.022>.
- Singleton RS, Liu-Yi P, Formenti F, Ge W, Sekirnik R, Fischer R, Adam J, Pollard PJ, Wolf A, Thalhammer A, et al. 2014. OGFOD1 catalyzes prolyl hydroxylation of RPS23 and is involved in translation control and stress granule formation. *Proc Natl Acad Sci* **111**: 4031–4036. <http://www.pnas.org/cgi/doi/10.1073/pnas.1314482111>.
- Slavov N, Semrau S, Airoidi E, Budnik B, van Oudenaarden A. 2015. Differential Stoichiometry among Core Ribosomal Proteins. *Cell Rep* **13**: 865–873. <https://linkinghub.elsevier.com/retrieve/pii/S2211124715010815>.
- Sloan KE, Warda AS, Sharma S, Entian K-D, Lafontaine DLJ, Bohnsack MT. 2017. Tuning the ribosome: The influence of rRNA modification on eukaryotic ribosome biogenesis and function. *RNA Biol* **14**: 1138–1152.
- Soto-Gamez A, Demaria M. 2017. Therapeutic interventions for aging: the case of cellular senescence. *Drug Discov Today* **22**: 786–795. <http://www.ncbi.nlm.nih.gov/pubmed/28111332>.
- Squires JE, Patel HR, Nusch M, Sibbritt T, Humphreys DT, Parker BJ, Suter CM, Preiss T. 2012. Widespread occurrence of 5-methylcytosine in human coding and non-coding RNA. *Nucleic Acids Res* **40**: 5023–5033. <https://academic.oup.com/nar/article/40/11/5023/2409239>.
- Steffen KK, McCormick MA, Pham KM, MacKay VL, Delaney JR, Murakami CJ, Kaeberlein M, Kennedy BK. 2012. Ribosome Deficiency Protects Against ER Stress in *Saccharomyces cerevisiae*. *Genetics* **191**: 107–118. <http://www.genetics.org/lookup/doi/10.1534/genetics.111.136549>.
- Steitz TA. 2008. A structural understanding of the dynamic ribosome machine. *Nat Rev Mol Cell Biol* **9**: 242–53. <http://www.ncbi.nlm.nih.gov/pubmed/18292779>.
- Strittmatter AW, Fischer C, Kleinschmidt M, Braus GH. 2006. FLO11 mediated filamentous growth of the yeast *Saccharomyces cerevisiae* depends on the expression of the ribosomal RPS26 genes. *Mol Genet Genomics* **276**: 113–125. <http://link.springer.com/10.1007/s00438-006-0127-7>.
- Sugihara Y, Honda H, Iida T, Morinaga T, Hino S, Okajima T, Matsuda T, Nadano D. 2010. Proteomic Analysis of Rodent Ribosomes Revealed Heterogeneity Including Ribosomal Proteins L10-like, L22-like 1, and L39-like. *J Proteome Res* **9**: 1351–1366. <https://pubs.acs.org/doi/abs/10.1021/pr9008964>.

- Suh Y, Atzmon G, Cho M-O, Hwang D, Liu B, Leahy DJ, Barzilai N, Cohen P. 2008. Functionally significant insulin-like growth factor I receptor mutations in centenarians. *Proc Natl Acad Sci* **105**: 3438–3442. <http://www.pnas.org/cgi/doi/10.1073/pnas.0705467105>.
- Sun D-L, Jiang X, Wu QL, Zhou N-Y. 2013. Intragenomic Heterogeneity of 16S rRNA Genes Causes Overestimation of Prokaryotic Diversity. *Appl Environ Microbiol* **79**: 5962–5969. <http://aem.asm.org/lookup/doi/10.1128/AEM.01282-13>.
- Syntichaki P, Troulinaki K, Tavernarakis N. 2007. eIF4E function in somatic cells modulates ageing in *Caenorhabditis elegans*. *Nature* **445**: 922–6.
- Takahashi A, Okada R, Nagao K, Kawamata Y, Hanyu A, Yoshimoto S, Takasugi M, Watanabe S, Kanemaki MT, Obuse C, et al. 2017. Exosomes maintain cellular homeostasis by excreting harmful DNA from cells. *Nat Commun* **8**: 15287. <http://www.nature.com/articles/ncomms15287>.
- Talens RP, Christensen K, Putter H, Willemsen G, Christiansen L, Kremer D, Suchiman HED, Slagboom PE, Boomsma DI, Heijmans BT. 2012. Epigenetic variation during the adult lifespan: Cross-sectional and longitudinal data on monozygotic twin pairs. *Aging Cell* **11**: 694–703.
- Taoka M, Nobe Y, Yamaki Y, Sato K, Ishikawa H, Izumikawa K, Yamauchi Y, Hirota K, Nakayama H, Takahashi N, et al. 2018. Landscape of the complete RNA chemical modifications in the human 80S ribosome. *Nucleic Acids Res* **46**: 9289–9298. <https://academic.oup.com/nar/article/46/18/9289/5091956>.
- Tassabehji M. 2003. Williams-Beuren syndrome: a challenge for genotype-phenotype correlations. *Hum Mol Genet* **12**: R229–37. <https://academic.oup.com/hmg/article-lookup/doi/10.1093/hmg/ddg299>.
- Tchkonia T, Zhu Y, van Deursen J, Campisi J, Kirkland JL. 2013. Cellular senescence and the senescent secretory phenotype: therapeutic opportunities. *J Clin Invest* **123**: 966–72. <http://www.ncbi.nlm.nih.gov/pubmed/23454759>.
- Terlecki-Zaniewicz L, Lämmermann I, Latreille J, Bobbili MR, Pils V, Schosserer M, Weinmüller R, Dellago H, Skalicky S, Pum D, et al. 2018. Small extracellular vesicles and their miRNA cargo are anti-apoptotic members of the senescence-associated secretory phenotype. *Aging (Albany NY)* **10**: 1103–1132. <http://www.aging-us.com/article/101452/text>.
- Terlecki-Zaniewicz L, Pils V, Bobbili MR, Lämmermann I, Perrotta I, Grillenberger T, Schwestka J, Weiß K, Pum D, Arcalis E, et al. 2019. Extracellular Vesicles in Human Skin: Cross-Talk from Senescent Fibroblasts to Keratinocytes by miRNAs. *J Invest Dermatol* **139**: 2425–2436.e5. <https://linkinghub.elsevier.com/retrieve/pii/S0022202X19317543>.
- Terry DF, Nolan VG, Andersen SL, Perls TT, Cawthon R. 2008. Association of longer telomeres with better health in centenarians. *J Gerontol A Biol Sci Med Sci* **63**: 809–812.
- Teuscher AC, Statzer C, Pantasis S, Bordoli MR, Ewald CY. 2019. Assessing Collagen Deposition During Aging in Mammalian Tissue and in *Caenorhabditis elegans*. *Methods Mol Biol* **1944**: 169–188.
- Thompson PM. 2005. Abnormal Cortical Complexity and Thickness Profiles Mapped in Williams Syndrome. *J Neurosci* **25**: 4146–4158. <http://www.jneurosci.org/cgi/doi/10.1523/JNEUROSCI.0165-05.2005>.
- Tibshirani R, Friedman JH, Mayeda TK, Lyons TW, Devlin SJ, Rajagopalan B, Lall U, Vajda I, Grassberger P, Stuetzle W, et al. 2011. The Structure of the Eukaryotic Ribosome at 3.0 Å Resolution. *Science (80-)* **331**: 1524–1529.
- Tijsterman M, Okihara KL, Thijssen K, Plasterk RHA. 2002. PPW-1, a PAZ/PIWI protein required for efficient germline RNAi, is defective in a natural isolate of *C. elegans*. *Curr Biol* **12**: 1535–40.
- Tiku V, Kew C, Mehrotra P, Ganesan R, Robinson N, Antebi A. 2018. Nucleolar fibrillarin is an evolutionarily conserved regulator of bacterial pathogen resistance. *Nat Commun* **9**: 1–10.
- Tilstra J, Robinson A, Wang J. 2012. NF-κB inhibition delays DNA damage–induced senescence and aging in mice. *J* **122**. <http://www.jci.org/articles/view/45785?ref=nf>.
- Trixl L, Lusser A. 2019. The dynamic RNA modification 5-methylcytosine and its emerging role as an

- epitranscriptomic mark. *Wiley Interdiscip Rev RNA* **10**: e1510.
- Turowski TW, Tollervey D. 2015. Cotranscriptional events in eukaryotic ribosome synthesis. *Wiley Interdiscip Rev RNA* **6**: 129–39. <http://www.ncbi.nlm.nih.gov/pubmed/25176256>.
- Turowski TW, Tollervey D. 2016. Transcription by RNA polymerase III: insights into mechanism and regulation. *Biochem Soc Trans* **44**: 1367–1375. <http://biochemsoctrans.org/lookup/doi/10.1042/BST20160062>.
- Tushev G, Glock C, Heumüller M, Biever A, Jovanovic M, Schuman EM. 2018. Alternative 3' UTRs Modify the Localization, Regulatory Potential, Stability, and Plasticity of mRNAs in Neuronal Compartments. *Neuron* **98**: 495–511.e6.
- Urbán Z, Riazi S, Seidl TL, Katahira J, Smoot LB, Chitayat D, Boyd CD, Hinek A. 2002. Connection between elastin haploinsufficiency and increased cell proliferation in patients with supravalvular aortic stenosis and Williams-Beuren syndrome. *Am J Hum Genet* **71**: 30–44.
- Valiathan R, Ashman M, Asthana D. 2016. Effects of Ageing on the Immune System: Infants to Elderly. *Scand J Immunol* **83**: 255–66. <http://www.ncbi.nlm.nih.gov/pubmed/26808160>.
- van Spaendonk RML, Ramesar J, van Wigcheren A, Eling W, Beetsma AL, van Gemert G-J, Hooghof J, Janse CJ, Waters AP. 2001. Functional Equivalence of Structurally Distinct Ribosomes in the Malaria Parasite, *Plasmodium berghei*. *J Biol Chem* **276**: 22638–22647. <http://www.jbc.org/lookup/doi/10.1074/jbc.M101234200>.
- Vannini A, Cramer P. 2012. Conservation between the RNA Polymerase I, II, and III Transcription Initiation Machineries. *Mol Cell* **45**: 439–446. <http://dx.doi.org/10.1016/j.molcel.2012.01.023>.
- Velichutina IRINA V., ROGERS MJ, McCUTCHAN TF, LIEBMAN SW. 1998. Chimeric rRNAs containing the GTPase centers of the developmentally regulated ribosomal rRNAs of *Plasmodium falciparum* are functionally distinct. *RNA* **4**: S1355838298980049. http://www.journals.cambridge.org/abstract_S1355838298980049.
- Vieira N, Bessa C, Rodrigues AJ, Marques P, Chan FY, de Carvalho AX, Correia-Neves M, Sousa N. 2017. Sorting nexin 3 mutation impairs development and neuronal function in *Caenorhabditis elegans*. *Cell Mol Life Sci* 1–18.
- Vijg J, Campisi J. 2008. Puzzles, promises and a cure for ageing. *Nature* **454**: 1065–71. <http://www.ncbi.nlm.nih.gov/pubmed/18756247>.
- Villeda SA, Luo J, Mosher KI, Zou B, Britschgi M, Bieri G, Stan TM, Fainberg N, Ding Z, Eggel A, et al. 2011. The ageing systemic milieu negatively regulates neurogenesis and cognitive function. *Nature* **477**: 90–94. <http://www.nature.com/articles/nature10357>.
- von Zglinicki T, Saretzki G, Ladhoff J, d'Adda di Fagagna F, Jackson SP. 2005. Human cell senescence as a DNA damage response. *Mech Ageing Dev* **126**: 111–7. <http://www.ncbi.nlm.nih.gov/pubmed/15610769>.
- Voorhees RM, Ramakrishnan V. 2013. Structural basis of the translational elongation cycle. *Annu Rev Biochem* **82**: 203–36. <http://www.ncbi.nlm.nih.gov/pubmed/23746255>.
- Wang C, Jurk D, Maddick M, Nelson G, Martin-Ruiz C, von Zglinicki T. 2009. DNA damage response and cellular senescence in tissues of aging mice. *Aging Cell* **8**: 311–23. <http://www.ncbi.nlm.nih.gov/pubmed/19627270>.
- Wang Y, Hekimi S. 2015. Mitochondrial dysfunction and longevity in animals: Untangling the knot. *Science* **350**: 1204–7. <http://www.ncbi.nlm.nih.gov/pubmed/26785479>.
- Warnecke PM, Stirzaker C, Song J, Grunau C, Melki JR, Clark SJ. 2002. Identification and resolution of artifacts in bisulfite sequencing. *Methods* **27**: 101–7.
- Waterhouse AM, Procter JB, Martin DMA, Clamp M, Barton GJ. 2009. Jalview Version 2--a multiple sequence alignment editor and analysis workbench. *Bioinformatics* **25**: 1189–91.
- Weir HJ, Yao P, Huynh FK, Escoubas CC, Goncalves RL, Burkewitz K, Laboy R, Hirschey MD, Mair WB. 2017.

- Dietary Restriction and AMPK Increase Lifespan via Mitochondrial Network and Peroxisome Remodeling. *Cell Metab* **26**: 884–896.e5. <http://www.ncbi.nlm.nih.gov/pubmed/29107506>.
- Westendorp RGJ, van Heemst D, Rozing MP, Frölich M, Mooijaart SP, Blauw G-J, Beekman M, Heijmans BT, de Craen AJM, Slagboom PE, et al. 2009. Nonagenarian siblings and their offspring display lower risk of mortality and morbidity than sporadic nonagenarians: The Leiden Longevity Study. *J Am Geriatr Soc* **57**: 1634–7. <http://www.ncbi.nlm.nih.gov/pubmed/19682117>.
- Willcox BJ, Donlon TA, He Q, Chen R, Grove JS, Yano K, Masaki KH, Willcox DC, Rodriguez B, Curb JD. 2008. FOXO3A genotype is strongly associated with human longevity. *Proc Natl Acad Sci* **105**: 13987–13992. <http://www.pnas.org/cgi/doi/10.1073/pnas.0801030105>.
- Williams GC. 1957. Pleiotropy, Natural Selection, and the Evolution of Senescence. *Evolution (N Y)* **11**: 398. <https://www.jstor.org/stable/2406060?origin=crossref>.
- Wu Q, Niebuhr E, Yang H, Hansen L. 2005. Determination of the ‘critical region’ for cat-like cry of Cri-du-chat syndrome and analysis of candidate genes by quantitative PCR. *Eur J Hum Genet* **13**: 475–485. <http://www.nature.com/articles/5201345>.
- Xu M, Palmer AK, Ding H, Weivoda MM, Pirtskhalava T, White TA, Sepe A, Johnson KO, Stout MB, Giorgadze N, et al. 2015. Targeting senescent cells enhances adipogenesis and metabolic function in old age. *Elife* **4**: e12997. <http://www.ncbi.nlm.nih.gov/pubmed/26687007>.
- Xue S, Barna M. 2012. Specialized ribosomes: a new frontier in gene regulation and organismal biology. *Nat Rev Mol Cell Biol* **13**: 355–69.
- Yang G, Heisenberger C, Kos-Braun IC, Polacek N, Grillari J, Schosserer M, Kos M. 2020. Cellular senescence and quiescence are associated with altered ribosomal RNA methylation and processing. *bioRxiv* 2020.04.01.019653. <http://biorxiv.org/content/early/2020/04/02/2020.04.01.019653.abstract>.
- Yang J, Sharma S, Watzinger P, Hartmann JD, Ko P, Entian K. 2016. Mapping of Complete Set of Ribose and Base Modifications of Yeast rRNA by RP-HPLC and Mung Bean Nuclease Assay. 1–18.
- Yarunin A, Panse VG, Petfalski E, Dez C, Tollervey D, Hurt EC. 2005. Functional link between ribosome formation and biogenesis of iron-sulfur proteins. *EMBO J* **24**: 580–588.
- Yokoyama W, Hirota K, Wan H, Sumi N, Miyata M, Araoi S, Nomura N, Kako K, Fukamizu A. 2018. rRNA adenine methylation requires T07A9.8 gene as rram-1 in *Caenorhabditis elegans*. *J Biochem* **163**: 465–474. <https://academic.oup.com/jb/article/163/6/465/4827711>.
- Yousefzadeh MJ, Zhao J, Bukata C, Wade EA, McGowan SJ, Angelini LA, Bank MP, Gurkar AU, McGuckian CA, Calubag MF, et al. 2020. Tissue specificity of senescent cell accumulation during physiologic and accelerated aging of mice. *Aging Cell* e13094. <http://www.ncbi.nlm.nih.gov/pubmed/31981461>.
- Yu Y, Ji H, Doudna JA, Leary JA. 2009. Mass spectrometric analysis of the human 40S ribosomal subunit: Native and HCV IRES-bound complexes. *Protein Sci* **14**: 1438–1446. <http://doi.wiley.com/10.1110/ps.041293005>.
- Yuan Z, Chen P, Zhang T, Shen B, Chen L. 2019. Agenesis and Hypomyelination of Corpus Callosum in Mice Lacking Nsun5, an RNA Methyltransferase. *Cells* **8**: 552. <http://www.ncbi.nlm.nih.gov/pubmed/31174389>.
- Zarkower D. 2006. Somatic sex determination. *WormBook*. http://www.wormbook.org/chapters/www_somaticsexdeterm/somaticsexdeterm.html.
- Zeidan Q, Wang Z, De Maio A, Hart GW. 2010. O -GlcNAc Cycling Enzymes Associate with the Translational Machinery and Modify Core Ribosomal Proteins ed. M.B. Omary. *Mol Biol Cell* **21**: 1922–1936. <https://www.molbiolcell.org/doi/10.1091/mbc.e09-11-0941>.
- Zhang C, Cuervo AM. 2008. Restoration of chaperone-mediated autophagy in aging liver improves cellular maintenance and hepatic function. *Nat Med* **14**: 959–65. <http://www.ncbi.nlm.nih.gov/pubmed/18690243>.

- Zhang G, Li J, Purkayastha S, Tang Y, Zhang H, Yin Y, Li B, Liu G, Cai D. 2013. Hypothalamic programming of systemic ageing involving IKK- β , NF- κ B and GnRH. *Nature* **497**: 211–6. <http://www.ncbi.nlm.nih.gov/pubmed/23636330>.
- Zhang T, Chen P, Li W, Sha S, Wang Y, Yuan Z, Shen B, Chen L. 2018. Cognitive deficits in mice lacking Nsun5, a cytosine-5 RNA methyltransferase, with impairment of oligodendrocyte precursor cells. *Glia* **67**: 1–15. <http://doi.wiley.com/10.1002/glia.23565>.
- Zhou J, Lancaster L, Donohue JP, Noller HF. 2014. How the ribosome hands the A-site tRNA to the P site during EF-G-catalyzed translocation. *Science* **345**: 1188–91. <http://www.ncbi.nlm.nih.gov/pubmed/25190797>.
- Zhu Y, Doornebal EJ, Pirtskhalava T, Giorgadze N, Wentworth M, Fuhrmann-Stroissnigg H, Niedernhofer LJ, Robbins PD, Tchkonja T, Kirkland JL. 2017. New agents that target senescent cells: the flavone, fisetin, and the BCL-XL inhibitors, A1331852 and A1155463. *Aging (Albany NY)* **9**: 955–963. <http://www.aging-us.com/article/101202/text>.
- Zhu Y, Tchkonja T, Fuhrmann-Stroissnigg H, Dai HM, Ling YY, Stout MB, Pirtskhalava T, Giorgadze N, Johnson KO, Giles CB, et al. 2016. Identification of a novel senolytic agent, navitoclax, targeting the Bcl-2 family of anti-apoptotic factors. *Aging Cell* **15**: 428–435. <http://doi.wiley.com/10.1111/ace.12445>.
- Zou L, Wu D, Zang X, Wang Z, Wu Z, Chen D. 2019. Construction of a germline-specific RNAi tool in *C. elegans*. *Sci Rep* **9**: 2354.

7 Appendix

7.1 Abbreviations

ac ⁴ C	Acetylated cytosine
AMPK	AMP-activated protein kinase signalling
ATP	Adenosine 5'- triphosphate
CHO	Chinese hamster ovary
COBRA	Combined bisulfite restriction analysis
CR	Caloric restriction
DBA	Diamond-Blackfan anaemia
DCS	Decoding site
DDR	DNA-damage response
DKC1	Dyskerin
DNMT2	DNA methyltransferase 2
eNoSC	Energy-dependent nucleolar silencing complex
ESC	Embryonic stem cells
EV	Extracellular vesicle
GnRH	Gonadotropin-releasing hormone
HSC	Hematopoietic stem cells
HDF	Human dermal fibroblast
HH	Hoyeraal-Hreidarsson
IGF	Insulin/insulin-like growth factor
IIS	Insulin/insulin-like growth factor signalling
IL	Interleukin
IRES	Internal ribosomal entry sites
MEF	Mouse embryonic fibroblast
mTOR	Mammalian target of rapamycin
m ⁶ ₂ A	<i>N,N</i> -dimethyladenosine
m ⁶ A	<i>N</i> ⁶ -methyladenosine
m ⁷ G	<i>N</i> -methylguanosine

m ¹ acp ³ Ψ	<i>N</i> -methyl- <i>N</i> -aminocarboxypropylpseudouridine
m ¹ A	<i>N</i> ¹ -methyladenosine
m ⁵ C	<i>C</i> ⁵ -methylcytosine
m ³ U	<i>N</i> ³ - methyluridine
NF-κB	Nuclear factor kappa-light-chain-enhancer of activated B cells
NML	Nucleomethylin
NOL1/NOP2/SUN	NSUN
OPP	O-propargyl-puromycin
PTC	Peptidyl transferase centre
PTM	Post-translational modification
PUS	Pseudouridine synthase
qMS	Quantitative mass spectrometry
Rcm1p	rRNA cytosine methyltransferase
ROS	Reactive oxygen species
RP	Ribosomal protein
rRNA	Ribosomal RNA
RRP8	Ribosomal RNA-processing protein 8
SA-β-gal	Senescence-associated β-galactosidase
SAM	S-adenosyl methionine
SASP	Senescence associated secretory phenotype
shRNA	Small hairpin RNA
SIPS	Stress-induced premature senescent
SIRT1	Sirtuin1
snoRNA	Small nucleolar RNA
WBS	Williams-Beuren syndrome
X-DC	X-linked Dyskeratosis Congenita

7.2 Thesis related publications

7.2.1 A novel *Caenorhabditis elegans* proteinopathy model shows changes in mRNA translational frameshifting during aging – Cell Physiol Biochem. 2019

7.2.2 Cellular senescence and quiescence are associated with altered ribosomal RNA methylation and processing – bioRxiv preprint

Both publications are mentioned and cited throughout the thesis. For full citation including doi, please see 6. References.



Published in final edited form as:

Cell Physiol Biochem. 2019 ; 52(5): 970–983. doi:10.33594/0000000067.

A Novel *Caenorhabditis Elegans* Proteinopathy Model Shows Changes in mRNA Translational Frameshifting During Aging

Frauke Adaml^a, Jarod Rollins^b, Matthew Newsom^b, Santina Snow^b, Markus Schosserer^c, Clemens Heissenberger^c, Jordan Horrocks^b, Aric N. Rogers^b, Zoya Ignatova^a

^aDepartment of Chemistry and Biochemistry, University of Hamburg, Hamburg, Germany,

^bMDI Biological Laboratory, Davis Center for Regenerative Biology and Medicine, Salisbury Cove, ME, USA,

^cDepartment of Biotechnology, BOKU-University of Natural Resources and Life Sciences, Vienna, Austria

Abstract

Background/Aims: Regulation of mRNA translation is central to protein homeostasis and is optimized for speed and accuracy. Spontaneous recoding events occur virtually at any codon but at very low frequency and are commonly assumed to increase as the cell ages.

Methods: Here, we leveraged the polyglutamine(polyQ)-frameshifting model of huntingtin exon 1 with CAG repeat length in the pathological range (Htt51Q), which undergoes enhanced non-programmed translational –1 frameshifting.

Results: In body muscle cells of *Caenorhabditis elegans*, –1 frameshifting occurred at the onset of expression of the zero-frame product, correlated with mRNA level of the non-frameshifted expression and formed aggregates correlated with reduced motility in *C. elegans*. Spontaneous frameshifting was modulated by IFG-1, the homologue of the nutrient-responsive eukaryotic initiation factor 4G (eIF4G), under normal growth conditions and NSUN-5, a conserved ribosomal RNA methyltransferase, under osmotic stress.

Conclusion: Our results suggest that frameshifting and aggregation occur at even early stages of development and, because of their intrinsic stability, may persist and accelerate the onset of age-related proteinopathies.

Keywords

Translation; Frameshifting; Aging; CAG repeat; Polyglutamine; *C. elegans*; Aggregation

Zoya Ignatova and Aric N. Rogers, Inst. of Biochemistry and Molecular Biology, Univ. of Hamburg, Hamburg (Germany); MDI Biological Laboratory; Davis Center for Regenerative Biology and Medicine, Salisbury Cove (USA) Tel. 4940428382332, zoya.ignatova@uni-hamburg.de; arogers@mdibl.org.

Disclosure Statement

The authors declare that there are no conflicts of interest.

Introduction

Translation is central to genetic decoding and is orchestrated by the ribosome which translates, codon by codon, the information stored in the mRNA. Translation is highly dynamic and optimized for speed and accuracy [1]. However, the cost of maintaining high translation levels is reduced accuracy resulting in some aberrancies in translation, like recoding or misincorporation of amino acids. Translational recoding, or frameshifting, is due to local “out-of-register” decoding in which the ribosomes shift from the normal reading frame to either the -1 frame or the $+1$ frame. Both -1 and $+1$ frameshifting result in different *trans*-frame protein products. Spontaneous recoding events may occur virtually at any codon with relatively low frequency, resulting in expression of an aberrant protein product [2, 3]. In contrast, programmed recoding occurs more frequently at specific signals in the open reading frame (e.g. slippery site, secondary structure) [2–5]. Programmed frameshifting is frequently employed in viral genomes and is seen as an evolutionary tool to expand protein repertoire and maintain stoichiometry of protein complexes [4, 6, 7].

Incidental or non-programmed frameshifting is a stochastic process that uses atypical mechanisms of recoding. For example, mutation-based extension of a homopolymeric polyCAG stretch of huntingtin (Htt) exon 1 or ataxin-3, both implicated in neurodegenerative repeat pathologies, undergo -1 and $+1$ frameshifting with different underlying mechanisms [8–14]. $+1$ frameshifting is induced at an atypical slippery sequence 5'-upstream of the CAG repeat and this ribosomal slippage is facilitated by the increased secondary structure propensity of the expanded CAG-repeat. In contrast, -1 frameshifting is more frequent and is triggered by depletion of charged tRNA^{Gln}CUG that reads the CAG codon [10, 11]. Despite mechanistic differences in their origin, the *trans*-frame products (e.g. polyS from $+1$ frameshifting or polyQ/A from -1 frameshifting) are refractory to degradation and aggregate in the cell [8, 10, 15, 16].

Decades ago, the hypothesis was put forward that translation efficiency decreases with age and errors in translation accumulate [17]. Yet, direct experimental evidence of this longstanding assumption is missing. In general, aging is defined as a time-dependent progressive loss of physiological integrity and molecular activities which increases the vulnerability to death [18, 19]. One of the key players in physiological integrity, protein homeostasis or proteostasis, deteriorates with aging [18, 20]. Translation is intimately linked to proteostasis, hence compromised proteostasis integrity with age has been also extrapolated to alterations in translation fidelity. Furthermore, the level of many translation-associated factors, e.g. some ribosomal proteins, initiation factors, and modifying enzymes, declines with age, leading to general downregulation of protein synthesis (reviewed in [21]). But does the decreased translation that occurs with age correlate with errors in translation?

Using lysates prepared from young and old human fibroblasts, Luce and Bunn observed a sevenfold increase in cysteine misincorporation in aged human fibroblast cell line IMR-90 [22]. By contrast, other studies do not find any correlation between translation errors and aging [23, 24]. Furthermore, a recent study demonstrated that longer-lived species had lower basal rates of translation errors [25], suggesting that translation fidelity coevolved with the longevity of the organism. Measurements of the global protein synthesis in germ cells of

Drosophila melanogaster show that differentiating cells have higher protein output compared to stem cells [26]. Does this increased translation activity in differentiated cells lead to higher translational errors?

To address whether and how translation fidelity changes with age in differentiated cells, we used *Caenorhabditis elegans*, a widely-used model organism to study aging. Under a muscle-specific promoter, we integrated a reporter with an expanded polyCAG stretch which is sensitive to translation recoding errors and reports on -1 frameshifting (Htt51Q(-1)). By analyzing the frameshifting frequency as a function of age, from larvae to late adult state, we found that translational recoding errors accompany the zero-frame product from the onset of its expression in a manner that correlates with the overall level of gene expression. To test the influence of translational regulation that increases lifespan and resistance to age-related disease, we used knockdown of the nutrient-responsive eukaryotic translation initiation factor 4G/ *ifg-1* [27] or ribosomal RNA methyltransferase gene *nsun-5* [28]. We find that the toxicity associated with the Htt51Q(-1) aggregates is modulated by IFG-1 under normal growth conditions and by NSUN-5 under osmotic stress.

Materials and Methods

Design of a frameshifting reporter and generation of *C. elegans* transgenic strain

The reporter of frameshifting was adopted from [10], containing eCFP in zero frame to Htt exon 1 with 51 CAG repeats and mCherry in -1 (eCFP-Htt51Q(-1)-mCherry) generating the strain ANR105 (rogEx103[unc54p::CFP::Q51::mCherry]). It was cloned into pPD30.38 containing the promoter and enhancer elements from *unc-54* for body wall muscle expression. To bypass an independent translational start for mCherry, its N-terminal Met was mutated to Val. Integration of extrachromosomal arrays was carried out into the Bristol N2 nematodes using UV irradiation. Integrated lines were backcrossed three times into N2 wild-type to guarantee a wild-type genetic background generating the strain ANR144 (rogEx103[unc54p::CFP::Q51(2 151_2152insC)::mCherry]). Three independent lines were isolated and they all showed same phenotype.

C. elegans strains and maintenance

Besides ANR105, ANR144 and N2, the strain AM141 (rmIs133[unc-54p::Q40::YFP]) expressing a polyCAG-stretch alone and C-terminally fused to YFP was used. Furthermore, we included the strain AM881 (rmEx336[unc54p::htt171Q75::YFP] as a control (a kind gift from R.I. Morimoto, Northwestern University). AM881 expressed Htt exon 1 with 75 CAG repeats fused to YFP. All Htt variants were under the control of the body wall muscle specific promoter *unc-54*. ANR127 (rogIs113[sca-1p::GFP + myo-2::mCherry]) expressing mCherry and GFP only was used as a positive control. Strains were maintained at 20°C on nematode growth media (NGM) plates seeded with *Escherichia coli* OP50. For age synchronization, young adult animals were placed on NGM plates and were allowed to lay eggs. After about eight hours adult nematodes were removed and hatchlings were used for experiments. All experiments were carried out at 20°C. During reproductive stage, *C. elegans* individuals were transferred to fresh NGM plates every second day to avoid contamination by progeny.

Imaging

For light and fluorescence microscopy, synchronized nematodes were immobilized using either 5 mM levamisole or 10 mM NaN₃. The animals were imaged with a Leica DMi8 or Leica DFC310 FX (Leica Microsystems) and BZ-9000 (Keyence), respectively. It should be noted, that in general the mCherry fluorescence was hardly detectable under the same settings used to detect the zero-frame CFP-labeled Htt51Q, hence for the animals were usually longer exposed when recording the mCherry fluorescence. Intensity of fluorescence was quantified by using *ImageJ* 1.44p software.

RNAi experiments

RNAi bacteria strains expressing dsRNA *ifg-1* (M110.4), *daf-2* (Y55D5A_391.b), *daf-16* (R13H8.1), *nsun-5* (Y53F4B.4), *hsf-1* (Y53C10A.12), *qars-1* (Y41E3.4), *yars-1* (Y105E8A.19) (from the Ahringer library and from the Vidal library), including empty vector L4440 (Addgene, Cambridge, MA, USA.), were cultured as previously described [29]. 1 mM isopropyl β -D-thiogalactopyranoside (IPTG) was used for induction of dsRNA. *C. elegans* strains were synchronized via timed-egg lay, transferred to RNAi plates 48 hours after hatching and exposed to RNAi for 48 hours. Compared to N2 wild-type, the animals expressing Htt51Q exhibited delayed developing time. Therefore, they were monitored over a longer period until they reached adulthood phase comparable to that of the N2 animals. The knockdown of the gene of interest was verified by qRT-PCR or in case of *ifg-1* by immunoblot and *nsun-5* by COBRA.

Life span assay

Synchronized populations of 100 individual *C. elegans* nematodes were used for life-span assays starting from first day of adulthood. Life-span assays were carried out at 20°C on NGM plates spotted with *E. coli* OP50. Nematodes were scored every second day for survival and animals that failed to respond to a touch-provoked stimulus were referred as dead. Worms were censored if they died because of vulva burst or internal hatching of progeny. For life-span assays of AM141, the survival was scored starting from the first day of adulthood. 100 or more animals were used per condition (RNAi *ifg-1* or control RNAi L4440) and put on seeded RNAi plates containing 200 μ M fluorodeoxyuridine (FUDR). Survival was plotted by means of Kaplan-Meier survival curves and statistically analyzed by log-rank test, both integrated in *GraphPad Prism* 5.

Motility assay

Thrashing rate of individually synchronized nematodes was determined as described previously [30]. Briefly, one individual worm was transferred into 15 μ l of M9 or S-basal medium. After a recovery of 1 min the body bends were counted for 30 s. A body bend was defined as a change in direction of bending at midbody of the animals as described in [31]. Statistical analysis was performed by unpaired Student's *t*-test integrated in *GraphPad Prism* 5. Differences with $p < 0.05$ were considered as significant.

To determine motility traces, single one-day old adult worms of wild-type N2 and ANR144 were placed onto NGM plates with *E. coli* OP50 and allowed to move freely for 60 min at 20°C. Afterwards, their traces were imaged using Leica DMi8 (Leica Microsystems) with

10x objective. Assembling of one mosaic image from multiple smaller images was done to obtain a defined field size (here 6×6, software module “Tile Scan”).

RNA isolation and qRT-PCR

From synchronized *C. elegans* populations grown on NGM or RNAi plates the total RNA was isolated with TRIzol reagent (Ambion, ThermoFisher Scientific) following manufacturer’s protocol for chloroform extraction. The integrity of the RNA was analyzed with RNA Nano Chip 2100 (Bioanalyzer, Agilent Technologies). 0.5 µg total RNA was treated with RNase-free DNase I (Thermo Scientific) and reverse transcribed using oligo(dT)-primers and Revert Aid Reverse Transcriptase (Thermo Scientific). qRT-PCR was performed in a SYBR green-based approach (Qiagen) on a real-time PCR system (TOptical, Analytic Jena). mRNA expression of target genes was normalized to the housekeeping gene *act-2*.

Immunoblotting analysis and filter-retardation assay

A large population of animals (i.e. several thousands) were synchronized via timed egg lay and collected at different time points, starting from the first day of adulthood. *C. elegans* individuals were placed in 100 µl standard lysis buffer (8 M urea, 2% SDS, 50 mM DTT, 50 mM Tris pH 7.4, 1x Halt Protease Inhibitor Cocktail (Thermo Scientific)) on ice for several hours and then frozen. The protein concentrations of the lysates were determined using DC Protein Assay (Bio-Rad) and analyzed by immunoblotting using anti-GFP monoclonal antibody (1:1000, Thermo Scientific) or anti-mCherry (1:1000, St. John’s laboratory). For loading control, membranes were stripped with buffer containing 0.4 M NaOH, washed twice (5 minutes each), and immunostained with antibodies against beta-tubulin (1:500, Developmental Studies Hybridoma Bank). As a positive control, protein lysate of mCherry-expressing ANR127 strain were loaded.

For filter-retardation assays [32] a defined number of individual synchronized *C. elegans* were picked and lysed by boiling for 15 min in 15 µl of lysis buffer (50 mM DTT, 2% SDS). The lysates were loaded onto a cellulose acetate membrane with a defined pore size of 0.2 µm and polyQ variants were detected by immunoblotting.

Osmotic stress test

Nematodes were synchronized via timed egg lay on *nsun-5* RNAi plates or control RNAi, respectively. At one day of adulthood, *C. elegans* were moved to plates containing 50 mM, 100 mM or 200 mM NaCl. After 24 hours, animals were harvested for filter-retardation assay.

Detection of NSUN-5-specific methylation at C2381 of 26S rRNA by COBRA

C2381 methylation was detected by COBRA as previously described [28, 33] with minor modifications. Worms exposed to *nsun-5* or control RNAi were subjected to total RNA extraction and on-column DNase I digestion using the Direct-zol™ RNA Miniprep Kit (Zymo Research). 0.5 µg total RNA were bisulfite-converted using the EZ RNA Methylation™ Kit (Zymo Research) and subsequently cDNA was generated using Super Script IV (Life Technologies). PCR using OneTaq® DNA Polymerase was performed to

generate a 101 bp PCR product surrounding C2381 with forward and reverse primers specific for the cDNA after bisulfite conversion (i.e., 5'-GGGAGTAATTATGATTTTCTAAGGTAG-3' and 5'-ATAATAAATAAAAAACAATAAAAAATCTCACTAATCCATTCATACAC-3'). The PCR product was digested with *MseI* (New England Biolabs) and loaded on a Novex™ TBE Gel, 20%, 10 well (Life Technologies). Two products of 45 and 56 bp were formed, if C2381 was methylated and three products of 15, 30 and 56 bp, if C2381 was not methylated.

Results

-1 frameshifted species appears early in the development of *C. elegans*

To determine the age-dependent effect on frameshifting in *C. elegans*, we generated a reporter construct with the fluorescent mCherry protein fused C-terminally in -1 reading frame to human *Htt* exon 1 with a repeat in the pathological range encoding 51 glutamines (Htt51Q) (Fig 1A). N-terminally of Htt, the reporter carries eCFP in the zero-reading frame, enabling detection of the overall expression level (Fig 1A). For simplicity, we named the full-length constructs eCFP::Htt_exon1(Q51)::mCherry(-1) as Htt51Q(-1). The reporter was cloned under the control of the *unc-54* promoter, which normally drives expression of the myosin heavy chain in body muscle (Fig 1A). Expression in muscle cells was chosen as expression of polyQ proteins produces a toxic effect that reduces locomotion in *C. elegans* [34]. Using the mCherry fluorescence as a read-out of frameshifting, we detected abundant -1 frameshifting (Fig 1B). In parallel, we produced a similar construct that reports on +1 frameshifting (Htt51Q(+1)) to compare both recoding events. However, +1 frameshifting was extremely rare (i.e. far less than 1%), which precluded further analysis and so, we focused only on -1 frameshifting. This observation agrees with results from mammalian cell cultures in which +1 frameshifting was also much more rarely detected than -1 [10, 11].

We used two different *C. elegans* strains, ANR144 with the integrated -1 frameshift reporter and ANR105 strain expressing Htt extrachromosomally. Overall, the expression of the integrated frameshift reporter was similar to that already observed in nematodes expressing Htt extrachromosomally, but with fewer mCherry-positive -1-frameshifted species (Fig. 1B and Fig. S1A - for all supplemental material see www.cellphysiolbiochem.com). On average, we detected 1.9 vs 4.6 red fluorescent spots per animal with integrated *Htt51Q(-1)* gene vs extrachromosomal array, respectively (Fig S1B). The mCherry fluorescence reporting on -1 frameshifting was detectable in every animal tested and appeared during larval development as hyper-fluorescent puncta (Fig. 1C and S1C). Expression of both Htt51Q(-1) and Htt51Q was more prominent in the head of the transgenic animals and rarely detectable in the rest of the body wall muscle cells (Fig. 1B, C and Fig. S1A, C). Notably, the zero-frame Htt51Q, detected through eCFP, exhibited rather diffuse fluorescence throughout the body wall muscle cells, whereas the foci were exclusively red (Fig. 1B). mCherry-foci that were clearly visible in young adults and characterized by sharp and distinct boundaries which disappeared with age (Fig. 1D and Fig. S1D). Instead, the red fluorescence was dominated by mostly intestinal age-associated autofluorescence from day 5 on (Fig. 1D and Fig. S1D). Limited expression to the head region was also observed for

the AM881 strain (Fig. S1G), another *C. elegans* model expressing Htt exon 1 with a polyQ stretch within the pathological range (Htt75Q).

To determine the relative accumulation of the -1 *trans*-frame product with age, we measured the ratio of mCherry to eCFP fluorescence of the main zero-frame Htt51Q product by integrating the fluorescence over the head area of the animals (Fig. 1E and Fig. S1E). The ratio of mCherry to CFP fluorescence increased with age (Fig. 1E and Fig. S1E). But when analyzing the zero- and *trans*-frame products separately, we realized that changes in the ratio were mostly due to a decrease of CFP fluorescence, while the mCherry fluorescence changed only marginally (Table S1 and S2), suggesting higher stability or higher aggregation propensity of polyA stretches compared to polyQ. Supportive of this, in the polyA pathologies, much shorter expansions of polyA confer cellular dysfunction [35].

The amount of the zero-frame protein Htt51Q decreased with age in both animals with genome-integrated or extrachromosomal expression (Fig. 1D, E, Fig. S1D, E and Table S1, S2). Compared to the *C. elegans* strain AM141 expressing solely the polyQ stretch under the control of the same muscle-specific promoter the average number of the zero-frame Htt51Q(-1) aggregates per young animal was much lower (Fig S1B) [34]. The decrease in fluorescence of the zero-frame Htt51Q strongly correlated with the decline in mRNA levels over time for both animal groups with genome-integrated and extrachromosomal expression of Htt51Q(-1) (Fig 1F and Fig S1F) which corroborates previous observations for age-dependent decrease in mRNA levels in muscle tissues [36].

-1 frameshifted protein alone forms aggregates that persist with age

The mCherry fluorescence reporting on -1 frameshifting remained relatively unchanged with age on the background of decreased zero-frame Htt51Q product (Table S1 and S2), which raised the question as to whether zero- and *trans*-frame proteins exhibit different stability, and/or the CFP fluorescence might be quenched by interactions with cellular proteins or through the Htt51Q aggregation itself. Hence, we performed immunoblotting to monitor the expression of SDS-soluble proteins (Fig. 2A, C) and filter-retardation assays to detect detergent-insoluble aggregates (Fig. 2B). The zero-frame Htt51Q protein was detectable at early adulthood and declined with age (Fig 2C). By contrast, we were not able to detect mCherry biochemically in the first days of adulthood (Fig. 2A, C) despite visible detection of mCherry fluorescence during this time (Fig. 1B, D); Htt51Q(-1) protein expression might be under the detection limit of the immunoblots (Fig. 2A). At a later age, between day 5 and 11 of adulthood, we detected frameshifted species (Fig. 2A, C), which in the mCherry-immunostained blot exhibited higher molecular weights, most likely oligomers and persisted over time (Fig. 2A). Furthermore, the SDS-insoluble aggregates were mCherry-positive (Fig. 2B). Together, these results demonstrate that frameshifting in Htt51Q occurs early in life, presumably due to the high level of expression driven by the *unc-54* promoter at this time, and that the frameshifted product formed aggregates that were present throughout the life cycle of the animal. Our data suggests that the increase in aggregates with age might be due at least in part, to decreased turnover of frameshifted products.

In parallel, some phenotypic observations on the effect of Htt51Q(-1) expression on nematode behavior were made. When placed in liquid, *C. elegans* thrash about as they try to

get traction. This is frequently used to measure motility, which decreases with age and which is malleable under certain genetic or environmental conditions. The impact on morphological development of *C. elegans* with integrated *Htt51Q(-1)* was severe and locomotion was severely limited (Fig 2D). When placing animals on NGM plates spotted with *E. coli* OP50 to track their traces within the bacteria lawn, after 60 min transgenic animals with genome-integrated *Htt51Q(-1)* expression remained in close proximity to the start point, while the wild-type N2 had traversed almost the entire *E. coli* lawn (Fig S2A). This defect in exploratory locomotion was observed beginning from young larvae right after hatching; they remained near their hatching spot. Although wild-type nematodes moved slower with age, they retained coordinated thrashing behavior. In contrast, movements of transgenic animals with the integrated reporter were characterized by uncoordinated thrashing even at young age with some animals exhibiting paralysis. Impaired locomotion was also detectable by the egg laying pattern with eggs laid in clusters or straight lines. Very often, egg-laying adults stayed within a close proximity to the eggs. We isolated three independent transgenic lines with genome-integrated *Htt51Q(-1)* and these severe phenotypic changes were observed in all three which argues that the phenotype was not caused by the point of chromosomal insertion.

The mean survival was significantly reduced by ~40% compared to wild-type N2 ($p < 0.001$, log-rank test, Fig 2E). Many animals were censored during life-span assays because of internal hatching of larvae (Fig S2B). In contrast, the overall life span of the *Htt51Q(-1)* animals with the extrachromosomal array was not altered (Fig. S2C), although the thrashing rate of *Htt51Q(-1)* animals with the extrachromosomal array decreased compared to N2 wild-type animals (Fig S2D), despite exhibiting typical sinusoidal movements. With increasing age, the cuticles of transgenic animals became crumpled and the locomotion decreased. The *Htt51Q(-1)* animals with extrachromosomal array showed comparable motility with different polyglutamine-expressing strains (e.g. *Htt75Q-YFP* and *poly40Q-YFP*; Fig S2E).

IFG-1 and NSUN-5 modulate toxicity associated with aggregation

Next, we tested which cellular proteins influence translational frameshifting. We silenced several genes involved in regulation of translation and lifespan using interfering RNA (RNAi), e.g. *daf-16* and *daf-2* (abnormal dauer formation), *hsf-1* (heat shock factor 1), *ifg-1* (homologue of the eukaryotic initiation factor 4G (eIF4G)), *rsks-1* (worm homologue of S6 kinase), *qars-1* (glutamyl-tRNA synthetase, QARS) *yars-1* (tyrosyl-tRNA synthetase, YARS) and *nsun-5* (NOP2/Sun RNA methyltransferase family member 5). *daf-2* and *daf-16* were chosen for their role in regulating life span and longevity: *daf-16* encodes a FOXO transcription factor and *daf-2* an insulin-like receptor tyrosine kinase. Attenuation of DAF-2 activates DAF-16, which translocates to the nucleus and activates expression of stress response and longevity assurance genes [37]. HSF-1 is the heat shock transcription factor regulating transcription of heat shock genes, e. g. chaperones, assisting in refolding misfolded proteins [38]. IFG-1 was selected as its knock-down has been shown to decrease global translation rates [39, 40] and increases life span in *C. elegans* [27, 37, 39–41]. RSKS-1 activates ribosomal protein S6 through phosphorylation and also decreases global translation rates. Similar to *ifg-1*, knockdown of *rsks-1* results in life span extension of *C.*

elegans [40]. Our previous studies in mammalian cell culture models have shown that frameshifting frequency depends on the availability of charged glutamyl-tRNA^{Gln}CUG that reads the CAG codon [10]. Hence, to decrease the amount of charged glutamyl-tRNA^{Gln}CUG, we down regulated *qars-1* encoding the QARS which aminoacylates tRNA^{Gln}CUG with glutamine. As a control, *yars-1* encoding tyrosyl-tRNA synthetase (YARS) was selected, which charges tRNAs unrelated to the translation of CAG repeats. The down-regulation of the tested genes was verified by qPCR (Fig S3A), Western blot (Fig. S3B), or Combined Bisulfite Restriction Analysis (COBRA) methylation activity assay (Fig S3C, D). NSUN-5 introduces an m⁵C modification at C2381 of 26S ribosomal RNA and its depletion extends the mean lifespan and increases paraquat resistance, without affecting growth, pharyngeal pumping or locomotion [28].

The low intensity of the frameshifted Htt51Q(-1) species in the immunoblots precluded quantifiable comparison of the frameshifting yields following the knockdown of various genes. Instead, we compared the thrashing rates of individual nematodes subjected to different selected RNAi as readout of changes in proteotoxicity and associated changes in frameshifting products. In both nematodes strains with extrachromosomal or integrated expression of *Htt51Q(-1)* we observed the highest accumulation of frameshifted species at one day of adulthood, which coincides with the highest amount of *Htt51Q(-1)* mRNA (Fig 1F, S1F). Thus, we compared the thrashing rates following exposure to selected RNAi only at that age. In general, the motility was very low and the animals exhibited uncoordinated movements as also seen for nematodes grown on bacteria without any RNAi background (Fig 2D, 3A). For the majority of the genes with downregulated expression, we did not observe any effect on thrashing (Fig 3A). Day-one adult animals subjected to *ifg-1* knockdown in the previous 48 hours exhibited the highest variation in their body bends and the motility increased significantly compared to empty RNAi vector controls (Fig 3A). This may be due to enhanced activation of heat shock responsive genes when translation is attenuated in this manner [27]. Furthermore, many individuals presented the same sinusoidal movements on solid media and the same coordinated thrashing behavior in liquid characteristic for the N2 wild-type strain albeit with a slower frequency, showing the protective effect of the *ifg-1* knockdown. Furthermore, the *ifg-1* knockdown significantly reduced the fluorescence ratio of mCherry to eCFP over the head area of the animals (Fig S3E). Moreover, a positive and protective effect of *ifg-1* knockdown was also observed on the life span of nematodes expressing poly40QYFP (Fig S3F). A downregulation of aminoacyl-tRNA-synthetases (here QARS and YARS) may influence translation globally and consequently it was difficult to disentangle the effect of QARS on the overall lowered translation from that on the frameshifting frequency.

Following knockdown of *nsun-5*, we observed only a marginal impact on the thrashing rate in day 1 adult nematodes causing more heterogeneity without changing the mean (Fig 3A). Since it is known that loss of RCM1, the yeast orthologue of NSUN-5, decreases ribosome stability at high salt concentrations or oxidative stress and alters translation fidelity [28, 33], we next tested the effect of *nsun-5* depletion on aggregation of frameshifted products under osmotic stress. After one day, animals with reduced *nsun-5* levels formed more mCherry-positive aggregates when subjected to osmotic stress suggesting higher frameshifting frequency when rRNA methylation is altered (Fig 3B). This increase was visible under high

salt conditions (200 mM), whereas at lower salt concentration (100 mM) the amount of the aggregates containing frameshifted species was comparable to the control (Fig 3B). These results demonstrate that the presence of msC2381 of 26S rRNA as mediated by NSUN-5 is required for translation fidelity and maintenance of protein homeostasis under osmotic stress. Furthermore, relief of the toxic effect of aggregates on locomotion is specific to low IFG-1 and not shared with other RNAi treatments known to promote longevity and decrease translation, like *rsks-1* and *daf-2*.

Discussion

Translation fidelity plays an important role in maintaining proteostasis which, in turn, is a key player in protecting cellular function. Here, we took advantage of the multicellular model organism *C. elegans* to explore the frequency of translation recoding as a function of age and mRNA expression level. Spontaneous recoding is a relatively rare event, which occurs at rates comparable to the background rate [42] of translational errors $\sim 5 \times 10^{-4}$ per codon [43]. Such low rates are difficult to detect, and hence we leveraged the polyQ-frameshifting model with an expanded glutamine stretch which undergoes an enhanced and detectable non-programmed +1 and -1 frameshifting [10, 11]. By expressing the Htt51Q(-1) frameshift reporter either extrachromosomally or through genome integration we determined the incidental frameshifting frequency in the body wall muscle cells as the nematode aged. Intriguingly, the frameshifting is readily detectable during larval development, but changes little during the remaining life cycle of the nematodes. Frameshifting correlates with the expression level of the zero-frame protein. The latter declines because of a decrease in the steady-state *Htt51Q* mRNA levels with age (Fig 1F). Earlier studies demonstrate that mRNA levels of transgenic polyCAG and endogenous genes expressed in muscle cells (under the control of the *unc-54* promoter) decrease after the first day of adulthood in *C. elegans* [36, 44]. Moreover, decline in the expression of polyQ protein in muscle cells has been reported earlier: In nematodes expressing polyQ fragments only, aggregation did not increase over time [34] suggesting that the polyQ expression was most likely largely diminished with age. Nematodes with the integrated reporter show a shorter life span as well as reduced motility rates compared to the ones with the extrachromosomal array suggesting that the genetic background or expression level in general may also influence the turnover. In light of our observations, the spontaneous frameshifting occurs at the onset of Htt51Q expression during larval development, but the aggregation frequency remains constant with age likely due to a global decrease in Htt51Q expression.

The modulatory effect of IFG-1 on locomotion under normal growth was modest, albeit significant and easily detected. The IFG-1 effect on translation depends on the mRNA steady-state levels [39, 40], hence the decline in *Htt51Q(-1)* mRNA steady-state levels with aging likely weakens the IFG-1 effect. Similarly, the NSUN-5 effect is more pronounced at early time points of growth and weakens with aging because of the general decline in the *Htt51Q* mRNA steady-state levels.

The animals expressing the Htt51Q(-1) frameshift reporter either extrachromosomally or genome-integrated show significant locomotion alterations implying a toxic effect, which likely comes from both zero-frame and *trans*-frame proteins in light of the gain-of-toxicity

effect described for polyQ and polyA containing aggregates [45–47], which result in reduced motility when expressed in muscle cells [34]. We do not see an increase of the amount of aggregates, but rather a persistent small fraction that remains unchanged with age implying that the effect may originate from the onset of Htt51Q(–1) expression. Moreover, the hyperfluorescent aggregate foci of the trans-frame Htt51Q(–1) disappear early in adulthood suggesting a different turnover as compared to aggregates formed by polyQ stretch only, which are refractory to degradation [30, 34, 48]. Lee and coworkers, who also used full-length exon 1 instead of the polyQ stretch by itself, observed very modest aggregation behavior [49]. The native sequences flanking polyQ within exon 1 largely influence its aggregation propensity [50, 51].

Conclusion

Together, our results suggest that frameshifting is exacerbated when polyQ-containing mRNA is expressed at higher levels. Furthermore, spontaneous translational recoding occurs at the onset of expression. Some *trans*-frame products might be efficiently cleared by proteasome- or autophagy-mediated pathways, while *trans*-frame products of some transcripts may produce more persistent or even toxic products, like the example here, whose repetitive expanded polyamino acid stretch is refractory to clearance by the proteasome [52] and the aggregates of it likely alter the proteostasis network [53]. *Trans*-frame products produced at early age may risk accumulation because of their intrinsic stability or age-related deregulation of proteostasis, which, in turn, might be of importance in age-related proteinopathies.

Supplementary Material

Refer to Web version on PubMed Central for supplementary material.

Acknowledgements

The work was funded by the Innovation Award from the MDI Biological Laboratory Maine to Z.I., the James L. Boyer Fellowship at the MDI Biological Laboratory and the Austrian Science Fund (FWF: P30623-B26) to M.S. We thank Kevin Strange and Dustin Updike from the MDI Biological Laboratory in Maine, USA, for providing RNAi libraries. We thank R. Morimoto from the Northwestern University for the kind gift of the *C. elegans* strain AM881. N2 wild-type *C. elegans* was provided by the CGC, which is funded by NIH Office of Research Infrastructure Programs (P40 OD010440).

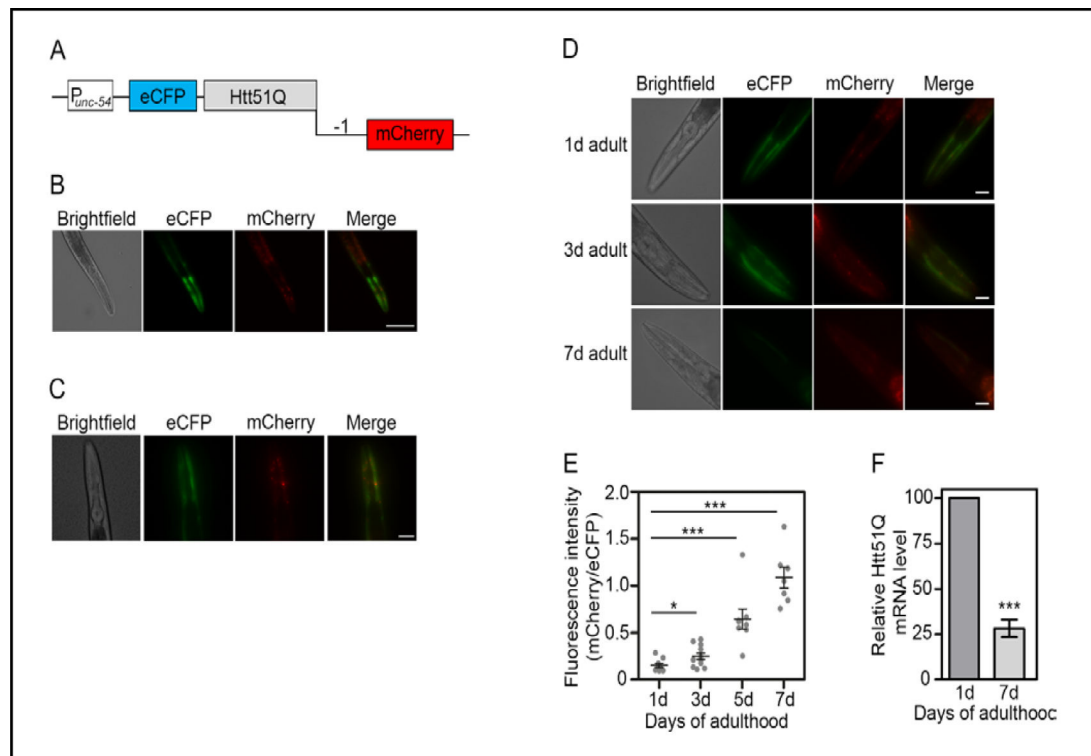
References

1. Rodnina MV, Wintermeyer W: The ribosome as a molecular machine: The mechanism of trna-mrna movement in translocation. *Biochem Soc Transact* 2011;39:658–662.
2. Advani VM, Dinman JD: Reprogramming the genetic code: The emerging role of ribosomal frameshifting in regulating cellular gene expression. *BioEssays: News Rev Mol Cell Develop Biol* 2016;38:21–26.
3. Dinman JD: Control of gene expression by translational recoding. *Adv Prot Chem Struct Biol* 2012;86:129–149.
4. Atkins JF, Loughran G, Bhatt PR, Firth AE, Baranov PV: Ribosomal frameshifting and transcriptional slippage: From genetic steganography and cryptography to adventitious use. *Nucl Acids Res* 2016;44:7007–7078. [PubMed: 27436286]

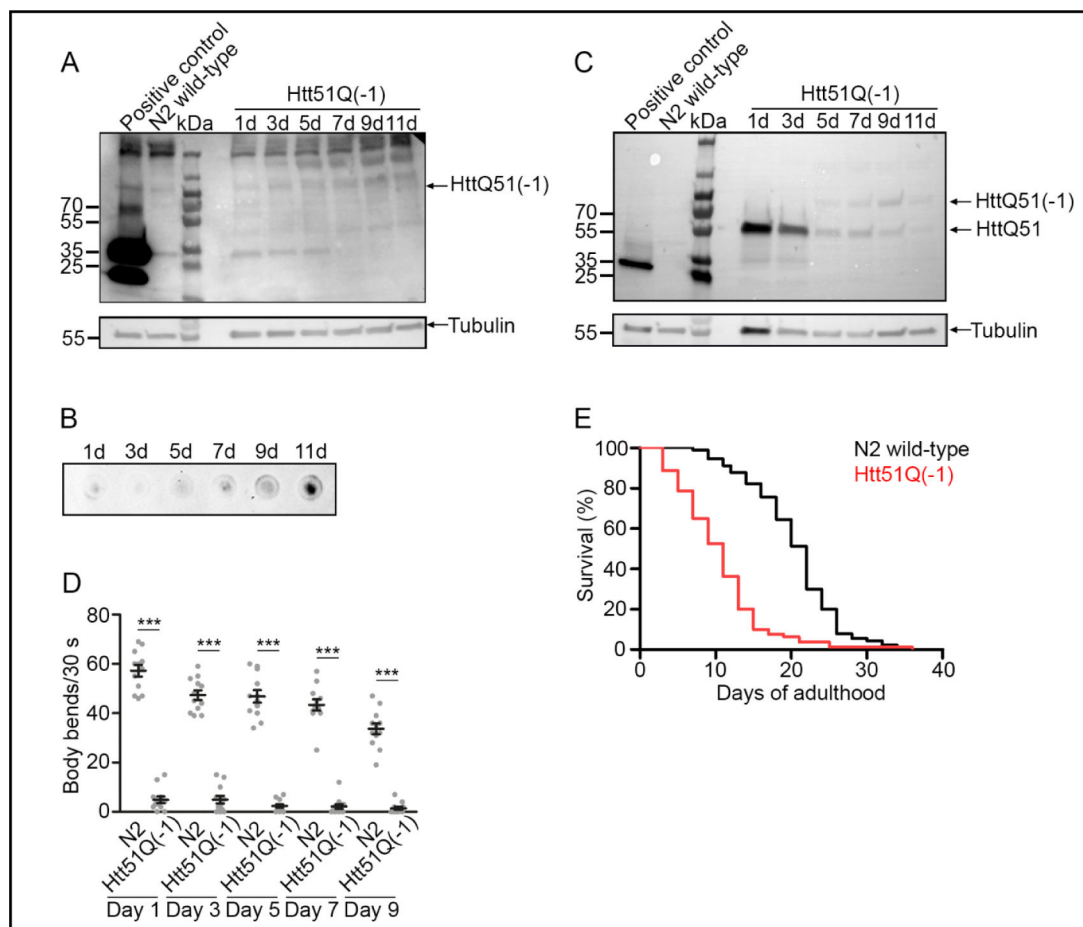
5. Dinman JD: Mechanisms and implications of programmed translational frameshifting. *Wiley Interdiscip Rev RNA* 2012;3:661–673. [PubMed: 22715123]
6. Giedroc DP, Cornish PV: Frameshifting rna pseudoknots: Structure and mechanism. *Virus Res* 2009;139:193–208. [PubMed: 18621088]
7. Namy O, Rousset JP, Naphine S, Brierley I: Reprogrammed genetic decoding in cellular gene expression. *Mol Cell* 2004;13:157–168. [PubMed: 14759362]
8. Davies JE, Rubinsztein DC: Polyalanine and polyserine frameshift products in huntington's disease. *J Med Genet* 2006;43:893–896. [PubMed: 16801344]
9. Gaspar C, Jannatipour M, Dion P, Laganier J, Sequeiros J, Brais B, Rouleau GA: Cag tract of mjd-1 may be prone to frameshifts causing polyalanine accumulation. *Human Mol Genet* 2000;9:1957–1966. [PubMed: 10942424]
10. Girstmair H, Saffert P, Rode S, Czech A, Holland G, Bannert N, Ignatova Z: Depletion of cognate charged transfer rna causes translational frameshifting within the expanded cag stretch in huntingtin. *Cell Rep* 2013;3:148–159. [PubMed: 23352662]
11. Saffert P, Adamla F, Schieweck R, Atkins JF, Ignatova Z: An expanded cag repeat in huntingtin causes +1 frameshifting. *J Biol Chem* 2016;291:18505–18513. [PubMed: 27382061]
12. Stochmanski SJ, Therrien M, Laganier J, Rochefort D, Laurent S, Karemera L, Gaudet R, Vyboh K, Van Meyel DJ, Di Cristo G, Dion PA, Gaspar C, Rouleau GA: Expanded atxn3 frameshifting events are toxic in drosophila and mammalian neuron models. *Human Mol Genet* 2012;21:2211–2218. [PubMed: 22337953]
13. Toulouse A, Au-Yeung F, Gaspar C, Roussel J, Dion P, Rouleau GA: Ribosomal frameshifting on mjd-1 transcripts with long cag tracts. *Human Mol Genet* 2005;14:2649–2660. [PubMed: 16087686]
14. Zhang G, Fedyunin I, Miekley O, Valleriani A, Moura A, Ignatova Z: Global and local depletion of ternary complex limits translational elongation. *Nucl Acid Res* 2010;38:4778–4787.
15. Lam YA, Pickart CM, Alban A, Landon M, Jamieson C, Ramage R, Mayer RJ, Layfield R: Inhibition of the ubiquitin-proteasome system in alzheimer's disease. *Proc Natl Acad Sci USA* 2000;97:9902–9906. [PubMed: 10944193]
16. van Leeuwen FW, de Kleijn DP, van den Hurk HH, Neubauer A, Sonnemans MA, Sluijs JA, Koycu S, Ramdjielal RD, Salehi A, Martens GJ, Grosveld FG, Peter J, Burbach H, Hol EM: Frameshift mutants of beta amyloid precursor protein and ubiquitin-b in alzheimer's and down patients. *Science* 1998;279:242–247. [PubMed: 9422699]
17. Orgel LE: The maintenance of the accuracy of protein synthesis and its relevance to ageing. *Proc Natl Acad Sci USA* 1963;49:517–521. [PubMed: 13940312]
18. Lopez-Otin C, Blasco MA, Partridge L, Serrano M, Kroemer G: The hallmarks of aging. *Cell* 2013;153:1194–1217. [PubMed: 23746838]
19. Maynard Smith J: Review lectures on senescence - i. The causes of ageing. *Proc Royal Soc B* 1962; DOI:10.1098/rspb.1962.0065.
20. Balch WE, Morimoto RI, Dillin A, Kelly JW: Adapting proteostasis for disease intervention. *Science* 2008;319:916–919. [PubMed: 18276881]
21. Gonskikh Y, Polacek N: Alterations of the translation apparatus during aging and stress response. *Mech Ageing Develop* 2017;168:30–36.
22. Luce MC, Bunn CL: Decreased accuracy of protein synthesis in extracts from aging human diploid fibroblasts. *Exp Gerontol* 1989;24:113–125. [PubMed: 2721600]
23. Mori N, Hiruta K, Funatsu Y, Goto S: Codon recognition fidelity of ribosomes at the first and second positions does not decrease during aging. *Mech Ageing Develop* 1983;22:1–10.
24. Filion AM, Laughrea M: Translation fidelity in the aging mammal: Studies with an accurate in vitro system on aged rats. *Mech Ageing Develop* 1985;29:125–142.
25. Ke Z, Mallik P, Johnson AB, Luna F, Nevo E, Zhang ZD, Gladyshev VN, Seluanov A, Gorbunova V: Translation fidelity coevolves with longevity. *Aging Cell* 2017;16:988–993. [PubMed: 28707419]
26. Sanchez CG, Teixeira FK, Czech B, Preall JB, Zamparini AL, Seifert JR, Malone CD, Hannon GJ, Lehmann R: Regulation of ribosome biogenesis and protein synthesis controls germline stem cell differentiation. *Cell Stem Cell* 2016;18:276–290. [PubMed: 26669894]

27. Howard A, Rogers AN: Role of translation initiation factor 4g in lifespan regulation and age-related health. *Ageing Res Rev* 2014;13:115–124. [PubMed: 24394551]
28. Schosserer M, Minois N, Angerer TB, Amring M, Dellago H, Harreither E, Calle-Perez A, Pircher A, Gerstl MP, Pfeifenberger S, Brandl C, Sonntagbauer M, Kriegner A, Linder A, Weinhausel A, Mohr T, Steiger M, Mattanovich D, Rinnerthaler M, Karl T et al.: Methylation of ribosomal rna by nsun5 is a conserved mechanism modulating organismal lifespan. *Nat Commun* 2015;6:6158. [PubMed: 25635753]
29. Kamath RS, Martinez-Campos M, Zipperlen P, Fraser AG, Ahringer J: Effectiveness of specific rna-mediated interference through ingested double-stranded rna in *caenorhabditis elegans*. *Genome Biol* 2001;2:RESEARCH0002. [PubMed: 11178279]
30. Brignull HR, Moore FE, Tang SJ, Morimoto RI: Polyglutamine proteins at the pathogenic threshold display neuron-specific aggregation in a pan-neuronal *caenorhabditis elegans* model. *J Neurosci* 2006;26:7597–7606. [PubMed: 16855087]
31. Miller KG, Alfonso A, Nguyen M, Crowell JA, Johnson CD, Rand JB: A genetic selection for *caenorhabditis elegans* synaptic transmission mutants. *Proc Natl Acad Sci USA* 1996;93:12593–12598. [PubMed: 8901627]
32. Scherzinger E, Lurz R, Turmaine M, Mangiarini L, Hollenbach B, Hasenbank R, Bates GP, Davies SW, Lehrach H, Wanker EE: Huntingtin-encoded polyglutamine expansions form amyloid-like protein aggregates *in vitro* and *in vivo*. *Cell* 1997;90:549–558. [PubMed: 9267034]
33. Gigova A, Duggimpudi S, Pollex T, Schaefer M, Kos M: A cluster of methylations in the domain iv of 25s rna is required for ribosome stability. *RNA* 2014;20:1632–1644. [PubMed: 25125595]
34. Morley JF, Brignull HR, Weyers JJ, Morimoto RI: The threshold for polyglutamine-expansion protein aggregation and cellular toxicity is dynamic and influenced by aging in *caenorhabditis elegans*. *Proc Natl Acad Sci USA* 2002;99:10417–10422. [PubMed: 12122205]
35. Amiel J, Trochet D, Clement-Ziza M, Munnich A, Lyonnet S: Polyalanine expansions in human. *Human Mol Genet* 2004;13 Spec No 2:R235–243. [PubMed: 15358730]
36. Adamla F, Ignatova Z: Somatic expression of *unc-54* and *vha-6* mRNAs declines but not pan-neuronal *rgef-1* and *unc-119* expression in aging *caenorhabditis elegans*. *Sci Rep* 2015;5:10692. [PubMed: 26031360]
37. Henderson ST, Johnson TE: Daf-16 integrates developmental and environmental inputs to mediate aging in the nematode *caenorhabditis elegans*. *Curr Biol* 2001;11:1975–1980. [PubMed: 11747825]
38. Hsu AL, Murphy CT, Kenyon C: Regulation of aging and age-related disease by *daf-16* and heat-shock factor. *Science* 2003;300:1142–1145. [PubMed: 12750521]
39. Hansen M, Taubert S, Crawford D, Libina N, Lee SJ, Kenyon C: Lifespan extension by conditions that inhibit translation in *caenorhabditis elegans*. *Aging Cell* 2007;6:95–110. [PubMed: 17266679]
40. Pan KZ, Palter JE, Rogers AN, Olsen A, Chen D, Lithgow GJ, Kapahi P: Inhibition of mrna translation extends lifespan in *caenorhabditis elegans*. *Aging Cell* 2007;6:111–119. [PubMed: 17266680]
41. Curran SP, Ruvkun G: Lifespan regulation by evolutionarily conserved genes essential for viability. *PLoS Genet* 2007;3:e56. [PubMed: 17411345]
42. Farabaugh PJ: Translational frameshifting: Implications for the mechanism of translational frame maintenance. *Prog Nucl Acid Res Mol Biol* 2000;64:131–170.
43. Parker J: Errors and alternatives in reading the universal genetic code. *Microbiol Rev* 1989;53:273–298. [PubMed: 2677635]
44. Meyer JN, Boyd WA, Azzam GA, Haugen AC, Freedman JH, Van Houten B: Decline of nucleotide excision repair capacity in aging *caenorhabditis elegans*. *Genome Biol* 2007;8:R70. [PubMed: 17472752]
45. Bates GP, Dorsey R, Gusella JF, Hayden MR, Kay C, Leavitt BR, Nance M, Ross CA, Scahill RI, Wetzel R, Wild EJ, Tabrizi SJ: Huntington disease. *Nat Rev Dis Primers* 2015;1:15005. [PubMed: 27188817]
46. Labbadia J, Morimoto RI: Huntington's disease: Underlying molecular mechanisms and emerging concepts. *Trends Biochem Sci* 2013;38:378–385. [PubMed: 23768628]

47. van Eyk CL, McLeod CJ, O'Keefe LV, Richards RI: Comparative toxicity of polyglutamine, polyalanine and polyleucine tracts in drosophila models of expanded repeat disease. *Human Mol Genet* 2012;21:536–547. [PubMed: 22021427]
48. Mohri-Shiomi A, Garsin DA: Insulin signaling and the heat shock response modulate protein homeostasis in the caenorhabditis elegans intestine during infection. *J Biol Sci* 2008;283:194–201.
49. Lee AL, Ung HM, Sands LP, Kikis EA: A new caenorhabditis elegans model of human huntingtin 513 aggregation and toxicity in body wall muscles. *PLoS One* 2017;12:e0173644. [PubMed: 28282438]
50. Bhattacharyya A, Thakur AK, Chellgren VM, Thiagarajan G, Williams AD, Chellgren BW, Creamer TP, Wetzel R: Oligoproline effects on polyglutamine conformation and aggregation. *J Mol Biol* 2006;355:524–535. [PubMed: 16321399]
51. Thakur AK, Jayaraman M, Mishra R, Thakur M, Chellgren VM, Byeon IJ, Anjum DH, Kodali R, Creamer TP, Conway JF, Gronenborn AM, Wetzel R: Polyglutamine disruption of the huntingtin exon 1 n terminus triggers a complex aggregation mechanism. *Nat Struct Mol Biol* 2009;16:380–389. [PubMed: 19270701]
52. Venkatraman P, Wetzel R, Tanaka M, Nukina N, Goldberg AL: Eukaryotic proteasomes cannot digest polyglutamine sequences and release them during degradation of polyglutamine-containing proteins. *Mol Cell* 2004;14:95–104. [PubMed: 15068806]
53. Labbadia J, Morimoto RI: The biology of proteostasis in aging and disease. *Ann Rev Biochem* 2015;84:435–464. [PubMed: 25784053]

**Fig. 1.**

The frequency of -1 frameshifting with age. (A) Schematic of the frameshift reporter *Htt51Q(-1)* for expression in body wall muscle cells under control of *unc-54* promoter. N-terminal eCFP is expressed in zero frame and mCherry reports on -1 frame. (B) Representative fluorescence images of one day-old nematodes with genome-integrated expression of *Htt51Q(-1)* in the body wall muscle cells. For better visualization, eCFP fluorescence is depicted in green. Scale bar, 25 μ m. (C) Representative fluorescence images of synchronized nematodes at larval stage L4. Scale bar, 25 μ m. (D) Representative fluorescence images of synchronized nematodes imaged at different ages. Starting at day 5, autofluorescence in the intestine becomes visible. Scale bar, 25 μ m. (E) Quantification of the ratio between mCherry and CFP fluorescence of the animals expressing *Htt51Q(-1)* at different age (n = 7–11 animals). Fluorescence was integrated over the head area since the expression was more prominent in the head and only this region was considered in the quantifications. Note that the mCherry channel was disproportionally enhanced in panels B–D compared to the blue CFP channel for better visualization. The quantification, however, was performed with non-enhanced images. *, p<0.05; ***, p<0.001, Student's *t*-test. See also Table S1. (F) qPCR analysis of adult nematodes with genome-integrated *Htt51Q(-1)* expression. *Htt51Q(-1)* mRNA was normalized to *act-2*. Expression in day 1 adults was set to 100%. Data are means \pm SEM (n = 3). ***, p<0.001, Student's *t*-test.

**Fig. 2.**

Aggregates containing -1 frameshifted Htt51Q persist with age in *C. elegans* with genome-integrated frameshift reporter. (A,C) Immunoblot of synchronized nematodes at different ages to detect soluble trans-frame and zero-frame proteins. $50 \mu\text{g}$ of protein were loaded per lane and *trans*-frame proteins were detected with anti-mCherry antibodies (A) and zero-frame proteins with anti-GFP antibody (C). Arrows indicate the position of the Htt51Q(-1) or Htt51Q monomers, respectively. Note the extended exposure in mCherry channel (A) compared to CFP channel (C) to enable detection of frameshift products, which were produced in very low amounts. Immunoblot membranes were stripped and reprobed with anti-tubulin antibody (A,C). As a positive control animals expressing both, GFP and mCherry, were used (ANR127). The signal at 250 kDa results from unspecific binding of mCherry antibodies. As a negative control, N2 animals were loaded. Note, the tubulin signal overlaps with CFP-polyQ in size; hence, the enhanced tubulin amount at 1d might be due to inefficient stripping in this part of the blot (C). (B) Filter-retardation assay of synchronized animals at different ages. 30 animals were loaded per sample and frameshifted Htt51Q(-1) was detected with anti-mCherry antibodies. (D) Motility assay on different days of adulthood. Each dot represents one single nematode, the horizontal line indicates the mean thrashing rate (\pm SEM, $n = 10$ animals for each strain and time point). Data among one time-point are normalized to the body bends of N2 wild-type. *** $p < 0.001$ (Student's t -test). (E)

Life span assay of wild-type N2 and nematodes expressing Htt51Q(-1). Kaplan-Meier survival curves were compared using log-rank test. Median lifespan of 12.5 days for animals with integrated expression of Htt51Q(-1) vs. 22 days for N2. $p < 0.001$ for animals with integrated Htt51Q(-1) vs. N2, (log-rank test). See also Fig. S2B.

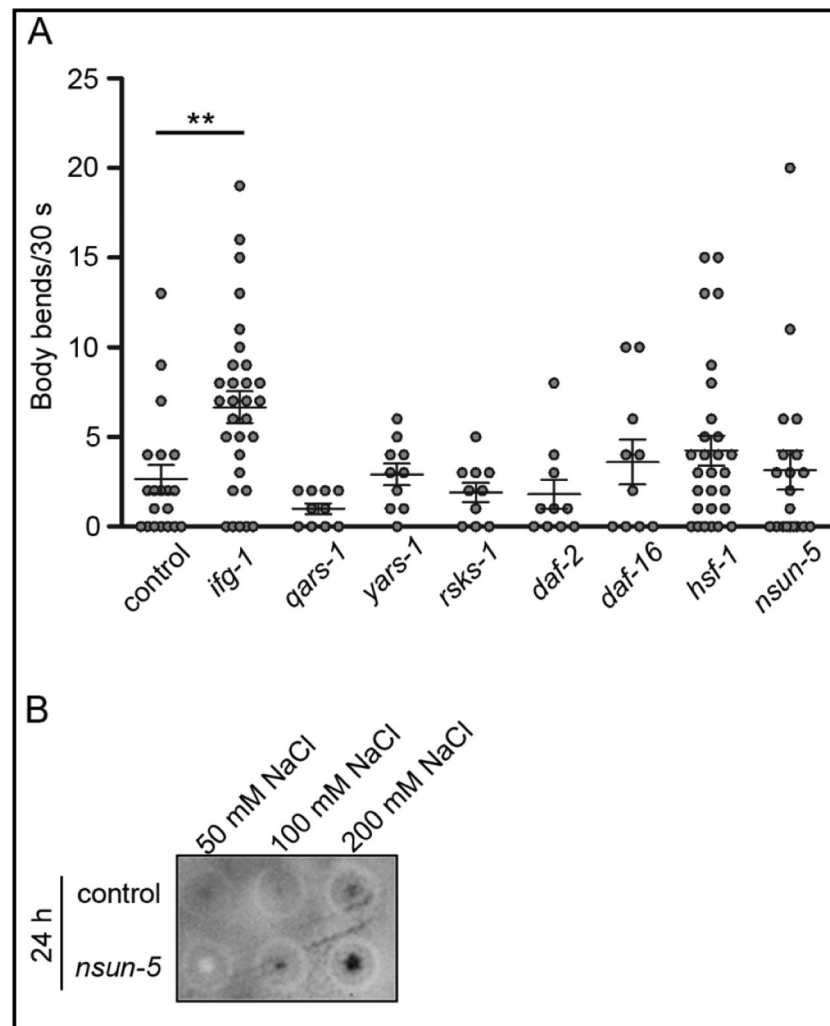


Fig. 3. Thrashing rate of 1d-old Htt51Q(-1) *C. elegans* after RNAi knockdown. (A) Motility was analyzed by counting the body bends for each nematode within 30 s. Each dot represents one individual, the horizontal bar represents mean \pm SEM ($n = 10$ for *qars-1*, *yars-1*, *rsks-1*, *daf-2*, *daf-16*; $n = 20$ for control RNAi/empty L4440 vector, $n = 30$ for *hsf-1*, *ifg-1*). Data were normalized to the thrashing rate of control animals. ** $p < 0.01$ for *ifg-1* compared to the control, differences between all other knockdowns were not significant. (B) Filter-retardation assay of synchronized animals expressing Htt51Q(-1) grown on control RNAi/L4440 vector or *nsun-5* RNAi and subjected at 1d of adulthood to various doses of osmotic stress. 30 animals were loaded onto a cellulose-acetate membrane and frameshifted Htt51Q(-1) detergent-insoluble aggregates were detected using anti-mCherry antibodies.

Cellular senescence and quiescence are associated with altered ribosomal RNA methylation and processing

Guohuan Yang^{1,2}, Clemens Heisenberger², Isabelle C. Kos-Brauni, Norbert Polacek³, Johannes Grillari², Markus Schosserer^{2,*} and MaUWin Koã^{1,*}

1. Biochemistry Center (BZH), Heidelberg University, Heidelberg, Germany

2. Institute of Molecular Biotechnology, Department of Biotechnology, University of Natural Resources and Life Sciences, Vienna, Vienna, Austria.

3. Department of Chemistry and Biochemistry, University of Bern, Bern, Switzerland

* These authors contributed equally

Total: 10289 characters;

Abstract: 566; Text: 4762; References: 3181; Fig. legend: 815; Acknowledgements: 501

Abstract

The 2'-O-methylation (2'-O-Me) of ribosomal RNA (rRNA) shows plasticity potentially associated with specific cell phenotypes. We used RiboMeth-seq profiling to reveal 2'-O-Me patterns specific to stress induced premature senescent (SIPS), quiescent and proliferating human dermal fibroblasts. The altered methylation levels in SIPS and quiescence partially correlated with the expression of specific snoRNAs but not fibrillarin. Senescence and quiescence were accompanied by a trend towards preferred usage of one of the two alternative ribosome biogenesis pathways.

Introduction

The accumulation of senescent cells is one of the main drivers of biological ageing mainly due to the characteristic pro-inflammatory senescence-associated secretory phenotype (SASP) (Coppe et al., 2010). Eliminating senescent cells extends the healthy lifespan of mice (Baker et al., 2016; Xu et al., 2018). Thus, strategies to deplete senescent cells or block the SASP offer therapeutic opportunities. Ribosomes represent a promising novel target, as delayed rRNA processing promotes induction of senescence by activation of p53 (Nishimura et al., 2015), and accumulation of pre-ribosomes maintains the senescent state by engaging retinoblastoma protein (Lessard et al., 2018). The protein composition of ribosomes in senescent cells was found to vary (Shi et al., 2017), but other ribosome features, such as rRNA modifications, were not yet explored.

The 2'-O-methylation (2'-O-Me), the most abundant modification in rRNA, is introduced by ribonucleoprotein complexes of four conserved proteins, including the methyltransferase fibrillarin (FBL), and a small nucleolar RNA (snoRNA) specifying the methylated site (Kiss, 2002). Recently, the plasticity of the 2'-O-Me modification of rRNA in response to stress was shown to contribute to the heterogeneity of ribosomes and affect their translational activity (Erales et al., 2017; Krogh et al., 2016). Here we show that the rRNA 2'-O-methylation is altered in senescent and quiescent human cells.

Results and discussion

We induced senescence in the human dermal fibroblasts (HDF) from three different donors by exposure to hydrogen peroxide (Lämmermann et al., 2018) and confirmed their senescent phenotype by changes in morphology, increased senescence-associated β -Galactosidase activity (SA- β -gal) and absence of proliferation by incorporation of 5-Bromo-2'-deoxyuridine (BrdU) (Supp. Inf. Fig. S1). The contact-inhibited quiescent (Q) and proliferating (P) cells derived from each donor served as controls.

We used RiboMeth-seq to profile 104 2'-O-Me sites in the rRNA of SIPS, Q and P cells and assigned the RMS score (0 = non-methylated, 1 = fully methylated) to each modified position as described (Krogh et al., 2016) (Fig. 1 and Supp. Inf. Tables S2, S3). While the majority of sites were highly methylated (RMS > 0.9), the scores of nine positions in SIPS and Q cells appeared lower (SSU-C1391, LSU-C3680) or higher (SSU: C797, G867, C1272 and G1447; LSU: G1303, G3723 and G4588) compared to P cells (Fig. 1). The methylation at SSU-C797, G867, C1272 and LSU-G1303 was nearly identical in Q and SIPS but different in P cells, pointing to a general role in proliferation. The SSU-C1391, G1447, and LSU-C3680, G3723 methylation in SIPS differed from P or Q cells suggesting a specific association with SIPS, however the biological variance between donors at these sites precludes a conclusion from the current data (Fig. 1; Supp. Inf. Tables S2, S3).

The RMS scores were overall slightly higher in Q and SIPS than P cells. In a recent study, the expression levels of FBL affected methylation at specific positions (Sharma et al., 2017). However, in our model the methylation in Q/SIPS and P cells did not correlate with FBL expression, which did neither change at mRNA nor at protein level in any of the tested conditions (Supp. Inf. Fig. S1D-F).

In contrast, methylation at the hypomodified sites correlated with expression of snoRNAs guiding modification at those sites. Even small methylation changes were accompanied by comparable alterations in the snoRNAs levels (Fig. 1BD, Supp. Inf. Fig. S2, S3). Importantly, the expression of all snoRNAs for the hypomodified sites was very low and thus the hypomethylation might be due to the limiting levels of the snoRNAs.

Contrary to previous reports of delayed early rRNA processing in cellular senescence (Lessard et al., 2018; Nishimura et al., 2015), the 47 pre-rRNA did not accumulate in SIPS revealing that neither transcription nor early processing were affected (Fig. 2ABC). Conversely, the relative levels of 21S and 18S-E pre-rRNAs decreased in SIPS, indicating an altered kinetics of the late SSU biogenesis (Fig. 2DE). Intriguingly, Q and SIPS cells showed a trend towards preference for the rRNA processing pathway B, represented by an increase in the 30S:41S pre-rRNA ratio (41S and 30S pre-rRNAs are produced only by the pathway A or B respectively) (Fig. 2A and 2FGH). A similar switch between two pre-rRNA processing pathways in response to stress was described in yeast (Kos-Braun et al., 2017). Alternative pathways can provide means to produce distinct ribosomes.

In summary, we identified nine 2'-O-Me sites that appear to be differentially modified in non-proliferating cells (Q and SIPS). Their methylation correlated with the snoRNAs levels that are likely at limiting concentrations. Upon growth arrest, the pre-rRNA processing in SIPS and Q cells shifted towards the pathway B. Our results provide a basis for further study of ribosomes in cellular senescence as plausible targets for novel therapeutic interventions.

ACKNOWLEDGEMENTS

We thank Uschi Göbels and Elena Stelzer for technical assistance. GY was supported by the China Scholarship Council (201608310107). The work was supported by Deutsche Forschungsgemeinschaft 280594475 to MK, Austrian Science Fund (FWF) I2514 to JG and the Swiss National Science Foundation 310030E-162559/1 to NP; and by FWF and Herzfelder'sche Familienstiftung P30623-B26 to MS.

AUTHOR CONTRIBUTIONS

GY, CH and IKB performed experiments and analyzed data. NP, JG, MS and MK designed experiments and analyzed data. GY, MS and MK wrote the paper.

CONFLICTS OF INTEREST

104 JG is co-founder and shareholder of Evercyte GmbH and TAmiRNA GmbH.

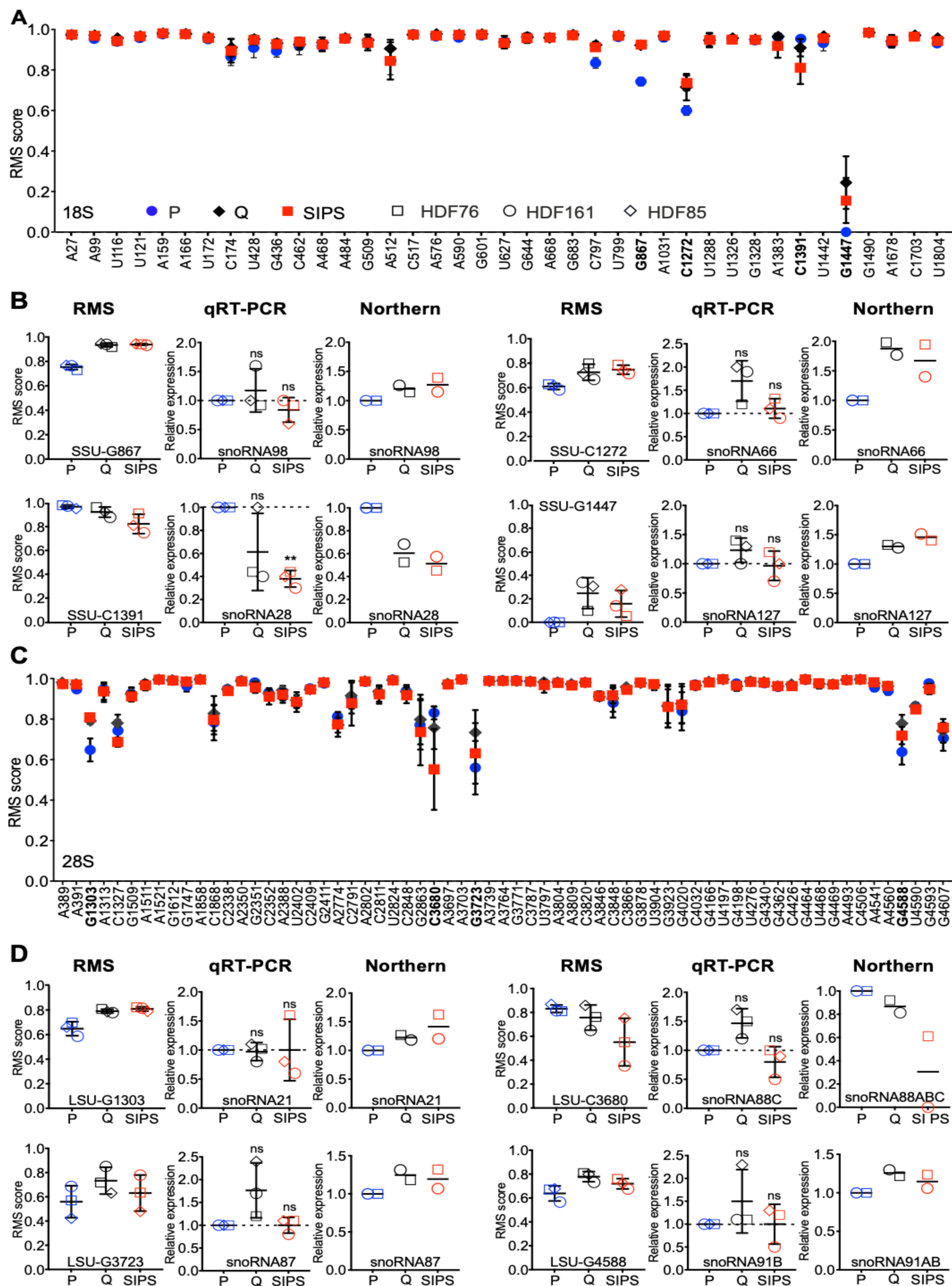
REFERENCES

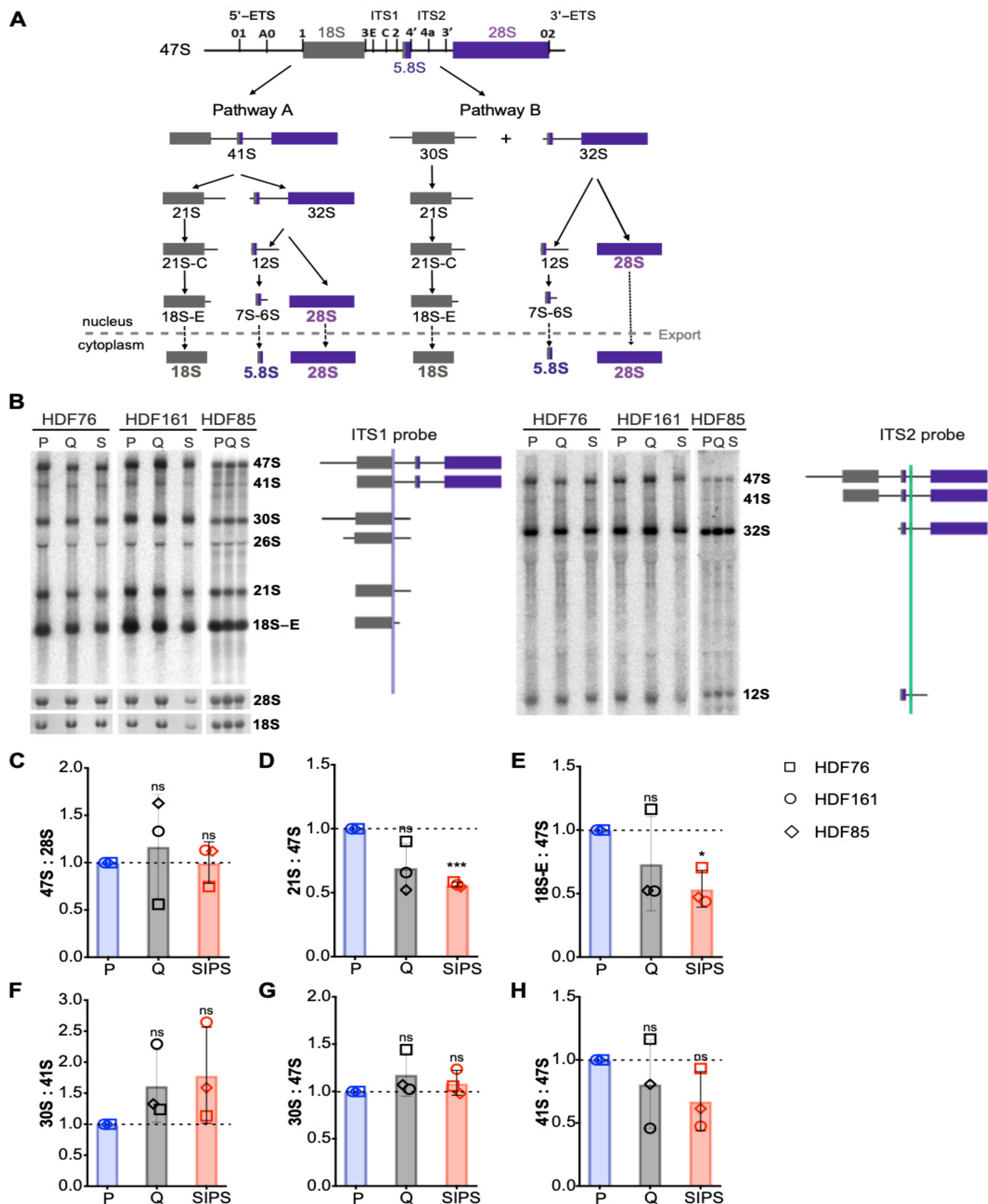
- Baker, D. J., Childs, B. G., Durik, M., Wijers, M. E., Sieben, C. J., Zhong, J., ... Deursen, J. M. Van. (2016). Naturally occurring p16 Ink4a -positive cells shorten healthy lifespan. *Nature*, 530(7589), 184–189. DOI:10.1038/nature16932
- Coppe, J. P., Desprez, P. Y., Krtolica, A., & Campisi, J. (2010). The senescence-associated secretory phenotype: The dark side of tumor suppression. *Annu Rev Pathol*, 5, 99–118. DOI:10.1146/annurev-pathol-121808-102144
- Erales, J., Marchand, V., Panthu, B., Gillot, S., Belin, S., Ghayad, S. E., ... Diaz, J.-J. (2017). Evidence for rRNA 2'-O-methylation plasticity: Control of intrinsic translational capabilities of human ribosomes. *Proceedings of the National Academy of Sciences*, 114(49), 12934–12939. DOI:10.1073/pnas.1707674114
- Kiss, T. (2002). Small nucleolar RNAs: An abundant group of noncoding RNAs with diverse cellular functions. *Cell*, 109(2), 145–148.
- Kos-Braun, I. C., Jung, I., & Koš, M. (2017). Tor1 and CK2 kinases control a switch between alternative ribosome biogenesis pathways in a growth-dependent manner. *PLoS Biology*, 15(3). DOI:10.1371/journal.pbio.2000245
- Krogh, N., Birkedal, U., Christensen-Dalsgaard, M., Nielsen, H., Jansson, M. D., Häfner, S. J., ... Lund, A. H. (2016). Profiling of 2'-O-Me in human rRNA reveals a subset of fractionally modified positions and provides evidence for ribosome heterogeneity. *Nucleic Acids Research*, 44(16), 7884–7895. DOI:10.1093/nar/gkw482
- Lämmermann, I., Terlecki-Zaniewicz, L., Weinmüllner, R., Schosserer, M., Dellago, H., de Matos Branco, A. D., ... Grillari, J. (2018). Blocking negative effects of senescence in human skin fibroblasts with a plant extract. *Npj Aging and Mechanisms of Disease*, 4(1). DOI:10.1038/s41514-018-0023-5

- 129 Lessard, F., Igelmann, S., Trahan, C., Huot, G., Saint-Germain, E., Mignacca, L., ... Ferbeyre, G. (2018).
130 Senescence-associated ribosome biogenesis defects contributes to cell cycle arrest through
131 the Rb pathway. *Nature Cell Biology*, 20(7), 789. DOI:10.1038/s41556-018-0127-y
- 132 Mullineux, S.-T., & Lafontaine, D. L. J. (2012). Mapping the cleavage sites on mammalian pre-rRNAs:
133 Where do we stand? *Biochimie*, 94(7), 1521–1532. DOI:10.1016/j.biochi.2012.02.001
- 134 Nishimura, K., Kumazawa, T., Kuroda, T., Katagiri, N., Tsuchiya, M., Goto, N., ... Kimura, K. (2015).
135 Perturbation of Ribosome Biogenesis Drives Cells into Senescence through 5S RNP-Mediated
136 p53 Activation. *Cell Reports*, 10(8), 1310–1323. DOI:10.1016/j.celrep.2015.01.055
- 137 Sharma, S., Marchand, V., Motorin, Y., & Lafontaine, D. L. J. (2017). Identification of sites of 2'-O-
138 methylation vulnerability in human ribosomal RNAs by systematic mapping. *Scientific*
139 *Reports*, 7(1), 1–15. DOI:10.1038/s41598-017-09734-9
- 140 Shi, Z., Fujii, K., Kovary, K. M., Genuth, N. R., Röst, H. L., Teruel, M. N., & Barna, M. (2017).
141 Heterogeneous Ribosomes Preferentially Translate Distinct Subpools of mRNAs Genome-
142 wide. *Molecular Cell*, 67(1), 71-83.e7. DOI:10.1016/j.molcel.2017.05.021
- 143 Xu, M., Pirtskhalava, T., Farr, J. N., Weigand, B. M., Palmer, A. K., Weivoda, M. M., ... Kirkland, J. L.
144 (2018). Senolytics improve physical function and increase lifespan in old age. *Nature*
145 *Medicine*, 24(8), 1246–1256. DOI:10.1038/s41591-018-0092-9

Fig. 1: RiboMeth-seq and snoRNA expression. (A, C) Average RMS scores for each 2'-O-methylated nucleotide in 18S (A) and 28S (C) rRNAs from proliferating (P), quiescent (Q) and senescent (SIPS) HDFs from three donors (HDF76, HDF161, HDF85). Error bars represent standard deviation. (B and D) Relative levels of snoRNAs guiding modification at the variable sites. Values were corrected for loading by snoRNA57 (northern) and 5.8S RNA (qRT-PCR).

Fig. 2 Pre-rRNA processing in SIPS. (A) Scheme of the human pre-rRNA processing (modified from (Mullineux & Lafontaine, 2012)). (B) Northern blots of total RNA using two probes to detect different pre-rRNAs shown on the right. (C-H) Quantification of changes in pre-rRNAs expressed as ratios: (C) 47S:28S; (D) 18S-E:47S; (E) 21S:47S; (F) 30S:41S; (G) 30S:47S; (H) 41S:47S.





CURRICULUM VITAE

DIPL-ING. BSc Clemens Heissenberger



PERSONAL INFORMATION

Name Clemens Heissenberger
Date of birth 03 October 1990
Place of birth Neunkirchen
Nationality Austria
Address Hauptstraße 31
 2824 Seebenstein
Email clemens_h@gmx.net
Phone +43 676 9560046

LANGUAGE SKILLS

German fluently
English fluently
Italian basics

SCIENTIFIC SKILLS

Programs CorelDRAW, SigmaPlot
 CytExpert, Kaluza,
 SnapGene, ImageJ/Fiji, R
 (basics)
Laboratory Cell culture
 Cell culture-based assays
 Molecular biology
 Mouse and *C. elegans*

ADDITIONAL QUALIFICATIONS / INTERESTS

Computer skills Windows
 Microsoft Office
Driving Licence B
Hobbies Beekeeping
 Nature and
 sports in general

WORK EXPERIENCE

Mar 16 – now **University of Natural Resources and Life Sciences, Vienna, Austria**
Doctoral program
 - Conducting the doctoral study at the Department of Biotechnology according to the FWF guideline
Aug 13 – Sep 13 **Internship: Vöslauer Mineralwasser AG**
 - QM and QC
 - Responsible for sample-drawing and analysis
Jul 12 – Aug 12 **Internship: Baumit Wopfinger**
 - R&D
 - Formulation and hands-on of new building materials
Aug 10 – Sep 10 **Internship: Reckitt Benckiser**
 - QM and QC
 - Delivery control and regular analytical testing of products

EDUCATION

Mar 16 – now **University of Natural Resources and Life Sciences, Vienna, Austria**
Doctoral program
 - Doctoral Thesis: The role of specialized ribosomes in healthy aging and stress
 - At the Department of Biotechnology in the working group of Assoc. Prof. Johannes Grillari
 - First author publication: "Loss of the ribosomal RNA methyltransferase NSUN5 impairs global protein synthesis and normal growth", 2019, Nucleic Acids Research
Oct 13 – Dec 15 **University of Natural Resources and Life Sciences, Vienna, Austria**
Master's program in Biotechnology
 - Master Thesis on *Regulation of NSUN5 and SAMS1 in healthy aging*
 - Department of Biotechnology in the working group of Assoc. Prof. Johannes Grillari
 - **Degree: Dipl.-Ing. (equal to MSc) – passed with distinction**
Oct 10 – Oct 13 **University of Natural Resources and Life Sciences, Vienna, Austria**
Bachelor's program in Lebensmittel –und Biotechnologie
 - Bachelor Thesis: *Purification and characterisation of two synthetic peroxidases expressed in E.coli and P.pastoris*
 - Department of Chemistry in the working group of Ao. Prof. Paul Furtmüller
 - **Degree: Bachelor of Science – passed with distinction**
Oct 09 – Jul 10 **Cumprulsory community service**
 - Red cross, Aspang
 - Paramedic
Sep 05 – Jun 09 **Bundesoberstufenrealgymnasium (BORG) Wiener Neustadt**
 - *Secondary school*
Sep 01 – Jun 05 **Hauptschule Scheiblingkirchen**
 - *Secondary school*